CZECH TECHNICAL UNIVERSITY IN PRAGUE
FACULTY OF CIVIL ENGINEERING
DEPARTMENT OF STEEL AND TIMBER STRUCTURES

Mechanical properties of cold-formed stainless steel

A dissertation thesis for obtaining the degree of "Doctor" abbreviated to Ph.D.

Ing. Jan Mařík

Ph.D. Programme: Civil Engineering
Branch of study: Building Structures

Supervisor: doc. Ing. Michal Jandera, Ph.D.

Prague, 2017

Autorovo prohlášení

Prohlašuji, že jsem předloženou práci vypracoval samostatně pod vedením školitele doc. Ing. Michala Jandery, Ph.D., že uvedené výstupy a závěry jsou výsledkem původního výzkumu a že jsem uvedl veškeré použité informační zdroje v souladu s Metodickým pokynem o dodržování etických principů při přípravě vysokoškolských závěrečných prací.

Disertační práce vznikla v souvislosti s řešením projektů:

GAČR P105/12/P307 “Influence of Cold-Forming on Stainless Steel Mechanical Properties”, SGS12/123/OHK1/2T/11, SGS14/125/OHK1/2T/11

V Praze dne 23. října 2017 Jan Mařík

Author's declaration

I hereby declare that this thesis work presented herein is my own and outputs, results and conclusions stated below are issues of my original research under the supervision of doc. Ing. Michal Jandera, Ph.D. All information sources used in the thesis are cited in accordance with Methodical instruction for ethical principles obeying within preparing of qualification theses.

The support of the Czech Science Foundation grant P105/12/P307 “Influence of Cold-Forming on Stainless Steel Mechanical Properties” is gratefully acknowledged, internal Czech technical university grants SGS12/123/OHK1/2T/11, SGS14/125/OHK1/2T/11 as well.

In Prague October 23th 2017 Jan Mařík

Abstrakt

Korozivzdorná ocel je specifický materiál, který se svým chováním liší od uhlíkové oceli, což vyžaduje odlišný přístup při navrhování stavebních konstrukcí. Jedním z hlavních znaků všech korozivzdorných ocelí, který doposud nebyl uspokojivě prozkoumán a nebyl zohledněn v normách pro navrhování, je výrazná změna pracovního diagramu způsobená tvářením za studena během výroby zejména dutých průřezů. V posledních desetiletích byly stanoveny různé vztahy pro popis základních materiálových charakteristik těchto profilů, které využívají rozdílných parametrů potřebných pro výpočet a získávají i rozličné výsledné hodnoty. Některé jsou přesnější pro malá přetvoření (očekávaná ve stavebních konstrukcích), jiné jsou přesnější pro vyšší hodnoty deformace. Současně publikovaný výzkum se také liší ve stanovení základních materiálových charakteristik jako modulu pružnosti, parametrech nelinearity, smluvní meze kluzu a pevnosti či tažnosti. Zvláště pro za studena tvářené oceli se tyto veličiny mohou významně lišit.

Níže uvedený výzkum zahrnuje experimentální program zaměřený na zkoušky netvářeného i tvářeného materiálu ze čtyř druhů ocelí: austenitické (1.4404), feritické (1.4003), austeniticko-feritické = duplexní (1.4462) a nízkolegované austeniticko-feritické, tzv. lean-duplexní (1.4162). Tyto vybrané druhy reprezentují nejvíce používané typy korozivzdorných ocelí pro konstrukční účely zpracovávané tvářením zastudena. Získaná data společně s ostatními dostupnými výsledky dalších výzkumů slouží jako podklad pro analytickou část práce.

Hlavním úkolem disertační práce bylo stanovit analytické řešení pro popis pracovního diagramu celého průřezu vyrobeného pomocí tváření za studena do formy hranaté nebo kruhové trubky. Dalším cílem bylo určit vztahy pro další mechanické vlastnosti průřezu, jako jsou tažnost nebo mez pevnosti, jelikož tato problematika nebyla dosud dostatečně prozkoumána. Uvedené závěry mohou přispět k nejnovějším postupům pro navrhování a pomoci zpřesnit výpočty metodou konečných prvků využívající zvýšené mechanické vlastnosti zastudena tvářených prvků.

Klíčová slova: korozivzdorná ocel, pracovní diagram, tváření zastudena, mechanické vlastnosti.

Abstract

Stainless steel is material of many specific properties. Structural behaviour significantly differs from carbon steel and demands more sophisticated structure design. One of the main attributes of all stainless steel grades that haven't been satisfactorily investigated is the significant change of stress-strain behaviour due to cold-forming in fabrication process of structural elements. In the last decades some proposals for the most basic material properties have been developed. These models work with various material parameters and result in different values. Some of them show a good agreement in the range of strain expected in service of load-bearing structures, other are in good agreement at higher strains. Current experimental results obtained from the recent approaches demonstrate also different values for basic material characteristics, especially for the modulus of elasticity, parameters of nonlinearity, 0.2% proof strength, ultimate tensile strength or ductility. Particularly, material properties of steel in cold worked conditions can differ a lot as it is stated herein.

Presented research project involves testing programme focused on virgin and cold-worked elements of four stainless steel grades: austenitic (1.4404), ferritic (1.4003), duplex (1.4462) and lean duplex (1.4162). Selected grades represent the most used families of stainless steel specific for structural purposes and used for section fabricating via cold-forming. Gathered data together with other available experimental results serve as a base for the analytical part of the thesis.

The main task of the thesis was to establish an analytical solution for a stress-strain diagram of a whole structural section represented by rectangular or circular hollow sections. Further objective was to establish relationships for mechanical properties such as ductility or ultimate strength as these issues of current research have not been sufficiently investigated yet. Conclusions stated herein might contribute to the newest design codes and help to precise finite element analyses using enhanced properties of cold-worked stainless steel.

Key words: stainless steel, stress-strain diagram, cold-forming, mechanical properties

Poděkování

Poděkování patří zejména mému školiteli doc. Michalu Janderovi, pod jehož přátelským vedením jsem mohl provádět všechny práce a výzkumné činnosti, a jehož cenné připomínky a rady po celou dobu studia výrazně přispěly k jeho průběhu a výsledkům.

Díky patří také všem členům katedry ocelových a dřevěných konstrukcí za jejich přátelství a otevřené dveře při řešení nejrůznějších problémů. Zvláště bych chtěl poděkovat mému kolegovi Martinu Prachařovi za jeho trpělivost a pomoc s fakultní agendou v průběhu našich společných studií.

Všechny zkoušky byly provedeny v laboratořích fakulty stavební s částečnou přípravou vzorků v Kloknerově ústavu. Provedené experimenty by nebyly možné bez profesionálního přístupu pracovníků těchto institucí.

Závěrem je třeba poděkovat také za finanční podporu grantům GAČR P105/12/P307 "Influence of Cold-Forming on Stainless Steel Mechanical Properties", SGS12/123/OHK1/2T/11, SGS14/125/OHK1/2T/11 a Nadaci Františka Faltuse, bez jejichž podpory by nebylo možné provést řadu činností, obzvláště experimentální program.

Acknowledgement

I am highly grateful to Dr. Michal Jandera for his kind guidance and well-aimed points to my work and research. His advices and comments were extremely valuable and helped me a lot.

I would like to thank to all members of the Department of Steel and Timber Structures of Faculty of Civil Engineering for their kindness a friendship, especially to my colleague and friend Martin Prachař for his patience and assistance with study issues during the whole time spent at Faculty.

Professor Leroy Gardner supervised my research during my three-month stay at Imperial College London in 2015 and I am extremely grateful to him for the great opportunity to study there and for all his friendly guidance and good points to my work. Also, I would like to thank to the students and staff at Imperial College London for their support and kindness, especially to Dr. Sheida Afshan.

All experiments were carried out in laboratories of Faculty of Civil Engineering CTU with partial preparing of samples in Klokner's institute. Executed tests would not have been feasible without professional attitude of the staff of these institutions.

The support of the Czech Science Foundation grant P105/12/P307 "Influence of Cold-Forming on Stainless Steel Mechanical Properties" is gratefully acknowledged, internal Czech technical university grants SGS12/123/OHK1/2T/11, SGS14/125/OHK1/2T/11 and Foundation of František Faltus as well.

Content

Chapter 1

Introduction

1.1 Foreword

Stainless steel is a relatively new and widely used material, which price generally ranges about three to six times the carbon steel price. Therefore stainless steel is demanded for relatively low thickness section members where the material is effectively used as much as possible, for the aesthetic sheeting, architectural important objects or for members, situated in the high corrosive environment, with long-term durability requirements. Full use of material benefits might contribute to decreasing of construction costs and environmental impact. Also continual increasing demand of stainless steel products require new approaches for the design as they become one of the most exposed members in structures with relatively high acquisition costs and aesthetical appearance.

Relatively high acquisition costs determine stainless steel structure to be used in harsh environment, for constructions with limited access for maintenance or due to high quality of surface finish, for architectural important structures, for offshore structures or pedestrian bridges. More and more stainless steel is used also for traditional bridge construction allowing decrease of maintenance costs and avoiding corrosion losses estimations (e.g. as it stated in recent studies for weathering steel [1]).

In addition, there is a new progressive method for considering the whole life costs with respect to sustainability and environmental impact, Life – cycle costing. It affects choice of material for main load-bearing structure in terms of initial, operating costs and residual value of material. From this point of view stainless steel distinguish by minimal maintenance and residual costs. Thus increase of stainless steel constructions could be expected. Therefore the thesis is aimed at structural applications which efficient use in designing is demanded for.

1.2 Stainless steel for structural purposes

Stainless steel differs in chemical composition in comparison with carbon steel a lot. Corrosion resistance is given by chromium (an essential alloy with minimal content of 10.5%), molybdenum and nitrogen content. Stainless steel may contain also carbon, nickel, manganese, copper, silicon, phosphorus, sulphur and niobium or titanium.

Traditionally structural stainless steel is divided into several basic groups according to its microstructure. These main groups represent austenitic, ferritic, duplex (i.e. ferritic - austenitic), martensitic and precipitation-hardening grades (see Figure 1.1). Each group differs in material properties, corrosion resistance or way of fabrication. For structural purposes the first three ones are the mostly used.

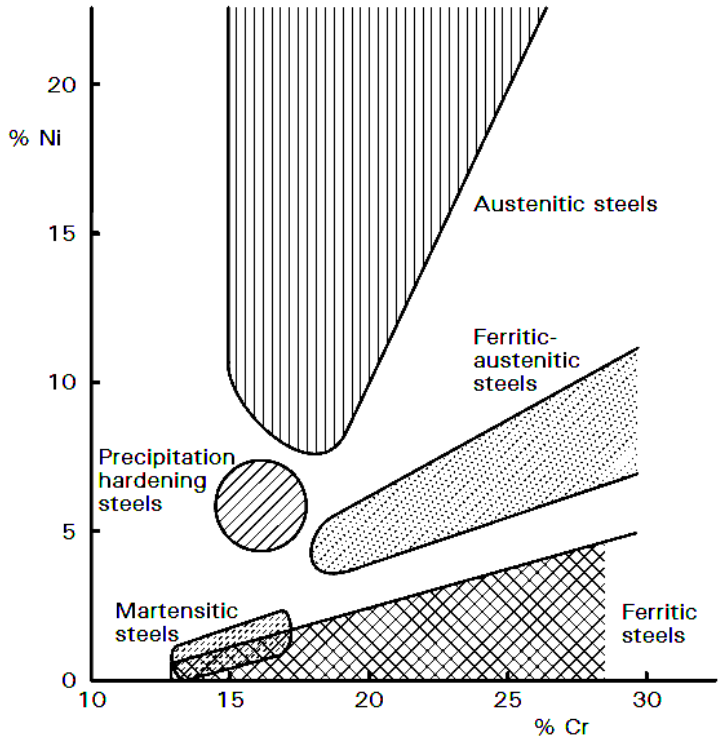

Figure 1.1 *Stainless steel grades according to content of nickel and chromium* [2]

Austenitic Grades

The austenitic family is the most commonly used, especially grades: 1.4301 (widely known as 304 according to the American standard AISI) and 1.4401 (known as 316). Other widespread grades are 1.4404 (known as 316L) and 1.4307 (known as 304L).

They are characterized by non-magnetism, excellent behaviour in elevated temperatures (see Figure 1.2), very high ductility, good corrosion resistance and they are readily weldable. All properties mentioned determine them to use for cold-formed sections, applications demanding high plastic deformations and for applications exposed to high temperatures.

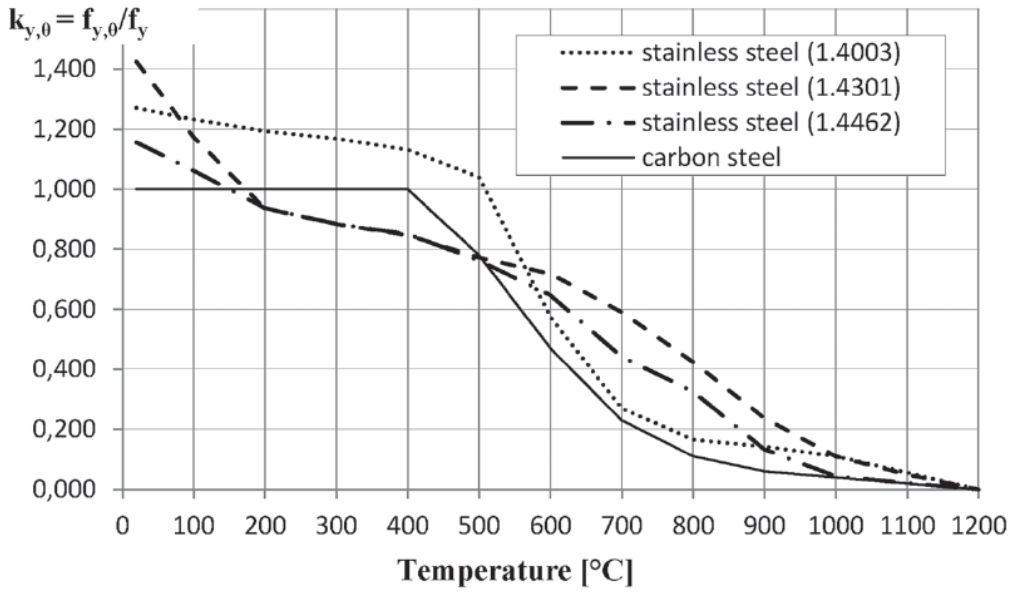

Figure 1.2 *Reduction factor for yield (proof) strength under fire: comparison of carbon and stainless steel* [3]

Ferritic Grades

Ferritic steels almost do not contain nickel. They are mostly poorly weldable, characterized by low ductility. Their advantage is stable low price and good corrosion resistance. These grades are generally used for exhaust systems, domestic equipment or building sheeting. Quite new grades have been joined for structural purposes, i.e. 1.4509 which exhibits improved weldability with workability and 1.4521 with improved corrosion resistance.

Austenitic-ferritic (Duplex) Grades

Duplex steels contain larger content of chromium and lower nickel content. It is relatively equal mix of two phases – ferritic and austenitic. They exhibit high strength and corrosion resistance with relatively high ductility and good weldability. Enhanced properties are in balance with high price. In case of duplex steels there is a new grade of lean-duplex (low alloy duplex) steel 1.4162 with reduced content of nickel and molybdenum. It keeps similar mechanical and corrosion properties in comparison with duplex grades, but lower price as well. Main application field is their use for exposed bridge load-bearing elements.

Martensitic Grades

Martensitic grades are hard steels exhibiting magnetism and high strength with low ductility and toughness used for bearings etc.

Precipitation Hardening Grades

The precipitation hardening stainless steels have properties similar to a mix of martensitic and austenitic steels. They can be heat treated to provide high tensile strengths. They are used in the specific applications such as nuclear and aerospace industry.

In case of structural section fabrication there are several main production methods, i.e. hot-rolling, cold-rolling and press-braking when a sheet material is formed into the final shape by individual bends. Current product market offers mostly cold-rolled sections.

1.3 Fabrication

The final stainless steel products involve thin and thick plates sheet, bars, hollow sections, both hot-rolled and cold-rolled open cross sections etc. The most common are circular, square and rectangular hollow sections (CHS, SHS, RHS), thick-walled H, I cross sections, thin-walled U, C or angles. Structural section production is shown in Figure 1.3). In civil engineering, stainless steel is mainly used in lightweight structures as thin-walled cold-rolled or cold-formed structure elements due to the high efficiency, ease of transport and handling on site.

The two main cold forming routes are press-braking and cold-rolling.

Cold-rolled structural cross sections represent the most widely used stainless steel sections for members in civil engineering. The principle of fabrication process can be described as passing a coiled sheet through series of shaped rollers to form both open and hollow section types. Cold rolling allows producing of large volumes of the identical structural sections with low fabrication tolerances. The hollow sections production route using flat material allows manufacturing more than one box size with the same size of rolls. This means it does not require change of rollers and thus it is possible to produce small batches without greater costs.

Press-braking is a process of cold-forming of sections from a flat sheet. Longitudinal fold is being created along the sheet by a tool pressing the material into a die. This process is used to create open sections such as angles and channels. Drawbacks of the press-braking are limited sort of cross section fabricated and shorter length of the final products (according to the manufacturing machine). It is particularly used for small batches of bespoke sections or for cross section prototypes.

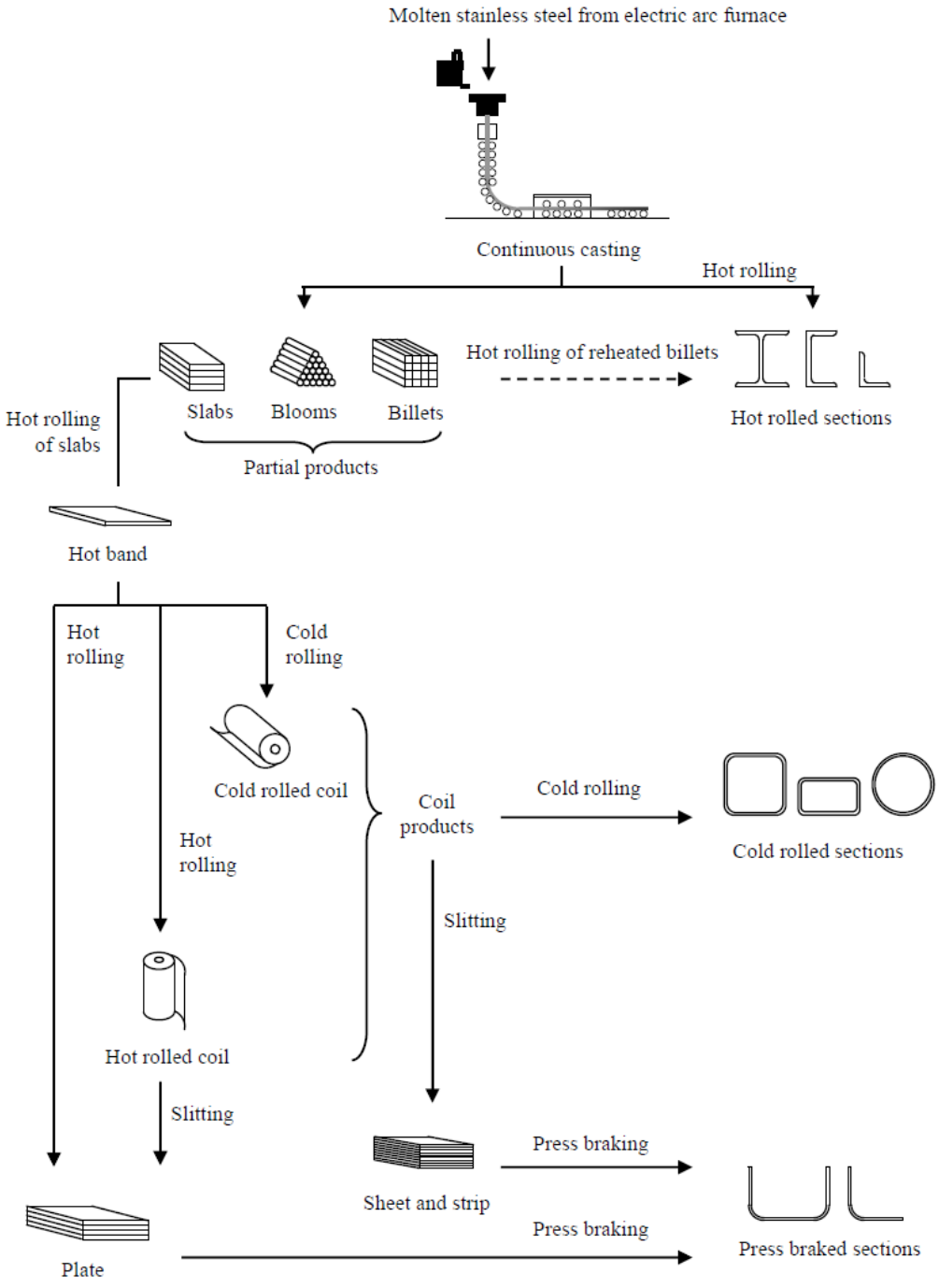

Figure 1.3 *Structural section production* [4]

1.4 Mechanical properties of stainless steel

Stainless steel is specific material. Main difference between common carbon steel and stainless steel is nonlinearity of stress-strain diagram (see Figure 1.4). Stainless steel doesn´t exhibit well-defined yield strength similar to aluminium alloys. Therefore the $\sigma_{0.2}$ is traditionally used, defined as a stress value for which plastic strain 0.2 % remains after unloading. Curvature of stress-strain diagram is dependent on material grade or level and type of cold-forming. Basic and essential material characteristics for stress-

strain diagram description are initial tangent modulus of elasticity, yield strength (0.2% proof strength) and parameters of nonlinearity (see Figure 1.5).

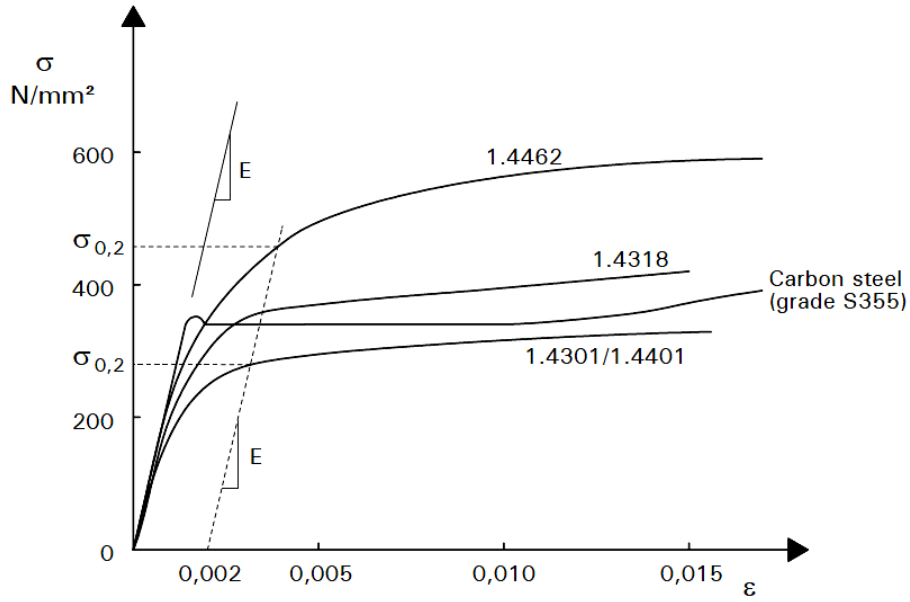

Figure 1.4 *Typical tension stress-strain diagram in annealed condition for selected stainless and carbon steel* [5]

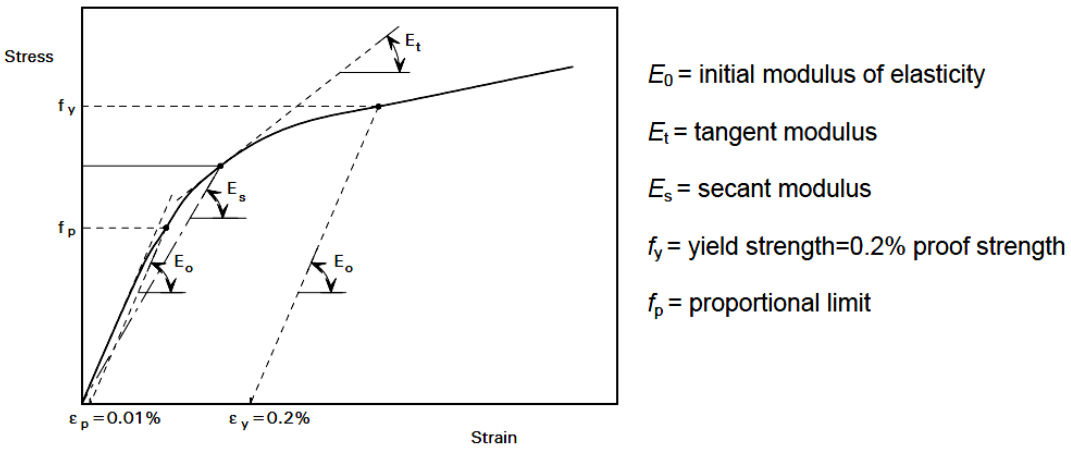

Figure 1.5 *Basic parameters used for the stress-strain diagram of stainless steel description* [6]

If stainless steel is cold-worked, it exhibits different mechanical properties in tension and compression, known as non-symmetry in stress-strain behaviour. Stainless steel also tends to demonstrate anisotropy in respect to the rolling direction (see Figure 1.6).

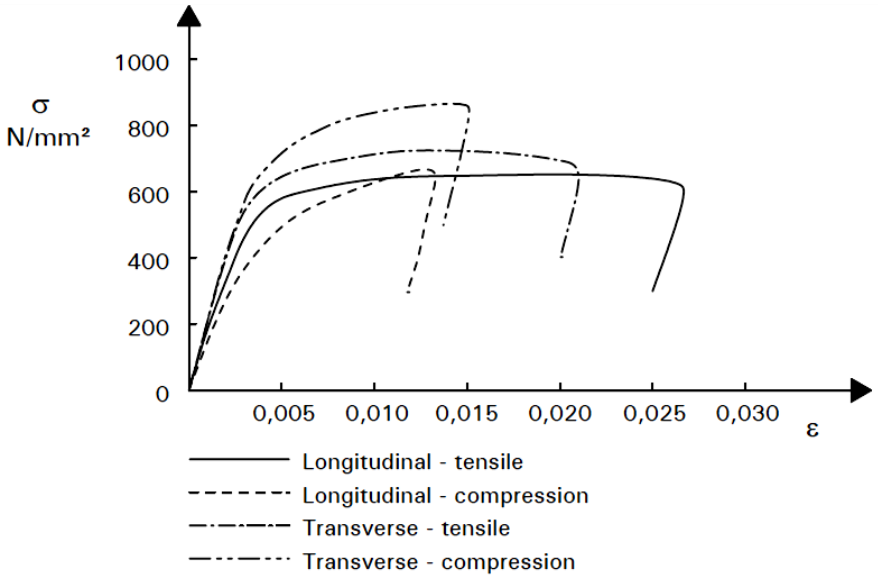

Figure 1.6 *Typical stress-strain diagram for cold-worked stainless steel 1.4318, level C850* [5]

In terms of stress-strain non-symmetry Shu et al. [7] observed within RHS and SHS testing that the proof strength $\sigma_{0.2}$ of the coupon made of the flat part in tension is slightly higher than the proof strength $\sigma_{0.2}$ of the coupon in compression. Executed tests for flat parts proved that the non-linearity parameter n is lower in tension than in compression. But differences for low levels of cold-working may be small, hence we can usually consider the values of $\sigma_{0.2}$ and non-linearity parameter n (see section 3.2) the same for tension and for compression. Also the value of initial modulus of elasticity was measured the same both for tension and compression.

Rossi et. al [8] analysed and compared available data of the 0.2% proof strength for tension and compression (see Figure 1.7). Results show 5% decrease for compression in comparison with tension in cold formed material.

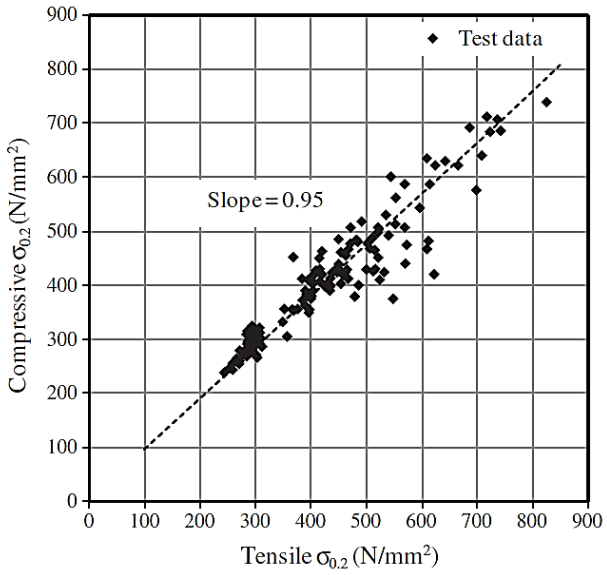

Figure 1.7 *Observed relationship between compressive and tensile proof strength* [8]

Numerical simulations performed at University of Sydney [9] proved negligible impact of anisotropy for common structural elements with difference of ultimate strength lower than 1% within elastic-plastic material model consideration.

It should be noted anisotropy increases with a level of cold-working (see section 4.3). If higher level of plastic deformation in one direction is induced the higher difference between strain hardening in the same and the transverse direction will be pronounced. Enhanced 0.2% proof strength is higher in the direction of original plastic deformation than in the transverse direction. Hence, where there is no dominant direction of loading the nominal value of the strength in transverse direction should be used in design as the safe value.

1.5 Cold - forming

In cold-formed sections plastic deformation occurs during the fabrication process, that increases the yield strength and ultimate tensile strength [2], but decreases ductility (see Figure 1.8). This increase is partially caused due to transformation of austenite to martensite. The transformation process is dependent on the forming rate and material temperature during forming process. The low the temperature induced the higher content of martensite will occur. Strength increase is dependent on alloying elements, especially on nickel and chromium content.

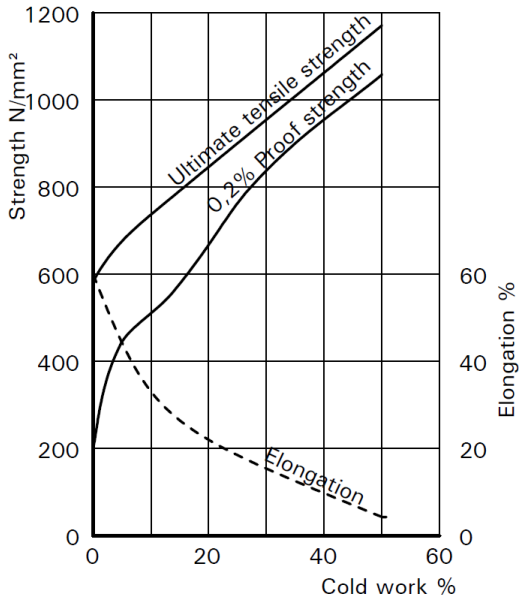

Figure 1.8 *Cold forming effect* [2]

1.6 Plastic deformation and plasticity

Plastic deformation of structural element means permanent deformation remaining after unloading. It occurs, when material under load exceeds yield point or yield surface in the stress space (in fact the proportional limit). The simplest model of the stress space consists of elastic stress state and plastic stress state.

For ductile materials such as metals, the simplest and most common material model of yield condition is von Mises criterion (see Figure 1.9). The material is assumed to be perfectly elastic-plastic (i.e. hardening caused by cold forming is not accounted for).

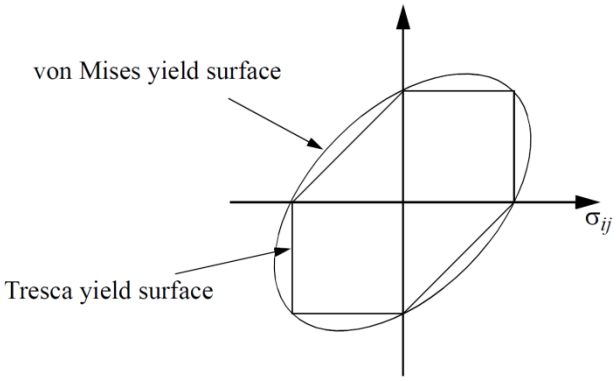

Figure 1.9 *Comparison of von Mises yield surface with Tresca yield surface* [10]

The simplest model describing strength increase is isotropic hardening. The new yield surface after particular hardening is affine in respect to the original one. The loading surfaces can be obtained from the form of the previous yield function by the different yield stress value (Figure 1.10).

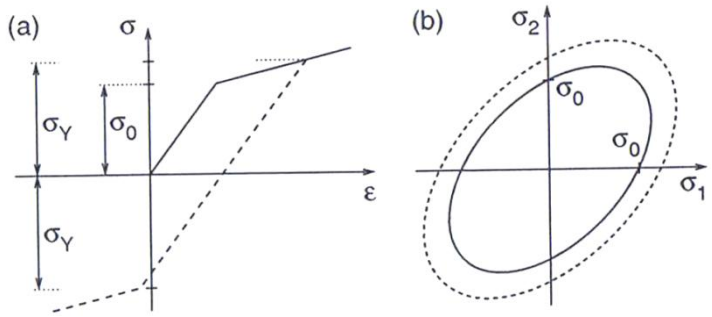

Figure 1.10 *a) uniaxial stress strain diagram, b) evolution of the yield surface in the biaxial stress plane* [11]

This model does not involve the Bauschinger effect. In case when the material is preloaded into the plastic range in one direction and then reloaded in another direction, Bauschinger effect (i.e. the different yield values for different axis due to internal or residual stresses and dislocations structures) occurs. A model affecting this behaviour is called kinematic hardening. The current loading surface is assumed not to expand, but to move as a unit as it is introduced in Figure 1.11.

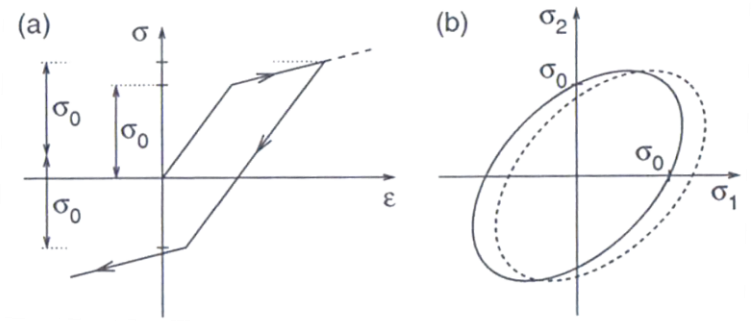

Figure 1.11 *a) uniaxial stress strain diagram, b) evolution of the yield surface in the biaxial stress plane* [11]

However, the kinematic hardening is not even in agreement with the real material response (see Figure 1.12). Hence, advanced multiple surface models for stainless steel respecting hardening, Bauschinger effect, different plastic moduli were proposed by Granlund[12] or Olsson[13].

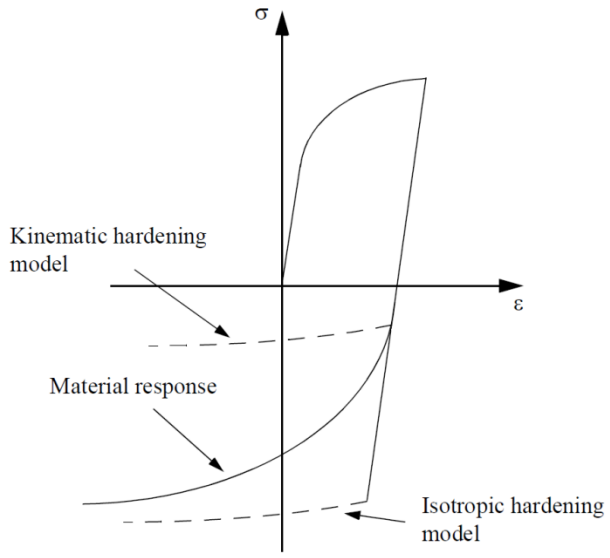

Figure 1.12 *Comparison of material response with simple models* [10]

Fabrication routes involve more complex processing of the material than simple uniaxial loading and hardening. Structural section fabricating consists of coiling, bending and other steps. That makes the stress and strain state very complicated and difficult to describe.

For instance, practical description of stress distribution and neutral surface location in sheet bend after plastic deformation induction was set out by Hill [14].

Chapter 2

Thesis objectives and thesis outline

The recent formulas or suggestions don´t involve all possibilities and ranges of the cold-forming and determine only a few material properties. They particularly contain methods for the specification of the yield strength especially in corner areas and flat parts of sections. In addition these methods are limited in use as they concern specific bending methods and steel grades. In civil engineering, sections bent in different angles, CHS, RHS or oval sections made of different steel grades are often used. Different bending processes have been recently concerned by Rossi et al. with sophisticated finite element modelling [15].

Demands of more efficient use of high cost materials require constant research efforts to establish new progressive and safe methods that can satisfy them. In case of stainless steel various materials offer wide field for enhancing of current relationships. Considering the high degree of the cold-forming in most of the stainless steel sections, it would be very favourable to employ the enhancing effect into calculations. That leads to the significant precision and effectiveness in member design. For members subjected to tension it implies strong increase of resistance, however for buckling mode there is possible resistance decrease (related to the enhanced tensile resistance) due to the higher proportion of the non-linearity.

The research covers the basic austenitic, duplex, ferritic and also lean duplex stainless steel grades.

The main objective of the thesis is to contribute to determining of stress-strain response and fundamental mechanical properties for whole sections of cold-rolled hollow sections.

The aim of the research presented herein can be divided into 2 parts:

1) Experimental research including data collection
2) Analytical modelling of forming process

1) Experimental research including data collection

The aim was to establish experimental data for further use in advanced material modelling in terms of stress-strain response of the main stainless steel families. The various proportion of the plastic strain was induced and measured at experimental patterns. Afterwards tensile tests of specimens were performed. Set of experiments was executed to record the most important mechanical properties of austenitic, ferritic and duplex grades. Both virgin and cold-worked samples serve for further evaluation of different cold-formed material modelling and as a base for use of enhanced structural stainless steel properties. Detailed description of the experimental programme is stated in the separate Chapter 4. Results obtained from the tests are supposed to be employed for an analytical model of stress-strain behaviour.

2) Analytical modelling of forming process

The thesis compares previously published relationships for enhanced mechanical properties with own conclusions stated in the thesis. It is focused on prediction of material properties such as the non-linearity degree of the stress-strain diagram or the ductility.

Gradually there is introduced an analytical description for a corner and a flat face of hollow sections. Finally, there is established a solution for the whole section stress-strain description based on the analytical models (see Chapter 5) describing stress-strain behaviour which might lead to more accurate structure design. The formulas determination for the cold-forming effect resulted from the analytical model was calibrated and verified by recent experimental data.

Conclusions of the presented experimental programme and material modelling may serve as a base for possible extension of the design standard EN 1993-1-4 [16].

Chapter 3

Literature review

3.1 Foreword

Stainless steel has been researched for several decades whilst cold-forming (resp. cold-working) effect on stainless steel has been researched for approximately 25 years and results of research have been utilized for only one design method (valid in Europe), which has been nowadays used in the National annex of British Standard EN 1993-1-4. There are several important research workplaces including e.g. Imperial College London, Hong Kong Polytechnic University, The University of Hong Kong, Polytechnic University of Catalonia, KU Leuven and University Liege. These institutions are considered to be major centres of stainless steel research.

This chapter summarizes recent relationships, approaches and data related to stainless steel mechanical properties. Especially, there are mentioned stress-strain models with methods for determination of enhanced strength in corners and flat faces of rectangular hollow sections. The chapter compares codified mechanical properties for stainless steel according to different design standards as well.

3.2 Stress – strain diagram description

J.L. Holmquist and A. Nadai [17] in 1939 investigated plastic collapse of tubes under external pressure. It was found that the resistance to collapse depends on the shape of the stress-strain curve. Because of different kind of materials (such as carbon steel, stainless steel or even brass) not all pronouncing a well-defined yield point a new stress-strain function was used [17]:

$$\varepsilon = \frac{\sigma}{E_0} \qquad \sigma \leq \sigma_p \tag{3.1}$$

$$\varepsilon = \frac{\sigma}{E_0} + \varepsilon_y \left(\frac{\sigma - \sigma_p}{\sigma_y - \sigma_p} \right)^n \qquad \sigma > \sigma_p \tag{3.2}$$

where ε_y denotes plastic strain at yield strength σ_y, σ_p – proportional limit, E_0 – Young´s modulus, n – nonlinearity parameter.

Later Ramberg and Osgood [18] in 1943 contributed to the research of the stainless steel stress-strain behaviour. They published the three-parameters expression for the stress-strain diagram of chrome-nickel, aluminium alloy and carbon steel, which idealised notation related to 0.2% plastic strain of elongation was obtained as:

$$\varepsilon = \frac{\sigma}{E_0} + K \left(\frac{\sigma}{E_0} \right)^n \tag{3.3}$$

The expression was modified one year later by Hill [19] in following equation:

$$\varepsilon = \frac{\sigma}{E_0} + c \left(\frac{\sigma}{R_p} \right)^n \tag{3.4}$$

where R_p denotes proof strength and c corresponding plastic strain.

Thus, the formula (for generally adopted 0.2% proof strength) is given by:

$$\varepsilon = \frac{\sigma}{E_0} + 0.002 \left(\frac{\sigma}{\sigma_{0.2}} \right)^n \tag{3.5}$$

where the Ramber-Osgood parameter n defining the strain-hardening nonlinearity is in the form:

$$n = \frac{\ln(\varepsilon_{p2}/\varepsilon_{p1})}{\ln(\sigma_2/\sigma_1)} = \frac{\ln(20)}{\ln(\sigma_{0.2}/\sigma_{0.01})} \tag{3.6}$$

σ_2, σ_1 are stresses for two points on the stress-strain diagram ($\sigma_2 > \sigma_1$) and ε_{p2}, ε_{p1} corresponding plastic strain.

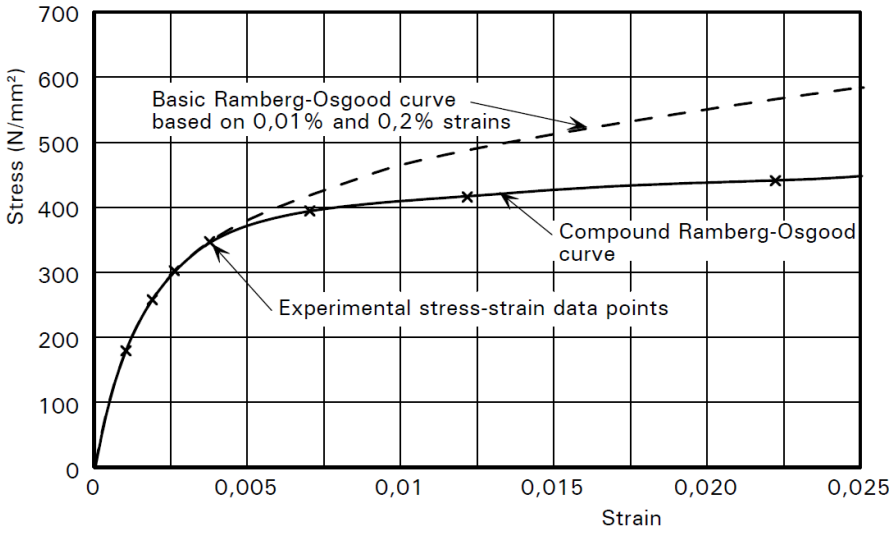

Figure 3.1 *Comparison of the Ramberg-Osgood model with the compound R-O model (and a test of a specimen)* [2]

Figure 3.1 shows, that the R-O model doesn´t sufficiently fit the stress-strain behaviour of stainless steel for stress over the yield (proof) strength. In 2000, Mirambell and Real [20] proposed a model using the R-O expression until the 0.2 % plastic strain limit, but the further description of the behaviour is in the form:

$$\varepsilon = \frac{(\sigma - \sigma_{0.2})}{E_{0.2}} + \varepsilon_{pu}\left(\frac{\sigma - \sigma_{0.2}}{\sigma_u - \sigma_{0.2}}\right)^m + \varepsilon_{ty} \qquad \sigma \geq \sigma_{0.2} \tag{3.7}$$

where $E_{0.2}$ is the tangent modulus at the proof strength $\sigma_{0.2}$, ε_{pu} the strain at the ultimate strength, ε_{ty} the plastic strain at the proof strength, σ_u the ultimate strength and n is the parameter of nonlinearity obtained as:

$$m = 1 + 3.5\,\frac{\sigma_{0,2}}{\sigma_u} \tag{3.8}$$

Annex C of the European standard EN 1993-1-4 contains this expression, with a little adjustment, as an appropriate model for finite elements method analyses. Nevertheless this formulation indicates different values of the strain ε at the ultimate strength σ_u. Gardner and Nethercot [21] in 2004 modified the Mirambell-Real´s expression and defined the new one by the following formula:

$$\varepsilon = \frac{(\sigma - \sigma_{0.2})}{E_{0.2}} + \left(0.008 - \frac{\sigma_{1.0} - \sigma_{0.2}}{E_{0.2}}\right)\left(\frac{\sigma - \sigma_{0.2}}{\sigma_{1.0} - \sigma_{0.2}}\right)^{n'_{0.2,1.0}} + \varepsilon_{t0,2} \tag{3.9}$$

where $E_{0.2}$ is the tangent modulus at $\sigma_{0.2}$, $\sigma_{1.0}$ is the 1.0% proof strength, $\varepsilon_{t0.2}$ the strain at the proof strength $\sigma_{0.2}$, $n'_{0.2,1.0}$ the parameter of nonlinearity for the second stage.

In 2000, MacDonald, Rhodes and Taylor [22] published the stress-strain curve based on the different mathematical basis in the following form:

$$\varepsilon = \frac{\sigma}{E_0} + 0.002 \left(\frac{\sigma}{\sigma_1}\right)^{\left(i+j\left(\frac{\sigma}{\sigma_1}\right)^k\right)} \tag{3.10}$$

where i, j and k are constants set from the stress-strain diagram in the range from 2.5 to 6 depending on the material thickness. Stress $\sigma_1 = \sigma_{0.2}$. The expression was established for only one steel grade (1.4301), particularly for one thickness of cold-formed channel. It indicated an excellent agreement between the model and tested samples.

Rassmusen [23] modified a Mirambell-Real´s model based on the Ramberg-Osgood diagram, which requires only three essential parameters (E_0, $\sigma_{0.2}$ and n, where E_0 is the initial modulus). Another two parameters can be determined using the equation:

$$\frac{\sigma_{0.2}}{\sigma_u} = 0.2 + 185e \tag{3.11}$$ for austenitic and duplex alloys

$$\frac{\sigma_{0.2}}{\sigma_u} = \frac{0.2 + 185e}{1\text{-}0.0375(n\text{-}5)} \tag{3.12}$$ for all alloys

where $$e = \frac{\sigma_{0.2}}{E_0} \tag{3.13}$$

Then, the full-range stress-strain curve can be described as follows:

$$\varepsilon = \frac{\sigma}{E_0} + 0.002 \left(\frac{\sigma}{\sigma_{0.2}}\right)^n \quad \text{for } \sigma \leq \sigma_{0,2} \tag{3.14}$$

$$\bar{\varepsilon} = \frac{\bar{\sigma}}{E_{0.2}} + \bar{\varepsilon}_{u_p} \left(\frac{\bar{\sigma}}{\bar{\sigma}_u}\right)^m \quad \text{for } \sigma > \sigma_{0,2} \tag{3.15}$$

$\bar{\varepsilon} = \varepsilon - \varepsilon_{0.2}$ (3.16) $\bar{\sigma} = \sigma - \sigma_{0.2}$ (3.17) $\bar{\sigma}_u = \sigma_u - \sigma_{0.2}$ (3.18)

$\bar{\varepsilon}_{u_p} \approx \varepsilon_u$ (3.19) $m = 1 + 3.5 \frac{\sigma_{0.2}}{\sigma_u}$ (3.20)

$\varepsilon_u = 1 - \frac{\sigma_{0.2}}{\sigma_u}$ (3.21) $E_{0.2} = \frac{E_0}{1 + 0.002 n E_0 / \sigma_{0.2}}$ (3.22)

This curve is more appropriate for description of a whole stress-strain diagram than the one-stage R-O expression and requires knowledge of only design code defined parameters (see Figure 3.2 and Figure 3.3).

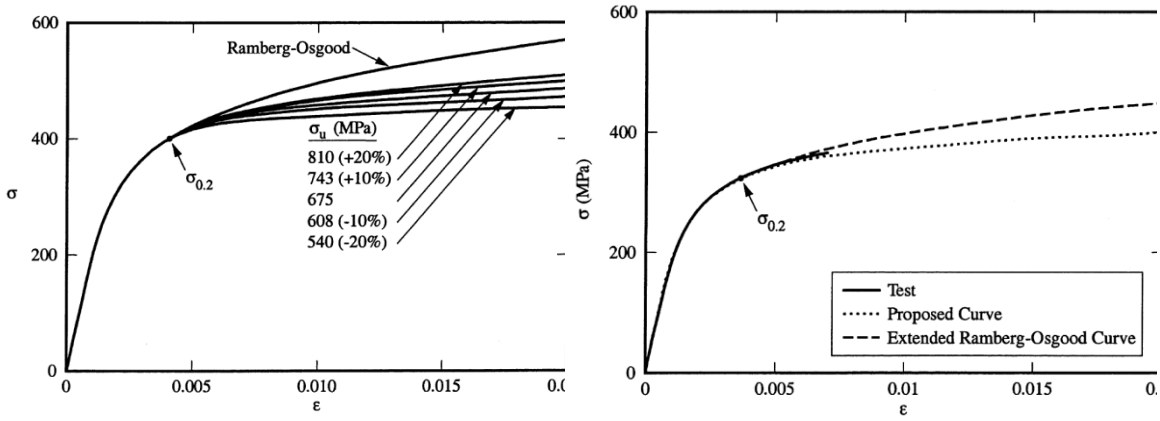

Figure 3.2 *Comparison of the R-O model, tested specimen and the Rasmussen´s expression of the stress-strain curve depending on the ultimate strength* σ_u [23]

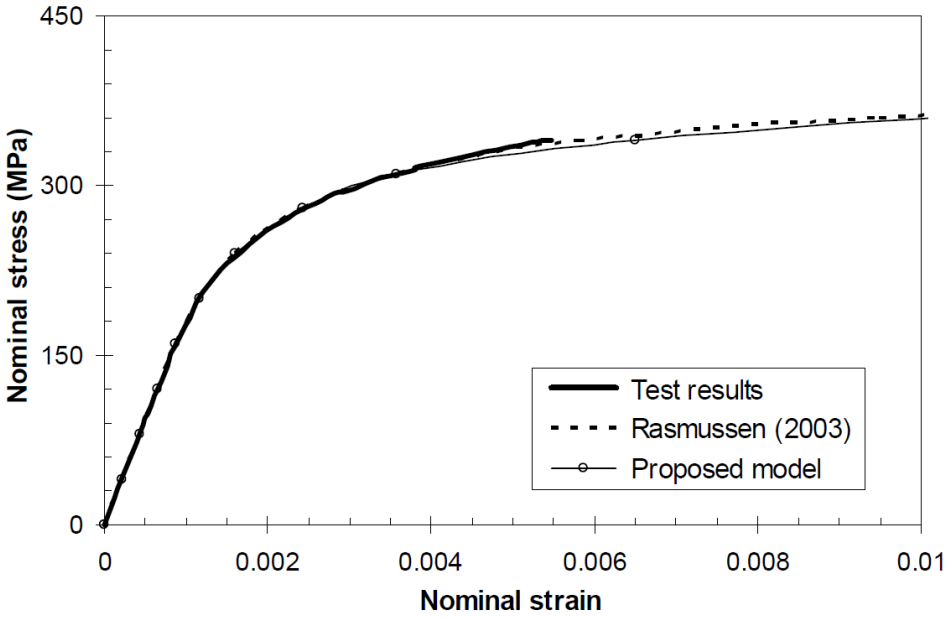

Figure 3.3 *Nominal stress-strain curves for the longitudinal tension, coupon cut out from the ferritic stainless steel plate tested by Korvink et al.* [24] *with comparison of the Rasmussen model.* [25]

Three-stage stress-strain model for both tensile and compressive strains was published in 2005 by Quach [25]. The model is more accurate and uses the Ramberg-Osgood formula for strains up to 0.2% plastic limit. Behind this limit the relationship based on the Gardner-Nethercot description for plastic strain up to 2% is used and for higher strains it assumes that the curve is a straight line passing through the 2% proof strength $\sigma_{2.0}$ and the ultimate strength σ_u.

Full description of the model is given by following formulas: In Eq. (3.25) the upper sign denotes tension; the lower sign is related to compression.

$$\varepsilon = \frac{\sigma}{E_0} + 0.002 \left(\frac{\sigma}{\sigma_{0.2}} \right)^n \qquad \sigma \leq \sigma_{0.2} \qquad (3.23)$$

$$\varepsilon = \frac{(\sigma - \sigma_{0.2})}{E_{0.2}} + \left[0.008 + (\sigma_{1.0} - \sigma_{0.2}) \left(\frac{1}{E_0} - \frac{1}{E_{0.2}} \right) \right] \left(\frac{\sigma - \sigma_{0.2}}{\sigma_{1.0} - \sigma_{0.2}} \right)^{n'_{0.2,1.0}} + \varepsilon_{t0.2} \qquad \sigma_{0.2} < \sigma \leq \sigma_{2.0} \qquad (3.24)$$

$$\varepsilon = \frac{\sigma - a}{b \mp \sigma} \qquad \sigma > \sigma_{2.0} \qquad (3.25)$$

$$a = \sigma_{2.0}(1 \pm \varepsilon_{2.0}) - b\varepsilon_{t0.2} \qquad (3.26)$$

$$b = \frac{\sigma_u(1 \pm \varepsilon_u) - \sigma_{2.0}(1 \pm \varepsilon_{2.0})}{\varepsilon_u - \varepsilon_{2.0}} \qquad (3.27)$$

with $$\varepsilon_{2.0} = \frac{\sigma_{2.0}}{E_0} + 0.02 \qquad (3.28)$$

and $$\sigma_{2.0} = \frac{1 + \left(\frac{\sigma_{1.0}}{\sigma_{0.2}} - 1 \right) A^{1/n'_{0.2,1.0}}}{1 + \frac{\sigma_{2.0}}{E_0} \left(\frac{E_0}{E_{0.2}} - 1 \right) \left(\frac{\sigma_{1.0}}{\sigma_{0.2}} - 1 \right) \frac{A^{1/n'_{0.2,1.0}}}{n'_{0.2,1.0} B}} \sigma_{0.2} \qquad (3.29)$$

Another model for explicit establishment of stress depending on strain was proposed by Abdella [26] in 2006 as a power law formula with exponent p:

$$\sigma = \frac{r\sigma_{0.2}\varepsilon/\varepsilon_{0.2}}{1 + (r-1)/(\varepsilon/\varepsilon_{0.2})^p} \qquad \varepsilon \leq \varepsilon_{0.2} \qquad (3.30)$$

$$\sigma = \sigma_{0.2} + \frac{r_2\sigma_{0.2}(\varepsilon/\varepsilon_{0.2} - 1)}{1 + (r^* - 1)\left(\frac{\varepsilon/\varepsilon_{0.2} - 1}{\varepsilon_u/\varepsilon_{0.2} - 1} \right)^{p^*}} \qquad \varepsilon > \varepsilon_{0.2} \qquad (3.31)$$

where the factors p, p^*, r, r^* and r_2 are calculated from the original model parameters E_0, $E_{0.2}$, $\sigma_{0.2}$, σ_u, $\varepsilon_{0.2}$, ε_u, n and m.

Later Arrayago, I., Real, E. & Mirambell, E. [27] in 2013 summarized modifications for EN 1993-1-4 as follows:

$$n = \frac{\ln(4)}{\ln\left(\frac{\sigma_{0.2}}{\sigma_{0.05}} \right)} \qquad (3.32)$$

$$m = 1 + 2.3 \frac{\sigma_{0.2}}{\sigma_u} \qquad \text{for austenitic} \qquad (3.33)$$

$$m = 1 + \frac{\sigma_{0.2}}{\sigma_u} \qquad \text{for ferritic} \qquad (3.34)$$

$$\frac{\sigma_{0.2}}{\sigma_{\mathrm{u}}} = 0.46+145\frac{\sigma_{0.2}}{E_0} \qquad \text{for ferritic} \qquad (3.35)$$

A generalized multistage model was presented by Hradil, Talja, Real, Mirambell and Rossi [28] in order to increase the accuracy of the material curve representation in 2013. It uses the Mirambell and Real´s concept to achieve a simple multistage form. For basic application and structural computations there was proposed three stages model for non-linear metallic materials.

$$\varepsilon = \frac{\sigma}{E_0}+0.002\left(\frac{\sigma}{\sigma_{0.2}}\right)^{n_{0\text{-}0.2}} \qquad \sigma \le \sigma_{0.2} \qquad (3.36)$$

$$\varepsilon = \frac{\sigma\text{-}\sigma_{0.2}}{E_{0.2}}+\varepsilon^{*}_{0.2}\left(\frac{\sigma\text{-}\sigma_{0.2}}{\sigma_{1.0}\text{-}\sigma_{0.2}}\right)^{n_{0.2\text{-}1.0}}+0.002+\frac{\sigma_{0.2}}{E_0} \qquad \sigma_{0.2} < \sigma \le \sigma_{1.0} \qquad (3.37)$$

$$\varepsilon = \frac{\sigma\text{-}\sigma_{1.0}}{E_{1.0}}+\varepsilon^{*}_{1.0}\left(\frac{\sigma\text{-}\sigma_{1.0}}{\sigma_{\mathrm{u}}\text{-}\sigma_{1.0}}\right)^{n_{1.0\text{-u}}}+0.01+\frac{\sigma_{1.0}}{E_0} \qquad \sigma_{1.0} < \sigma \le \sigma_{\mathrm{u}} \qquad (3.38)$$

where $$E_{0.2} = \frac{E_0}{1+0.002n(E_0/\sigma_{0.2})} \qquad (3.39)$$

$$E_{1.0} = \frac{E_{0.2}}{1+\varepsilon^{*}_{0,2}\, n_{0.2\text{-}1.0}(E_{0.2}/(\sigma_{1.0}-\sigma_{0.2}))} \qquad (3.40)$$

$$\varepsilon^{*}_{0.2} = 0.008\text{-}(\sigma_{1.0}\text{-}\sigma_{0.2})\left(\frac{1}{E_{0.2}}\text{-}\frac{1}{E_0}\right) \qquad (3.41)$$

$$\varepsilon^{*}_{1.0} = \left(\varepsilon^{\mathrm{pl}}_{\mathrm{u}}\text{-}0.01\right)\text{-}(\sigma_{\mathrm{u}}\text{-}\sigma_{1.0})\left(\frac{1}{E_{1.0}}\text{-}\frac{1}{E_0}\right) \qquad (3.42)$$

Currently, most of the stainless steel structures are made of austenitic and ferritic stainless steel. However, the lean duplex stainless steel has been developed and becoming an attractive choice for application in civil engineering due to its superior mechanical performance, comparable corrosion resistance to austenitic stainless steel and lower cost because of decreased Nickel content. Huang and Young investigated the lean duplex stainless steel material of 1.4162 (LDX2101) grade with the Nickel content around 1.5% [29]. Tensile tests results of samples made of RHS are shown in Figure 3.4 and Figure 3.5.

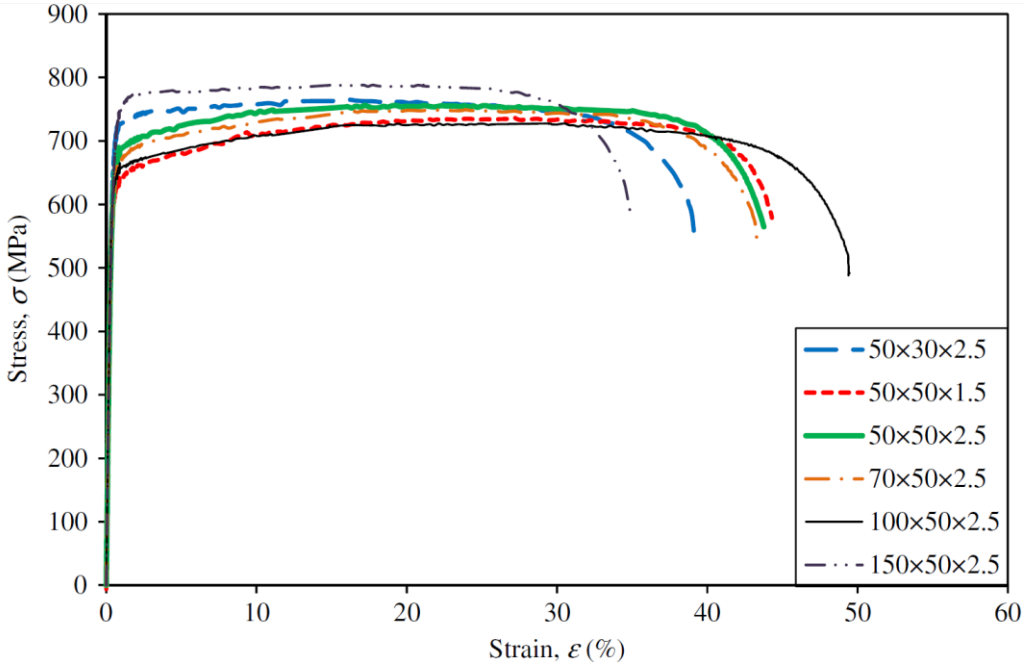

Figure 3.4 *Static stress–strain curves obtained from tensile coupon tests of flat portions cut out from RHS* [29].

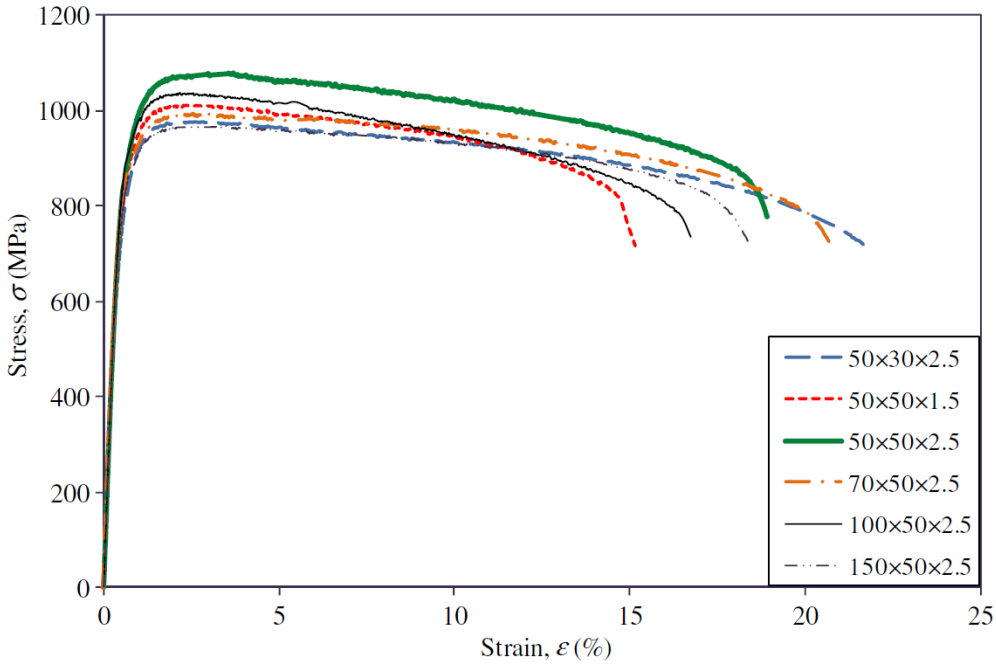

Figure 3.5 *Static stress–strain curves obtained from tensile coupon tests of corners cut out from RHS* [29].

Xing-Qiang Wang et al. [30] made a modification of the Rasmussen´s model and used a new formula for stress-strain description of RHS corners in 2014. Differences between the stress-strain behaviour of the flat material and the corner are shown in Figure 3.6. Hence, a different material model is required.

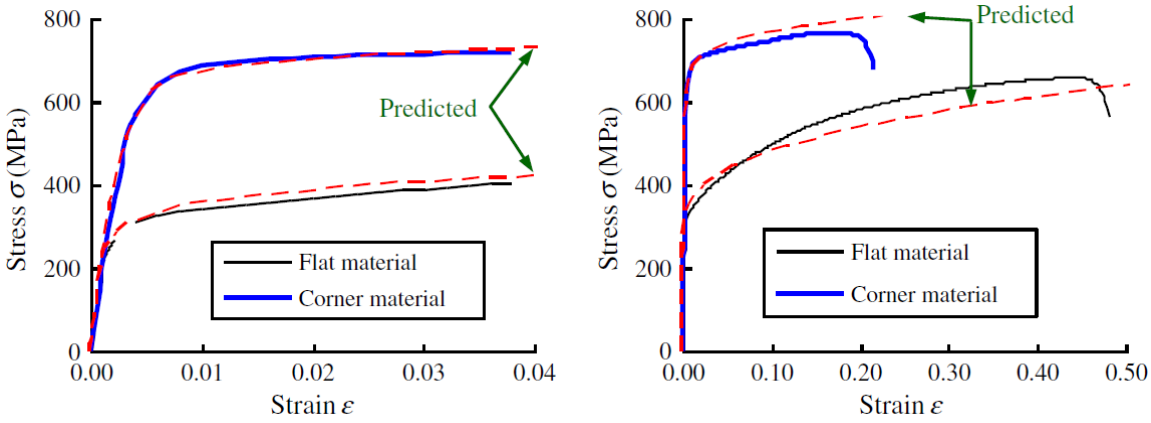

Figure 3.6 *Stress-strain curves of flat and corner regions prepared from the stainless steel RHS* [30].

Stress-strain response of a corner is given by analogy of the Rasmussen´s formula (subscript c means a corner property):

$$\varepsilon = \frac{\sigma}{E_{0,c}} + 0.002\left(\frac{\sigma}{\sigma_{0.2,c}}\right)^{n_c} \qquad \sigma \le \sigma_{0.2,c} \tag{3.43}$$

$$\varepsilon = 0.002 + \frac{\sigma_{0.2,c}}{E_{0,c}} + \frac{\sigma - \sigma_{0.2,c}}{E_{0.2,c}} + \varepsilon_{u,c}\left(\frac{\sigma - \sigma_{0.2,c}}{\sigma_{u,c} - \sigma_{0.2,c}}\right)^{m_c} \qquad \sigma_{0.2} < \sigma \le \sigma_{u,c} \tag{3.44}$$

where $$E_{0.2,c} = \frac{E_{0,c}}{1 + 0.002 n_c E_{0,c}/\sigma_{0.2,c}} \tag{3.45}$$

$$n_c = 0.9 n^2 e^{-0.3n} \tag{3.46}$$

$$m_c = 0.04\sigma_{0.2,c} - 8 \qquad \ge \mathrm{m} \tag{3.47}$$

$$\varepsilon_{u,c} = 1 - \frac{\sigma_{0.2,c}}{\sigma_{u,c}} \tag{3.48}$$

A more detailed approach of mechanical characteristics of steel exhibiting anisotropy and nonsymmetry under transverse and cyclic loading influence was performed by Olsson [13]. The conclusions were published in his doctoral thesis. There were undertaken many experiments with biaxial straining. Results of the tests proved that the stress-strain curve representing stress equilibrium in a higher strain range exhibit linear relation (see Figure 3.7). A rounded curve is utilized until the 2% strain limit. Then a linear function is employed similarly to the three stage model proposed by Quach. However difficult determination of particular constants (involving the anisotropy effect etc.) disables the use of this description in structural design practice. In addition, according to many studies the impact of anisotropy is not significant for the commonly used structural elements.

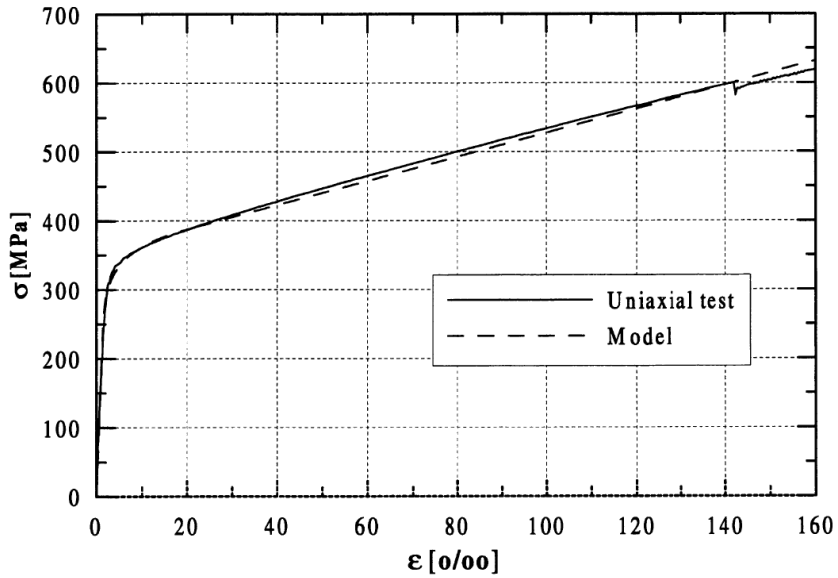

Figure 3.7 *Comparison of the Olsson´s model and the tested specimen of the 1.4301 steel at uniaxial stress* [13].

The stress-strain behaviour can be also expressed in a very simple form. For modelling purposes a multilinear isotropic material model may serve as a default material description as it was used for numerical modelling solving the prestressed stainless steel stayed columns [31] depicted in Figure 3.8.

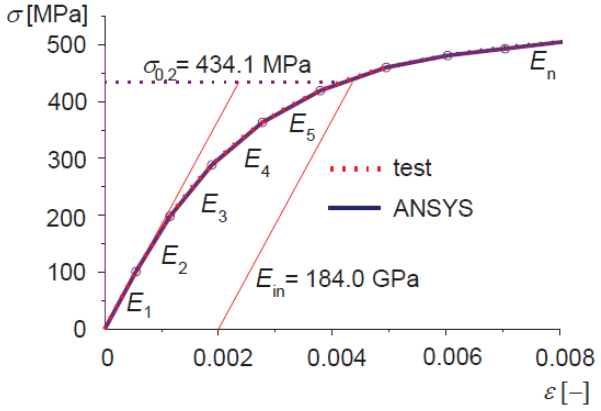

Figure 3.8 *Multilinear stress-strain model* [31].

3.3 Methods for the determination of enhanced strength after section cold-forming process

The first generally accepted model for the enhanced yield strength of carbon steel was established by Karren in 1967 [32]. The model provides a relation between the enhanced yield strength and the inner radius of a corner to the thickness ratio together with the original yield strength. It is suggested that since corner areas represent 5% - 30% of a cross sectional area, the influence of the enhanced strength should be involved in structural design.

$$f_{yc}=\frac{B_c}{(r_i/t)^m}f_{yv} \tag{3.49}$$

where

$$B_c=3.69\frac{f_{uv}}{f_{yv}}-0.819\left(\frac{f_{uv}}{f_{yv}}\right)^2-1.79 \tag{3.50}$$

$$m=0.192\frac{f_{uv}}{f_{yv}}-0.068 \tag{3.51}$$

f_{yc} – yield strength of corner material,
f_{yv} – yield strength of the virgin material,
f_{uc} – ultimate tensile strength of the virgin material,
r_i – inner bend radius,
t – sheet thickness.

Karren proved that the region of the increased strength overlaps the corner area by one or two wall thickness and the range depends on the method of cold-forming. The corner area means the region of the pure geometric corner extended by a part of the section wall. This area represents enhanced material properties as it is displayed in Figure 3.9.

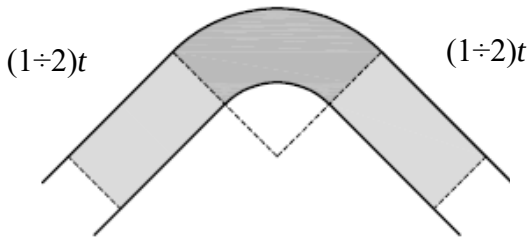

Figure 3.9 *Area of enhanced material properties.*

Belica [33] in 1969 tested press-braked sections (see Figure 3.10 and Figure 3.11). Distribution of enhanced mechanical properties is described in Figure 3.11; see another from 2008 performed by Cruise and Gardner [34] in Figure 3.12.

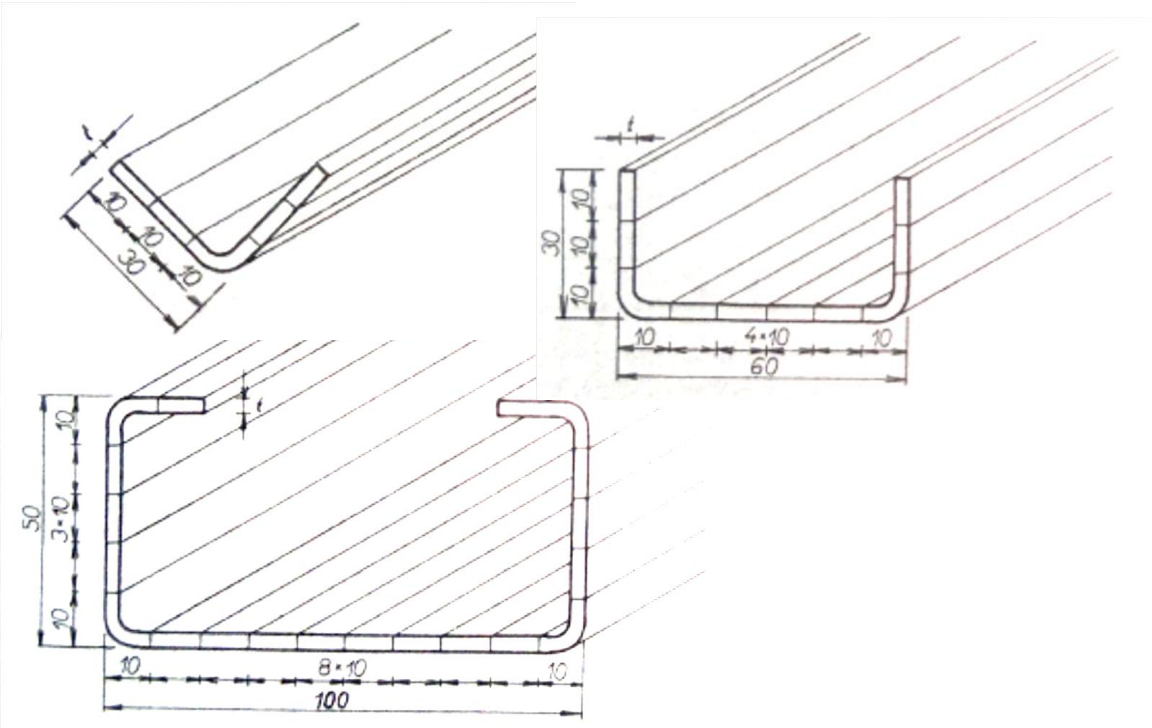

Figure 3.10 *Specimens tested by sectioning - press-braked cross-sections – angle L 30x4, channel 30x60x4, C 50x100x20* [33].

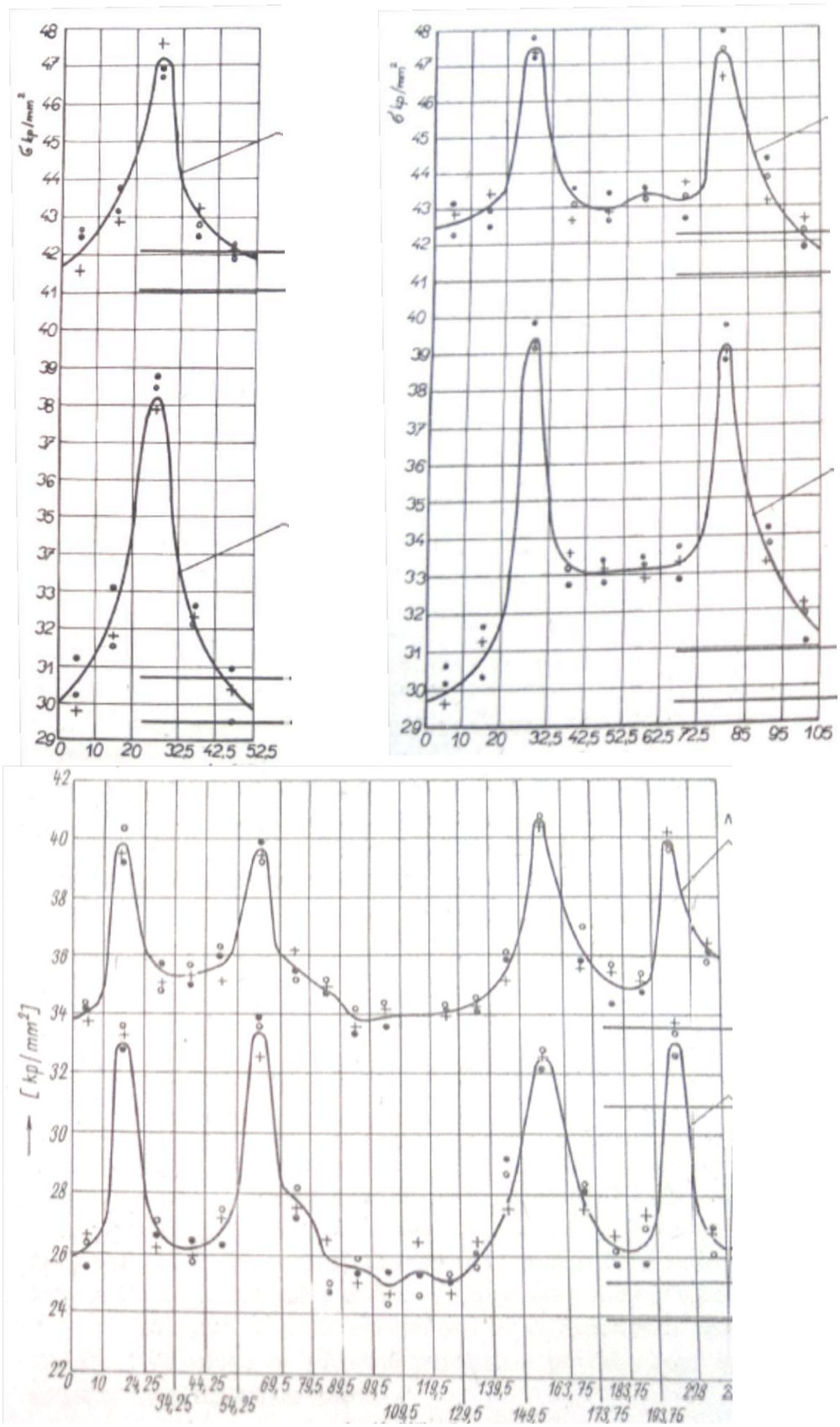

Figure 3.11 *Distribution of the yield and the ultimate tensile strength for the sections described in Figure 3.10* [33].

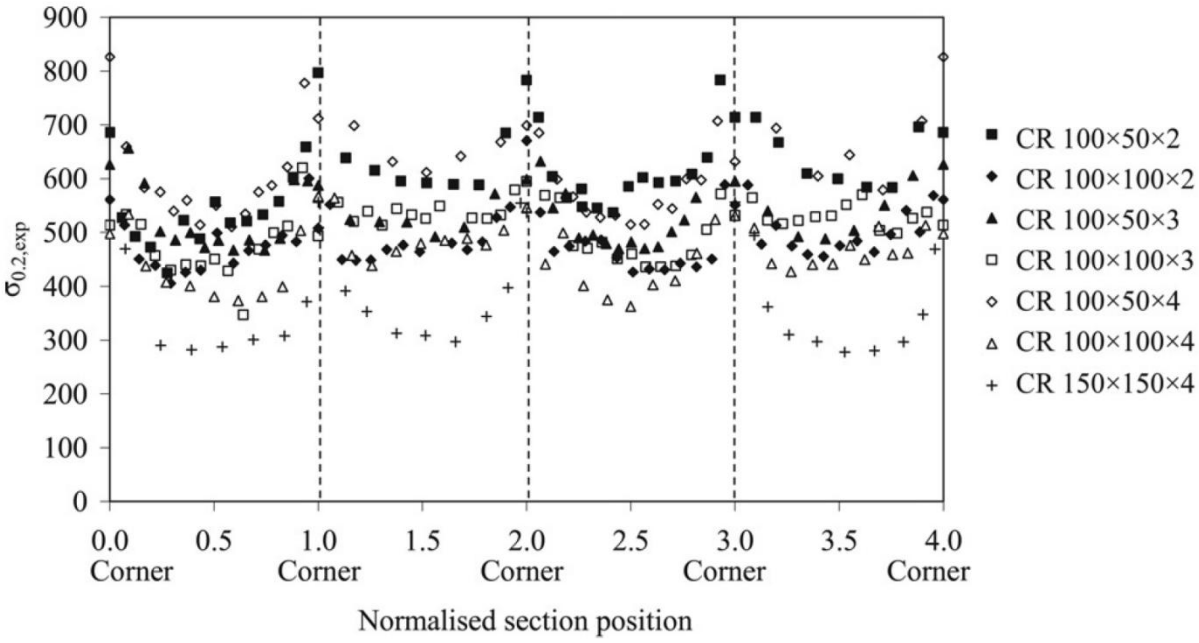

Figure 3.12 *The 0.2% proof strength for section flat faces and corners of stainless steel cold-rolled boxes* [34].

Consequently Karren and Winter (1967) suggested the relationship for the gross-sectional tensile yield strength f_{ya} for all cold formed sections as [35]:

$$f_{ya}=Cf_{yc}+(1-C)f_{yf} \tag{3.52}$$

where C is the ratio of corner area to the gross sectional area,
f_{yc} is the average tensile yield strength of corners cited above,
f_{yf} is the average tensile yield strength of flat parts, conservatively yield strength of the virgin material.

Compared to Karren and Winter recent European design standard EN 1993-1-3 [36] set the following formula for the yield strength of a cold-formed section made of carbon steel as:

$$f_{ya}=f_{yb}+\frac{knt^2}{A_g}\left(f_u-f_{yb}\right) \tag{3.53}$$, but $$f_{ya}\le\frac{f_u+f_{yb}}{2} \tag{3.54}$$

where f_{yb} is the nominal yield strength of the virgin material,
f_u is the nominal ultimate tensile strength ,
A_g is the cross-sectional area,
t is the sheet thickness before cold forming,
n is the number of 90° bends (bends with angles less than 90°, should be counted as a fractions of n),
k is the coefficient depending on a type of forming
= 7 for cold rolling
= 5 for other methods.

Abdel-Rahman and Sivakumaran [37] established the length of overlapping for press-braked carbon steel C cross-section as $\pi r_i/2$, where r_i is the inner corner radius. The yield strength for the corner region was determined as an average value of the higher yield strength in the corner area and the lower value of the yield strength in the overlapping. The increase varies from 13% to 16% in comparison with the measured yield strength outside of the corner region.

For stainless steel rectangular hollow sections Gardner and Nethercot (2004) determined the corner region based on numerical model correlation with experiments as the pure geometric corner area and the overlapping represented by the distance of double section thickness. There was also observed a linear relationship between the corner 0.2% proof strength and the flat face ultimate strength [38].

For stainless steel press-braked sections (according to Ashraf, Gardner and Nethercot [39]) the corner region is equal to the bend area extended by the dimension of only one thickness. From the research mentioned above global effect of enhanced mechanical properties in the corner area for rectangular hollow sections in compression is about 8% (without consideration of buckling). This increase refers to the section resistance involving the cold-forming effect also on flat parts.

Another extensive experimental research was published by Cruise [4]. Conclusions claimed the corner region is the bend area with two thicknesses overlapping at both sides for cold-rolled sections due to a set of narrow coupons tensile and hardness tests correlating to each other. However, for press-braked sections it was recommended to consider the corner region as only the bend area. Idealized distribution of the 0.2% proof strength is shown in Figure 3.13.

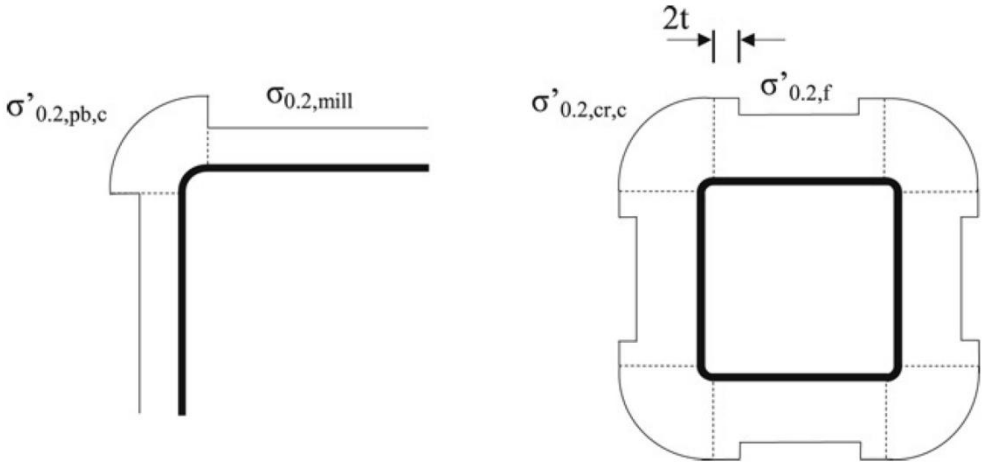

Figure 3.13 *Expected distribution of the 0.2% proof strength for a press-braked section and a cold-rolled box* [34].

Van den Berg and Van der Merwe [40] in 1992 made a comprehensive research of the corner properties of different stainless steel grades, i.e. 1.4301, 1.4512, 1.4016 and 1.4003. Samples with a various r_i/t ratios were press-braked for each of the four materials. The measured corner properties were then compared to the unformed material properties expressed by Karren's relationships. They established a new predictive equations for the corner 0.2% proof strength $\sigma_{0.2,c}$ estimation as:

$$\sigma_{0.2,c}=\frac{B_c\sigma_{0.2,v}}{\left(\frac{r_i}{t}\right)^m} \tag{3.55}$$

where $$B_c=3.289\left(\frac{\sigma_{u,v}}{\sigma_{0.2,v}}\right)-0.861\left(\frac{\sigma_{u,v}}{\sigma_{0.2,v}}\right)^2-1.34 \tag{3.56}$$

$$m=0.06\left(\frac{\sigma_{u,v}}{\sigma_{0.2,v}}\right)+0.031 \tag{3.57}$$

$\sigma_{0.2,v}$ is the 0.2% proof strength of the virgin material,
$\sigma_{u,v}$ is the ultimate strength of the virgin material.

In 2005, Ashraf et al. [41] provided a power model for stainless sections employing the 0.2% proof strength $\sigma_{0.2,v}$ or the ultimate strength $\sigma_{u,v}$ of the virgin material. The value of the enhanced corner proof strength $\sigma_{0.2,c}$ is given below:

$$\sigma_{0.2,c}=\frac{1.881}{(r_i/t)^{0.194}}\sigma_{0.2,v} \tag{3.58}$$

$$\sigma_{0.2,c}=\frac{C_1}{(r_i/t)^{C_2}}\sigma_{u,v} \tag{3.59}$$

where $$C_1=-0.382\frac{\sigma_{u,v}}{\sigma_{0.2,v}}+1.71 \tag{3.60}$$

$$C_2=0.176\frac{\sigma_{u,v}}{\sigma_{0.2,v}}-0.15 \tag{3.61}$$

The expression for relation between the corner proof strength and the section flat face ultimate strength $\sigma_{u,f}$ was also proposed as:

$$\sigma_{0.2,c}=0.85\sigma_{u,f} \tag{3.62}$$

The relationship (3.62) was previously proposed by Gardner in 2002 [42]:

The simple equation for the ultimate corner strength $\sigma_{u,c}$ was established from knowledge of only three properties by:

$$\sigma_{u,c}=0.75\sigma_{0.2,c}\left(\frac{\sigma_{u,v}}{\sigma_{0.2,v}}\right) \tag{3.63}$$

Cruise & Gardner [34] in 2008 modified previous expressions and proposed a new predictive model for the enhanced properties of austenitic stainless steel structural sections based on the experimental data set. The model covers corner regions and flat portions of a cross section. The formula employs the mill certificate 0.2% proof strength and dimensions of a rectangular hollow section. Nevertheless, the physical

interpretation doesn´t correspond to the factual behaviour because of the varying radius of the corner to thickness ratio.

$$\sigma_{0.2,f} = \frac{0.85\sigma_{0.2,mill}}{-0.19 + \frac{1}{12.45\left(\frac{\pi t}{2(B+D)}\right)+0.83}} \tag{3.64}$$

where $\sigma_{0.2,f}$ is the predicted enhanced 0.2% proof strength of the flat faces,
$\sigma_{0.2,mill}$ is the mill certificate 0.2% proof strength,
B and D are outer dimensions of a rectangular hollow section.

$$\sigma_{u,f} = \sigma_{u,mill}\left(0.19\frac{\sigma_{0.2,f}}{\sigma_{0.2,mill}} + 0.85\right) \tag{3.65}$$

where $\sigma_{u,f}$ is the predicted ultimate strength of faces of cold-rolled hollow sections,
$\sigma_{u,mill}$ is the mill certificate ultimate strength

$$\sigma_{0.2,pb,c} = \frac{1.673}{(r_i/t)^{0.126}}\sigma_{0.2,mill} \tag{3.66}$$

where $\sigma_{0.2,pb,c}$ is the predicted enhanced proof strength of press-braked corners

$$\sigma_{0.2,cr,c} = 0.83\sigma_{ult,f} \tag{3.67}$$

where $\sigma_{0.2,cr,c}$ is the predicted enhanced proof strength of cold-rolled hollow section corners

The corner value for the enhanced 0.2% proof strength set as 0.83 $\sigma_{ult,f}$ was obtained also in the stainless steel research aimed on residual stresses published by Jandera in his Ph.D. thesis [43].

The comparison with the experimental data from many researchers (Ashraf, Cruise, Gardner, Hyttinen, Talja et al.) provides good agreement of these models in higher ranges of r_i/t, more typical for press-braked sections.

For channel sections, an analytical model considering the influence of the fabrication process stages was proposed by Rossi and Jaspart [44] in 2010. There was used the finite element code METAFOR developed at the LTAS division of the University of Liege to simulate the cold-forming process of symmetric channel sections as it is shown in Figure 3.14 and Figure 3.15.

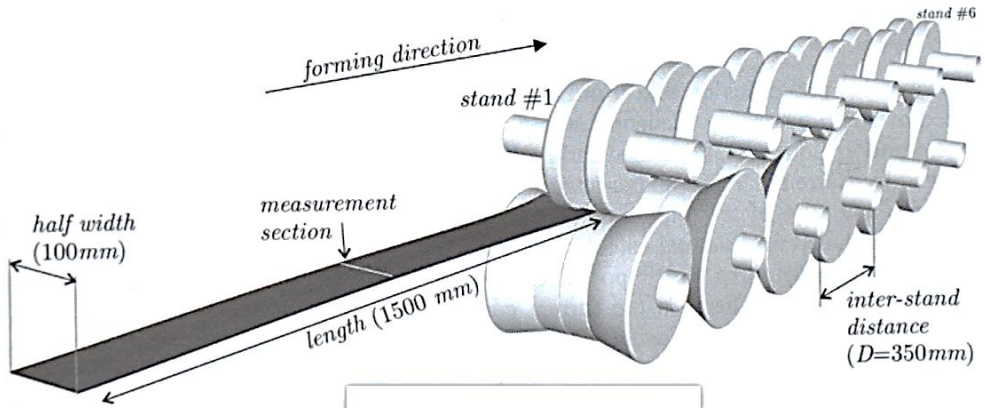

Figure 3.14 *Geometry of the forming line* [45].

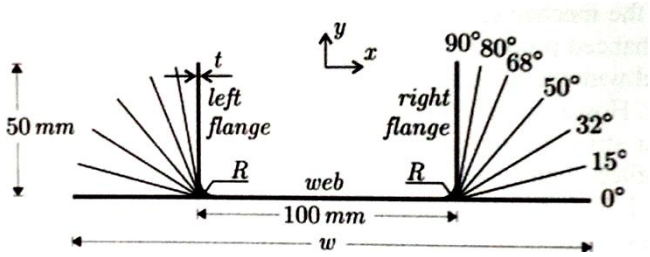

Figure 3.15 *Flow of channels fabrication process* [45].

Two different steels (ferritic stainless steel 1.4003 and high strength steel S 700 MC) were used for the cold-forming process simulation. Isotropic swift hardening laws which were used for modelling are plotted in Figure 3.16.

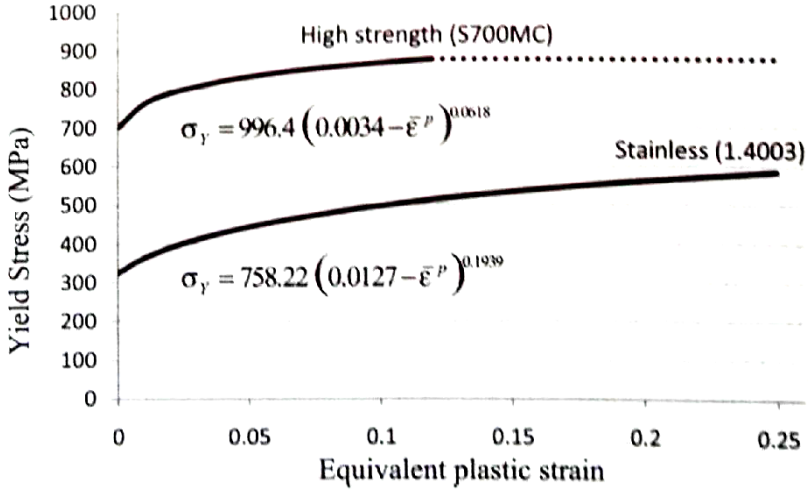

Figure 3.16 *Hardening laws of two different materials* [45].

Typically the mechanical properties enhancement is exhibited on cold-formed rectangular hollow sections, when the final shape is obtained by a few steps of cold-forming (see Figure 3.17).

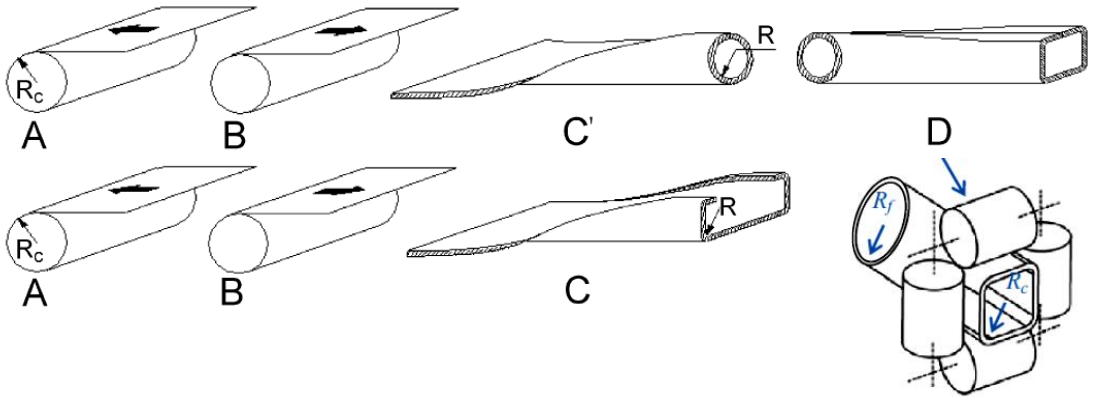

Figure 3.17 *Fabricating steps of cold-forming* [15].

In case of rectangular hollow sections the process can be divided into four steps, i.e. coiling-uncoiling (A+B), forming into a circular section and (C) and following deforming into a rectangular section (D).

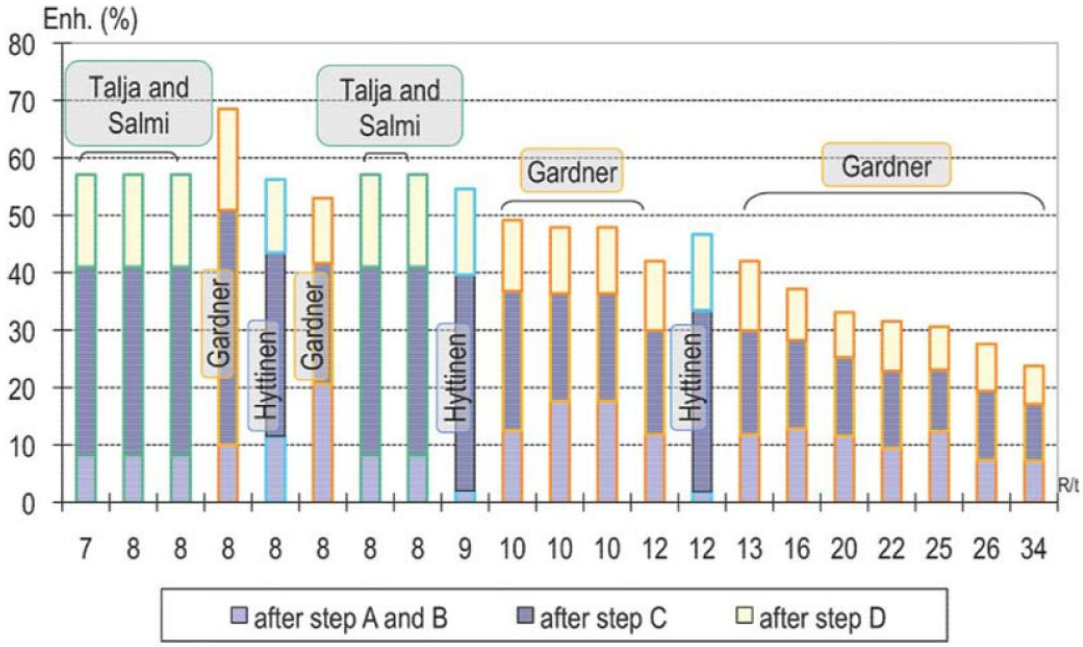

Figure 3.18 *Theoretical influence of fabricating steps on mechanical properties enhancement for rectangular hollow sections* [44].

According to the recent research, there is shown that even first steps of process (A+B) affect the enhancement (see Figure 3.18).

In 2011, Rossi, Boman and Degée [15] modified the predictive model for the strength increase of hollow sections depending on material properties $\sigma_{0.2,}$ σ_u and parameters included in the modified R-O expression for the stress-strain diagram published in recent research [23], resp. [20] and [46]. The new formulas are applicable for the radius to thickness ratio greater than 5 and for a different nonlinear material. For flats there is dominant impact of the forming into a circular section taken into account, for corner regions the last step of the process (the forming into a rectangular section) is decisive

(see Figure 3.18). As opposed to the Cruise´s model, this is generally applicable for materials with the nonlinear stress-strain behaviour (coefficients C_1, C_2, α depend on Ramberg – Osgood parameter n) as well as for open and hollow sections.

$$\frac{\sigma_u}{\sigma_{0.2,f\text{ or }c}-\sigma_{0.2}}=C_1\left(\frac{r_i}{t/2}\right)+C_2\left(\frac{r_i}{t/2}\right)^{\alpha} \tag{3.68}$$

where $\sigma_{0.2,f\text{ or }c}$ is the predicted enhanced proof strength of flat faces or corners of a cold-rolled hollow section,
r_i is the inner radius of a corner curvature or the circling radius for flat faces,
t is the thickness of the section wall.

$$C_1=\frac{\varepsilon_{0.2}\sigma_u}{r_2\sigma_{0.2}} \tag{3.69}$$

$$C_2=\frac{(r-1)\varepsilon_{0.2}\sigma_u}{r_2(\varepsilon_u-\varepsilon_{0.2})^p\sigma_{0.2}} \tag{3.70}$$

$$\alpha=(1-\dot{p}) \tag{3.71}$$

$$r=E_0\frac{\varepsilon_{0.2}}{\sigma_{0.2}} \tag{3.72}$$

$$r_2=E_{0.2}\frac{\varepsilon_{0.2}}{\sigma_{0.2}} \tag{3.73}$$

$$\dot{r}=E_{0.2}\frac{\varepsilon_u-\varepsilon_{0.2}}{\sigma_u-\sigma_{0.2}} \tag{3.74}$$

$$r_u=E_u\frac{\varepsilon_u-\varepsilon_{0.2}}{\sigma_u-\sigma_{0.2}} \tag{3.75}$$

$$p=r\frac{1-r_2}{r-1} \tag{3.76}$$

$$\dot{p}=\dot{r}\frac{1-r_u}{\dot{r}-1} \tag{3.77}$$

$$E_u=\frac{E_{0.2}}{1+(\dot{r}-1)m} \tag{3.78}$$

$$m=1+3.5\frac{\sigma_{0.2}}{\sigma_u} \tag{3.79}$$

Results obtained from the recent extensive investigations conducted by Rossi, Afshan and Gardner [47] and [8] in 2013 demonstrate also different values for basic material characteristics. The test programme was focused on cold-formed structural sections SHS, RHS and CHS and it contains results from 51 flat coupons, 28 corner coupons and 6 full section specimens. The results combined with measured data from other literature lead to amendments to the current design code EN 1993-1-4, especially for values of the model parameters n (Ramberg-Osgood nonlinear parameter) or the Young's modulus (initial modulus of elasticity) for commonly used stainless steel grades. Conclusions of experimental research show anticipated material parameters of nonlinearity n – the highest for ferric grades, intermediate for duplex grades and the lowest for austenitic grades. It is recommended considering the single value of Young's modulus as 195 GPa. Detailed information is displayed in Table 3.1 and Table 3.2.

Type	Grade	T/C	Table 8	Mean tensile values	EN 1993-1-4 [3]	AS/NZS 4673 [1]	SEI/ASCE-8 [2]
Austenitic	1.4301	T	5.6	5.6	6.0	7.5	8.3
		C	4.5		6.0	4.0	4.1
	1.4571	T	6.9		7.0	–	–
	1.4404	T	5.2		7.0	7.5	–
Ferritic	1.4003	T	8.4	7.9	7.0	9.0	–
		C	6.1		7.0	7.5	–
	1.4509	T	6.7		–	–	–
		C	6.3		–	–	–
Duplex	1.4462	T	6.5	7.2	5.0	5.5	–
Lean duplex	1.4162	T	7.3		–	–	–

Table 3.1 *Recommended and codified values of the R-O parameter n for stainless steel grades* [47].

The research points also slightly different R-O hardening exponent *n* depending on type of stainless steel, i.e. austenitic, ferritic, and duplex as opposed to the recent version of design code determining *n* according to steel grade and rolling direction.

Type	Grade	This study	EN 1993-1-4 [3]	AS/NZS 4673 [1]	SEI/ASCE-8 [2]
Austenitic	1.4301	192,000	200,000	195,000	193,000
	1.4571	191,000	200,000	–	–
	1.4404	195,000	200,000	195,000	–
Ferritic	1.4003	199,000	220,000	195,000	–
	1.4509	190,000	220,000	–	–
Duplex	1.4462	190,000	200,000	200,000	–
Lean duplex	1.4162	205,000	–	–	–

Table 3.2 *Recommended and codified values of the Young's modulus for stainless steel sections* [47].

In the study, a simple method for predicting the strength enhancement in cold-formed structural sections was presented depending on basic material and cross-sectional properties:

$$\sigma_{0.2,f,pred} = 0.85\left[p\left(\varepsilon_{f,av}+\varepsilon_{t,0.2}\right)^{q}\right] \quad \text{but} \le \sigma_{u,mill} \tag{3.80}$$

$$\sigma_{0.2,c,pred} = 0.85\left[p\left(\varepsilon_{c,av}+\varepsilon_{t,0.2}\right)^{q}\right] \quad \text{but} \le \sigma_{u,mill} \tag{3.81}$$

where $\sigma_{0.2,f,pred}$ is the predicted enhanced proof strength of the cold-rolled hollow section faces,

$\sigma_{0.2,c,pred}$ is the predicted enhanced proof strength of the cold-rolled hollow section corners,

$$\varepsilon_{f,av} = \left[(t/2)/R_{coiling}\right] + \left[(t/2)/R_{f}\right] \tag{3.82}$$

$$\varepsilon_{c,av} = 0.5\left[(t/2)/R_{c}\right] \tag{3.83}$$

$$R_f = \frac{b+h-2t}{\pi} \quad (3.84) \qquad R_c = r_i + t/2 \quad (3.85)$$

$$p = \frac{\sigma_{0.2,mill}}{\varepsilon_{t,0.2}^{q}} \quad (3.86) \qquad q = \frac{\ln\left(\sigma_{0.2,mill}/\sigma_{u,mill}\right)}{\ln\left(\varepsilon_{t,0.2}/\varepsilon_u\right)} \quad (3.87)$$

$$\varepsilon_{t,0.2} = 0.002 + \sigma_{0.2,mill}/E_0 \quad (3.88)$$

ε_u is the corresponding total strain at the $\sigma_{u,mill}$,
$R_{coiling}$ = 450 mm (average value recommended by Moen et al. [48]), for other parameters see Figure 3.19.

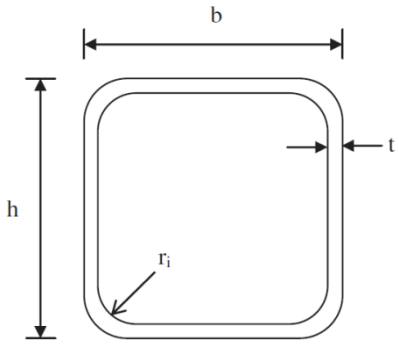

Figure 3.19 *Definition of parameters for SHS and RHS* [8].

Regarding strain at the ultimate tensile strength there was confirmed that the formula (in Annex C of EN 1993-1-4) given by Eq. (3.21) developed by Rasmussen [23] is valid and suitable for stainless steel. The correctness was proved on the basis of the collected data as it is shown in Figure 3.20.

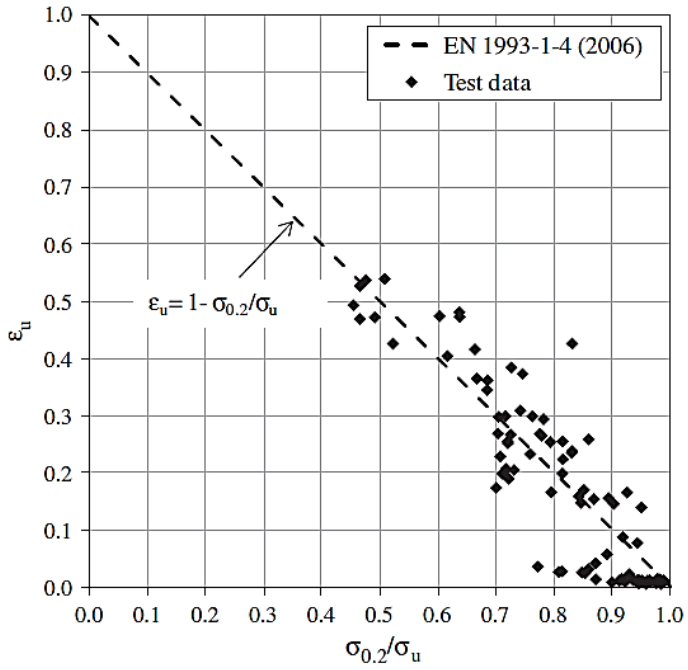

Figure 3.20 *Comparison of the predicted and measured strain* ε_u [47].

Thus the average enhanced cross-sectional 0.2% proof strength is obtained from following equations:

For press-braked sections:

$$\sigma_{0.2,\text{section}}=\frac{\left(\sigma_{0.2,\text{c,pred}}\,A_{\text{c,pb}}\right)+\left(\sigma_{0.2,\text{mill}}\left(A\text{-}A_{\text{c,pb}}\right)\right)}{A} \tag{3.89}$$

For cold-rolled sections:

$$\sigma_{0.2,\text{section}}=\frac{\left(\sigma_{0.2,\text{c,pred}}\,A_{\text{c,rolled}}\right)+\left(\sigma_{0.2,\text{f,pred}}\left(A\text{-}A_{\text{c,rolled}}\right)\right)}{A} \tag{3.90}$$

where

$$A_{\text{c,pb}}=A_{\text{c}}=\left(\frac{n_{\text{c}}\pi t}{4}\right)(2r_{\text{i}}+t) \tag{3.91}$$

$$A_{\text{c,rolled}}=A_{\text{c}}+4n_{\text{c}}t^2 \tag{3.92}$$

A is the gross cross-sectional area,
n_{c} is the number of 90°corners in a section.

Xing-Qiang Wang et al. in 2014 [30] proposed the 0.2% proof strength and the ultimate tensile strength expressions for corner given by:

$$\frac{\sigma_{0.2,\text{c}}}{\sigma_{0.2}}=1+0.05e^{900/\sigma_{0.2}} \qquad \text{where } \sigma_{0.2} \text{ is in MPa} \tag{3.93}$$

$$\frac{\sigma_{\text{u,c}}}{\sigma_{0.2,\text{c}}}=(0.56\,{\sigma_{0.2}}^{0.226}\text{-}1.4)\,\frac{\sigma_{\text{u}}}{\sigma_{0.2}} \qquad \text{where } \sigma_{0.2,\text{c}} \text{ is in MPa} \tag{3.94}$$

The relationship doesn´t consider the inner radius to thickness ratio that is one of the most important factors in strength increase.

The research and experimental data set published by Arrayago et al. in 2015 present recommendation for the nonlinearity parameter *n* defined in [49] as it is stated in Figure 3.21.

Family	Grade	RD/TD	T/C	Codified n			Recommended n
				EN 1993-1-4 [3]	AS/NZS-4673 [37]	SEI/ASCE-8 [38]	
Austenitic	1.4301	RD	T	6	7.5	8.3	7
	1.4301	RD	C	6	4.0	4.1	
	1.4435	RD	T	7	–	–	
	1.4541	RD	T	6	–	–	
	1.4307	RD	T	6	7.5	–	
	1.4571	RD	T	7	–	–	
	1.4404	RD	T	7	7.5	–	
	1.4318	RD	T	6	–	–	
	No. of curves:		367				
Ferritic	1.4016	RD	T	6	8.5	8.4	14
	1.4003	RD	T	7	9.0	–	
	1.4509	RD	T	–	–	–	
	1.4521	RD	T	–	11.0	–	
	No. of curves:		117				
	1.4016	TD	T	14	14.0	14.1	
	1.4003	TD	T	11	11.5	–	
	1.4509	TD	T	–	–	–	
	No. of curves:		32				
Duplex and lean duplex	1.4462	RD	T	5	5.5	–	8
	1.4162	RD	T	–	–	–	
	1.4162	RD	C	–	–	–	
	No. of curves:		92				
	1.4162	TD	T	–	–	–	
	1.4162	TD	C	–	–	–	
	No. of curves:		22				

Figure 3.21 *Codified and recommended values for the nonlinearity parameter n.*

Recently in Europe, only the National Annex (informative) to BS EN 1993-1-4:2006, Eurocode 3: Design of steel structures – Part 1-4: General rules – Supplementary rules for stainless steels [50] enable to consider the strength enhancement due to the cold-forming as follows:

a) press braking; an enhanced yield strength f_{ya} may be adopted to account for cold working in 90° section corners where inner radius to thickness ratio r_i/t is not greater than 5.

$$f_{ya} = \frac{f_{yb}\left(\left(A\text{-}A_{pb}\right)+A_{pb}\left(\frac{1.673}{(r_i/t)^{0.126}}\right)\right)}{A} \leq f_u \tag{3.95}$$

b) For austenitic cold rolled box sections (RHS and SHS) which have been formed via a circular tube and where t < 8 mm and r_i/t not greater than 5, an enhanced yield strength f_{ya} may be adopted to account for cold working in the section faces and an extended corner region.

$$f_{ya} = \frac{(A\text{-}A_{cr})\left(\frac{0.85f_{yb}}{\varepsilon_p\text{-}0.19}\right)+0.71A_{cr}f_u\left(\left(\frac{0.19}{\varepsilon_p\text{-}0.19}\right)+1\right)}{A} \leq f_u \tag{3.96}$$

where ε_p is the strain parameter defined as:

$$\varepsilon_p = \frac{1}{\left(12.42\left(\frac{\pi t}{2(b+h)}\right)+0.83\right)} \tag{3.97}$$

A is the gross cross-sectional area ,
A_{cr} is the total corner cross-sectional area for cold rolled box sections including a region of 2t which extends both

sides of each corner. A_{cr} can be obtained with the following expression:

$$A_{cr}=\pi t(2r_i+t)+16t^2 \quad (3.98)$$

r_i can be assumed to be equal to $2t$,
t is the sheet thickness before cold forming,
A_{pb} is the total corner cross-section area for press braked sections which can be calculated as:

$$A_{pb}=\frac{\pi n_c t}{4}(2r_i+t) \quad (3.99)$$

f_{yb}, f_u are the yield strength and the ultimate tensile strength of the basic material (i.e. the flat sheet material of which sections are made by cold forming),
f_u should be taken as the minimum value of the range specified in the material standard,
n_c is the number of 90° corners.

It´s clear, that the increase in the yield strength due to cold working should not be utilized for sections that are annealed or subject to heat treatment after forming which may produce softening.

c) For all section types, work hardening may be utilized in the design if the effect of work hardening has been verified by full size tests in accordance with Section 7 of EN 1993-1-4. For design of connections which are not part of the full size testing, nominal strength values should be used.

The design method for cold-rolled sections allows using accurate value of inner radius if it is obtainable. At the end an increasing inner radius leads to increasing strength of a full section because of an increasing area of corner enhancement. There is no influence of the inner radius to thickness ratio taken into account in terms of plastic strain level. Comparison of the recent methods exhibits unsafe trend of the 0.2% proof strength increase related to the inner radius to thickness ratio. Figure 3.22 depicts dependency of the 0.2% proof strength increase on this ratio for SHS 100x100x2 made of the 1.4404 grade. Other methods balance the influence of a larger corner area and decreased strength enhancement in corners whereas the method from the annex of BS EN 1993-1-4 only enlarges the area of enhancement.

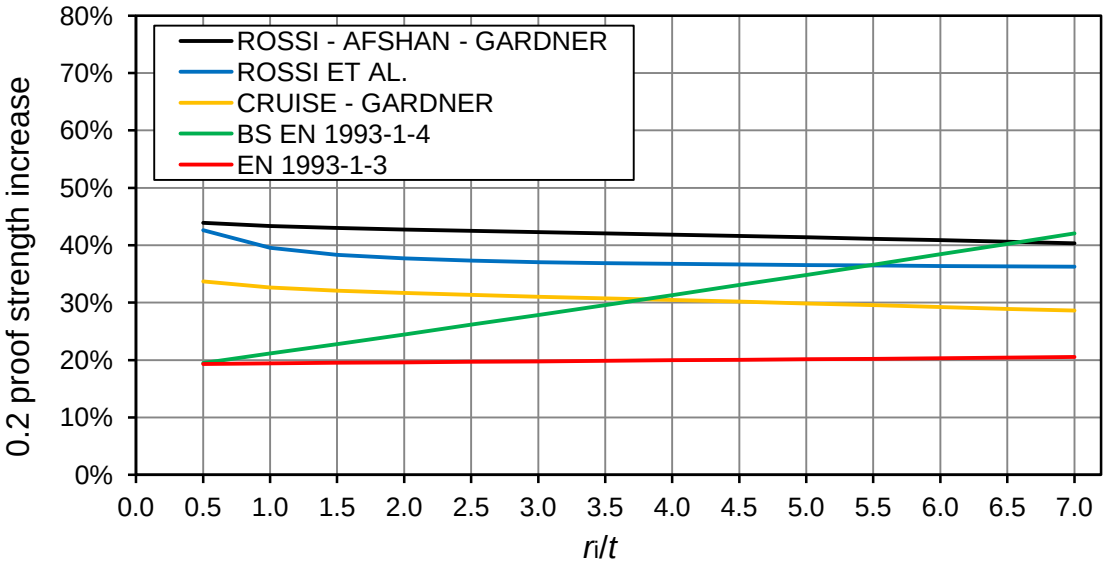

Figure 3.22 *Comparison of methods for the predicted 0.2% proof strength for a full section.*

3.4 Material ageing effect

Also material ageing may induce significant change of the stress-strain curve and increase of the ultimate and yield tensile strength. Hlaváček [51] concerns the ageing effect of the carbon steel as it is shown in Figure 3.23. After reaching the stress $\sigma_2 > \sigma_1$ (yield strength), a plastic deformation ε_{pl} remains. At re-loading, the yield strength reaches stress $\sigma_3 > \sigma_2$ on account of the ageing effect. The ultimate tensile strength increases as well. In case of carbon steel, when the plastic deformation is too large ($\varepsilon_{pl} >$ 25%) the steel becomes too brittle, that the yield strength reaches the ultimate strength and the ductility at the point of specimen collapse disappears. The higher the plastic deformation induced the lower the relative effect of ageing becomes. When the $\varepsilon_{pl} >$ 10% then the effect of ageing is not important. The ageing of carbon steel after plastic deformation induction is represented by a movement of elements with low atomic weight to dislocations. These elements resist to the further dislocations movements and increase the yield strength. This process takes several weeks at the room temperature and at higher temperature (100 – 200 °C) it could take only 30 minutes.

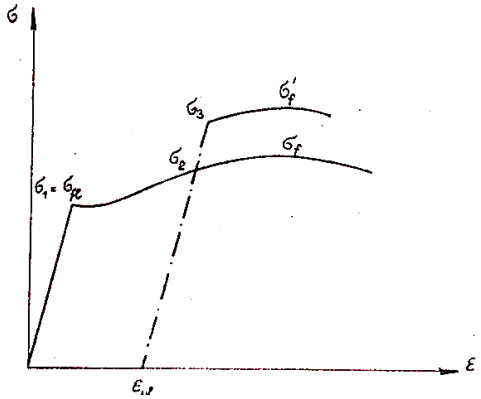

Figure 3.23 *Effect of the plastic deformation and ageing on the stress-strain curve* [51].

3.5 Residual stresses

A residual stress (stress without instant action of external forces or temperature etc.) significantly affects the structure behaviour, especially resistance of walls and members in compression. If plasticisation of material arises due to members' fabrication the residual stresses will occur. Residual stresses also arise due to temperature processes, such as rolling, welding or cold-forming, grinding and other processes. Not always residual stresses have to cause lower member resistance. E.g. a shot peening results in compressive residual stress at the surface of section and can help to increase the moment resistance or enhance life cycle in terms of corrosion resistance.

Residual stresses in austenitic steel were measured for instance by Cruise [4]. The research was focused on behaviour specific for cold-formed material. There was observed behaviour specific for cold-rolled and press-braked angles together with cold-rolled rectangular hollow sections. For the membrane stress, there was not established the idealized stress distribution. The average value of membrane stress (irrespective of the sign) was set up to 6 % of the 0.2% proof strength for angles and 13 % for rectangular hollow sections. The idealized distribution of the flexural stress component was determined as a constant value, different for the wall and corner. This model was established both for average values and for upper 5% fractile (Figure 3.24 and Figure 3.25).

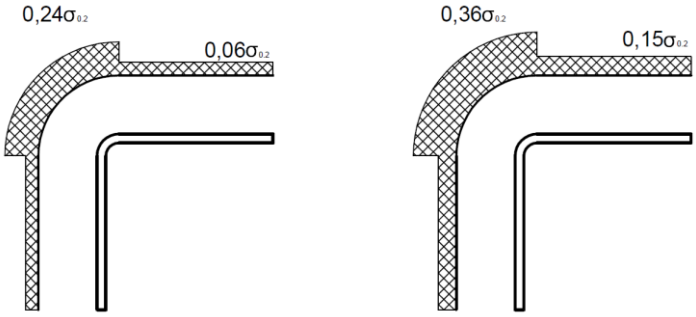

Figure 3.24 *Idealized distribution of the longitudinal flexural residual stress in press-braked angles from austenitic steel (left - average values, right hand – upper 5% fractile) according to* [4], *adopted from* [43].

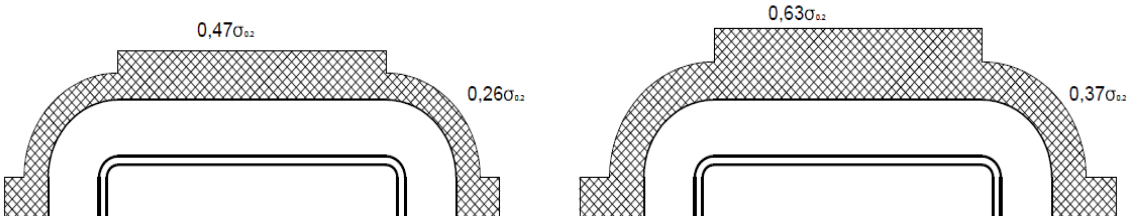

Figure 3.25 *Idealized distribution of the longitudinal flexural residual stress in cold-rolled rectangular hollow sections from austenitic steel (left - average values, right hand – upper 5% fractile) according to* [4], *adopted from* [43].

High stresses reflect high rate of the cold-forming. It is possible to suppose that the non-uniform distribution of the stress signifies also the non-uniform distribution of the 0.2% proof strength, alternatively the ultimate strength. These conclusions were confirmed by Cruise [4] by set of many hardness tests and the determination of the proof strength distribution corresponding with transversal residual stresses.

Cold-bending effect representing press-breaking in terms of residual stresses was also extensively investigated by Weng and White [52]. Set of experiments consisting of cold-bent thick plates with different angles and radii of bends was executed using sectioning and hole-drilling method for residual stresses evaluating. They observed the magnitude of the residual stresses on the inside surface exceeded the yield strength up to 90%. Residual stresses increase with increase of the yield strength of a virgin material and with an angle of the bend. On the other hand residual stresses decrease with increase of the inner radius of the bend.

Another sophisticated model using finite elements was established by Rossi et al. [53]. The model was proposed for nonlinear hardening materials considering fabrication steps as coiling, uncoiling and cold-bending with springback taken into account. It provides good agreement compared with the collected data.

Currently indeed, many researchers solve the cold-forming effect especially for high strength enhancement of stainless steels. However this topic has not been comfortably dealt yet.

3.6 Comparison of material properties in the design standards

3.6.1 Europe

Mechanical properties of stainless steel in annealed condition are specified in the European standard EN 10088 Part 1 [54] and Part 2 [55]. In the recent valid design standard EN 1993-1-4 [16] value of the 0.2% proof strength in annealed condition is given only for the transverse direction hence it does not take into account the material anisotropy. In addition by the annealed material it is probably meant a virgin one. It is thought a material in annealed condition exhibits a similar proof strength in both directions despite the fact that for cold-rolled products strength in transverse direction exhibits higher values of the 0.2% proof strength than in the parallel to the rolling direction. Figures in the standard differ according to the product form (cold rolled strip/hot rolled strip/hot rolled plate) and thickness. However, within the designing of structure it is not often possible to know what type of product form will be used. Consequently it is not applicable to employ enhanced properties of cold-worked materials except some specific products.

Despite this, design standard EN 1993-1-4 [16] allowed to use only materials with the yield strength up to 480 MPa. Just the most recent modification from June 2015 deleted this paragraph and allows use of any material such as new lean-duplex grade 1.4162 and enhances the strength of some other grades. The mechanical properties of some selected austenitic grades are listed in Table 3.3.

Grade	Product form(1)	Maximum thickness (mm)	Minimum 0.2% proof strength(2) (N/mm^2)	Minimum ultimate tensile strength (N/mm^2)
304 (1.4301)	C	6	230	540
	H	12	210	520
	P	75	210	520
316 (1.4401)	C	6	240	530
	H	12	220	530
	P	75	220	520
Notes: (1) C=cold rolled strip, H=hot rolled strip, P=hot rolled plate (2) Transverse properties				

Table 3.3 *Minimal mechanical properties according to product form* [6].

The code allows using cold-worked steel with the increased 0.2% proof strength and the ultimate strength providing two levels of hardening. However the application is possible only for a few austenitic grades.

EN 1993-1-4 defines the Ramberg-Osgood parameter *n* essential for the secant modulus of elasticity, necessary for the deflection or stability calculation. It provides values both for the direction parallel and transverse to the rolling. That could be slightly confusing for designers regarding different fabrication routes for structural members.

3.6.2 USA

American standards SEI/ASCE take into account the anisotropy and the asymmetry of the material (i.e. different behaviour in tension and compression) which becomes increasingly important as the level of the cold-working increases. SEI/ASCE, as well as European standards, determines the Ramberg-Osgood parameter *n* which is necessary for the tangential and secant modulus specification (for deflections estimating and buckling curves identification). Stress-strain curves and mechanical properties for austenitic grades 1.4301 and 1.4401 are presented in Figure 3.26 and Table 3.4.

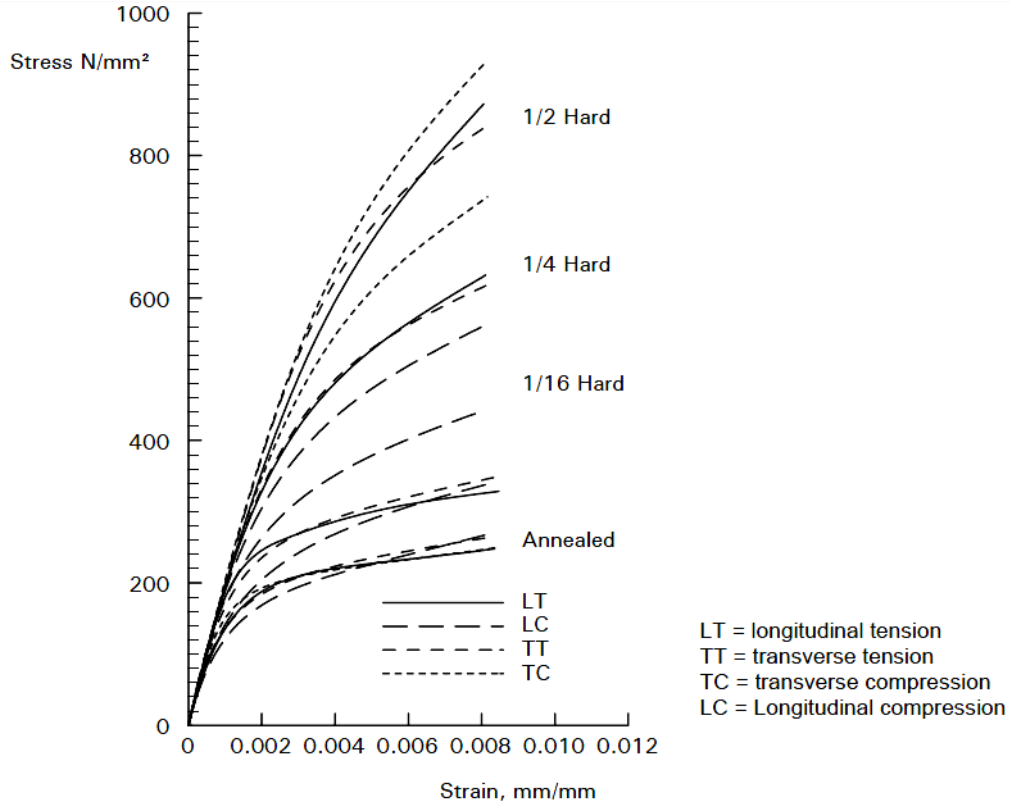

Figure 3.26 *Stress-strain curves for grade 304 in the annealed and cold-worked condition according to SEI/ASCE specification* [6].

Temper	Minimum yield strength (N/mm^2)			Minimum tensile strength (N/mm^2)
	Longitudinal tension and Transverse tension	Transverse compression	Longitudinal compression	
Annealed	206.9	206.9	193.1	517
1/16 hard	310.3	310.3	282.7	551.6 (grade 304) 586.1 (grade 316)
1/4 hard	517.1	621	344.8	862
1/2 hard	758.5	827.4	448.2	1034

Table 3.4 *Table gives minimal mechanical properties for grades 304 and 316 according to loading direction and degree of cold-working temper according to SEI/ASCE specification* [6]. *Degree of temper indicates a hardening level according to the surface hardness.*

3.6.3 Australia

Australian standards AS/NZS are based on the American standards. There is a comparison of the main standards in the Table 3.5 and Table 3.6.

Country	Grade	Minimum yield strength (N/mm^2)	Minimum ultimate tensile strength (N/mm^2)
Europe	304	210(1)	520
	316	220(1)	520
US	304 and 316	206.9 (LT, TT, TC)(2) 193.1 (LC)	517
Australia	304 and 316	205 (LT, TT, TC)(2) 195 (LC)	520
Notes: (1) For hot rolled plate, transverse properties (2) LT=longitudinal tension, TT=transverse tension, TC=transverse compression, LC=Longitudinal compression			

Table 3.5 *Comparison of mechanical properties for grades 304 and 316 in the annealed condition* [6].

Country		Longitudinal tension	Transverse tension	Transverse compression	Longitudinal compression
Europe	Grade 304	6.5	8.5	8.5	6.5
	Grade 316	7.0	9.0	9.0	7.0
US		8.31	7.78	8.63	4.10
Australia		7.5	5.5	7.0	4.0

Table 3.6 *Comparison of the Ramberg – Osgood parameter n for grades 304 a 316 in the annealed condition* [6].

Section	Annealed			C850		
	$\sigma_{0.2}$ (N/mm^2)	σ_u (N/mm^2)	E (N/mm^2)	$\sigma_{0.2}$ (N/mm^2)	σ_u (N/mm^2)	E (N/mm^2)
RHS 80 × 80 × 3—Face 1	571	864	190,000	713	1048	173,000
RHS 80 × 80 × 3—Face 2	469	805	185,000	590	1001	173,000
RHS 100 × 100 × 3—Face 1	530	830	195,000	666	971	183,000
RHS 100 × 100 × 3—Face 2	432	782	195,000	549	914	184,000
RHS 120 × 80 × 3—Face 1	619	886	197,000	763	1025	188,000
RHS 120 × 80 × 3—Face 2	459	796	202,000	553	916	192,000
RHS 140 × 60 × 3—Face 1	619	886	190,000	741	1038	187,000
RHS 140 × 60 × 3—Face 2	492	808	203,000	561	956	185,000

Table 3.7 *Comparison of measured tensile material properties in the annealed condition and cold-worked conditions* [56].

Table 3.7 displays measured mechanical properties in annealed conditions in comparison with measured values for cold-worked state of the material. Differences could be more significant as the specimens represent flat faces of rectangular sections and not the most affected parts of section – corners.

Chapter 4

Experimental program

The chapter describes set of experiments executed at the Department of steel and timber structures laboratory of the Faculty of Civil Engineering by the Czech Technical University in Prague. Specimens´ preparation was mostly provided by department technicians and by cooperation with the Klokner´s Institute. The work was focused on the stress-strain behaviour description of cold-formed stainless steel of all main grades, i.e. ferritic (1.4003), austenitic (1.4404), duplex (1.4462) and relatively new lean-duplex grade (1.4162) as well. The project involves tensile tests of coupons prepared of a cold-rolled steel sheet. Material tests of the virgin material preceded plastic strain induction procedure serving for tensile tests of cold-worked samples. Results obtained from the programme are evaluated and summarized. Detailed results and conclusions from the testing programme are stated herein and serve for the analytical part of the thesis.

4.1 Test rate sensitivity

Stress-strain curve is significantly affected by the test strain rate. The higher rate implies the higher strength and reduced ductility. Dependency on the strain rate is more pronounced in comparison with carbon steel also due to the nonlinear stress-strain behaviour. It is also more influenced (higher strength is recorded) by constant stress rate than constant strain rate. Thus all of executed tests were controlled by strain that provides safe measured strength values.

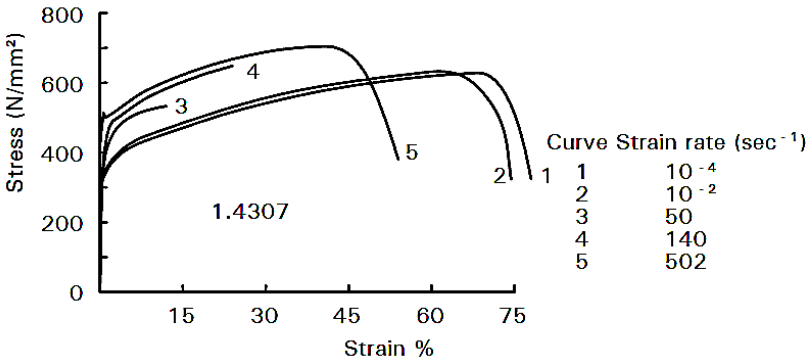

Figure 4.1 *Strain rate effect on 1.4307 grade* [2].

4.2 Material tensile tests

Specimens were made of cold-rolled sheet of 1.5 mm, resp. 2.0 mm (in case of the 1.4462 grade) thickness. All tensile tests were executed in the same configuration. Coupons were made in proportion to the EN ISO 6892-1 [57]. The geometry and coupons before and after a test are displayed in Figure 4.2.

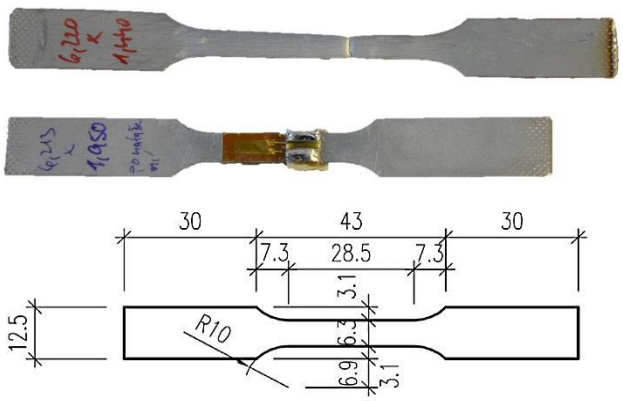

Figure 4.2 *Coupons before and after a tensile test with their geometry.*

Deflection, respectively strain was directly measured by foil strain gauges essential for accuracy of the initial part of strain response. An extensometer was used for higher strain ranges. Figure 4.3 graphically shows basic material parameters stated in following tables.

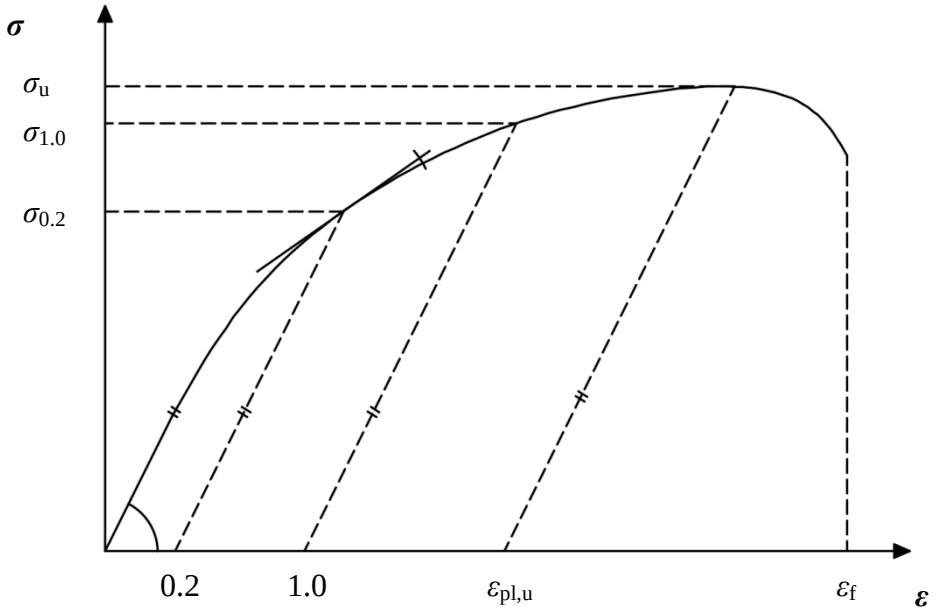

Figure 4.3 *Graphic declaration of material parameters.*

Determination process evaluating a slope of the linear elastic part of a uniaxial stress-strain diagram (Young´s modulus) was conducted in accordance with SEP 1235: Determination of the modulus of elasticity on steels by tensile testing at room temperature [58]. However difficulties with the modulus of elasticity caused by short linear region of the initial stress-strain curve also occurred and the initial modulus was evaluated for lower stress level than it is recommended. The common Ramberg-Osgood model (3.5) is used up to the 0.2% plastic strain. Beyond this limit, the Gardner-Nethercot description (3.9) is used with nonlinearity parameter established for the best agreement between the model curve and the recorded stress-strain response up to 3% plastic strain. Stress and strain values in tables are in engineering form. If the true stress and strain is used they are obtained by:

$$\sigma_{true}=\sigma_{nom}(1+\varepsilon_{nom}) \quad \text{for tension} \quad (4.1)$$

$$\varepsilon_{true}=\ln(1+\varepsilon_{nom}) \quad \text{for tension} \quad (4.2)$$

$$\sigma_{true}=\sigma_{nom}(1-\varepsilon_{nom}) \quad \text{for compression} \quad (4.3)$$

$$\varepsilon_{true}=-\ln(1-\varepsilon_{nom}) \quad \text{for compression} \quad (4.4)$$

The evaluated characteristics are as follows:

E_0 is the initial modulus of elasticity,
$E_{0,2}$ is the tangent modulus at the 0.2% proof strength,
$\sigma_{0.2}$ is the 0.2% proof strength,
$\sigma_{1.0}$ is the 1.0% proof strength,
σ_u is the ultimate tensile strength,
ε_f strain at coupon fracture,
$\varepsilon_{pl,u}$ plastic strain at ultimate strength,
n Ramberg-Osgood hardening exponent,
$n'_{0.2,1.0}$ compound Ramberg-Osgood model hardening exponent.

All tests were performed using the MTS Qtest 100 kN electromechanical testing machine with all data recording at 0.2 second interval by the SPIDER data acquisition system with CATMAN32 data acquisition software (see Figure 4.4). Strain control was used to drive the machine. The accepted strain rate for the first period of testing was 0.007% strain per second up to 1.5% strain and 0.2% strain per second until fracture according to the EN ISO 6892-1 [57]. The value of the 1.5% strain was determined to ensure the lower stress rate was used to reach the stress point of the 1.0% plastic deformation $\sigma_{1.0}$. The $\sigma_{1.0}$ value is often used for the stress-strain diagram description.

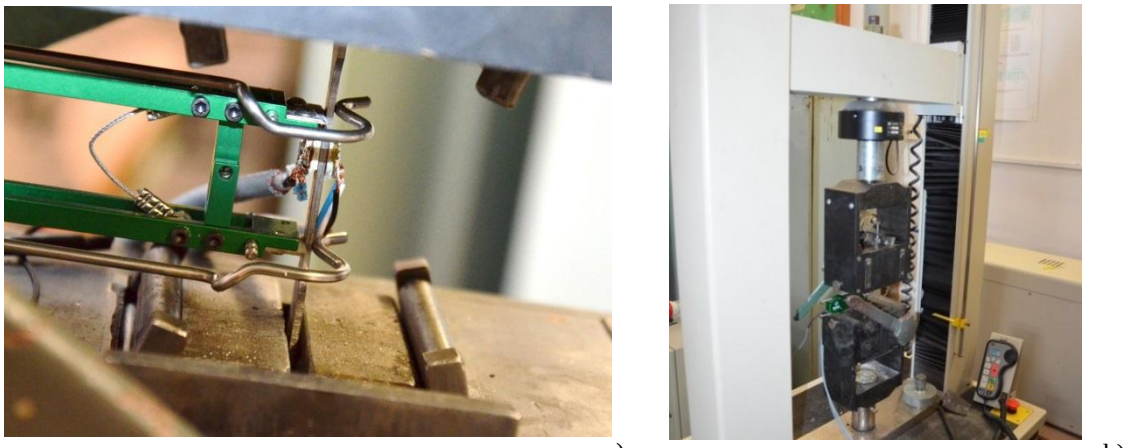

a) b)

Figure 4.4 *a) Detail of a coupon in testing machine jaws; b) Testing machine with jaws.*

4.2.1 Virgin material tests

First of all tensile material tests of the virgin sheet of all grades were executed. Tests were performed both for direction of rolling and direction transverse to the fabrication rolling of the sheet (see Figure 4.5). Material properties of the sheet were assumed by average of 3 samples. Obtained measurement is summarized in Table 4.1.

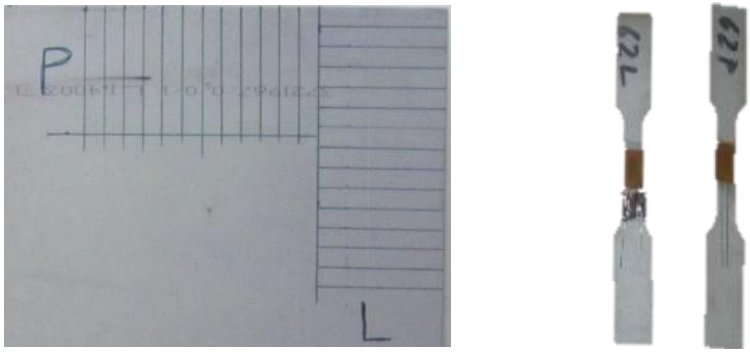

Figure 4.5 *Coupons made of sheet according to rolling direction. Letter "P" denotes letter mark "T" and "L" mark "P".*

Grade	Rolling direction	E_0	$E_{0.2}$	$\sigma_{0.2}$	$\sigma_{1.0}$	σ_u	ε_f	$\varepsilon_{pl.u}$	n	$n'_{0.2.1.0}$
		GPa	GPa	MPa	MPa	MPa	%	%	-	-
1.4003	P	198.3	7.5	326.7	357.1	492.3	22.1	18.0	8.4	1.8
1.4003	T	211.9	7.0	343.7	374.5	512.3	31.9	17.6	8.5	1.9
1.4404	P	189.0	14.1	259.8	307.3	620.8	61.8	48.7	3.7	2.1
1.4404	T	199.8	11.6	279.0	322.0	635.1	68.6	57.1	8.8	2.3
1.4162	P	193.3	21.9	551.6	623.7	785.9	37.9	24.1	7.3	3.0
1.4162	T	195.5	22.4	556.5	624.8	765.6	35.2	21.1	7.5	3.1
1.4462	P	195.8	25.2	600.1	676.6	843.0	34.3	22.6	6.9	2.9
1.4462	T	210.7	30.0	637.6	722.7	863.7	33.9	20.6	5.6	3.4

P – test parallel to the rolling directions. T – test transverse to the rolling direction

Table 4.1 *Mechanical properties of the cold rolled sheets according to the rolling direction.*

4.2.2 Tests after plastic strain induction

The next step included tensile plastic deformations induction on typical samples (described above) and special wide sheet samples from which new specimens were manufactured. Level of plastic deformation varies significantly in a range of several values, i.e. 1%, 3%, 5%, 10%, 15% and for other than ferritic grades also 20% or 50% (for austenitic grade only). Thus experimental set for each grade consists of 5 or 6 specimens for both directions depending on the rolling and in respect to the induced plastic strain direction and subsequent tensile test (according to the direction of the plastic strain induction). In total 92 coupons were prepared and tested.

Device for plastic strain induction in a wide sheet

For experimental purposes a device for plastic strain induction in a wide sheet was designed and fabricated. It is able to induce uniform plastic deformation through the whole width of a metal sample of special geometry. The sample geometry provides the best fitted stress distribution from shapes which were considered based on a simple Abaqus 2D model. That provides the desired strain distribution in the area which the new coupons are created (neck of the specimen) from as it is displayed in following figures. The idea about the stress distribution was confirmed by measurements consisting of 5 strain gauges. The progress and numerical results of different sample geometries are shown in Figure 4.6.

The device consists of two parts, in which the sample is attached by four bolts M16 8.8. There are two shear planes (represented by two plates and a sample) to ensure the best possible centric stress. The device is able to be clamped to a testing machine by a round bar hinged to jaws, which might eliminate eventual moment influence. The middle part of the sample serves to attaching an extensometer set with gauge length of 50 mm or less. Total load of the sample can be over 100 kN. The device with attached sample is shown in figures on the next page.

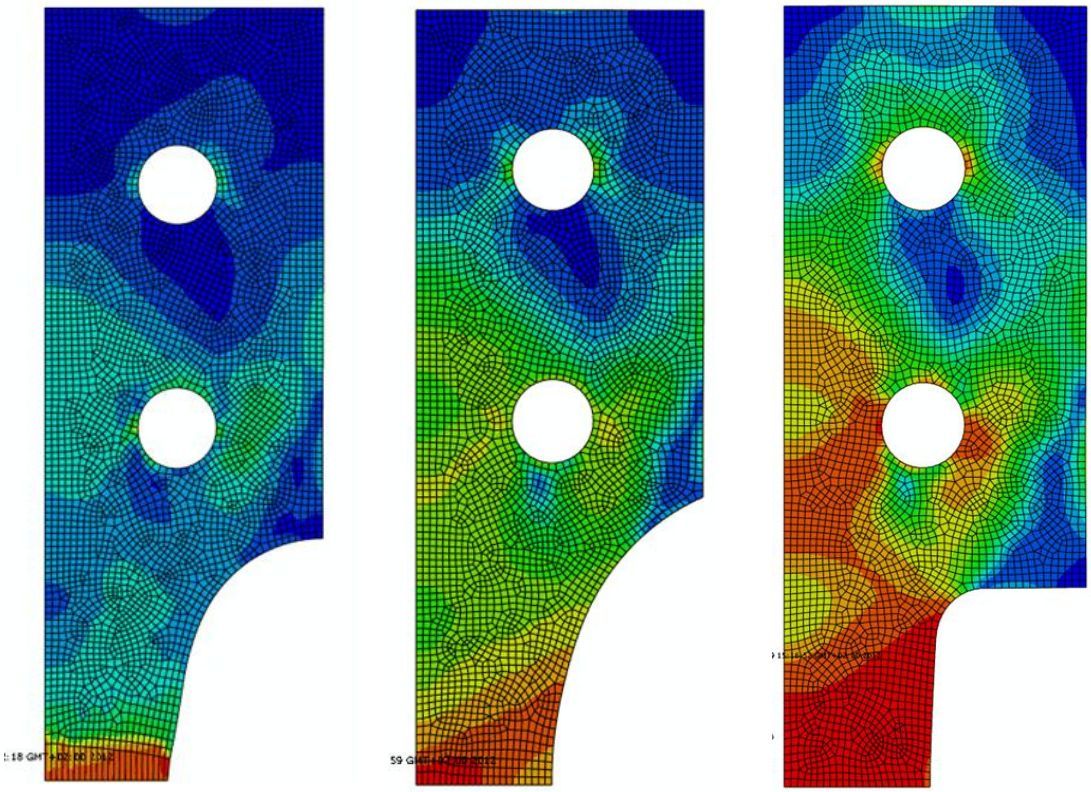

Figure 4.6 *Geometry of the sample in progress and the final geometry (uniform stress distribution) – right hand side (quarter of sample – symmetric).*

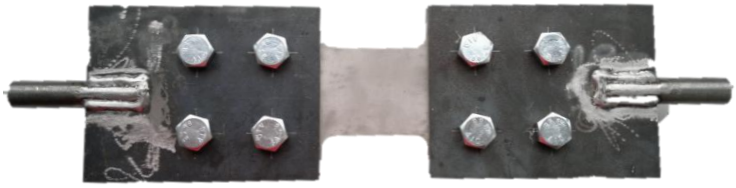

Figure 4.7 *The device for plastic strain induction in a wide sheet with sample.*

Figure 4.8 *The device for plastic strain induction in a wide sheet with sample (side view).*

Samples after cold-working represented by elongation with test description are shown in Figure 4.9. It describes directions of primary elongation and a subsequent test.

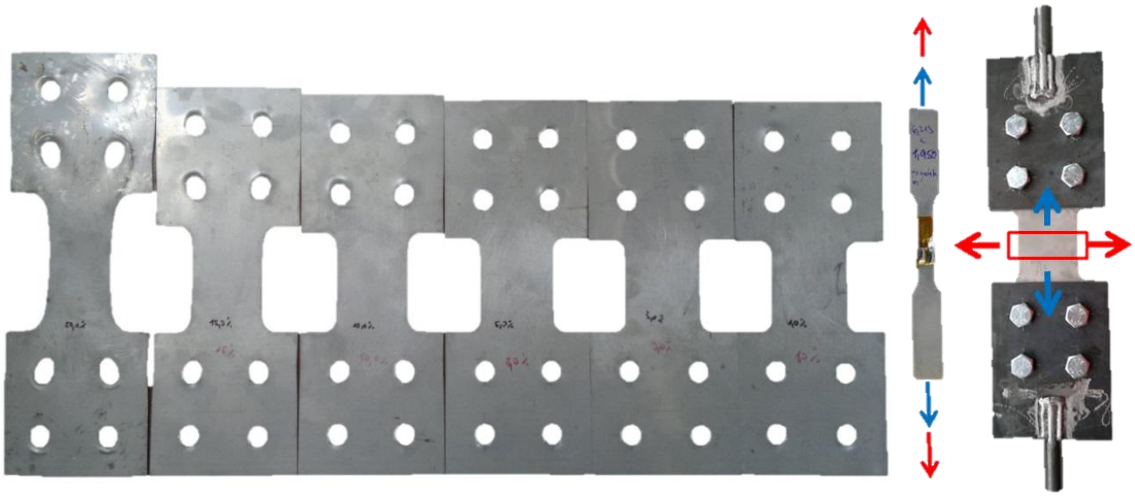

a) b)

Figure 4.9 *a) Different level of induced tensile plastic deformation; b) Cold-working and testing: the blue arrow marks the direction of elongation, the red arrow marks direction of the subsequent tensile test.*

Measured data is summarized in following tables. Explanation to shortcuts is stated as follows:

"RD" = Rolling direction; "LPSI" = Level of plastic strain induction; "PSI" = Plastic strain induction. Rolling direction (coupon cut out from sheet): "P" – parallel to the rolling directions, "T" – transverse to the rolling direction; Plastic strain induction (tensile test direction after elongation): "P" – parallel to the previous plastic strain induction, "T" – transverse to the previous plastic strain induction.

RD	LPSI (%)	PSI	E_0 GPa	$E_{0.2}$ GPa	$\sigma_{0.2}$ MPa	$\sigma_{1.0}$ MPa	σ_u MPa	$\varepsilon_{pl.u}$ %	ε_f %	n	$n'_{0.2.1.0}$
P	1.0	P	200.6	10.5	366.6	399.9	519.6	19.9	20.2	7.3	1.7
P	3.0	P	204.8	5.1	418.5	437.0	493.4	17.5	17.8	8.2	2.0
P	5.0	P	200.8	3.8	487.0	500.6	x	x	x	5.3	3.0
P	10.0	P	189.8	2.2	523.7	531.5	543.2	12.3	12.6	5.9	3.1
P	15.0	P	178.5	0.3	548.8	552.1	553.0	7.9	8.2	5.2	3.1
T	1.0	P	197.3	4.8	436.4	456.3	528.1	25.8	26.1	9.6	1.7
T	3.0	P	196.5	4.8	434.7	454.6	524.0	25.8	26.0	9.6	1.9
T	5.0	P	189.0	2.9	482.5	495.3	540.4	21.7	22.0	6.2	1.8
T	10.0	P	182.8	2.1	546.4	554.6	567.1	16.7	17.0	7.2	2.5
T	15.0	P	194.6	0.5	584.0	586.1	588.0	10.1	10.4	5.3	3.0

Table 4.2 *Mechanical properties of the tested coupons with induced plastic strain of the 1.4003 grade.*

RD	LPSI (%)	PSI	E_0 GPa	$E_{0.2}$ GPa	$\sigma_{0.2}$ MPa	$\sigma_{1.0}$ MPa	σ_u MPa	$\varepsilon_{pl.u}$ %	ε_f %	n	$n'_{0.2.1.0}$
P	1.0	T	192.1	18.2	354.1	407.2	455.0	x	x	9.2	3.1
P	3.0	T	202.6	21.2	420.2	469.1	503.2	x	x	4.0	4.0
P	5.0	T	194.6	32.1	453.7	517.7	526.5	x	x	3.9	5.0
P	10.0	T	189.2	47.8	492.0	581.4	581.4	11.7	12.0	3.3	5.0
P	15.0	T	184.9	35.0	585.7	649.6	650.6	7.6	8.0	5.3	5.0
T	1.0	T	190.7	19.6	368.0	415.7	528.0	15.7	16.0	6.3	2.5
T	3.0	T	207.3	36.3	408.2	481.7	534.1	29.7	30.0	3.4	4.9
T	5.0	T	197.6	30.2	464.7	518.2	551.0	21.7	22.0	4.7	4.5
T	10.0	T	197.2	36.3	561.1	612.3	632.4	9.7	10.0	4.2	4.0
T	15.0	T	201.8	40.0	577.1	x	643.5	6.5	6.8	4.1	4.0

Table 4.3 *Mechanical properties of the tested coupons with induced plastic strain of the 1.4003 grade – follow-up.*

RD	LPSI (%)	PSI	E_0 GPa	$E_{0.2}$ GPa	$\sigma_{0.2}$ MPa	$\sigma_{1.0}$ MPa	σ_u MPa	$\varepsilon_{pl.u}$ %	ε_f %	n	$n'_{0.2.1.0}$
P	1.0	P	195.2	7.2	336.7	369.7	655.0	44.8	56.6	8.2	2.0
P	3.0	P	184.5	20.2	356.8	398.8	656.3	43.0	56.2	3.2	2.2
P	5.0	P	170.4	6.6	416.9	440.5	643.8	39.5	51.5	5.8	1.8
P	10.0	P	198.1	15.9	513.1	539.0	695.8	32.5	45.2	2.8	1.9
P	15.0	P	199.5	44.6	550.9	588.4	700.9	28.9	40.2	2.6	2.1
P	50.0	P	193.2	54.5	927.3	954.7	960.9	x	7.5	2.4	2.1
T	1.0	P	201.4	11.3	328.9	364.2	649.1	53.4	64.0	5.8	2.0
T	3.0	P	210.7	13.7	375.1	406.1	663.2	52.7	62.9	4.0	1.8
T	5.0	P	202.9	14.4	419.5	448.2	676.0	48.2	60.6	3.7	1.8
T	10.0	P	188.8	11.0	506.7	525.6	653.4	36.9	49.4	3.1	2.2
T	15.0	P	197.6	10.4	548.0	571.0	748.8	43.9	56.2	2.7	1.8
T	50.0	P	197.4	56.0	925.6	960.5	981.7	x	17.8	3.1	15.0

Table 4.4 *Mechanical properties of the tested coupons with induced plastic strain of the 1.4404 grade.*

RD	LPSI (%)	PSI	E_0 GPa	$E_{0.2}$ GPa	$\sigma_{0.2}$ MPa	$\sigma_{1.0}$ MPa	σ_u MPa	$\varepsilon_{pl.u}$ %	ε_f %	n	$n'_{0.2.1.0}$
P	1.0	T	194.4	25.1	296.1	365.4	654.3	60.1	60.4	3.5	3.0
P	3.0	T	198.1	35.0	336.6	425.7	666.5	56.9	57.2	1.8	3.2
P	5.0	T	195.1	40.0	362.1	461.0	678.0	54.9	55.2	3.2	3.4
P	10.0	T	193.7	53.0	413.8	534.9	699.4	51.6	52.0	2.9	3.6
P	15.0	T	190.3	54.5	452.3	586.0	716.5	44.4	44.8	2.9	3.8
P	50.0	T	199.2		610.0	x	x	x	x	3.0	x
T	1.0	T	202.0	21.3	312.1	370.8	663.6	66.5	66.8	4.4	3.0
T	3.0	T	209.1	24.5	359.7	420.1	670.8	64.1	64.4	4.2	3.3
T	5.0	T	202.5	33.8	399.1	473.5	688.2	62.1	62.4	3.6	4.3
T	10.0	T	203.8	39.2	474.2	553.5	712.6	54.9	55.2	3.5	4.9
T	15.0	T	204.9	50.3	517.2	618.7	743.1	46.8	47.2	3.3	4.8
T	50.0	T	203.6	59.4	679.7	850.9	891.8	26.4	26.8	2.9	4.5

Table 4.5 *Mechanical properties of the tested coupons with induced plastic strain of the 1.4404 grade – follow-up.*

RD	LPSI (%)	PSI	E_0 GPa	$E_{0.2}$ GPa	$\sigma_{0.2}$ MPa	$\sigma_{1.0}$ MPa	σ_u MPa	$\varepsilon_{pl.u}$ %	ε_f %	n	$n'_{0.2.1.0}$
P	1.0	P	197.9	37.0	564.6	651.5	773.6	22.7	33.6	5.0	3.6
P	3.0	P	187.1	39.2	649.9	709.4	822.3	27.5	34.3	4.5	2.9
P	5.0	P	186.1	5.8	726.7	744.3	816.3	18.4	33.7	5.6	2.0
P	10.0	P	189.6	12.8	829.3	843.5	871.0	13.6	28.2	4.3	2.8
P	15.0	P	187.3	28.8	866.4	889.1	898.1	7.6	26.3	3.7	5.0
P	20.0	P	182.8	40.0	920.4	945.0	946.9	3.6	20.9	3.5	8.0
T	1.0	P	203.5	32.7	563.6	642.7	779.4	24.3	36.5	3.8	3.4
T	3.0	P	199.4	16.2	686.2	727.6	809.3	18.0	30.5	6.1	3.1
T	5.0	P	192.1	20.0	735.5	761.5	816.9	16.4	28.8	4.2	2.3
T	10.0	P	193.4	40.0	792.1	827.0	849.1	10.8	22.0	3.7	6.0
T	15.0	P	184.6	17.5	875.3	889.9	895.5	6.0	20.9	4.3	6.0
T	20.0	P	190.4	20.4	922.0	933.7	936.7	1.5	15.2	3.9	3.0

Table 4.6 *Mechanical properties of the tested coupons with induced plastic strain of the 1.4162 grade.*

RD	LPSI (%)	PSI	E_0 GPa	$E_{0.2}$ GPa	$\sigma_{0.2}$ MPa	$\sigma_{1.0}$ MPa	σ_u MPa	$\varepsilon_{pl.u}$ %	ε_f %	n	$n'_{0.2.1.0}$
P	1.0	T	193.6	54.5	511.8	668.2	815.5	40.0	40.4	2.6	4.5
P	3.0	T	200.3	59.4	546.4	721.6	824.6	37.6	38.0	2.9	3.3
P	5.0	T	200.2	44.6	637.6	782.3	857.9	32.8	33.2	7.2	3.1
P	10.0	T	190.3	59.4	596.0	835.0	911.4	24.7	25.2	2.7	3.1
P	15.0	T	197.1	72.6	626.9	880.1	956.1	17.9	18.4	2.5	2.7
P	20.0	T	201.8	75.4	653.6	937.0	1002.5	12.3	12.8	2.4	3.0
T	1.0	T	209.9	43.6	556.5	674.4	816.2	38.0	38.4	3.4	3.6
T	3.0	T	208.6	56.0	574.1	728.0	834.9	34.8	35.2	2.9	3.5
T	5.0	T	201.1	63.3	583.6	768.9	850.0	32.4	32.8	2.8	3.6
T	10.0	T	202.8	75.4	646.4	859.5	925.6	22.3	22.8	2.7	3.0
T	15.0	T	198.7	61.3	690.6	912.2	971.2	13.9	14.4	2.7	3.8
T	20.0	T	202.3	78.4	673.6	917.9	1006.9	11.5	12.0	1.8	3.0

Table 4.7 *Mechanical properties of the tested coupons with induced plastic strain of the 1.4162 grade – follow-up.*

RD	LPSI (%)	PSI	E_0 GPa	$E_{0.2}$ GPa	$\sigma_{0.2}$ MPa	$\sigma_{1.0}$ MPa	σ_u MPa	$\varepsilon_{pl.u}$ %	ε_f %	n	$n'_{0.2.1.0}$
P	1.0	P	193.3	22.3	665.2	713.0	834.2	28.0	39.6	6.6	2.4
P	3.0	P	195.1	7.9	741.7	763.1	843.5	17.1	28.9	5.5	1.9
P	5.0	P	195.3	29.7	745.4	790.5	867.2	16.4	29.6	3.9	3.2
P	10.0	P	188.1	10.2	876.6	888.8	913.6	15.7	24.4	4.6	2.6
P	15.0	P	192.0	40.8	931.5	959.8	961.3	5.5	19.3	3.2	8.0
P	20.0	P	192.6	27.2	981.8	997.4	1005.0	0.5	15.9	3.8	8.0
T	1.0	P	205.2	18.1	714.5	758.7	852.5	29.4	29.8	5.3	2.9
T	3.0	P	200.6	25.7	747.1	798.0	860.9	28.6	29.0	4.7	5.8
T	5.0	P	211.2	11.5	825.0	842.6	907.7	24.7	25.2	4.7	2.0
T	10.0	P	196.5	14.2	915.2	926.0	932.6	21.2	21.7	4.1	5.0
T	15.0	P	207.4	17.3	983.5	992.4	1005.3	16.1	16.6	3.9	6.0
T	20.0	P	200.2	26.7	1026.4	1036.0	1039.0	14.5	15.0	3.8	10.0

Table 4.8 *Mechanical properties of the tested coupons with induced plastic strain of the 1.4462 grade.*

RD	LPSI (%)	PSI	E_0 GPa	$E_{0.2}$ GPa	$\sigma_{0.2}$ MPa	$\sigma_{1.0}$ MPa	σ_u MPa	$\varepsilon_{pl.u}$ %	ε_f %	n	$n'_{0.2.1.0}$
P	1.0	T	191.1	39.2	608.2	665.8	882.4	33.5	34.0	3.2	3.0
P	3.0	T	194.5	44.2	647.5	756.6	890.3	30.3	30.8	3.8	3.4
P	5.0	T	195.0	56.6	720.2	873.6	940.4	22.3	22.8	3.2	3.8
P	10.0	T	196.2	63.9	747.7	933.9	994.1	16.3	16.8	3.0	4.2
P	15.0	T	188.2	66.1	844.5	1030.9	1072.2	10.2	10.8	2.9	4.3
P	20.0	T	188.8	66.8	897.3	1080.9	1116.0	7.0	7.6	3.0	4.2
T	1.0	T	211.0	43.3	648.4	757.2	900.9	38.4	38.8	3.7	3.6
T	3.0	T	208.9	58.8	691.6	836.8	927.6	32.0	32.4	2.7	4.0
T	5.0	T	208.4	51.2	732.3	860.3	939.3	24.3	24.8	3.3	4.0
T	10.0	T	209.2	57.1	827.2	933.9	994.1	19.9	20.4	3.5	4.3
T	15.0	T	203.1	66.1	865.9	1039.6	1117.4	16.2	16.8	3.2	4.4
T	20.0	T	213.5	67.6	887.3	1070.6	1115.4	15.1	15.6	3.1	4.8

Table 4.9 *Mechanical properties of the tested coupons with induced plastic strain of the 1.4462 grade – follow-up.*

4.3 Material tests outputs

This section describes graphic outputs resulting from the measured data. Figure 4.10 shows comparison of the different grades for the virgin material test according to the rolling directions.

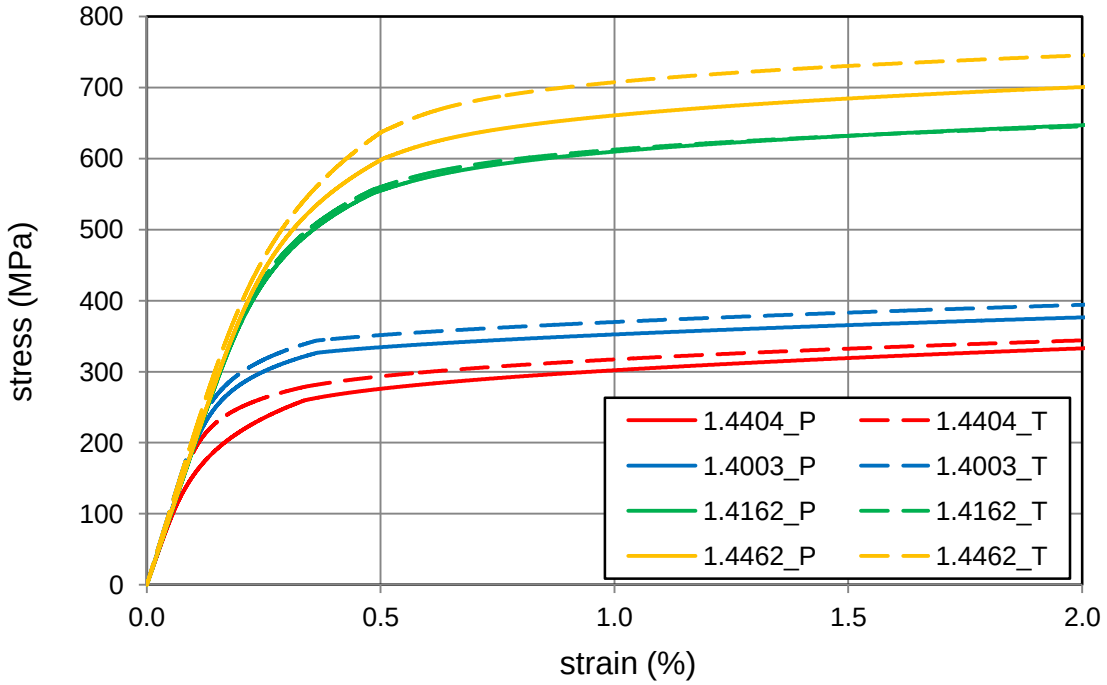

Figure 4.10 *Idealized stress-strain diagram of the coupons made of the cold-rolled sheet. P marks the test parallel to the rolling direction; T marks the test transverse to the rolling direction.*

All grades exhibit a higher strength in the transverse direction to the rolling. In case of the lean duplex grade 1.4162 there is almost the same stress-strain behaviour for both directions.

In terms of the anisotropy of the cold-rolled sheet with induced plastic strain there is displayed only the direction parallel to the rolling direction in following figures (Figure 4.11 - Figure 4.14). Coupons cut out in the transverse direction to the rolling exhibit similar behaviour.

Explanations for marks used in figures are given as:

First letter “P” denotes the samples manufactured parallel to the rolling direction, second letter denotes the plastic strain induced in the same direction as the subsequent tensile test (“P”) or the plastic strain induced in the transverse direction to the subsequent tensile test (“T”).

Results presented below confirm the dependency of anisotropy on the increasing level of cold-working. This effect is apparent for all grades. Differences are significant especially for the lean duplex and duplex grade. Also the stiffness (particularly before the 0.2% proof strength) differs a lot as it is obvious from the figures.

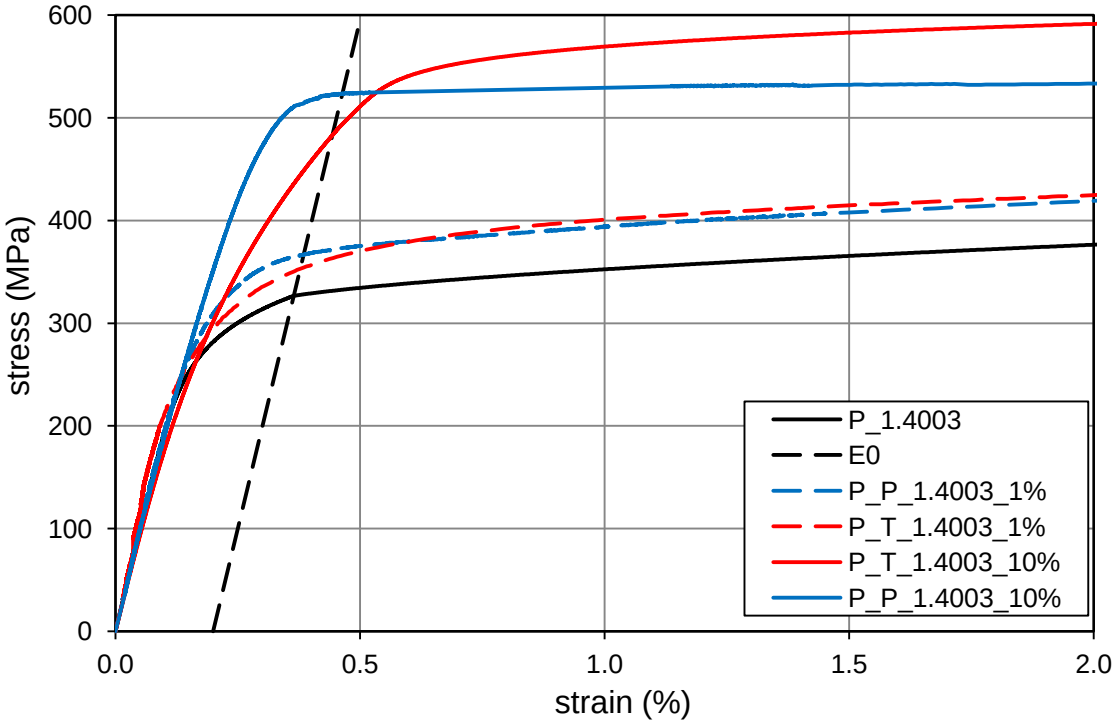

Figure 4.11 *Recorded stress-strain diagrams of selected 1.4003 samples.*

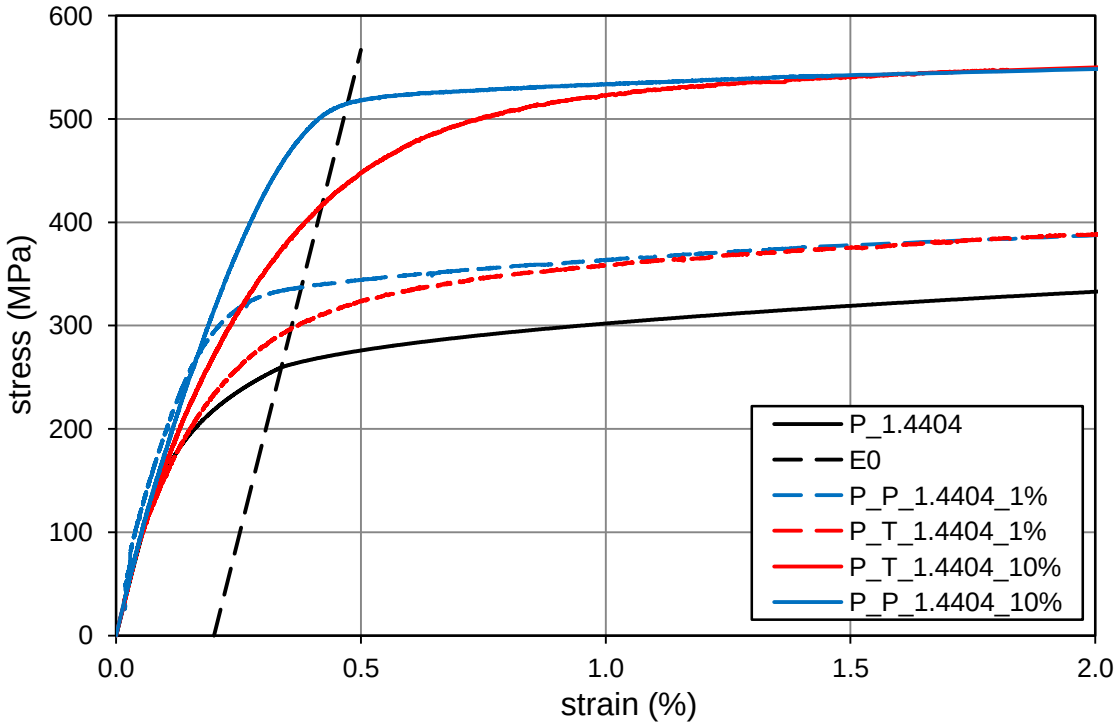

Figure 4.12 *Recorded stress-strain diagrams of selected 1.4404 samples.*

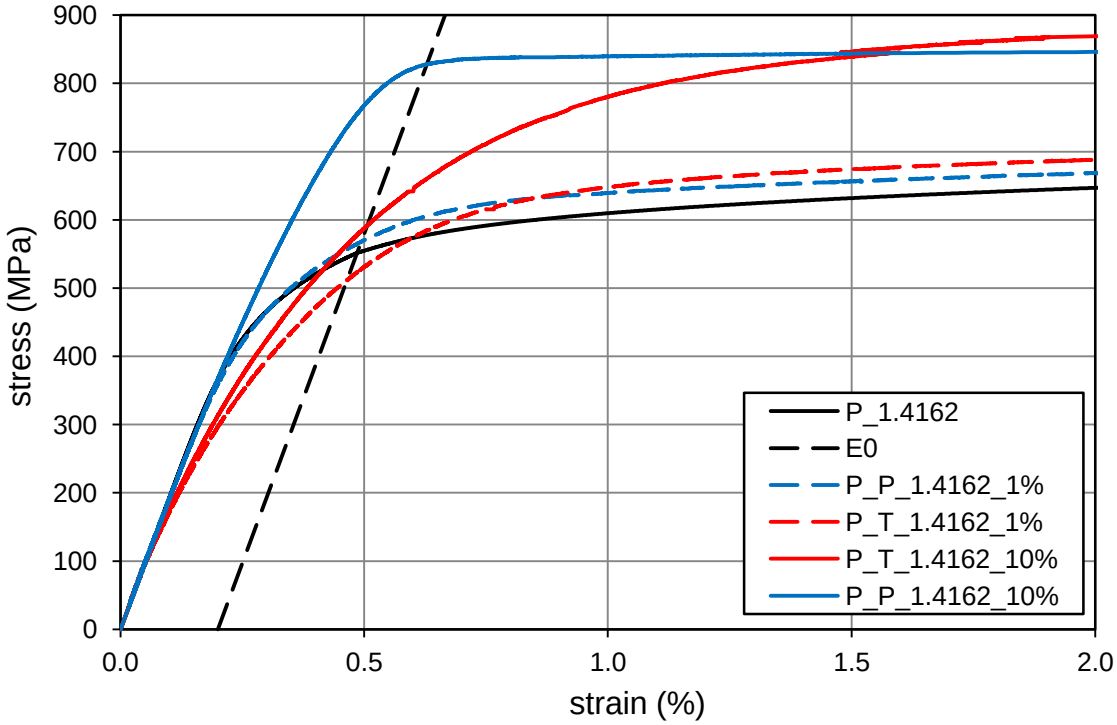

Figure 4.13 *Recorded stress-strain diagrams of selected 1.4162 samples.*

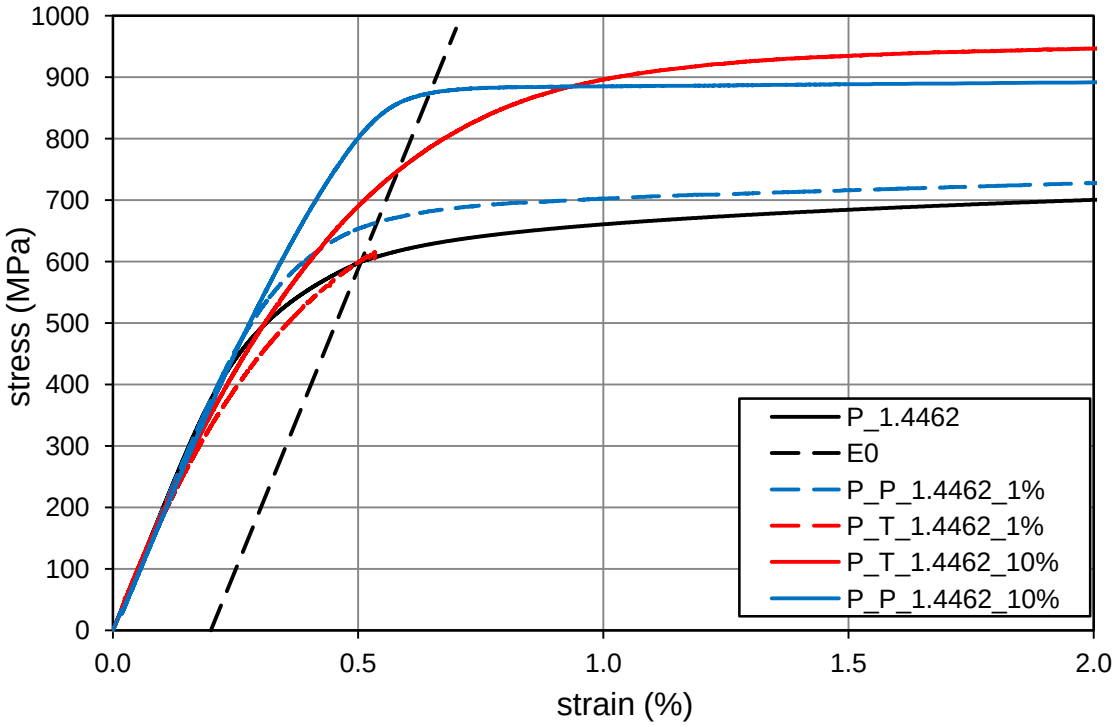

Figure 4.14 *Recorded stress-strain diagrams of selected 1.4462 samples.*

The effect of anisotropy is entirely opposite to the behaviour after cold-rolling where the 0.2% proof strength is higher for the direction transverse to the rolling. Cold-rolling is continuous process affecting an endless sheet through the thickness. Therefore this specific way of cold-working may produce a cold-rolled sheet with different mechanical properties in comparison to the uniaxial cold-working.

Figure 4.15 - Figure 4.18 display increase of the 0.2% proof strength for the cold-formed samples. Mark “P” denotes the subsequent tensile test parallel to the direction of plastic strain induction while mark “T” denotes the subsequent tensile test transverse to the direction of plastic strain induction. The curves determining the increase consists of the average value of 0.2% proof strength obtained both for direction parallel and transverse to the rolling direction as the comparing base representing virgin material mechanical properties. Plotted curves are compared with isotropic hardening obtained from stress-strain diagram of the unformed material.

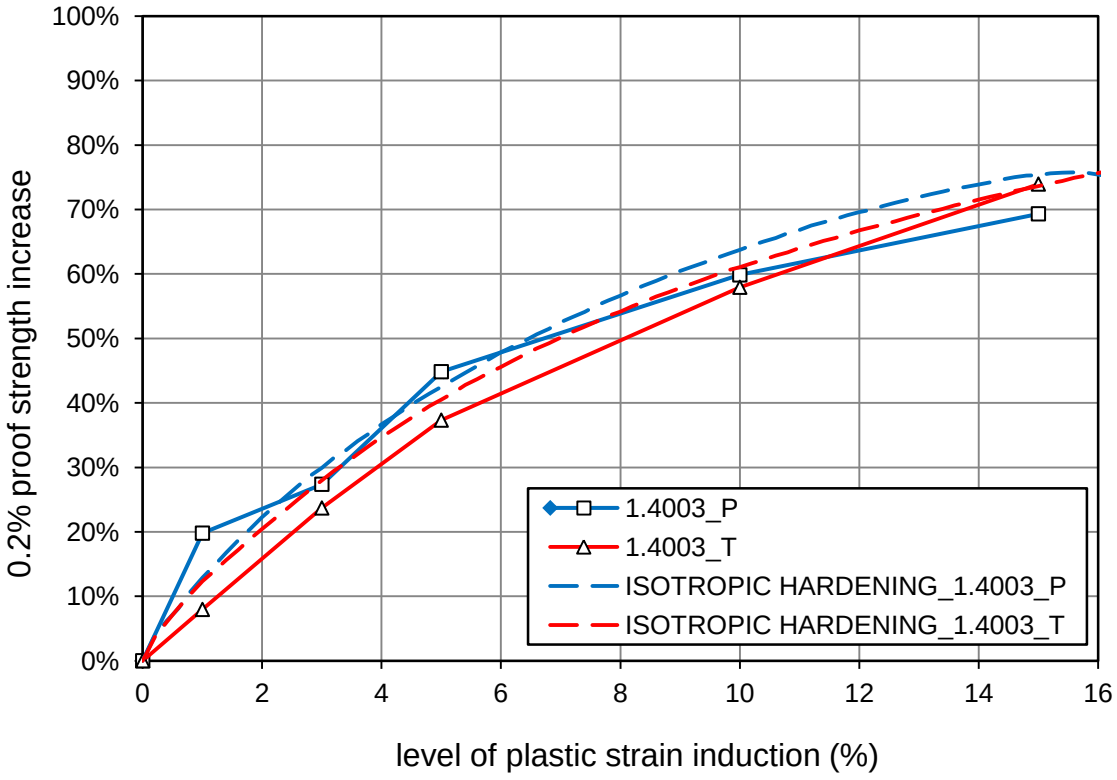

Figure 4.15 *Comparison of the measured strain hardening with the isotropic hardening model for the 1.4003 grade.*

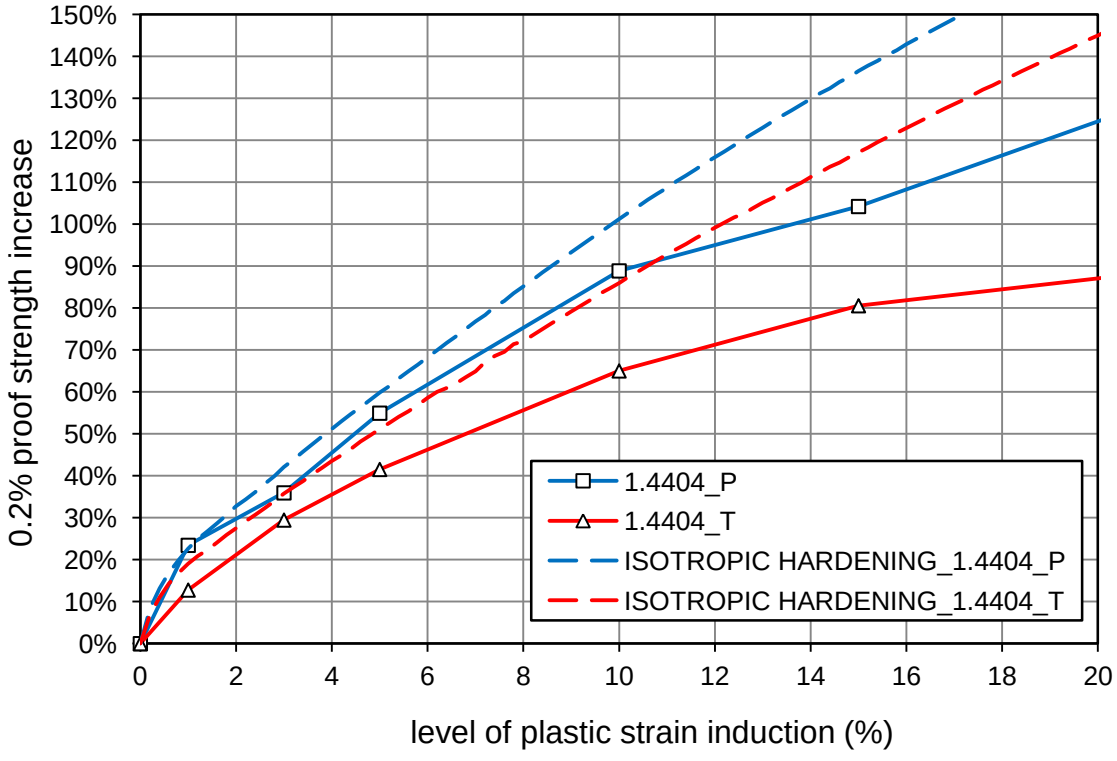

Figure 4.16 *Comparison of the measured strain hardening with the isotropic hardening model for the 1.4404 grade.*

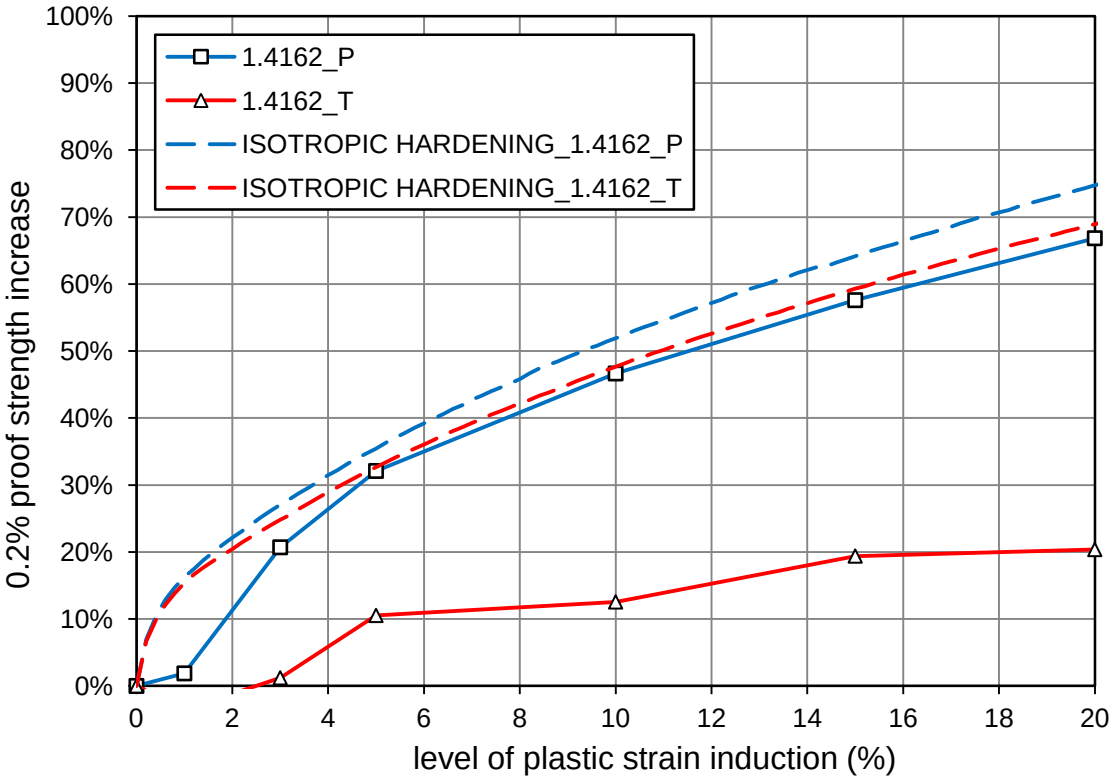

Figure 4.17 *Comparison of the measured strain hardening with the isotropic hardening model for the 1.4162 grade.*

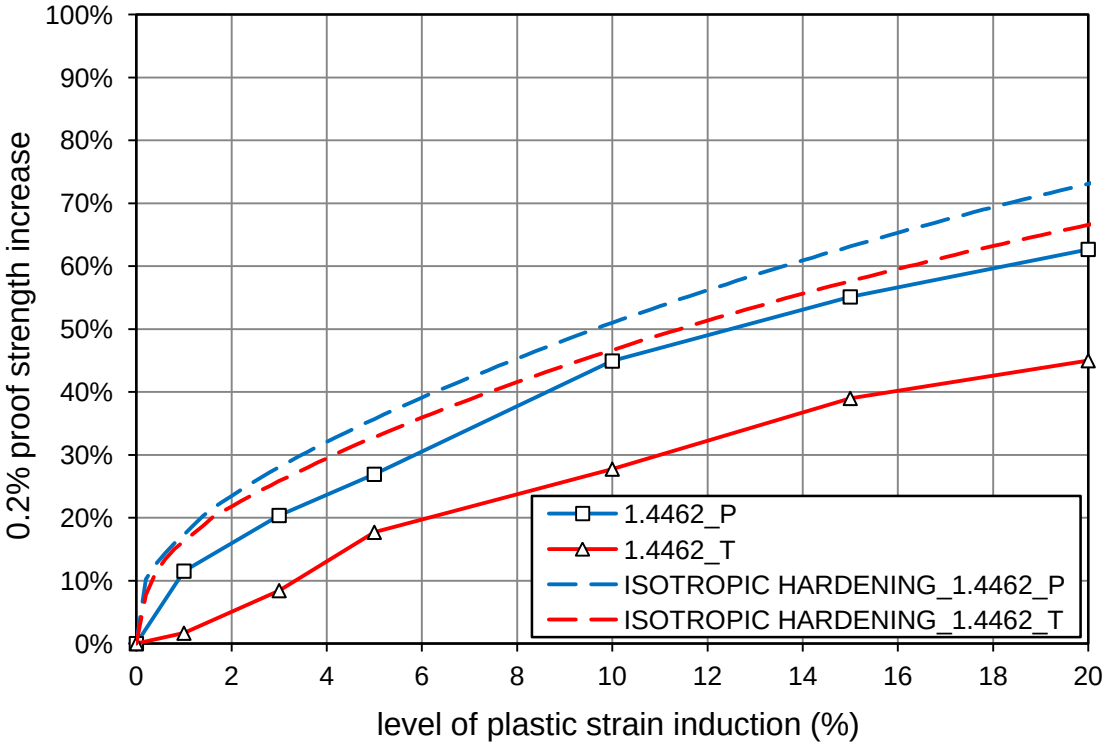

Figure 4.18 *Comparison of the measured strain hardening with the isotropic hardening model for the 1.4462 grade.*

Results provide relatively good agreement only in case of the isotropic hardening for the direction parallel to the previous elongation and confirm recent conclusions of non-suitability of the isotropic hardening for stainless steel. The effect of anisotropy is significant especially for the lean duplex 1.4162 grade.

Regarding to the small strain level for the 0.2% proof strength differences between true strain and true stress are negligible.

Entirely different case is the ultimate strength issue. Considering the true stress and strain there is no significant increase in the ultimate strength (see Figure 4.19) in contrast to the engineering form of these values (see Figure 4.20). This observation indicates the effect of partial change of the microstructure of the virgin material does not sufficiently affect resultant true ultimate strength which remains almost constant. This fact is a proof of ductility decrease, as well as move of the strain value at reaching the ultimate strength. Assuming following:

$$\sigma_{u,true,virgin} = \sigma_{u,true,pl} \tag{4.5}$$

The relationship of ultimate tensile strength $\sigma_{u,pl}$ dependency is given as follows:

$$\sigma_{u,pl} = \sigma_{u,virgin} \cdot \frac{1+\varepsilon_{tu,virgin}}{1+\varepsilon_{tu,pl}} \qquad \sigma_{u,pl} > \sigma_{u,virgin} \text{ and } \quad \varepsilon_{tu,virgin} > \varepsilon_{tu,pl} \tag{4.6}$$

where $\sigma_{u,true,virgin}$ is the true ultimate tensile strength of a initial sheet; $\sigma_{u,true,pl}$ is the true ultimate tensile strength of a stretched sample, $\sigma_{u,virgin}$ is the ultimate tensile strength in engineering values of a initial sheet; $\sigma_{u,pl}$ is the ultimate tensile strength of a stretched sample in engineering values; $\varepsilon_{tu,virgin}$ is the strain at the ultimate tensile strength in engineering value of a initial sheet and $\varepsilon_{tu,pl}$ the strain at the ultimate tensile strength in engineering value of a stretched sample.

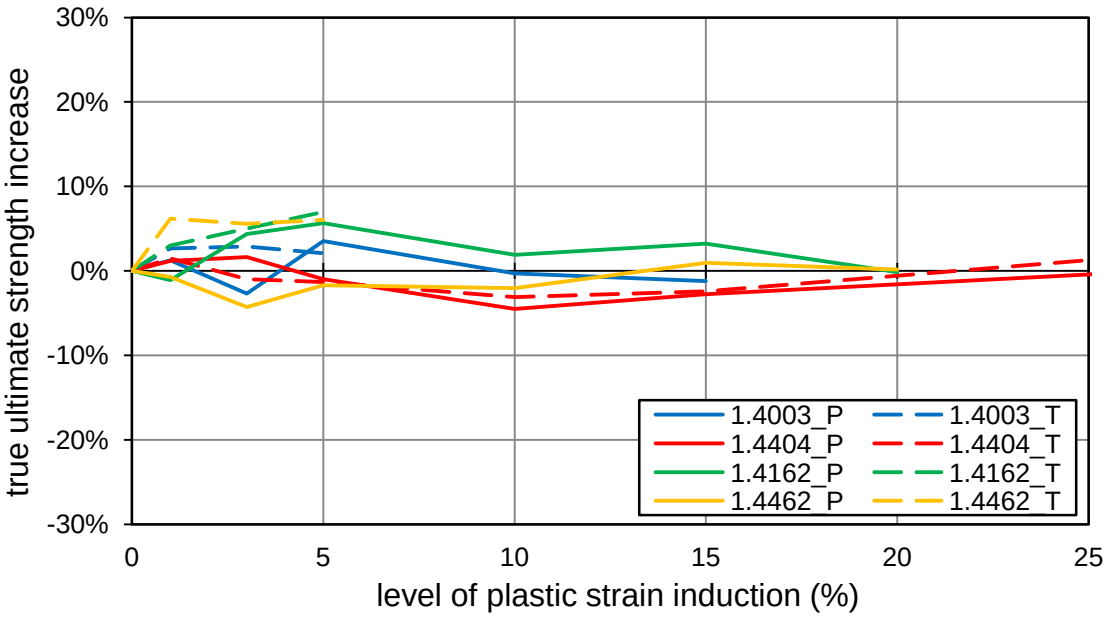

Figure 4.19 *Change of the ultimate strength according to the level of plastic strain induction with respect to the true values of stress and strain.*

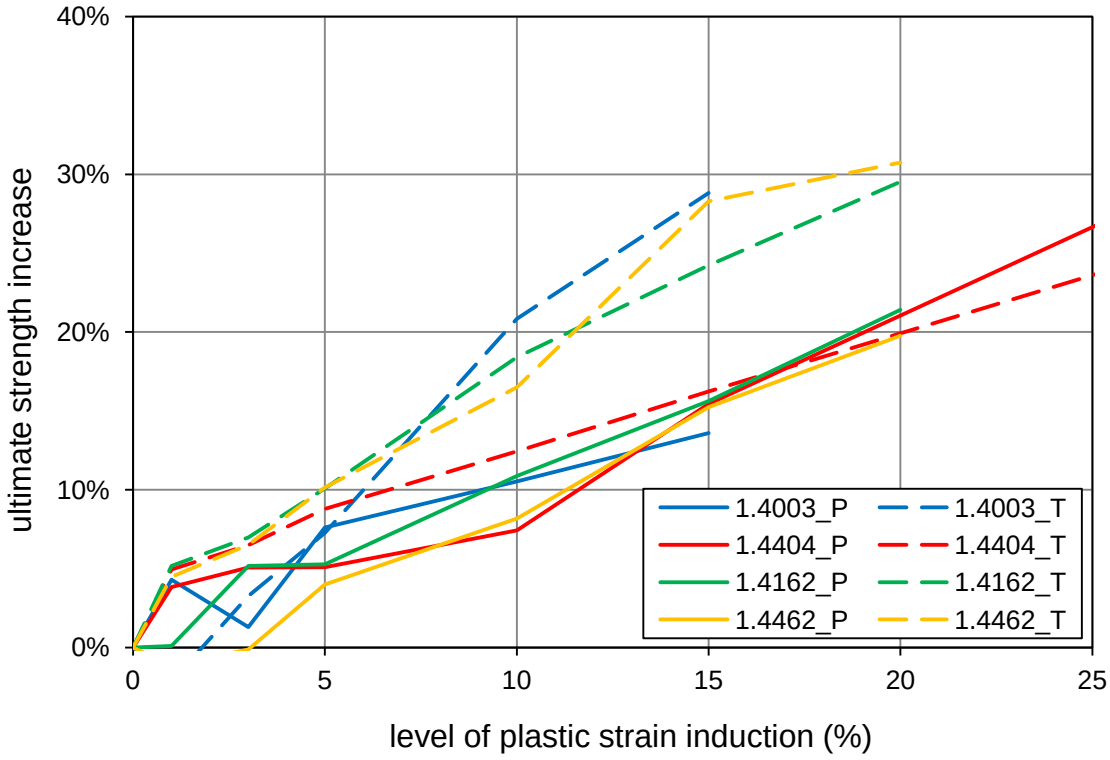

Figure 4.20 *Change of ultimate strength according to the level of plastic strain induction with respect to engineering values of stress and strain.*

Ductility decrease is significant for all investigated grades as it is shown in Figure 4.21. The largest decrease is exhibited by the ferritic grade in contrast to the austenitic grade with the smallest effect of cold-working affecting the ductility. Values for the duplex and lean duplex grade lie within the area bounded by the ferritic grade from the bottom and the austenitic grade from the top. The fact reflects the ductility of the virgin material. Ferritic grades exhibit the lowest values, following by the duplex and lean duplex grades. Austenitic grades are well-known for their ability to be cold-formed due to the high ductility in general and therefore it is not surprise that they exhibit the highest values among all tested grades.

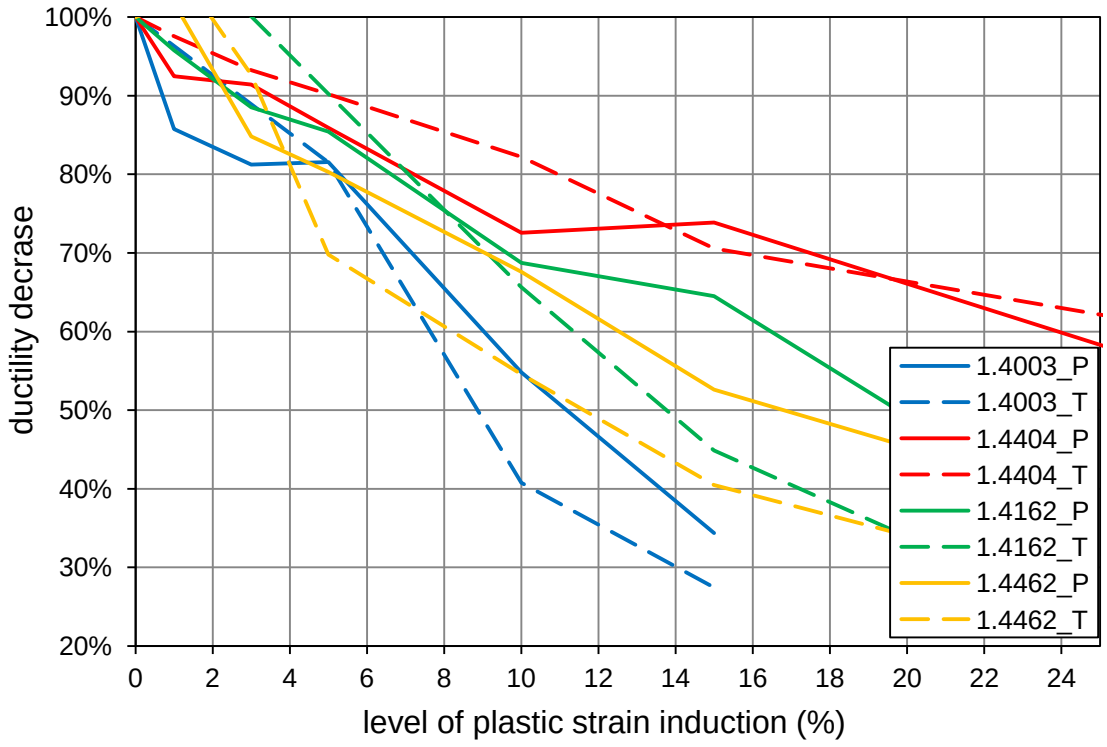

Figure 4.21 *Ductility decrease dependency on the level of plastic strain induction.*

Following figures describe ductility change dependency on the induced plastic strain and original value of ductility. It seems there is a linear relationship describing the decrease of ductility and the induced strain. If the basic assumption (stated bellow) is valid the slope of the linear regression function (a) will be evaluated as 1.0.

$$\varepsilon_{\mathrm{f}} - \varepsilon_{\mathrm{pl,i}} = a \cdot \varepsilon_{\mathrm{f,i}} \tag{4.7}$$

where
ε_{f} is the value of ductility of the unformed material,
$\varepsilon_{\mathrm{pl,i}}$ is the induced plastic strain,
$\varepsilon_{\mathrm{f,i}}$ is the ductility of the formed sample with induced plastic strain $\varepsilon_{\mathrm{pl,i}}$.

This assumption is virtually correct for all investigated grades in case of the uniaxial tensional hardening. The main task is to check the possibility of employing this observation for the structural sections properties.

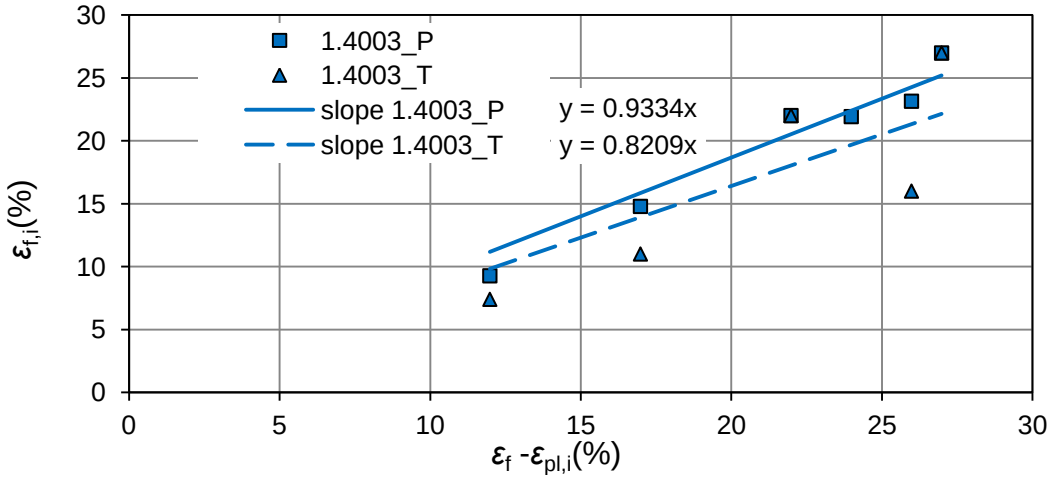

Figure 4.22 *Ductility dependency on the level of plastic strain induction and the original value of ductility for 1.4003.*

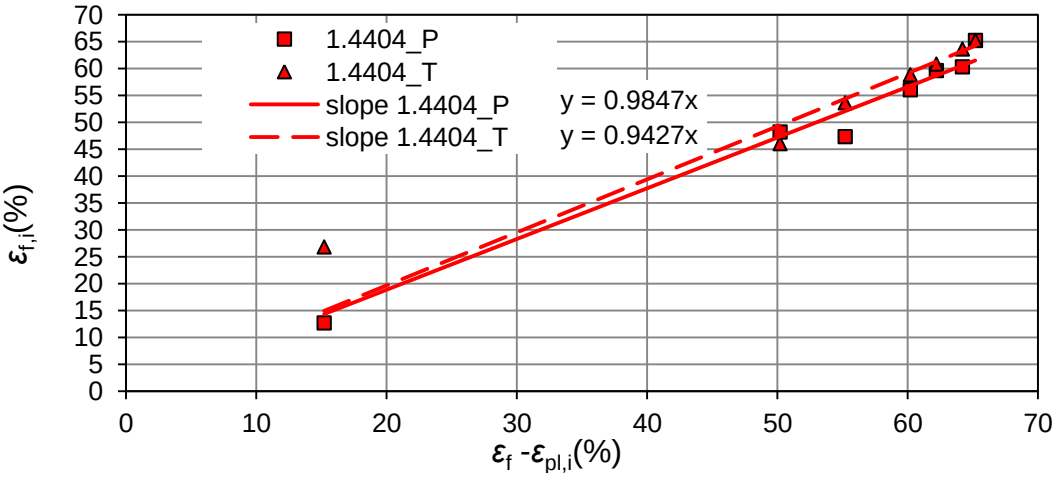

Figure 4.23 *Ductility dependency on the level of plastic strain induction and the original value of ductility for 1.4404.*

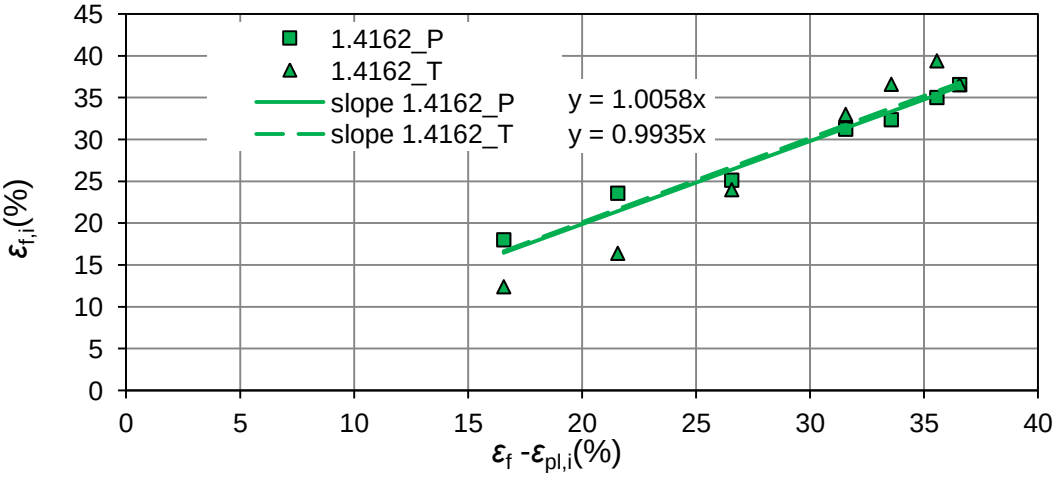

Figure 4.24 *Ductility dependency on the level of plastic strain induction and the original value of ductility for 1.4162.*

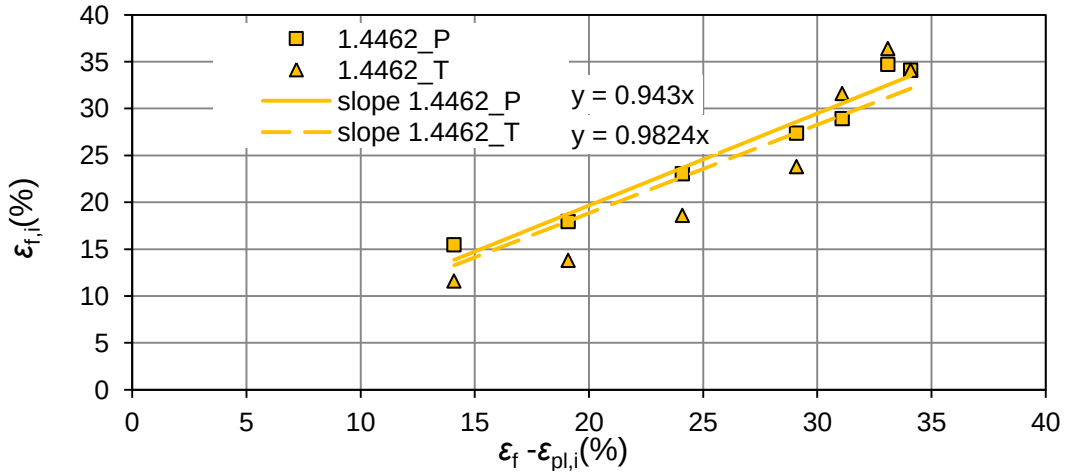

Figure 4.25 *Ductility dependency on the level of plastic strain induction and the original value of ductility for 1.4462.*

Also decrease of the parameter of nonlinearity is evident from Figure 4.26. The stress strain diagram of coupons with induced plastic strain exhibits more stiffness before the 0.2% proof strength and sharper intermediate area beyond the 0.2% proof strength.

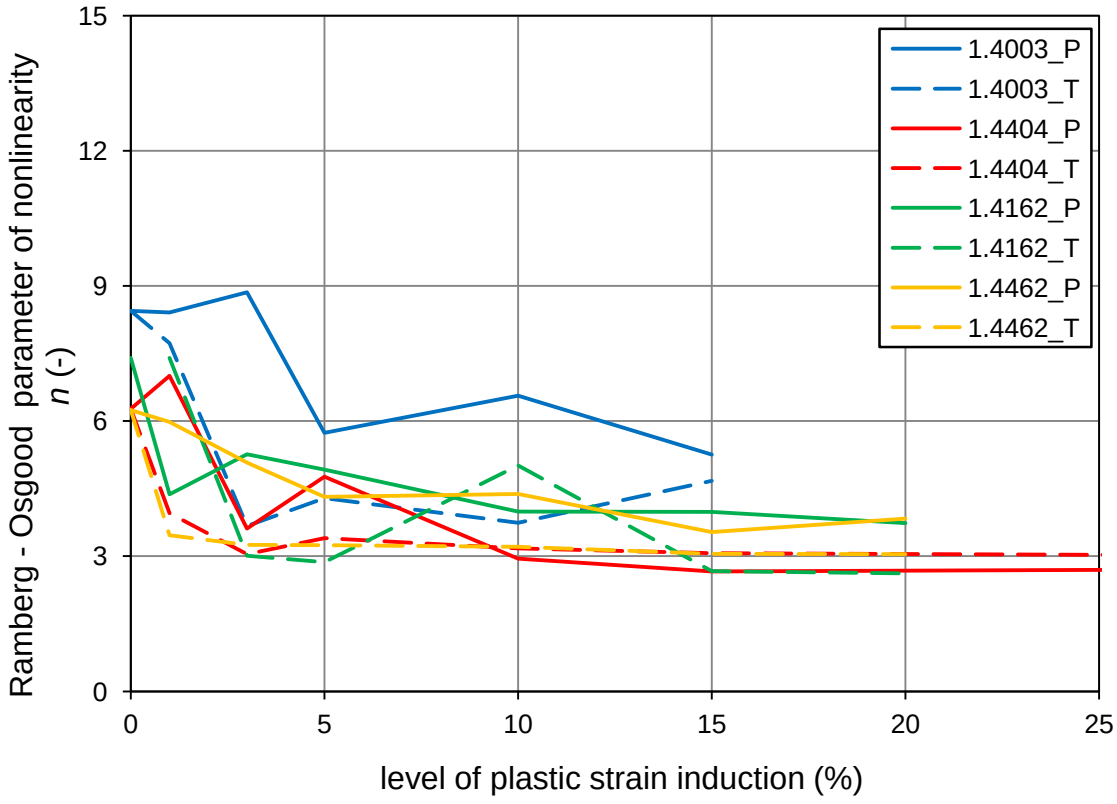

Figure 4.26 *Decrease of parameter of nonlinearity n.*

Similar to the true ultimate strength there is no significant change in the initial modulus of elasticity with respect to the different levels of induced plastic strain as it is shown in Figure 4.27. This was observed for all investigated grades.

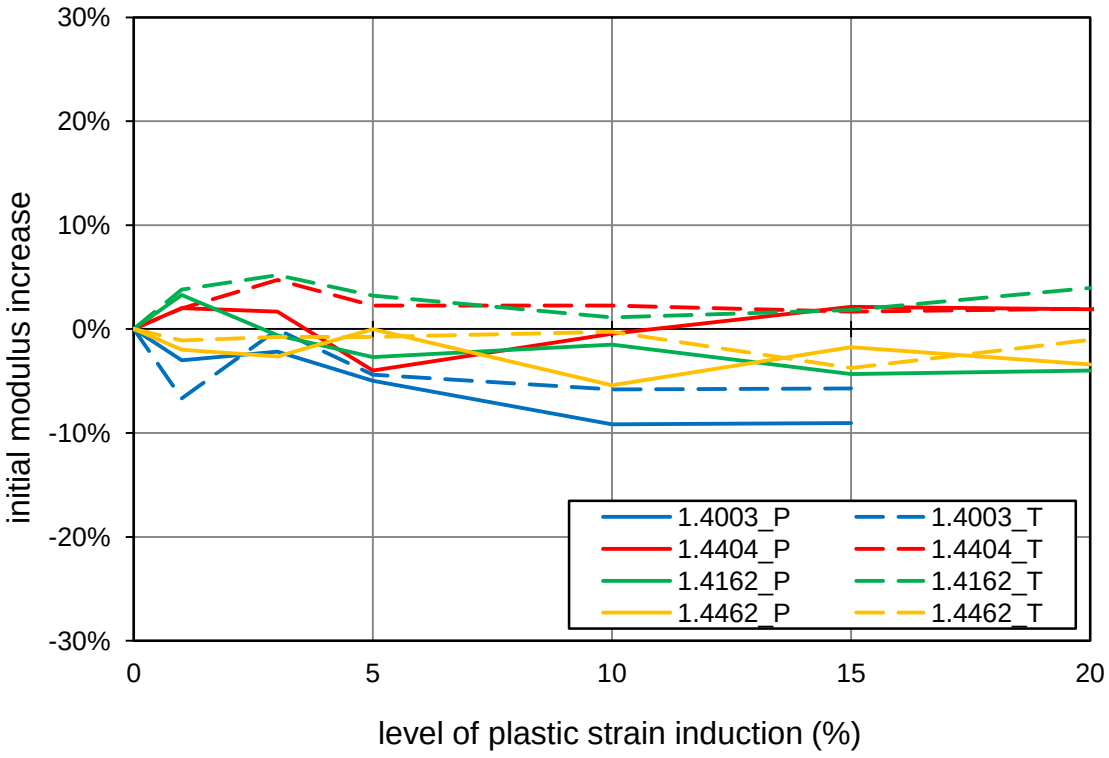

Figure 4.27 *Change of the initial modulus of elasticity according to the level of plastic strain induction.*

As Rossi et al.´s investigations [8] should be the most relevant a comparison of the predictive formulas and new test data were published. Average values of essential parameters of coupons cut out from the sheet in the direction of rolling and perpendicular to the rolling direction (see Table 4.1) were used both for basic material properties and predictive formulas as any mill certificate was not obtainable.

Expression for the strain from Eq. (3.80), resp. (3.81) is given by:

$$\left(\varepsilon_{\mathrm{f,av}} + \varepsilon_{\mathrm{t},0.2}\right), \text{ resp. } \left(\varepsilon_{\mathrm{c,av}} + \varepsilon_{\mathrm{t},0.2}\right) \tag{4.8}$$

For comparison purposes it is expressed as:

$$\left(\varepsilon_{\mathrm{pl,i}} + \varepsilon_{\mathrm{t},0.2}\right) \tag{4.9}$$

where
$\varepsilon_{\mathrm{pl,i}}$ is induced plastic strain (i.e. $\varepsilon_{\mathrm{pl,i}} \in (0.01; 0.15 \text{ or } 0.20 \text{ or } 0.5)$.

It should be noted that instead of $\varepsilon_{\mathrm{t},0.2}$ there should be used strain $\varepsilon_{t,i}$ at particular plastic strain, but the differences are negligible. Figures display dependency of the proof strength increase ($\sigma_{0.2}/\sigma_{0.2,\mathrm{O}}$-1) on the plastic strain level, where $\sigma_{0.2,\mathrm{O}}$ denotes the average value of the 0.2% proof strength of the virgin sheet according to Table 4.1. "P" mark denotes coupons tested parallel to the previous elongation. "T" mark denotes coupons tested transverse to the previous elongation (see Figure 4.9 both of "P" and "T" curve were calculated on basis of the average value from coupons cut out from the sheet in the rolling direction and perpendicular to the rolling direction. "PREDICTION 0.85"

denotes values obtained from the predictive formula. “PREDICTION” denotes values obtained from the predictive formula without the factor 0.85 which involves a 0.90 factor regarding variability of results and a 0.95 factor regarding the nonsymmetry effect as it is stated in section 1.4.

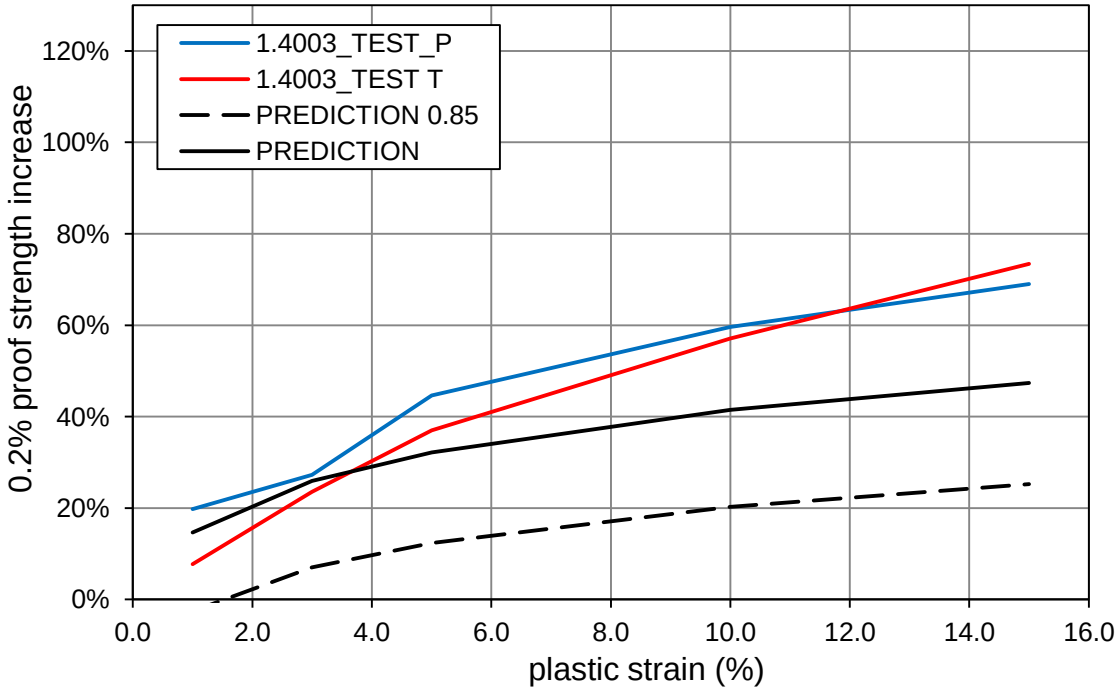

Figure 4.28 *Comparison of the measured proof strength increase and predicted proof strength increase for the 1.4003 grade.*

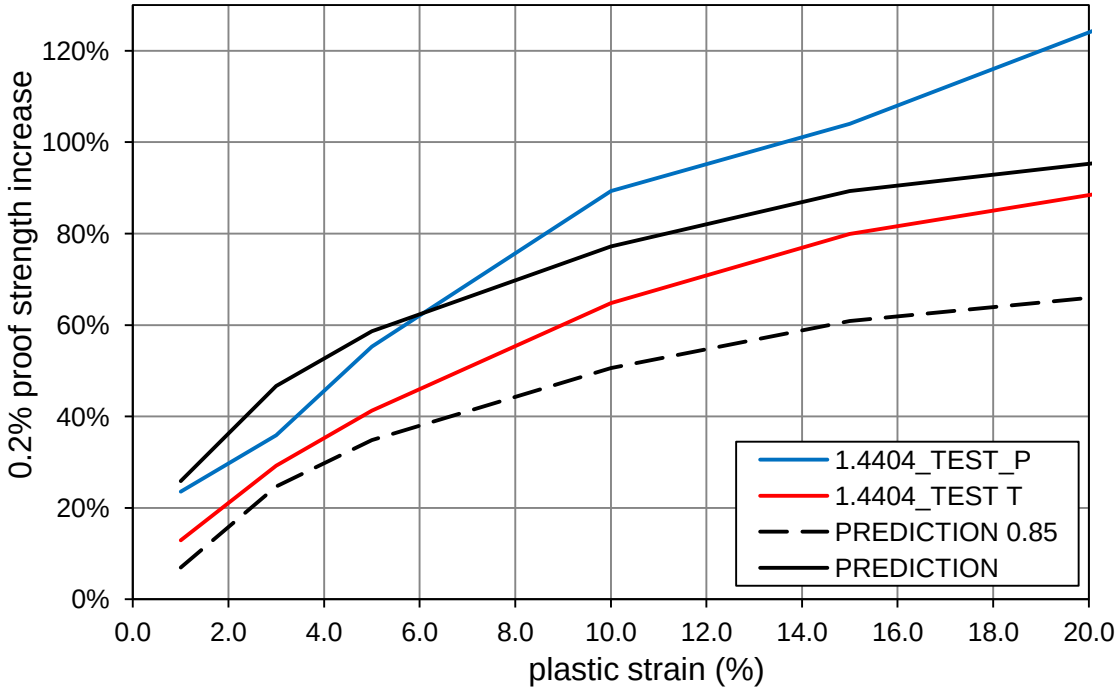

Figure 4.29 *Comparison of the measured proof strength increase and predicted proof strength increase for the 1.4404 grade.*

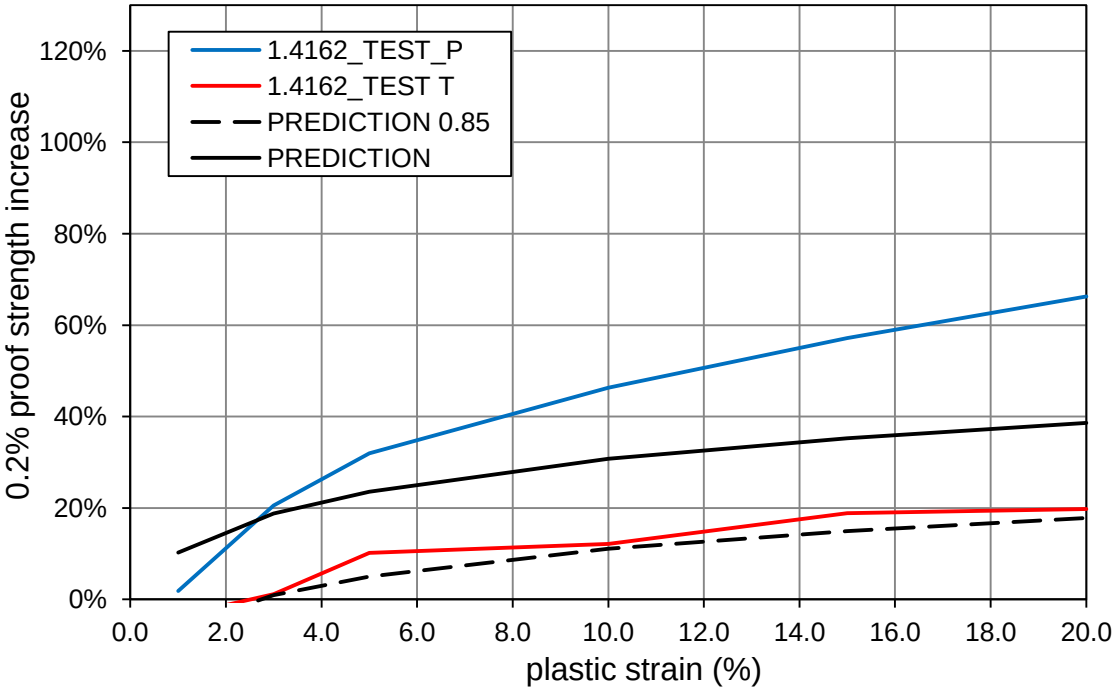

Figure 4.30 *Comparison of the measured proof strength increase and predicted proof strength increase for the 1.4162 grade.*

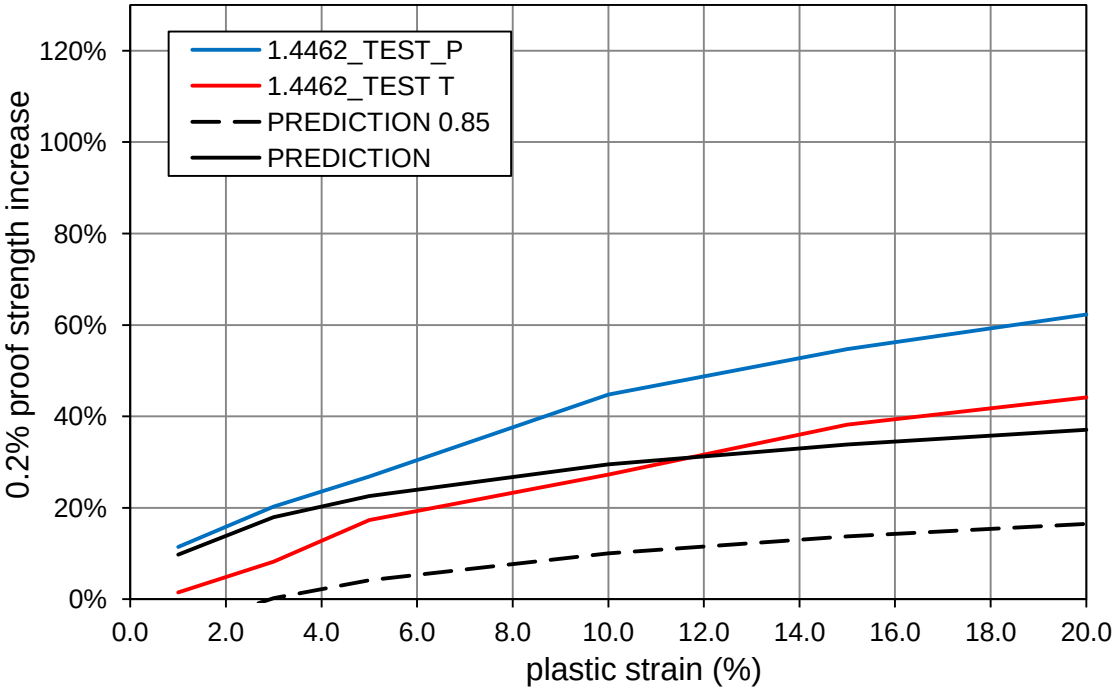

Figure 4.31 *Comparison of the measured proof strength increase and predicted proof strength increase for the 1.4462 grade.*

It seems the predictive relationship is more or less closer to the results of "T" samples although correct comparison is hardly possible due to the complex of other parameters (such as other fabrication steps, different levels of cold-forming in section portions etc.) It corresponds with the idea of acting of similar stresses in a member, i.e. strain induced within fabrication of RHS is transverse to the subsequent direction how a member is mostly used in structure. The slope of the 0.2% proof strength increase trends (except 1.4162 – T) is slightly higher than in case of the predictive curve. 0.2% proof strength enhancement of the ferritic grade exhibits the largest difference between the test and predictive model both for "T" samples and "P" samples. All of the covered materials exhibit higher values of the proof strength than what is proposed by the predictive formula. It can be assumed that due to impossibility of using the mill certificate, the predictions (in this comparison) are less safe than in case of using the mill certificate values as the mill certificate might give lower values of the 0.2% proof strength and the ultimate strength compared to the directly measured values.

4.4 Hot-rolled plate tests

Testing programme consists also of a set of compressive tests of hot rolled plate made of the austenitic grade 1.4404. Thickness of the plate was 4 mm and the specimen geometry according to the same code as in previous testing is depicted in the figure below.

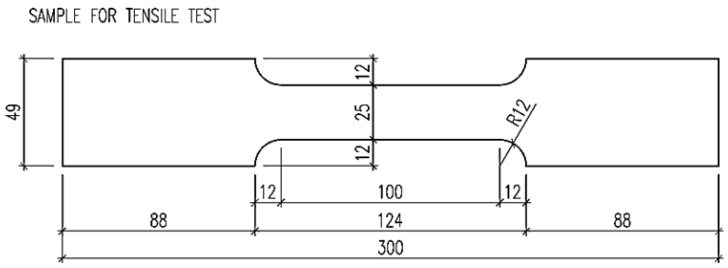

Figure 4.32 *Geometry of the specimen made of hot-rolled plate.*

The set consists of 3 specimens and average values of tests results are summarized in the following table.

Grade	E_0	$E_{0.2}$	$\sigma_{0.2}$	$\sigma_{1.0}$	σ_u	ε_f	$\varepsilon_{pl.u}$	n	$n'_{0.2.1.0}$
	GPa	GPa	MPa	MPa	MPa	%	%	-	-
1.4404	186.0	17.1	308.0	347.1	569.4	62.1	43.3	3.5	2.2

Table 4.10 *Mechanical properties of hot rolled plate.*

These tests proved that there is lot of factors causing high variability of final mechanical properties. Despite the lower strength of hot-rolled steel a higher strength was observed for the same grade. That means little change in chemical composition and way of

manufacturing are probably determining in this issue. It is possible that also hot rolling can affect some strength enhancement as well as cold rolling.

4.5 Annealing

Selected specimens were subjected to annealing process for a comparison of pure strength enhancement during the fabrication and material properties of a sheet after heat treatment. Annealed coupons involve basic coupons for tensile tests of all investigated stainless steel grades (1.4003, 1.4404, 1.4162 and 1.4462). Other annealed specimens were corners and flat faces of SHS and CHS (see Figure 4.33). The annealing process was discussed in detail with specialists from Faculty of Mechanical Engineering at CTU where the heat treatment procedure was also conducted.

First estimation of annealing temperature was made according to recommendations in [5]. Finally the annealing procedure was set as follows:

For the 1.4404, 1.4162 and 1.4462 steel the temperature was set up as 1050 °C for at least 40 min. For the 1.4003 steel the temperature was set up as 730 °C for at least 40 min as well as for other specimens.

All of specimens were subjected to natural cooling on air.

Figure 4.33 *Specimens after annealing (left figure), annealing furnace.*

Comparison of the average values of the annealed specimens and specimens made of the same cold-rolled sheet and grade is stated in Table 4.11 (extended Table 4.1). As for the previous testing, the stated values represent the average from 3 specimens.

Grade	Rolling direction or state	E_0	$E_{0.2}$	$\sigma_{0.2}$	$\sigma_{1.0}$	σ_u	ε_f	$\varepsilon_{pl.u}$	n	$n'_{0.2.1.0}$
		GPa	GPa	MPa	MPa	MPa	%	%	-	-
1.4003	P	198.3	7.5	326.7	357.1	492.3	22.1	18.0	8.4	1.8
1.4003	T	211.9	7.0	343.7	374.5	512.3	31.9	17.6	8.5	1.9
1.4003	A	210.1	-	309.8	309.1	500.2	-	-	-	2.9
1.4404	P	189.0	14.1	259.8	307.3	620.8	61.8	48.7	3.7	2.1
1.4404	T	199.8	11.6	279.0	322.0	635.1	68.6	57.1	8.8	2.3
1.4404	A	192.9	7.1	209.3	253.2	567.7	71.5	40.7	16.4	3.1
1.4162	P	193.3	21.9	551.6	623.7	785.9	37.9	24.1	7.3	3.0
1.4162	T	195.5	22.4	556.5	624.8	765.6	35.2	21.1	7.5	3.1
1.4162	A	196.9	35.1	451.1	517.2	750.9	25.9	-	3.7	3.2
1.4462	P	195.8	25.2	600.1	676.6	843.0	34.3	22.6	6.9	2.9
1.4462	T	210.7	30.0	637.6	722.7	863.7	33.9	20.6	5.6	3.4
1.4462	A	207.6	42.7	509.6	634.9	806.5	28.9	20.8	3.4	3.8

P – test parallel to the rolling direction. T – test transverse to the rolling direction.
A – annealed specimen.

Table 4.11 *Mechanical properties of the cold rolled sheet according to the rolling direction in comparison to the annealed specimens.*

All specimens subjected to the annealing exhibit more or less equal value of the initial modulus as the specimens made of the cold-rolled sheet. For annealed specimens of all grades lower values of the 0.2% proof strength are typical. That is a proof of the expectable assumption.

Comparison of the results for the austenitic grade is depicted in Figure 4.34. As it is stated above hot-rolled plate exhibits higher strength values despite of the cold-rolling effect.

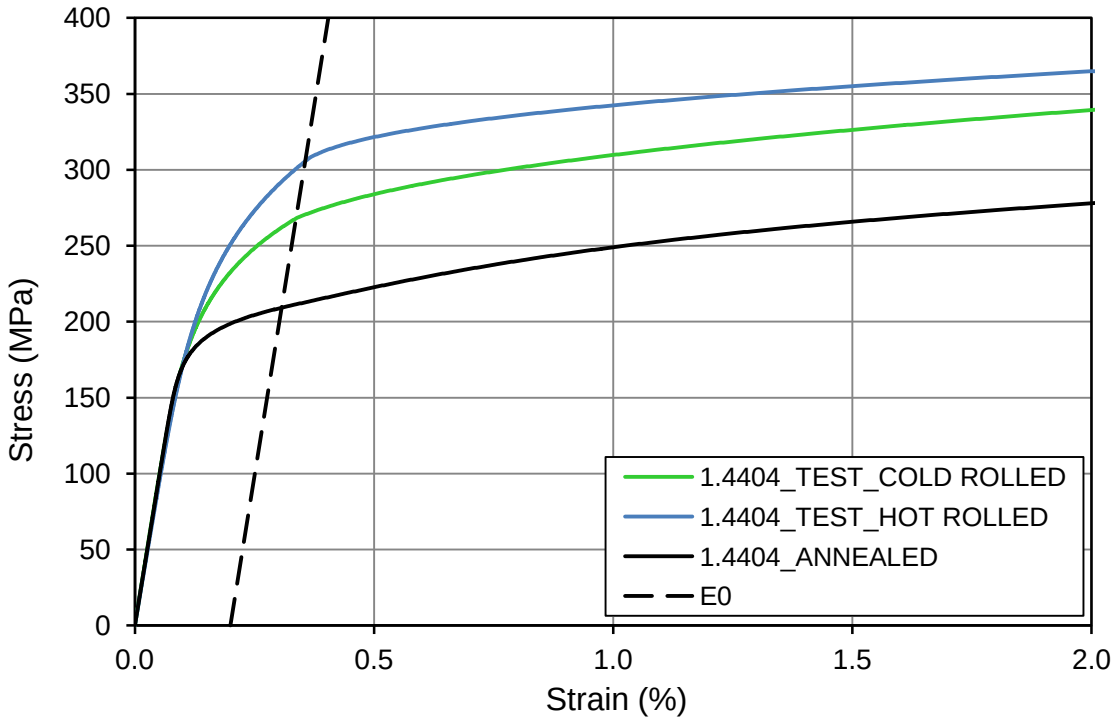

Figure 4.34 *Results comparison of the 1.4404 grade in the different treatment conditions.*

Annealed specimens of the ferrtitic 1.4003 grade exhibit dissimilar stress-strain behaviour. After the annealing the stress-strain curve refers to common carbon steel material. The difference between the diagram of the cold-rolled and annealed material is apparent from the Figure 4.35. As for the previous cases, the 0.2% proof strength is lower for the annealed material, however there is large plastic plateau (typical for carbon steel) with a following hardening stage. The annealed material also exhibits no rounded curve likewise the carbon steel. This behaviour was observed for all 3 annealed ferritic specimens. The reason for these results is probably the procedure of annealing and recrystallizing of the virgin material. Thus the annealed material is not appropriate for any validations at all.

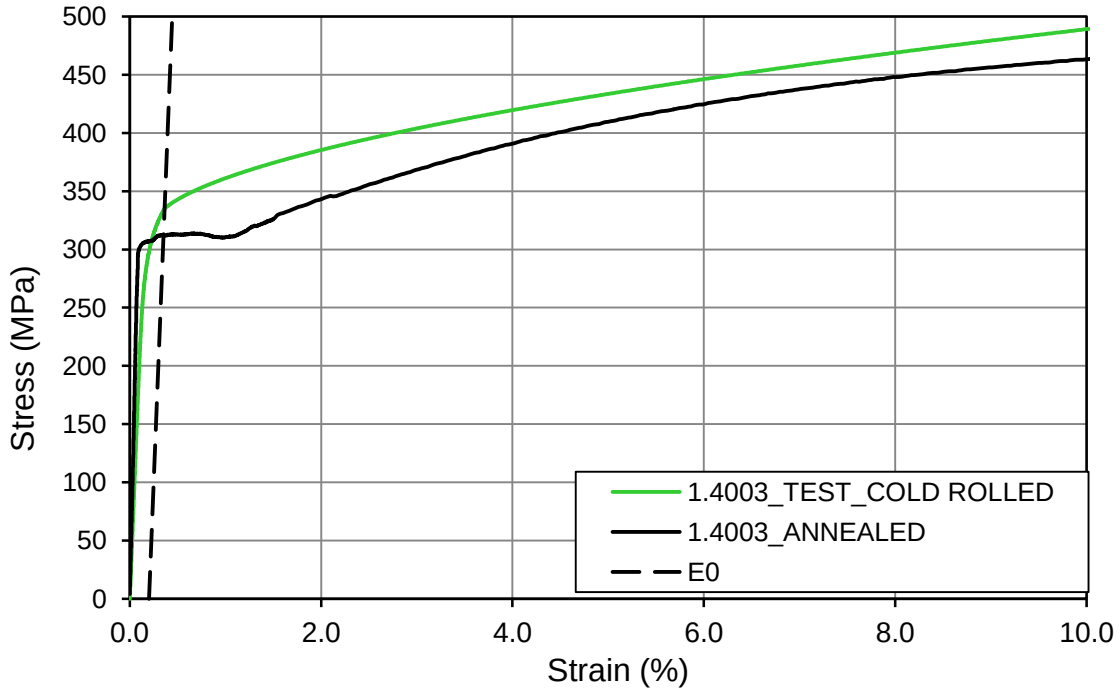

Figure 4.35 *Results comparison of the 1.4003 grade in different treatment conditions.*

4.6 Part of section tests

Tensile tests of flat faces and corners made of SHS and specimens prepared from circular hollow section (CHS) serve for the analytical model validation. Preparation of the coupons is shown in Figure 4.36 and Figure 4.37.

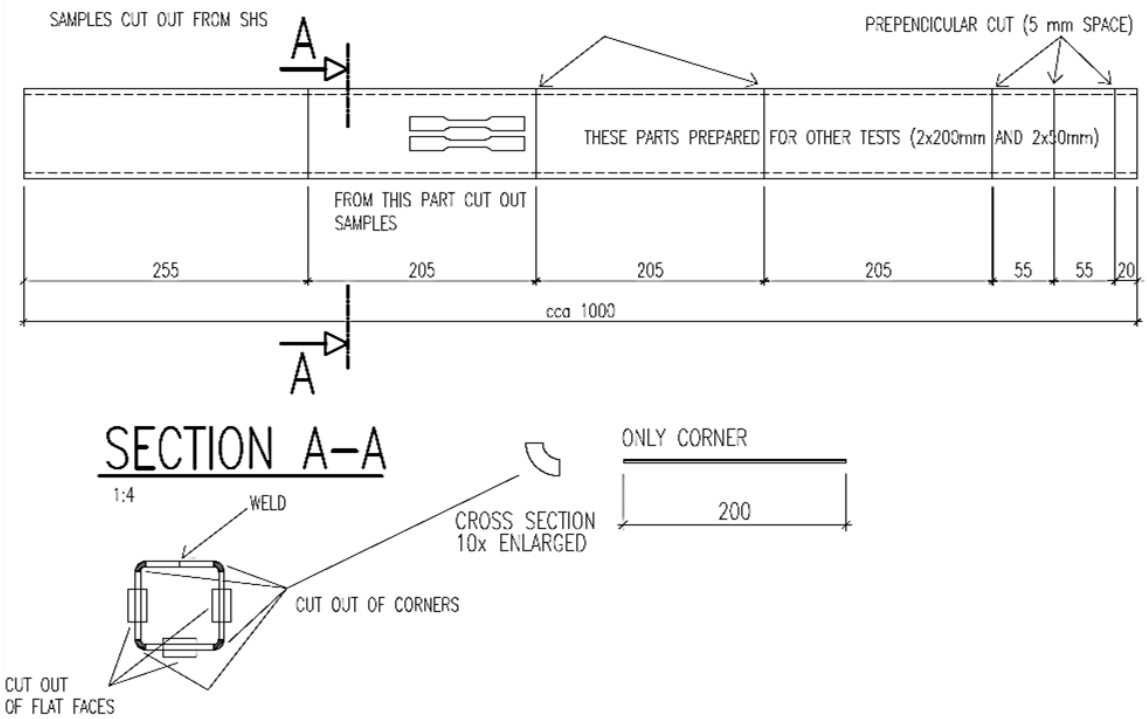

Figure 4.36 *Preparation of the specimens made of the SHS sections.*

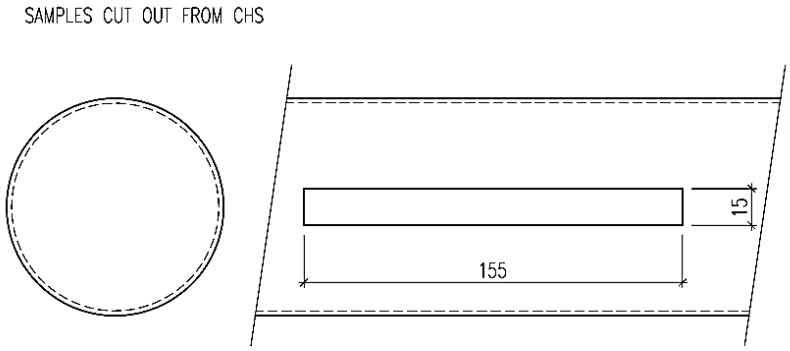

Figure 4.37 *Preparation of the specimens made of circular hollow sections.*

Test set-up consists of SHS 80x80x3 and SHS 80x80x5 and of 3 CHS, namely CHS 168.3x2, CHS 88.9x2 and CHS 42.4x2, all made of austenitic 1.4404 grade.

Results are stated in Table 4.12. The CHS 42.4x2 annealed specimen and virgin specimens after tests are shown below.

Figure 4.38 *CHS 42.4x2 specimens.*

The test programme involves 3 specimens for flat faces, 3 specimens for corners and one annealed corner specimen of each SHS section. CHS sections are represented by 3 virgin and 3 annealed specimens. Stated results are provided by averaging. Not all specimens were successfully tested due to difficulties with clamping into the testing machine. The non-representative values are not stated and marked by hyphen.

SECTION	Part of section	E_0	$E_{0.2}$	$\sigma_{0.2}$	$\sigma_{1.0}$	σ_u	ε_f	$\varepsilon_{pl.u}$	n	$n'_{0.2.1.0}$
		GPa	GPa	MPa	MPa	MPa	%	%	-	-
SHS 80x3	F	183.1	29.8	397.1	465.3	627.6	44.1	36.5	3.1	4.3
SHS 80x3	C	210.8	66.3	681.6	714.1	741.9	10.4	15.7	14.4	4.2
SHS 80x3	AC	-	-	246.0	284.0	579.9	-	-	-	-
SHS 80x5	F	190.5	29.3	448.1	516.2	627.4	53.8	-	3.4	4.5
SHS 80x5	C	215.3	17.5	726.3	764.5	771.8	16.9	4.6	15.4	6.2
SHS 80x5	AC	-	5.1	235.4	260.9	537.5	54.1	51.2	-	1.7
CHS 42.4x2	-	190.9	18.5	319.7	363.3	582.5	47.2	24.2	4.7	2.2
CHS 42.4x2	A	210.7	9.3	185.6	230.7	525.4	72.6	35.5	10.5	2.3
CHS 88.9x2	-	172.7	16.1	348.4	388.8	610.1	59.1	45.1	5.8	2.2
CHS 88.9x2	A	169.5	12.6	230.6	281.4	541.0	43.6	41.4	7.9	2.8
CHS 168.3x2	-	183.6	15.1	339.9	379.8	636.0	40.1	25.0	4.8	2.0
CHS 168.3x2	A	177.8	13.3	208.6	252.8	548.3	54.1	50.0	5.5	2.5

F – flat face. C – corner. AC – annealed corner specimen.

Table 4.12 *Mechanical properties of the specimens made of the sections.*

The mill certificate was known only for SHS. The mill certificate defines the 0.2% proof strength, the 1.0% proof strength and the ultimate strength for both SHS as follows:

$\sigma_{0.2}$	$\sigma_{1.0}$	σ_u
MPa	MPa	MPa
281.0	310.0	581.0

Table 4.13 *Mechanical properties for the SHS declared by the mill certificate.*

For modelling purpose other mechanical properties were assumed as it is stated below:

E_0	$E_{0.2}$	n	$n'_{0.2.1.0}$
GPa	GPa	-	-
195.0	22.2	5.6	1.9

Table 4.14 *Other assumed mechanical properties for the SHS.*

Stress-strain curve of the CHS virgin material was not modelled due to the lack of the mill certificate.

Charts comparing the stress-strain curves of the particular section parts are depicted in following figures.

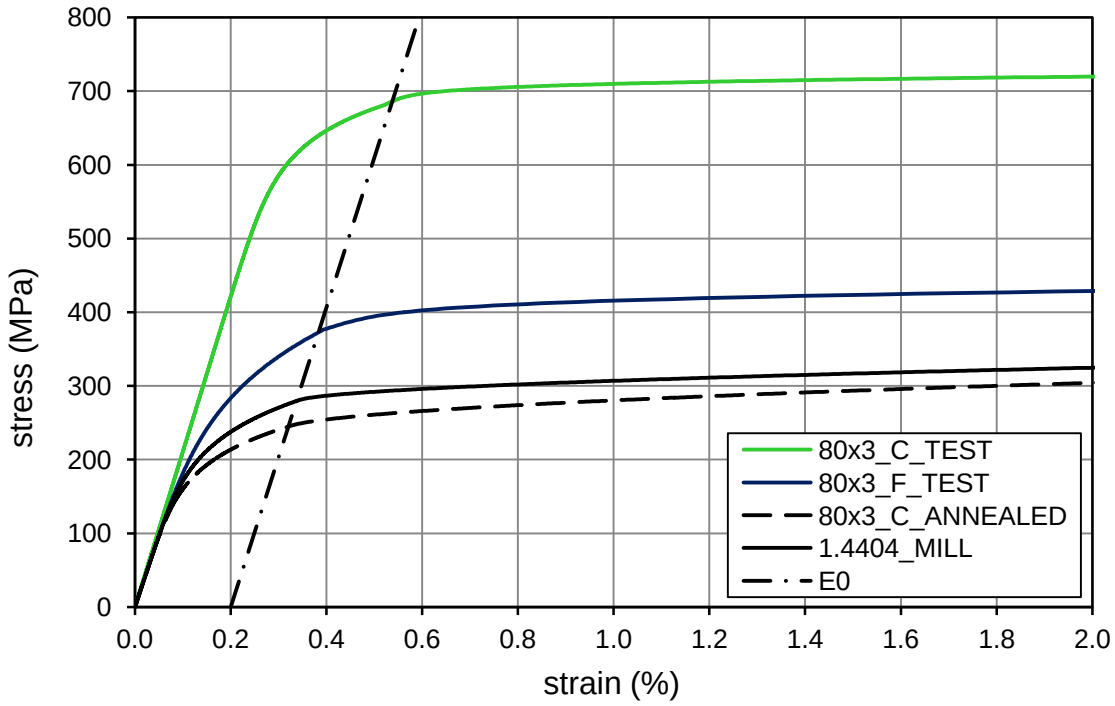

Figure 4.39 *Comparison of the stress-strain curve for the different parts of the SHS 80x3 section with the assumed virgin material (mill) and the annealed corner specimen.*

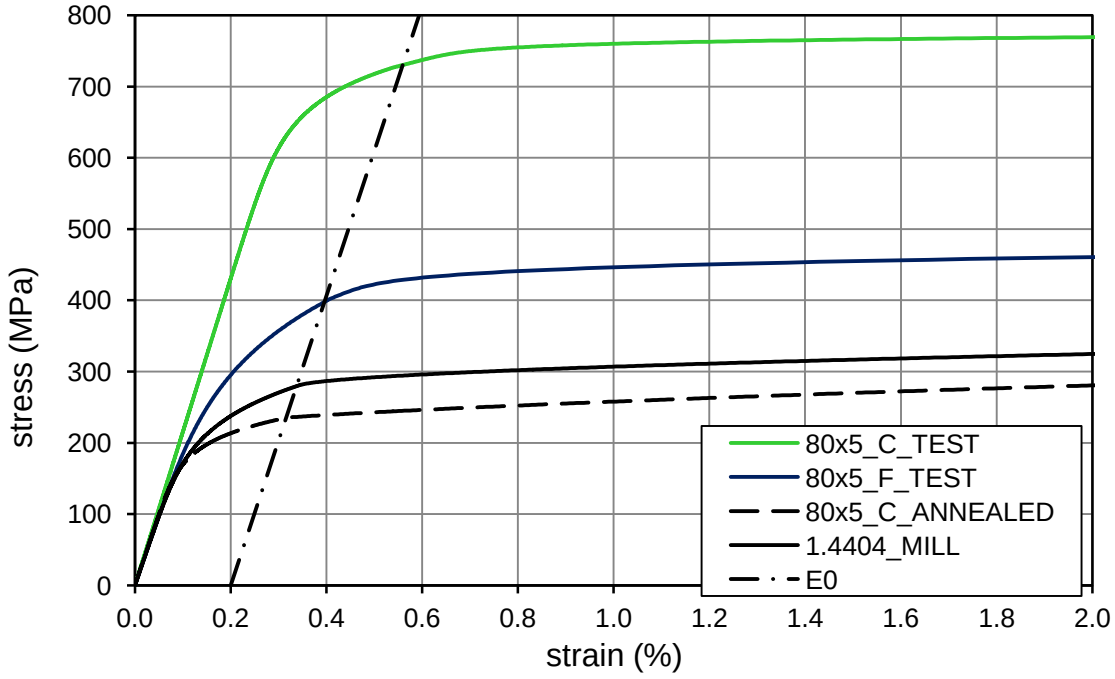

Figure 4.40 *Comparison of the stress-strain curve for the different parts of the SHS 80x5 section with the assumed virgin material (mill) and the annealed corner specimen.*

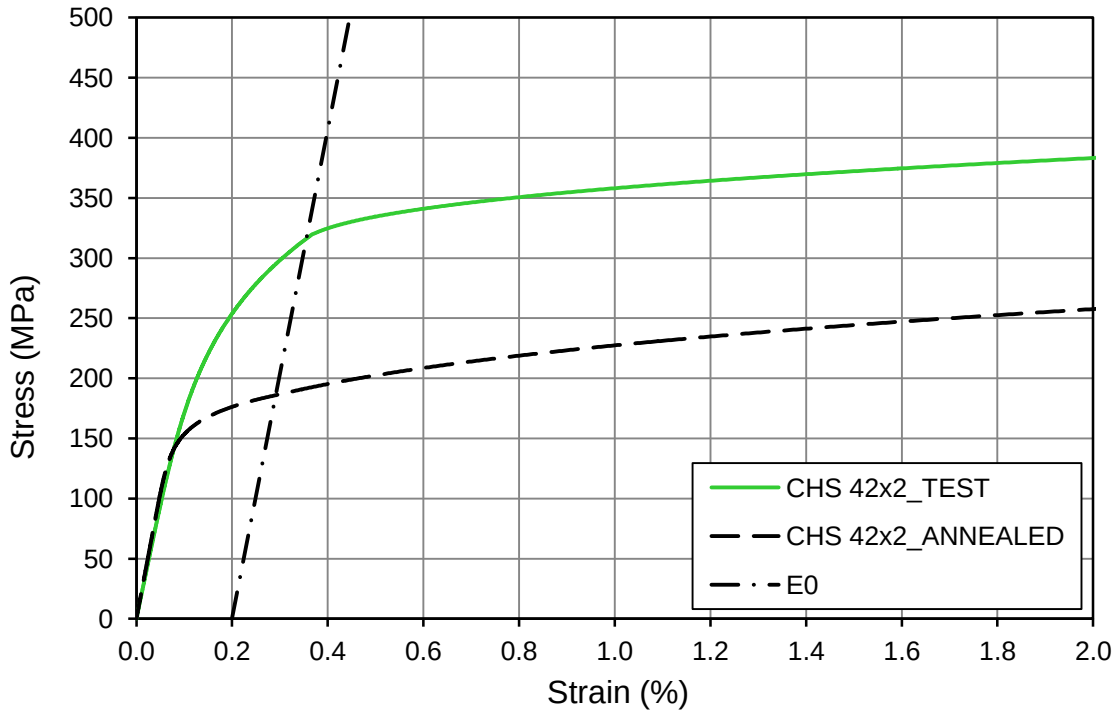

Figure 4.41 *Comparison of the stress-strain curve for the parts of the CHS 42.4x2 section with the annealed specimen.*

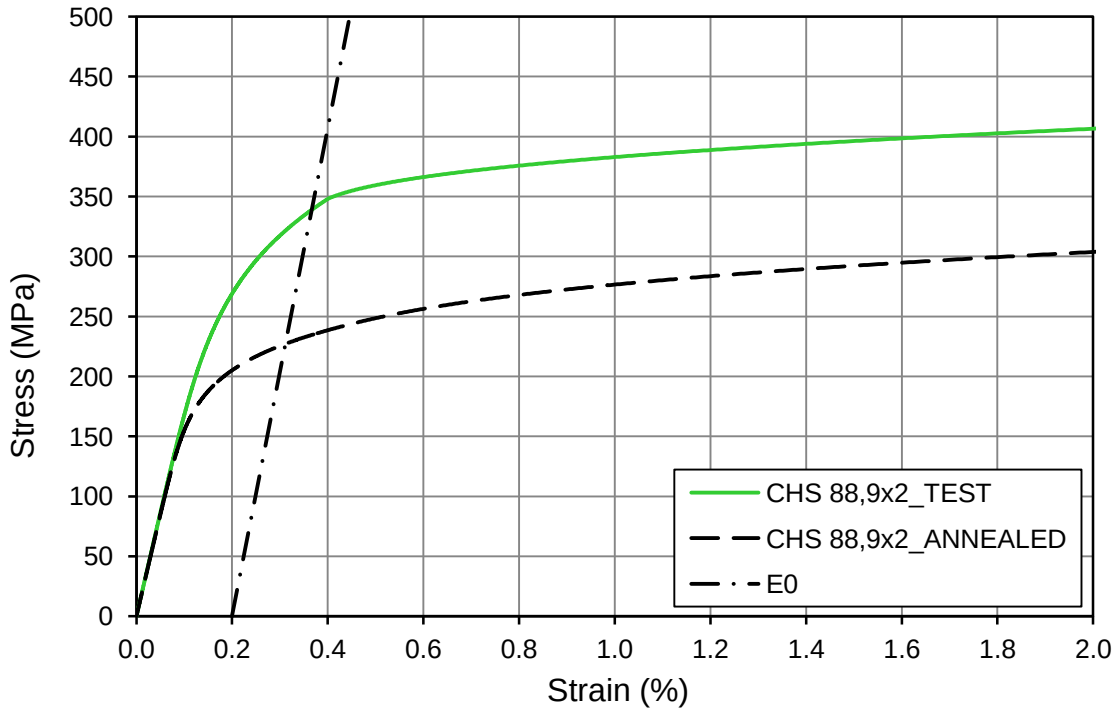

Figure 4.42 *Comparison of the stress-strain curve for the parts of the CHS 88.9x2 section with the annealed specimen.*

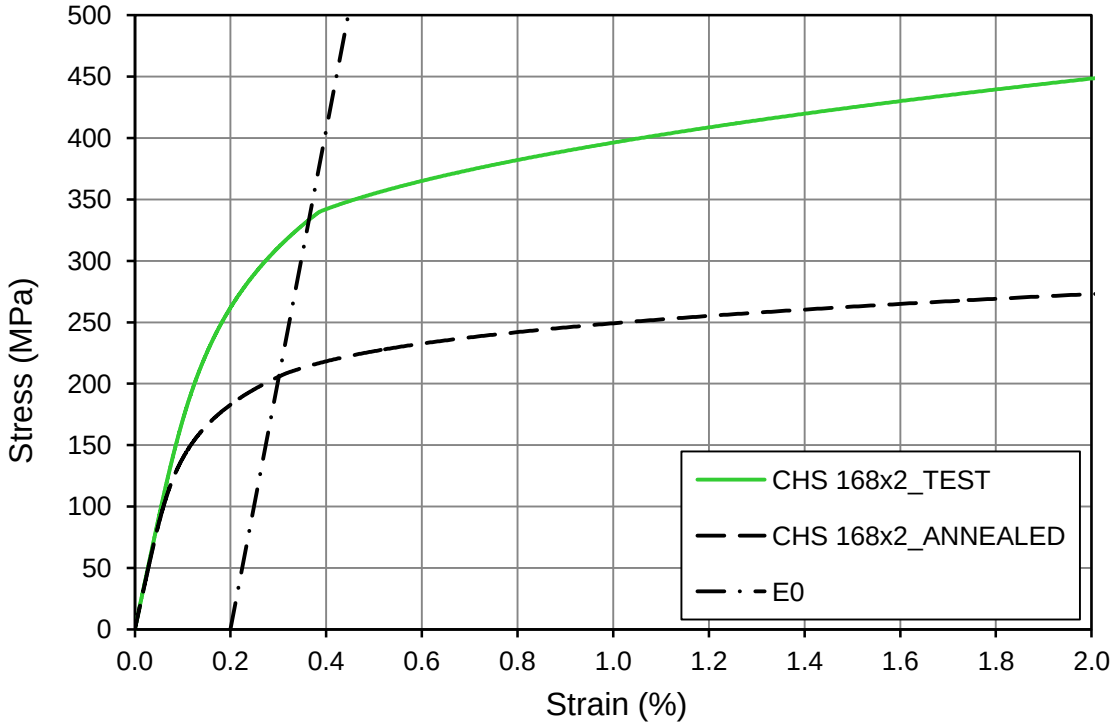

Figure 4.43 *Comparison of the stress-strain curve for the parts of the CHS 168.3x2 section with the annealed specimen.*

The set of specimens prepared from the sections is not very extensive. Nevertheless results obtained from the section testing show strength enhancement in the corners during all fabrication steps can reach almost 300% in comparison with the annealed material. The 0.2% proof strength of a corner to the 0.2% proof strength of a flat face ratio is 1.62, 1.72 respectively. Opposite to the assumed 0.2% proof strength of the virgin material the tested specimens exhibit at least 30% enhancement and there is no significant change in this effect in respect to the inner radius of circle hollow sections. It is necessary to mention there was no mill certificate for the CHS and despite to the fact the material for tubes is the same 1.4404, each section can exhibit different mechanical properties. 0.2% proof strength enhancement during fabrication of CHS (difference between annealed and section test) was 51% – 72%. Other mechanical properties are rather not representative due to the low count of specimens.

4.7 Conclusions

The presented results prove significant changes in many properties caused by the previous plastic forming. Also the influence of the forming direction in respect to the testing direction is clearly visible.

Current test results show particularly:

- Dependency of material properties on the induced plastic deformation was observed.

- Effect of anisotropy is different for the cold-rolling of a sheet and uniaxial cold-forming of a specimen made of a sheet.

- More than 100% increase of the 0.2% proof strength was observed for the austenitic steel in extreme (in case of the uniaxial cold-working of the steel sheet).

- Strength increase is significant for all investigated stainless steel grades (for the ferritic, the ductility may be limiting).

- The higher level of plastic strain induced the higher anisotropy effect is pronounced.

- The 0.2% proof strength is lower for the direction transverse to the previous strain induction.

- Material non-linearity differs according to the forming direction.

- There is no relevant ultimate tensile strength change in terms of the true values of stress and strain within cold-forming.

- There is no significant change of the initial modulus of elasticity within cold-forming.

- Decrease of the ductility corresponding with induced plastic strain and the relatively linear relationship was observed.

- Design expressions provide safe predictions of the proof strength increase, though the comparison of the test data to the recent predictive formulas does not provide perfect agreement.

- Difference of 5% – 33% between the annealed and virgin material for the 0.2% proof strength of the sheet material of all investigated grades was observed.

- In case of the section corner testing, there was observed the 0.2% proof strength enhancement of 300% in comparison with the annealed material.

- The 0.2% proof strength of a corner to the 0.2% proof strength of a flat face ratio 1.62, 1.72 respectively was observed.

The test programme on 160 coupons was executed and its results presented. The main material characteristics and stress-strain curves were also described. The presented strength increase shows, that the influence of cold forming is important not just for the austenitic grades, but also for the other stainless steel grades. However for ferritic grades, the ductility could be limiting. After the plastic strain induction in the specimen corresponding to strain during section cold-forming (in corners typically exceeding ten percent), the 0.2% proof strength could reach even 300% higher values. There is no change of the ultimate strength dependent on the level of cold-forming in terms of the true values of stress and strain (the ultimate strength increase is evident only for engineering values). Higher level of plastic strain induction implies lower values of Ramberg-Osgood nonlinearity parameter (more rounded stress-strain diagram) and ductility as well.

Measured values of mechanical properties serve for further development of the analytical model of the strength increase and a stress-strain behaviour description of a whole cold-formed stainless steel cross-section.

Chapter 5

Analytical part

This section describes an analytical solution for stress-strain response of a cold-formed stainless steel (primarily SHS) section. It allows to derivate the most important mechanical properties such as the 0.2% proof strength, initial modulus of elasticity, parameter of non-linearity, i.e. Ramberg-Osgood model hardening exponent essential for the structure design. The final model is based on the Quach analytical expression for coiling and uncoiling process and further relationships for forming into a circular respectively square hollow section. The solution stated herein employs a planar analysis of the sheet, thus only pure bending of a sheet involving different amounts of straining in the two orthogonal directions is considered with no stresses acting across the thickness. There are employed numerical simulations using Maple 18 software for a whole section stress-strain response evaluating. The preliminary Maple model has been already partially used for material properties estimation of stainless steel and published by Howlader, Jandera and Mařík [59] in 2016. Using mathematical software enables to process large amount of data together with its evaluation by iterating procedures in very favourable way and relatively short time and the resulting code can be easily checked.

5.1 Assumptions

Before proceeding further, there is essential to denote assumptions for further calculations. Assumptions are expressed in clear and simple way due to an effort of having simply working model. Main directions corresponding to stresses considered in this chapter are matched with coiling and uncoiling as well as with the longitudinal direction of resulting structural member that is denoted as "z". Width of the sheet refers to "*x*" direction and through-thickness *t* direction corresponds with "*y*" axis. Main directions identification is denoted in Figure 5.1 for more convenient.

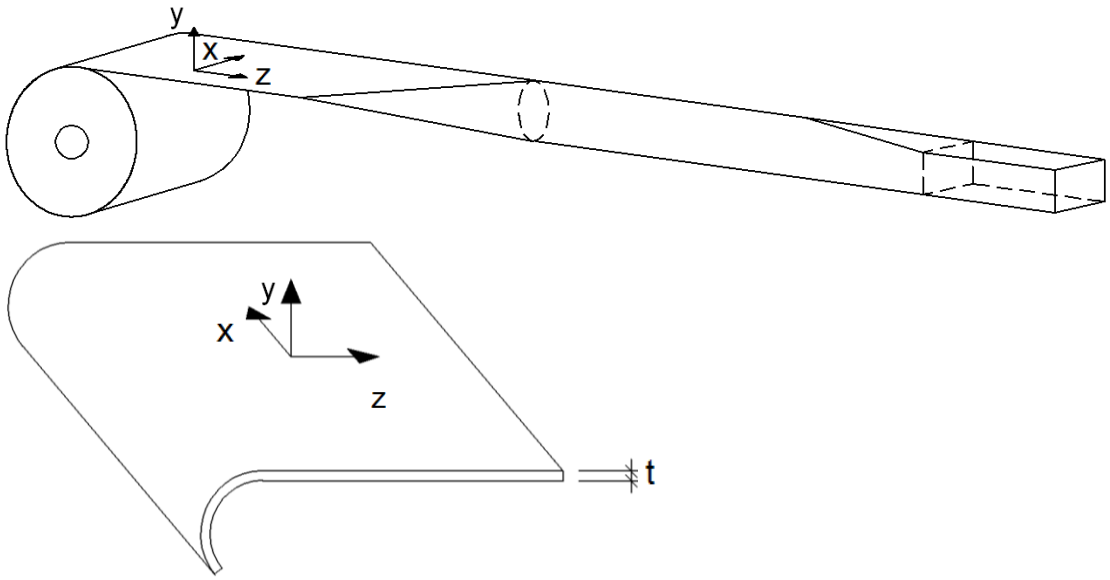

Figure 5.1 *Main directions identification.*

The study assumes the virgin material before coiling is free from residual stress that may be caused by cold-rolling with the stress-strain curve corresponding to the annealed material. Essential values can be obtained by measuring, mill-certificate or recent design codes. Regarding material hardening, the stainless steel is considered to be primarily isotropic material. Coiling, uncoiling and cold-forming are assumed as plane strain pure bending deducing stress and strain only in *y*-*z* plane. For most of calculations there is used coiling radius R_c=450 mm as it is recommended [48] (if not it is marked), as well as Poisson's ratio ν = 0.3. Sheet thickness remains unchanged during all fabrication stages. Equivalent plastic strain is considered in absolute value for more convenient.

5.2 Fabrication modelling

Analytical model developed by Quach [24] for residual stress prediction is adopted. The model is based on three main processes, i.e. coiling, uncoiling and corner bending. These stages are modified and compose into a complex description for a corner and a flat face of a rectangular hollow section. Stress strain response is expressed as the three stage material model: equations (3.23) - (3.25). During the evaluation of the analytical solution for fabricating the generally adopted two stage material model was also considered (equations (3.5), (3.9)) and processed for the whole fabrication model.

Although for strain range up to 2% it is sufficiently accurate, for higher strain ranges it doesn't provide quite correct results in terms of overall values of cold-formed parts.

5.2.1 Coiling and uncoiling

Coiling

During coiling an arbitrary point through the thickness is subjected to elastic or elastic-plastic straining. Amount of straining depends on the coiling curvature $\kappa_c = 1/R_c$ and distance y from the neutral surface (see Figure 5.2). Elastic in plane strains are given as follows:

$$\varepsilon_{z,c} = \frac{(\sigma_{z,c} - \nu\sigma_{x,c})}{E_0} \tag{5.1}$$

$$\varepsilon_{x,c} = \frac{(\sigma_{x,c} - \nu\sigma_{z,c})}{E_0} = 0 \tag{5.2}$$

where E_0 is the initial modulus of elasticity,
ν is the Poisson´s ratio,
$\sigma_{x,c}$, $\sigma_{z,c}$ = stresses in the directions according to subscripts due to the coiling,
$\varepsilon_{x,c}$ and $\varepsilon_{z,c}$ corresponding strains with $\varepsilon_{z,c} = \kappa_c y$

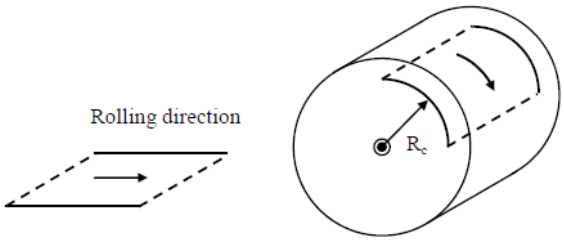

Figure 5.2 *Coiled sheet* [4].

Thus, the stress in an arbitrary point is given by:

$$\sigma_{z,c} = \frac{E_0}{(1-\nu^2)}\ \varepsilon_{z,c} \tag{5.3}$$

$$\sigma_{x,c} = \frac{\nu E_0}{(1-\nu^2)}\ \varepsilon_{z,c} \tag{5.4}$$

Within material plastic straining, there must be satisfied the von Mises yield criterion:

$$\bar{\sigma} = \sigma_{yc} \tag{5.5}$$

where σ_{yc} is the instantaneous yield stress reached at the end of coiling,

$$\bar{\sigma} = \sqrt{\sigma_{z,c}^2 + \sigma_{x,c}^2 - \sigma_{x,c}\sigma_{z,c}} \quad \text{is the equivalent stress} \tag{5.6}$$

At the onset of yielding the initial yield stress equals the instantaneous yield stress at the end of coiling ($\sigma_{y,0} = \sigma_{yc}$):

$$\sqrt{\sigma_{z,c}{}^2+\sigma_{x,c}{}^2-\sigma_{x,c}\sigma_{z,c}}=\sigma_{y,0} \tag{5.7}$$

where $\sigma_{y,0}$ is the initial yield stress.

Longitudinal strain $\varepsilon_{z,cy}$ at which yielding starts is obtained as:

$$\varepsilon_{z,cy}= \pm\sigma_{y,0}(1-\nu^2)/\left(E_0\sqrt{1-\nu+\nu^2}\right) \tag{5.8}$$

where "+" means tension (i.e. $y > 0$)

Central core remains elastic and size of the core is twice the value y_{cy} expressed as:

$$y_{cy}=\sigma_{y,0}(1-\nu^2)/\left(E_0\kappa_c\sqrt{1-\nu+\nu^2}\right) \tag{5.9}$$

Material points beyond the elastic central core and stress obey the von Mises criterion.
Letting the ratio $\omega_c= \sigma_{x,c/}\,\sigma_{z,c.}$ (5.10)

Coiling stresses at any point are given as:

$$\sigma_{z,c}= \pm\frac{\sigma_{y,c}}{\sqrt{1-\omega_c+\omega_c{}^2}} \tag{5.11}$$

$$\sigma_{x,c}= \pm\frac{\omega_c\sigma_{y,c}}{\sqrt{1-\omega_c+\omega_c{}^2}} \tag{5.12}$$

There is also limiting curvature at which the fibre of extreme surface starts to yield given by:

$$\kappa_{cy}=2\sigma_{y,0}(1-\nu^2)/\left(E_0 t\sqrt{1-\nu+\nu^2}\right) \tag{5.13}$$

It is evident the limit depends on material properties (yield point of virgin material, initial modulus of elasticity) and thickness of a sheet.

For isotropic material, the relationship between the equivalent stress and the equivalent plastic strain is the same as the uniaxial stress-strain relationship, so:

$$\bar{\sigma}=\sigma, \text{ when } \bar{\varepsilon_p}=\varepsilon_p \tag{5.14}$$

and $$d\bar{\sigma}=d\sigma, \text{ when } d\bar{\varepsilon_p}=d\varepsilon_p \tag{5.15}$$

with $$\varepsilon_p= \varepsilon- \sigma/E_0 \tag{5.16}$$

For strain-hardening materials σ_{yc} and ω_c are related to each other and it is necessary to establish them numerically for each *y*-location in terms of their increments.

Following slope of the equivalent stress-equivalent plastic strain relation H' equal to the corresponding slope of the uniaxial stress-plastic strain curve can be expressed as:

$$H' = \frac{d\bar{\sigma}}{d\bar{\varepsilon}_p} = \frac{d\sigma}{d\varepsilon_p} = \left(\frac{d\varepsilon}{d\sigma} - \frac{1}{E_0}\right)^{-1} \tag{5.17}$$

Stress ratio $\Omega_c = d\sigma_{x,c} / d\sigma_{z,c}$ is given in the form of: (5.18)

$$\Omega_c = \frac{4\nu H'\left(1-\omega_c+\omega_c^2\right) - E_0(2-\omega_c)(2\omega_c-1)}{E_0(2\omega_c-1)^2 + 4H'\left(1-\omega_c+\omega_c^2\right)} \tag{5.19}$$

Stress increment $d\omega_c$ is expressed as follows:

$$d\omega_c = \frac{2\left(1-\omega_c+\omega_c^2\right)(\Omega_c-\omega_c)}{\sigma\left[(2-\omega_c)+\Omega_c(2\omega_c-1)\right]} d\sigma \tag{5.20}$$

Hence, there can be used numerical calculations for the value of σ_{yc} and related stress ratio ω_c at each point y through the thickness.

Plastic strain under coiling curvature κ_c is then given by:

$$\varepsilon_{c,pl} = \varepsilon_{yc} - \sigma_{yc}/E_0 \tag{5.21}$$

where σ_{yc} is the instantaneous yield stress due to the coiling,
ε_{yc} is the corresponding strain to σ_{yc}

The increment of the longitudinal strain is expressed as:

$$d\varepsilon_{z,c} = \pm \begin{cases} \dfrac{[(1-2\omega_c)^2 - 2\nu(1-2\omega_c)(2-\omega_c) + (2-\omega_c)^2]\sigma}{2E_0(1-2\omega_c)\left(1-\omega_c+\omega_c^2\right)^{3/2}} d\omega_c \\ + \dfrac{(1-\omega_c)^2(1-2\nu)}{E_0(1-2\omega_c)\left(1-\omega_c+\omega_c^2\right)^{1/2}} d\sigma \end{cases} \tag{5.22}$$

Final values of σ_{yc} and corresponding stress ratio ω_c can be calculated numerically by step by step updating values of σ and ω_c via small assigned increment $d\sigma$, $d\omega_c$ respectively.

Uncoiling

When $\kappa_c > \kappa_{cy}$, in case of the natural uncoiling a sheet after the process exhibits a residual curvature (see Figure 5.3). The curvature is removed within fabrication process either before cold-forming or during cold-forming as a result of the final section overall stiffness. The solution assuming uncoiling including flattening is adopted and described herein. That means there is used the same uncoiling curvature κ_u as for coiling in the opposite direction.

$$\kappa_u = -\kappa_c \tag{5.23}$$

Total stress at an arbitrary point is then given by:

$$\sigma_{z,r} = \sigma_{z,c} + \sigma_{z,u} \tag{5.24}$$

$$\sigma_{x,r} = \sigma_{x,c} + \sigma_{x,u} \tag{5.25}$$

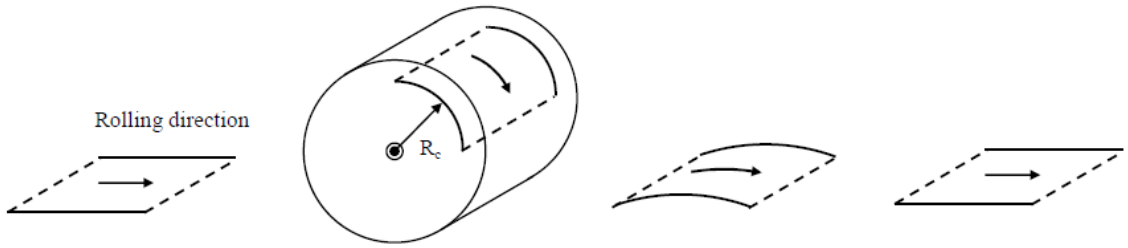

Figure 5.3 *Flattened sheet after uncoiling* [4].

As for the coiling there is similar condition for the limiting uncoiling curvature κ_{uy} when the extreme surface starts to yield described as follows:

$$\kappa_{uy} = -\frac{\sigma_{yc}(1-\nu^2)[2-\nu+(2\nu-1)\omega_c]}{E_0|y|\left(1-\nu+\nu^2\right)\sqrt{1-\omega_c+\omega_c^{\,2}}} \tag{5.26}$$

When the uncoiling curvature κ_u is lower than κ_{uy}, the uncoiling stresses are elastic given by:

$$\sigma_{z,u} = \frac{E_0}{(1-\nu^2)}\ \kappa_u y \tag{5.27}$$

$$\sigma_{x,u} = \frac{\nu E_0}{(1-\nu^2)}\ \kappa_u y \tag{5.28}$$

When the uncoiling curvature κ_u is greater than κ_{uy} the reverse yielding occurs and uncoiling stresses after the process are no longer only elastic given by:

$$\sigma_{z,r} = \mp\frac{\sigma_{y,r}}{\sqrt{1-\omega_u+\omega_u^{\,2}}} \tag{5.29}$$

$$\sigma_{x,r}=\mp\frac{\omega_u\sigma_{y,r}}{\sqrt{1-\omega_u+\omega_u^2}} \tag{5.30}$$

with $\omega_u=\sigma_{x,r}/\sigma_{z,r}=(\sigma_{x,c}+\sigma_{x,u})/(\sigma_{z,c}+\sigma_{z,u})$ (5.31)

Total equivalent plastic strain after uncoiling is similar to the previous one:

$$\varepsilon_{r,pl}=\varepsilon_r-\sigma_r/E_0 \tag{5.32}$$

where σ_r is the instantaneous yield stress with corresponding strain ε_r.

Similar to the coiling stage the stress ratio increment $d\omega_u$ is possible to consider as:

$$d\omega_u=\frac{2\left(1-\omega_u+\omega_u^2\right)(\Omega_u-\omega_u)}{\sigma\left[(2-\omega_u)+\Omega_u(2\omega_u-1)\right]}d\sigma \tag{5.33}$$

Stress ratio $\Omega_u=d\sigma_{x,r}/d\sigma_{z,r}$ is given in the form of: (5.34)

$$\Omega_u=\frac{4\nu H'\left(1-\omega_u+\omega_u^2\right)-E_0(2-\omega_u)(2\omega_u-1)}{E_0(2\omega_u-1)^2+4H'\left(1-\omega_u+\omega_u^2\right)} \tag{5.35}$$

The increment of the longitudinal strain for uncoiling is expressed as:

$$d\varepsilon_{z,u}=\pm\begin{cases}-\dfrac{[(1-2\omega_u)^2-2\nu(1-2\omega_u)(2-\omega_u)+(2-\omega_u)^2]\sigma}{2E_0(1-2\omega_u)\left(1-\omega_u+\omega_u^2\right)^{3/2}}d\omega_u\\ -\dfrac{(1-\omega_u)^2(1-2\nu)}{E_0(1-2\omega_u)\left(1-\omega_u+\omega_u^2\right)^{1/2}}d\sigma\end{cases} \tag{5.36}$$

Likewise the coiling final values of σ_r and corresponding stress ratio ω_u can be calculated integrally or numerically by step by step updating values of σ and ω_u in each step via small assigned increment $d\sigma$, $d\omega_u$ respectively.

The coiling-uncoiling process develops small strains in the sheet. Thus there is sufficient to use the stress-strain description in engineering values for evaluating of plastic strain and stress within the process. Differences between the true and nominal stress-strain behaviour are negligible. Differences have to be taken into consideration for higher strains as it is shown in Figure 5.4 and Figure 5.5. Also conclusions of Yu and Zhang [60] for pure bending with the centreline bending radius $R_c > 10t$ present the difference between maximum engineering and true logarithmic strain lower than 2.5%. Because of a coiling and uncoiling curvature (much larger than $10t$) engineering strain values provide more than good accuracy for calculations. However in case of cold bending (either cold-rolling or press-breaking) it is necessary to take the true strain into consideration and adapt the model.

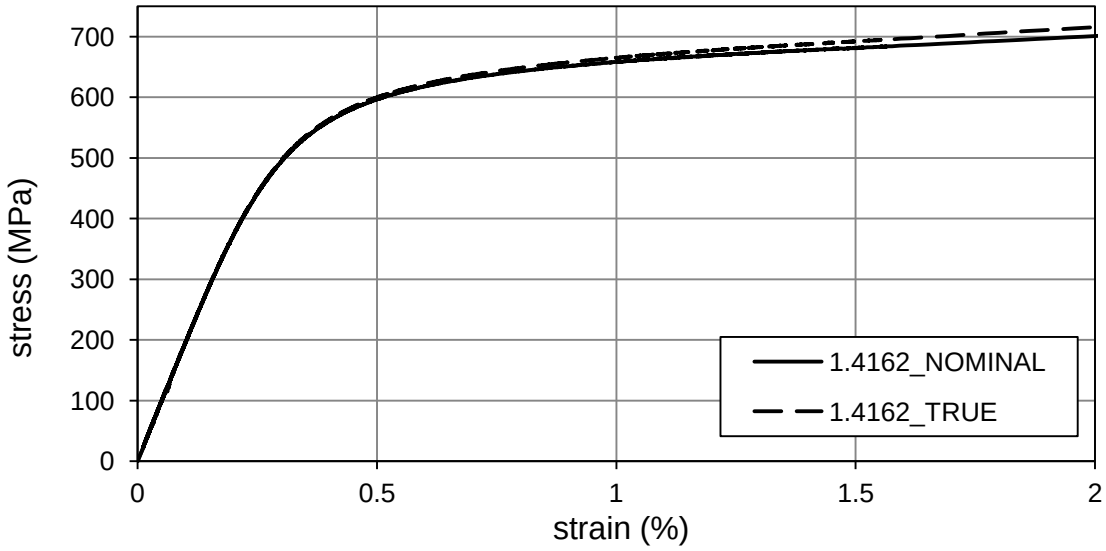

Figure 5.4 *Difference between the true and nominal stress-strain behaviour for the 1.4162 grade in small strain levels.*

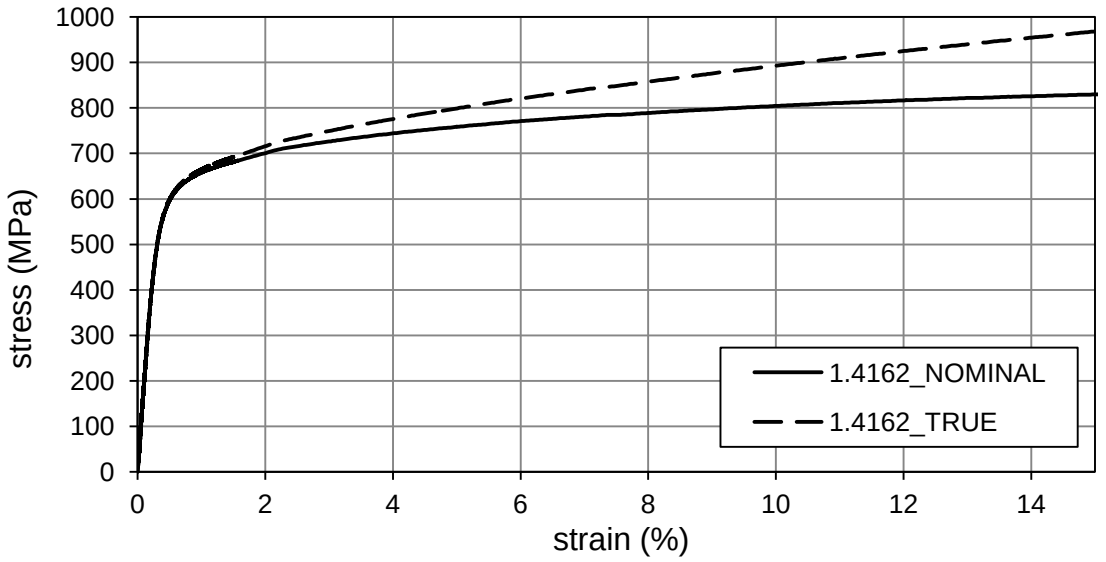

Figure 5.5 *Difference between true and nominal stress-strain behaviour for the 1.4162 grade in high strain levels.*

For more convenient, general process of coiling-uncoiling is displayed in Figure 5.6. The figure displays a general elastic-plastic material. However for the stainless steel there is no elastic region due to the rounded stress-strain response. Thus strain hardening across the whole section occurs from the start of coiling with different levels in relation to the location through the thickness. The diagram describes the "0-E-P" path representing the coiling. In case of stainless steel the path looks rounded starting at the point "0" and finishing at the point "P" missing the point "E". During elastic uncoiling following the "P-UE" path there is no additional plastic strain induction. Reverse yielding ("UE-UP") deduces further plastic strain and yield envelope expansion. Stress and strain distribution across the thickness is therefore non-linear.

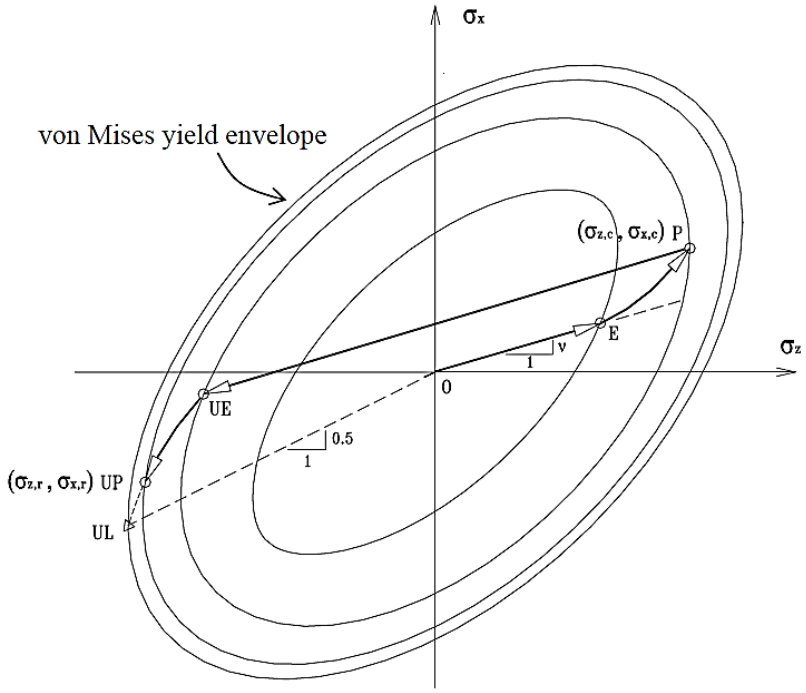

Figure 5.6 *Scheme of the coiling-uncoiling process* [24].

Distribution of stress and plastic strain after the coiling and uncoiling are displayed in following figures (Figure 5.7 - Figure 5.9). For highlighting the effect there is R_c = 250 mm used together with a 2 mm thin sheet made of an austenitic grade undergoing the coiling and uncoiling process and divided into 30 layers. Mechanical properties used for the following example are determined as:

Grade	E_0	$E_{0.2}$	$\sigma_{0.2}$	$\sigma_{1.0}$	σ_u	ε_u	n	$n'_{0.2,1.0}$
	GPa	GPa	MPa	MPa	MPa	%	-	-
1.4301	195.4	12.8	205.0	234.6	520.0	60.0	7.5	1.95

There are a few essential properties, i.e. the initial modulus of elasticity, the 0.2% proof strength, the ultimate strength and the Ramberg-Osgood parameter of nonlinearity. All other properties can be calculated from relationships stated below:

$$\sigma_{1.0}=\frac{0.542\sigma_{0.2}}{n}+1.072\sigma_{0.2} \tag{5.37}$$

Formula (5.37) was established by Quach [24] by analysing tension coupon test data as well as formula (5.38) determining compound Ramberg-Osgood nonlinearity parameter $n'_{0.2,1.0}$:

$$n'_{0.2,1.0}=\frac{12.225E_{0.2}\sigma_{1.0}}{E_0\sigma_{0.2}}+1.037 \tag{5.38}$$

Determination of the tangent modulus of elasticity at the 0.2% proof strength is based on Eq. (3.22).

Corresponding strain at the ultimate strength is adopted from Eq. (3.21) codified in EN 1993-1-4 and limited by the value of 60%. In case of ferritic steel the expression can be slightly modified according to results and observations from experimental programmes according to Bock et al. [61] as:

$$\varepsilon_u = 0.6 \left(1 - \frac{\sigma_{0.2}}{\sigma_u}\right) \tag{5.39}$$

However, in the Maple model the relationship for ε_u (Eq. (3.21)) is generally adopted for all grades. Although ferritic steels exhibit shorter area between the 0.2% proof strength and the ultimate stress they also exhibit relatively significant plateau at ultimate strength. Thus this observation within testing at CTU allows using the Eq. (3.21) for all grades. In addition by considering linearly increasing strains across the thickness from neutral surface to the outer or inner one during the fabricating, high plastic strains induced at surfaces of the bend area can even exceed original material ductility (in case of the corner bending with a low value of the inner radius). That means the bending with a low inner radius is more complex and not only planar behaviour and material acting through the thickness. The Maple model is based as a planar solution conservatively considering only lower values of plastic strain than ε_u.

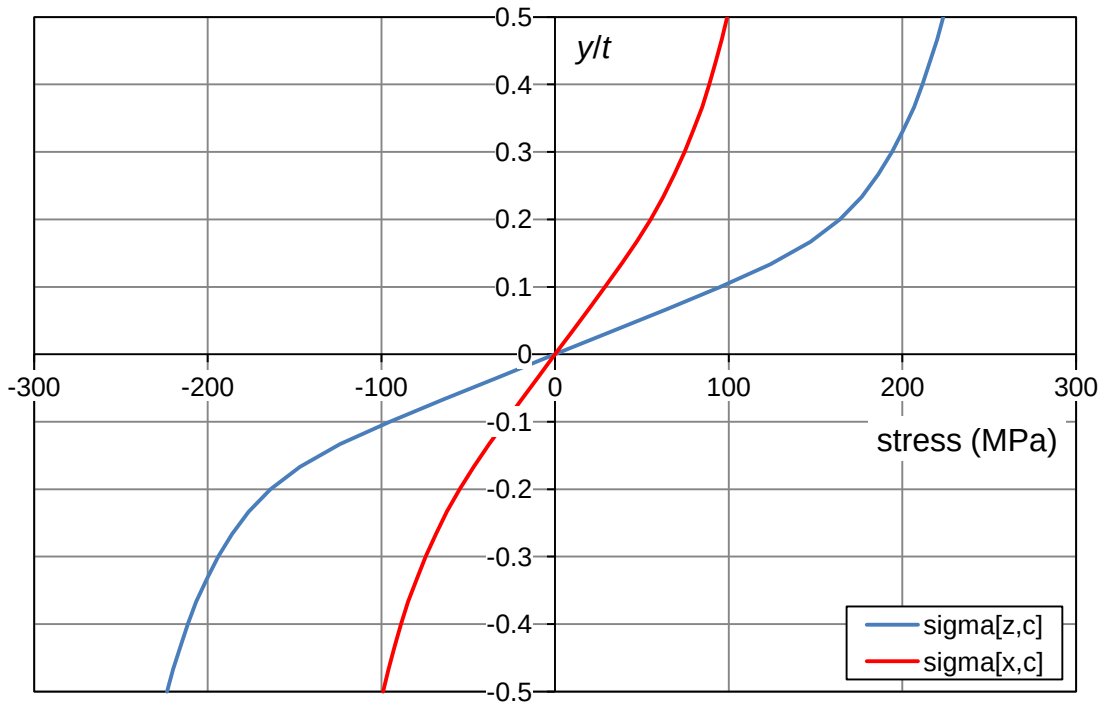

Figure 5.7 *Longitudinal and transverse stresses due to coiling according to the Maple model.*

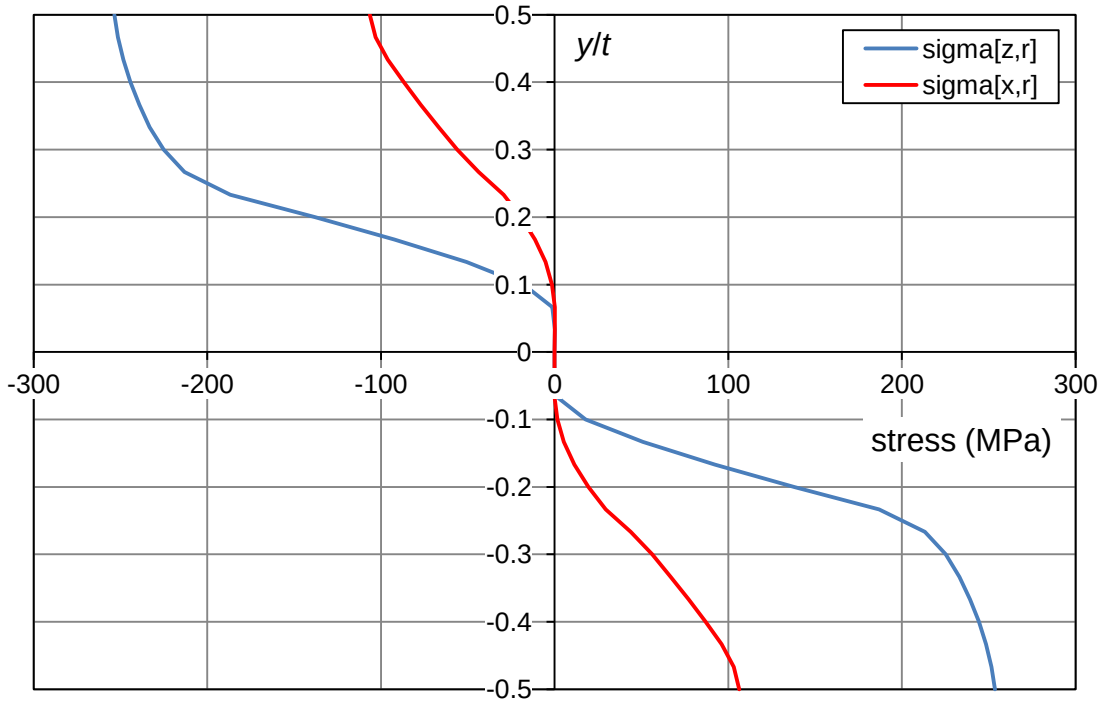

Figure 5.8 *Longitudinal and transverse stresses due to coiling-uncoiling according to the Maple model.*

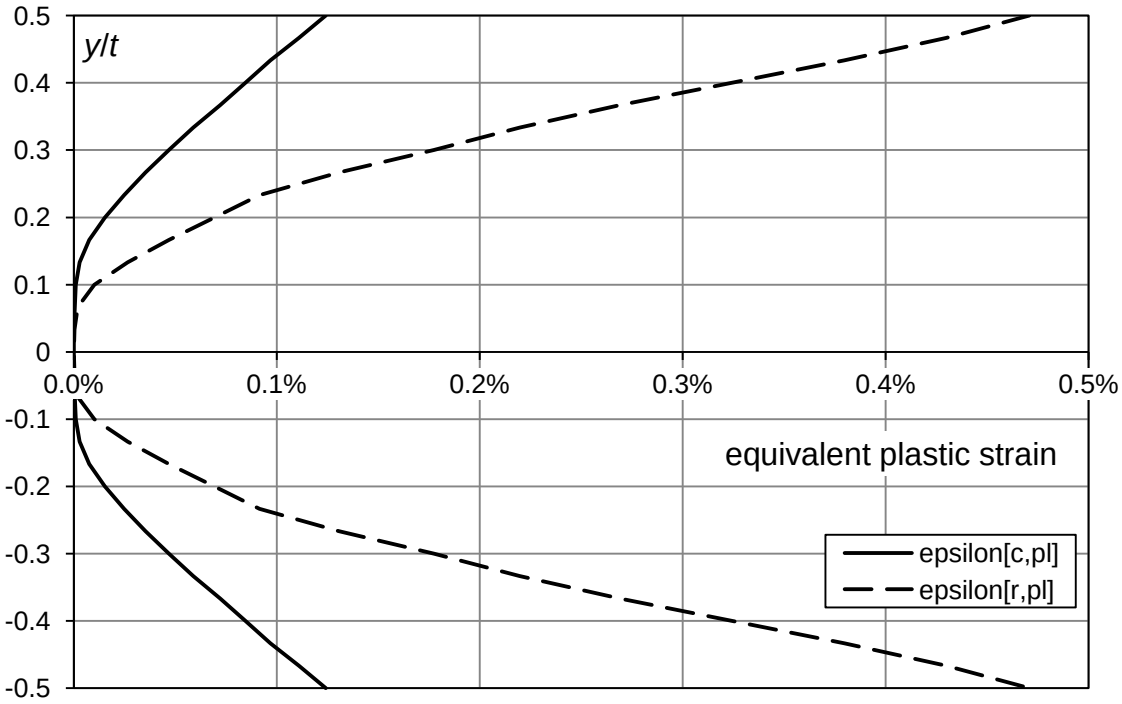

Figure 5.9 *Plastic strain after coiling and coiling-uncoiling according to the Maple model.*

5.2.2 Cold bending

This section describes an analytical solution both for press-breaking and cold-rolling of a sheet into a corner. It should be noted that within press-breaking the outer curved surface of a sheet becomes inner surface of the final bend. As the strains induced by cold-bending are much larger than in case of coiling-uncoiling the resulting state is mostly influenced by making a corner. The mathematical description stated herein is based on similar foundations as for the coiling-uncoiling assuming large bending curvature.

Cold-bending process affects relations across thickness of the corner [14]. For large curvatures (Rc < 10t) there is important effect of changing the neutral surface [60]. The neutral surface is not more the same as the middle one. It moves closer to the inner surface as the bending proceeds (see Figure 5.10). That means there is a zone within the thickness exposed to compression and following tension. It leads to a non-deformed surface during each step of the cold-bending where zero final strains occur.

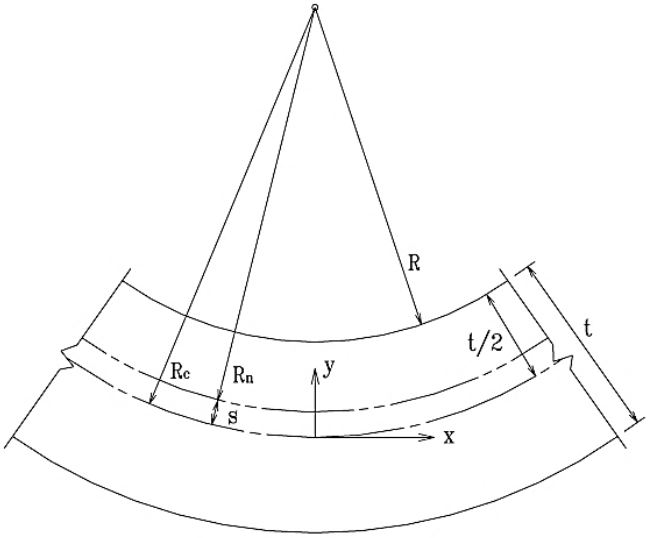

Figure 5.10 *Sheet under pure bending* [24].

When a sheet is cold-bent, its fibers undergo transverse straining. Amount of the straining depends on the location in relation to the current middle surface and a distance s between the neutral surface and the current middle surface and the centerline radius R_c. The true transverse strain is expressed as:

$$\varepsilon_{x,cs}=\ln\left(1+\left(\frac{s-y}{R_c-s}\right)\right) \tag{5.40}$$

As it was stated above no through-thickness stresses and strains are considered and similar to the coiling and uncoiling for elastic material longitudinal and transverse stresses are given by:

$$\sigma_{z,cs}=\frac{vE_0}{(1-v^2)}\ \varepsilon_{x,cs} \tag{5.41}$$

$$\sigma_{x,cs}=\frac{E_0}{(1-\nu^2)}\ \varepsilon_{x,cs} \tag{5.42}$$

The elastic stress is only theoretical issue due to the nonlinear stress-strain behaviour of the stainless steel, thus plastic straining occurs from the beginning of the process.

With stress ratio $\omega_{cs}= \sigma_{z,cs/}\ \sigma_{x,cs}$, (5.43)

stresses of points subjected to the plastic straining are expressed as:

$$\sigma_{z,cs}=\pm\frac{\omega_{cs}\sigma_{y,cs}}{\sqrt{1-\omega_{cs}+\omega_{cs}^{\ 2}}} \tag{5.44}$$

$$\sigma_{x,cs}=\pm\frac{\sigma_{y,cs}}{\sqrt{1-\omega_{cs}+\omega_{cs}^{\ 2}}} \tag{5.45}$$

Similar to Eq. (5.16), the equivalent plastic strain is given by:

$$\bar{\varepsilon}_{cs,pl}=\varepsilon_{y,cs}-\sigma_{y,cs}/E_0 \tag{5.46}$$

where $\sigma_{y,cs}$ is the instantaneous yield stress due to the cold-bending,
$\varepsilon_{y,cs}$ is the corresponding strain to σ_{yb}

Letting the stress ratio $\Omega_{cs} = d\sigma_{z,cs}/\ d\sigma_{x,cs}$ is given in the form of: (5.47)

$$\Omega_{cs}=\frac{4\nu H'\left(1-\omega_{cs}+\omega_{cs}^{\ 2}\right)-E_0(2-\omega_{cs})(2\omega_{cs}-1)}{E_0(2\omega_{cs}-1)^2+4H'\left(1-\omega_{cs}+\omega_{cs}^{\ 2}\right)} \tag{5.48}$$

Stress increment $d\omega_{cs}$ is expressed as follows:

$$d\omega_{cs}=\frac{2\left(1-\omega_{cs}+\omega_{cs}^{\ 2}\right)(\Omega_{cs}-\omega_{cs})}{\sigma\left[(2-\omega_{cs})+\Omega_{cs}(2\omega_{cs}-1)\right]}d\sigma \tag{5.49}$$

Then the value of $\sigma_{y,cs}$ and related stress ratio ω_{cs} at each point y through the thickness can be solved numerically.

Due to large curvatures and high strain levels it is necessary to use true values instead of engineering notation as it is stated above. Thus the true plastic strain ε_{tp} is expressed as:

$$\varepsilon_{t,pl}=\varepsilon_t-\sigma_t/E_0=\pm\ln(1\pm\varepsilon_n)-\frac{\sigma_n(1\pm\varepsilon_n)}{E_0} \tag{5.50}$$

where "+" denotes tension and "-" compression,
subscript "*t*" denotes true value and subscript "*n*" nominal value

Slope of the equivalent stress-equivalent plastic strain relation H' is still given by Eq. (5.17), however the strain rate $d\varepsilon/d\sigma$ must be replaced by $d\varepsilon_t/d\sigma_t$.

In terms of using three stage material model – Eq. (3.23)-(3.25) and for $d\sigma_t$ obtaining there is possible to employ following expression:

$$\frac{d\sigma_t}{d\sigma_n}=\begin{cases} 1\pm\left[\frac{2\sigma_n}{E_0}+0.002(n+1)\left(\frac{\sigma_n}{\sigma_{0.2}}\right)^n\right] & \sigma_n\le\sigma_{0.2} \quad (5.51)\\ 1\pm\left\{\varepsilon_{0.2}+\frac{(2\sigma_n-\sigma_{0.2})}{E_{0.2}}+\left[\left(n'_{0.2,1.0}+1\right)\sigma_n-\sigma_{0.2}\right]\cdot\right. & \sigma_{0.2}<\sigma_n\le\sigma_{2.0} \quad (5.52)\\ \left.\left[0.008+(\sigma_{1.0}-\sigma_{0.2})\left(\frac{1}{E_0}-\frac{1}{E_{0.2}}\right)\right]\frac{(\sigma_n-\sigma_{0.2})^{n'_{0.2,1.0}-1}}{(\sigma_{1.0}-\sigma_{0.2})^{n'_{0.2,1.0}}}\right\} & (5.53)\\ 1\pm\frac{(2\sigma_n-a)(b\mp\sigma_n)\pm\sigma_n(\sigma_n-a)}{(b\mp\sigma_n)^2} & \sigma_n>\sigma_{2.0} \quad (5.54)\end{cases}$$

First for the small increment of $d\sigma_n$ there is possible to establish $d\sigma_t$ and then $d\omega_{cs}$. Second, it is possible to calculate cold-bending stresses and equivalent plastic strain by determination $\sigma_{y,cs}$ and ω_{cs} that are as well as for previous stages related to each other.

As well as for the coiling and uncoiling the distribution of stress and plastic strain after cold-bending is shown below. The inner radius of bend is set as 4*t*. Parameters of the sheet remain the same as for the previous example. In Figure 5.11 and Figure 5.12 there is depicted how the final stresses and equivalent plastic strain are influenced by assuming stress-strain response in nominal or true values after coiling-uncoiling and cold-bending.

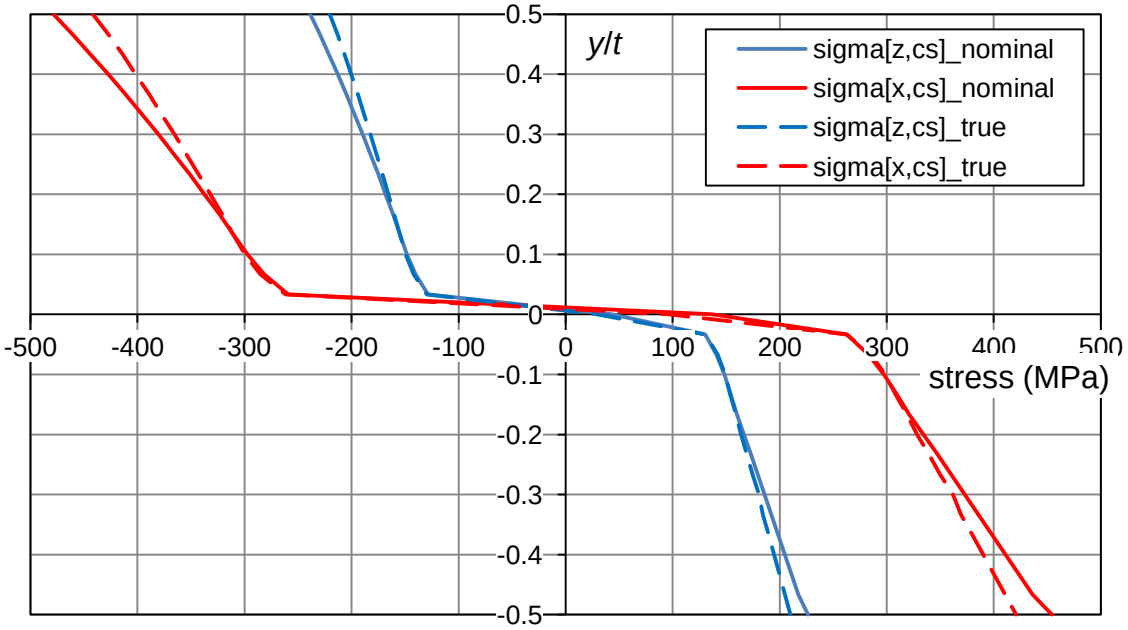

Figure 5.11 *Comparison of plane stresses according to the nominal and true stress-strain response for cold-bending in the Maple model.*

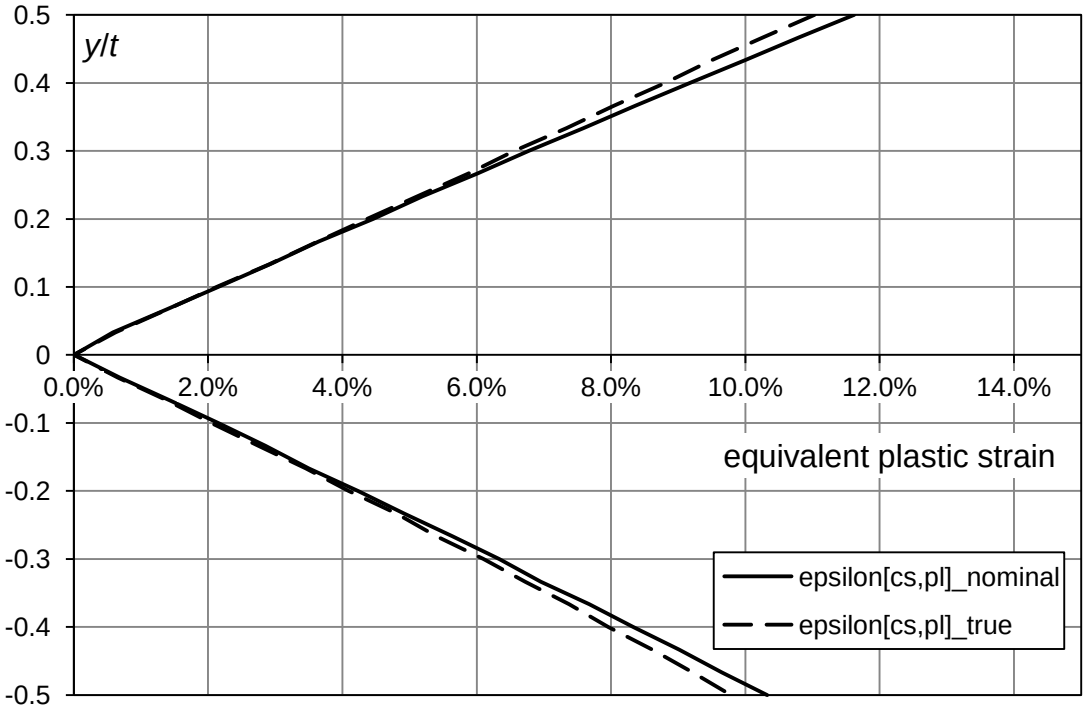

Figure 5.12 *Comparison of equivalent plastic strain according to the nominal and true stress-strain response for cold-bending in the Maple model.*

5.2.3 Cold bending including springback

When a steel sheet is subjected to the plastic strain induction during cold-bending followed by unloading, the final shape of the sheet is different from the originally bent one. Figure 5.13 displays a stress path of a cold-formed sheet in terms of the cold-bending of perfect elastic-plastic material as the simplest illustration of the effect. There should be remarked that residual stresses due to the elastic unloading (known as springback) occur within all fabrication steps. However the level of final stress distribution after each step is hard to determine. Herein it is assumed that important residual stresses arise after cold-forming into a corner.

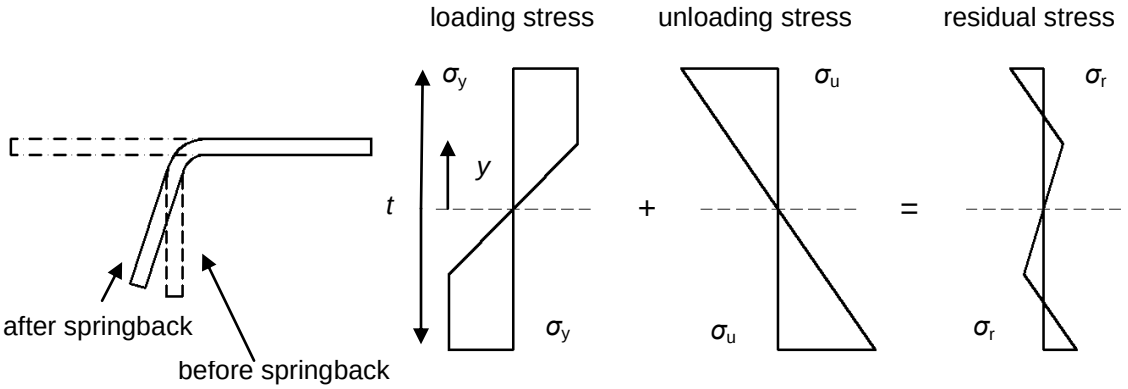

Figure 5.13 *Cold-bending of an elastic-plastic sheet with the stress path and resulting stress distribution in a corner.*

Thus the final Maple model employs residual stresses resulting from the elastic unloading after cold-bending (i.e. determination of residual stresses is based on the zero moment condition). Suitability of the proposed solution was verified by comparison with residual stress test data executed by Weng and White [52], Quach´s FEM solution [24] and Rossi et al.´s numerical analysis [53]. They all aimed on the same case of the cold-bending for the comparison. Residual stresses in *z* direction were compared only with Weng and White experiments together with Quach´s FE model due to the lack of other available data.

At first Weng and White (in 1990) executed an experimental investigation of residual stresses in cold-bent thick plates made of high-strength steel HY-80 (for material properties obtained from a coupon test see Table 5.1). The comparison of the results is proved for the sample of 1 inch thickness and with inner radius of bend 5.5*t*. Strain at the ultimate strength is obtained using Eq. (3.21). Transverse surface residual stresses in *z* direction were taken as average values resulting from experimental methods used within testing. (i.e. hole-drilling and sectioning).

t (mm)	σ_y (MPa)	σ_u (MPa)	E (GPa)	ν (-)	ε_u (%)
25.4	593.2	737.9	203.9	0.28	19.6

Table 5.1 *Mechanical properties of HY-80 steel.*

In 2005 Quach [24] used the finite element code ABAQUS for modelling the cold-bending process where both material and geometrical non-linearity were considered as well as interaction between the steel plate and the die or punch.

In 2007 Rossi et al. [53] modified previous equations proposed by Quach and incorporated a swift law to determine non-linear stress-strain behaviour of HY-80.

In the Maple model, the HY-80 steel is considered to be an elastic material until it reaches the yield strength and after it is assumed as an elastic hardening material as it is shown in Figure 5.14. The slope of hardening at the yield strength is then given by:

$$E_n = \frac{\sigma_u - \sigma_y}{\varepsilon_u - \sigma_y/E} = \frac{737.9 - 593.2}{0.196 - 593.2/203900} = 749.0 \text{ MPa} \tag{5.55}$$

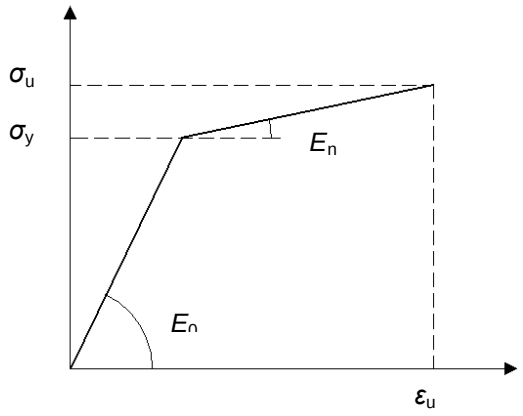

Figure 5.14 *Idealized material model of HY-80 steel.*

The simpler bilinear stress-strain description of the material with hardening is given by:

$$\sigma = \varepsilon E_0 \qquad \varepsilon \leq \sigma_y / E_0 \tag{5.56}$$

$$\sigma = \sigma_y + E_n \left(\varepsilon - \frac{\sigma_y}{E_0} \right) \qquad \varepsilon > \sigma_y / E_0 \tag{5.57}$$

Then the slope of the equivalent stress-equivalent plastic strain relation H' for $\sigma > \sigma_y$ is simply expressed as:

$$H' = \frac{E_0 E_n}{E_0 - E_n} \tag{5.58}$$

And the equivalent plastic strain can be obtained as:

$$\bar{\varepsilon}_{cs,pl} = \left(\sigma_{y,cs} - \sigma_y \right) \left[\frac{E_0 - E_n}{E_0 E_n} \right] \tag{5.59}$$

That simplifies previous expressions and thus it is easier to evaluate the analytical solution.

Figures below display a comparison of obtained results. Analytical solution is very close to the Rossi et al.´s numerical model while the confrontation with test results and FE model exhibits some differences that could be caused by boundary conditions entered in ABAQUS and only few strain gauges used for testing, because experimental measuring did not satisfy the condition of the required zero moment across the thickness. Overall the analytical solution provides good accuracy and it is employed for further applications.

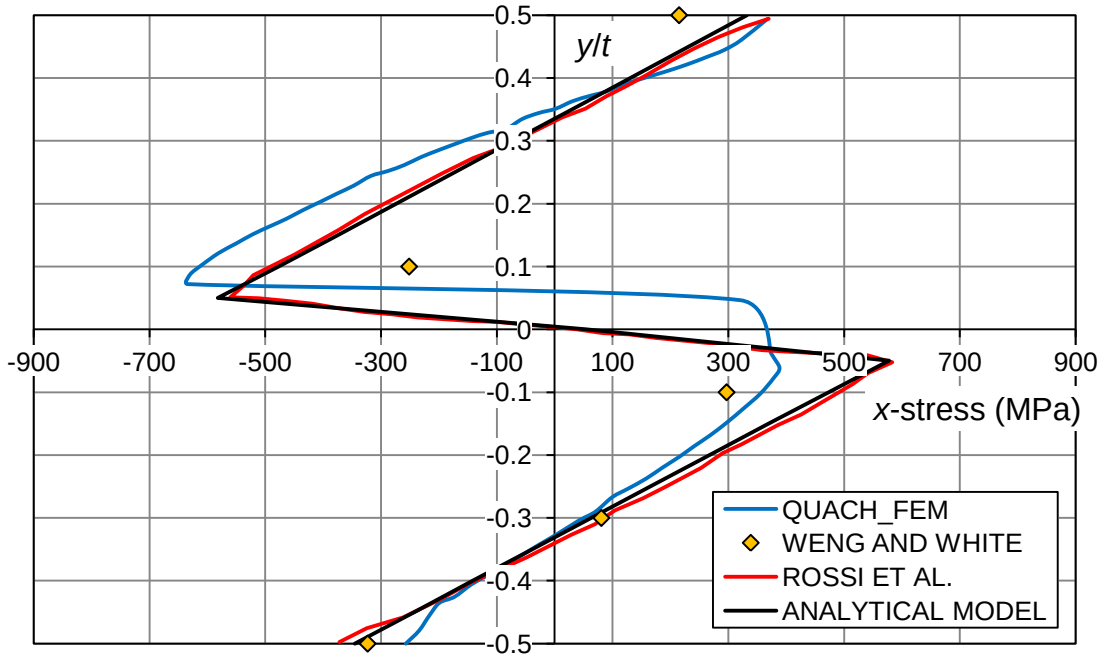

Figure 5.15 *Residual bending stresses σ_x across the thickness comparison.*

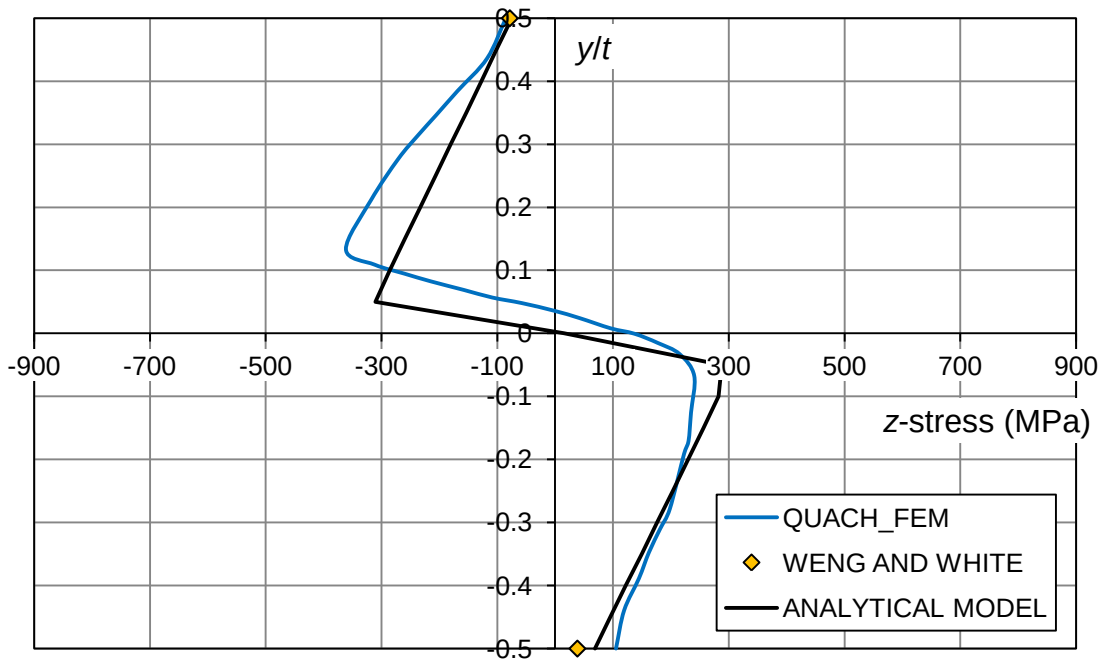

Figure 5.16 *Residual bending stresses σ_z across the thickness comparison.*

5.3 Stress-strain behaviour

The analytical solution of fabrication steps described above serves for residual stress and plastic strain evaluation. On the basis of these boundary conditions there is possible to determine awhole stress-strain behaviour for particular portions of a section as well as for a full section. Following sections deals with this issue.

5.3.1 Stress-strain behaviour of cold-bent corner and flat faces of SHS

A corner or SHS sections are modelled using the Maple via the three stage fabrication process consisting of the coiling stage followed by the uncoiling stage with the bending into the final shape as it was described above. The model is closer to the physical base of the cold-bending than for the cold-rolling due to the distribution of the enhanced strength as it was described by Cruise [4] for instance. From Figure 5.17 and Figure 5.18 it is evident that the idea of simple enhanced strength distribution with a relatively sharp border between a corner and a flat face is well applicable for press-braked sections. It also confirms the enhanced part of a section is solely represented by the pure geometric corner area. In opposite to press-braked sections the enhanced strength distribution for cold-rolled sections is much more complex with a peak at the border geometrically dividing the corner and the flat face. This peak continuously and almost linearly decreases on both sides and for the most of the flat the strength enhancement is the lowest in the section. For further corner properties the following Maple model considers the fabrication process of cold-rolling the same as for press-braking making the corner the most affected part of a section with dominant influence for resulting strength resistance of a full section in terms of the strength increase. However in case of flat faces there is appropriate to regard the complex effect of the cold-rolling. As it is shown in Figure 5.18, with respecting the previous assumption it could be incorrect to

assume the uniform enhanced strength with maximal amplitude for a whole flat face. In terms of determining of the enhanced strength properties the calculation of plastic strains essential for matching new material properties is the most important. Progress of the Maple model regarding this effect is stated herein. The model provides an average value of strain for the flat face as the representative strength enhancement used for a full section strength enhancement.

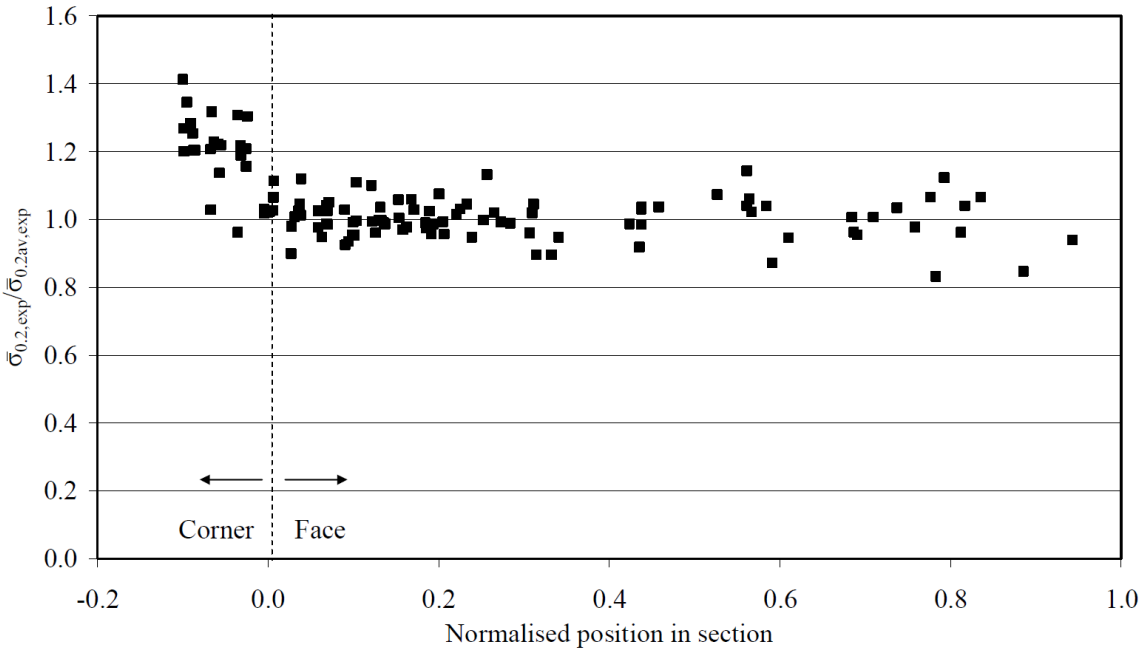

Figure 5.17 *Normalised 0.2% proof strength for press-braked section* [4].

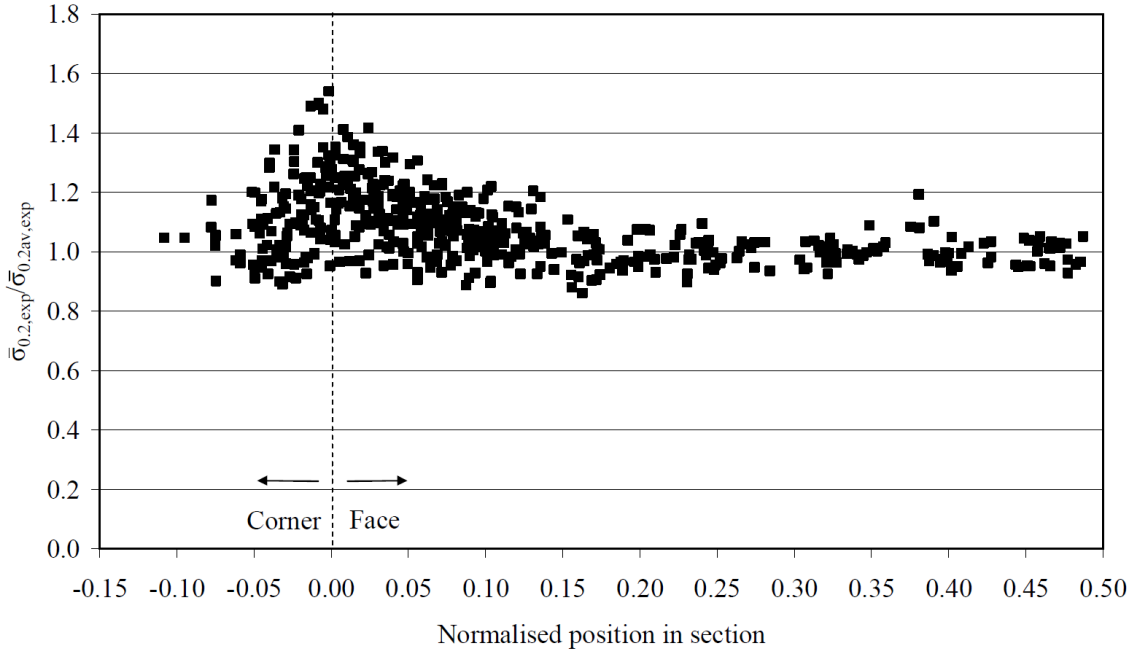

Figure 5.18 *Normalised 0.2% proof strength for cold-rolled section* [4].

In terms of flat faces the process of the cold-bending mostly consists of forming into a circular tube and further crushing it into flat parts of SHS. That means the primary bending followed by the secondary reverse bending with a curvature depending on the section dimensions. These steps take place in the residual stress and plastic strain calculation (see Figure 5.19).

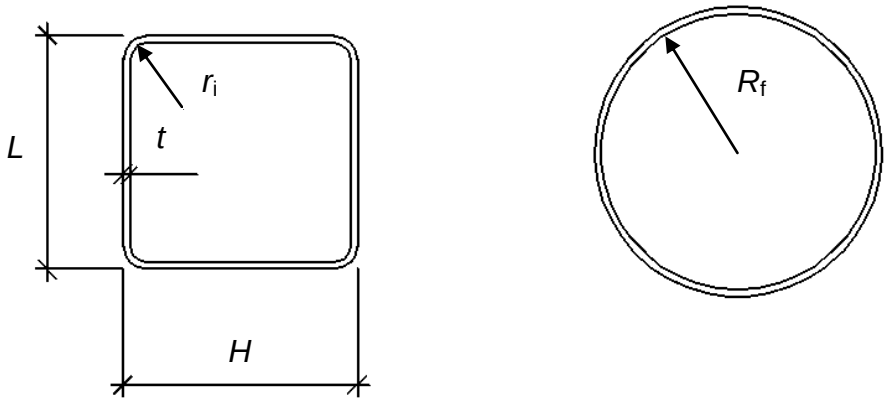

Figure 5.19 *Bending radius for a corner and a flat face.*

Bending radius for the flat faces regarding rounded corners of RHS is given by:

$$R_f = \frac{L+H-2t}{\pi} \tag{5.60}$$

The principle of the Maple model for the stress and strain calculation is based on the following steps. A part of a section (corner or flat face) is divided into several layers across the thickness to evaluate the residual stress and plastic strain. The model establishes plastic strains in absolute values for each layer. For obtaining a new stress-strain curve of a whole corner or flat face it is necessary to determine mechanical properties for each layer individually according to the plastic strain reached at the end of the fabricating process. Thus trends of the mechanical properties depending on the induced plastic strain level were gathered from the experimental data established at CTU (see Chapter 4 – section 4.2 and 4.3) and plotted in following figures. Trend functions were established on the basis of the tests executed transverse to the direction of previous plasticising (coupons denoted by "T" mark – right hand side - Figure 4.9). Linear and polynomic expressions were prescribed for insuring of a simple regression with no specific boundary conditions as it is shown in the figures. In some cases there would be suitable to perform additional tests to provide more data due to a relatively high scatter of measured values. In addition a few quadratic regressions exhibit both increasing and decreasing trends. Therefore for these cases two stage models were employed represented by a variable part and subsequent constant one. The constant expression for a particular property is used after the variable expression reaches the extreme. The dependency of *n* on the level of plastic strain induction represented by a constant value after reaching a particular limit was also observed by Hradil et al.[62]

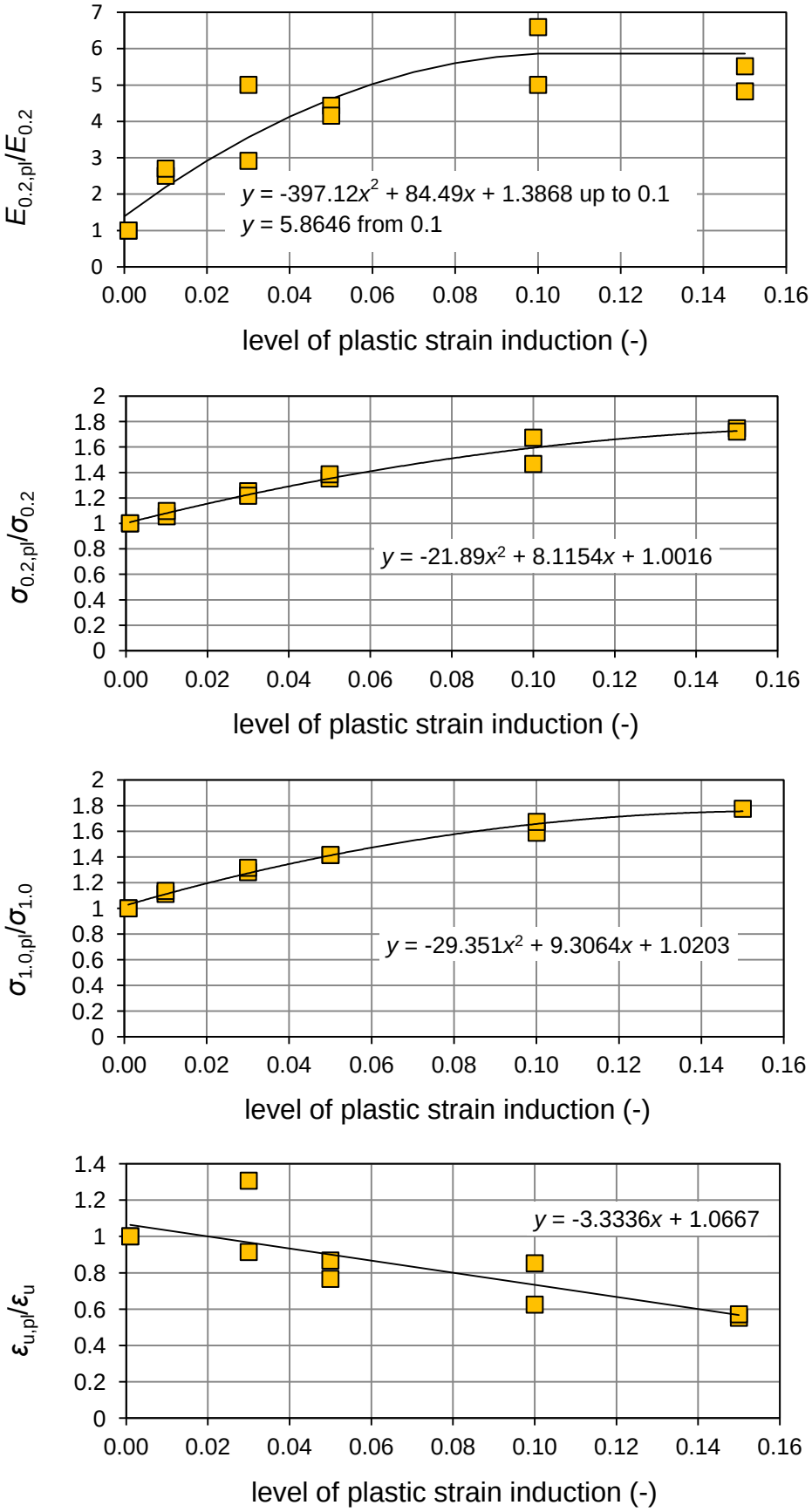

Figure 5.20 *Trends of the mechanical properties for the 1.4003 grade.*

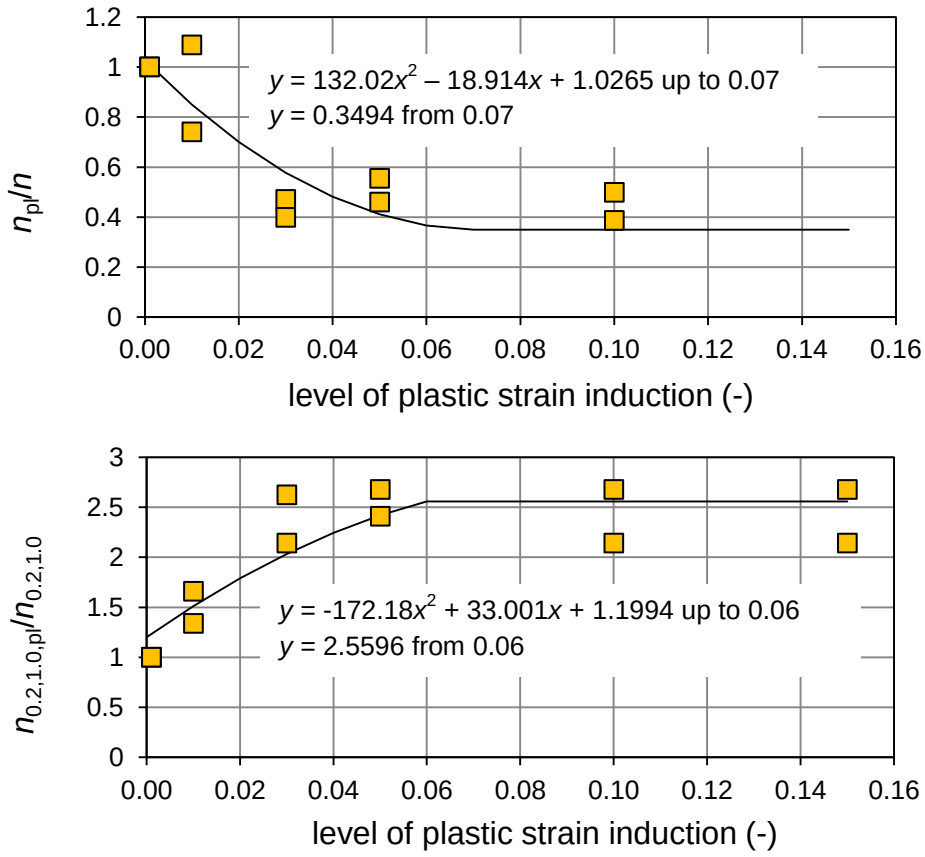

Figure 5.21 *Trends of the mechanical properties for the 1.4003 grade - follow up.*

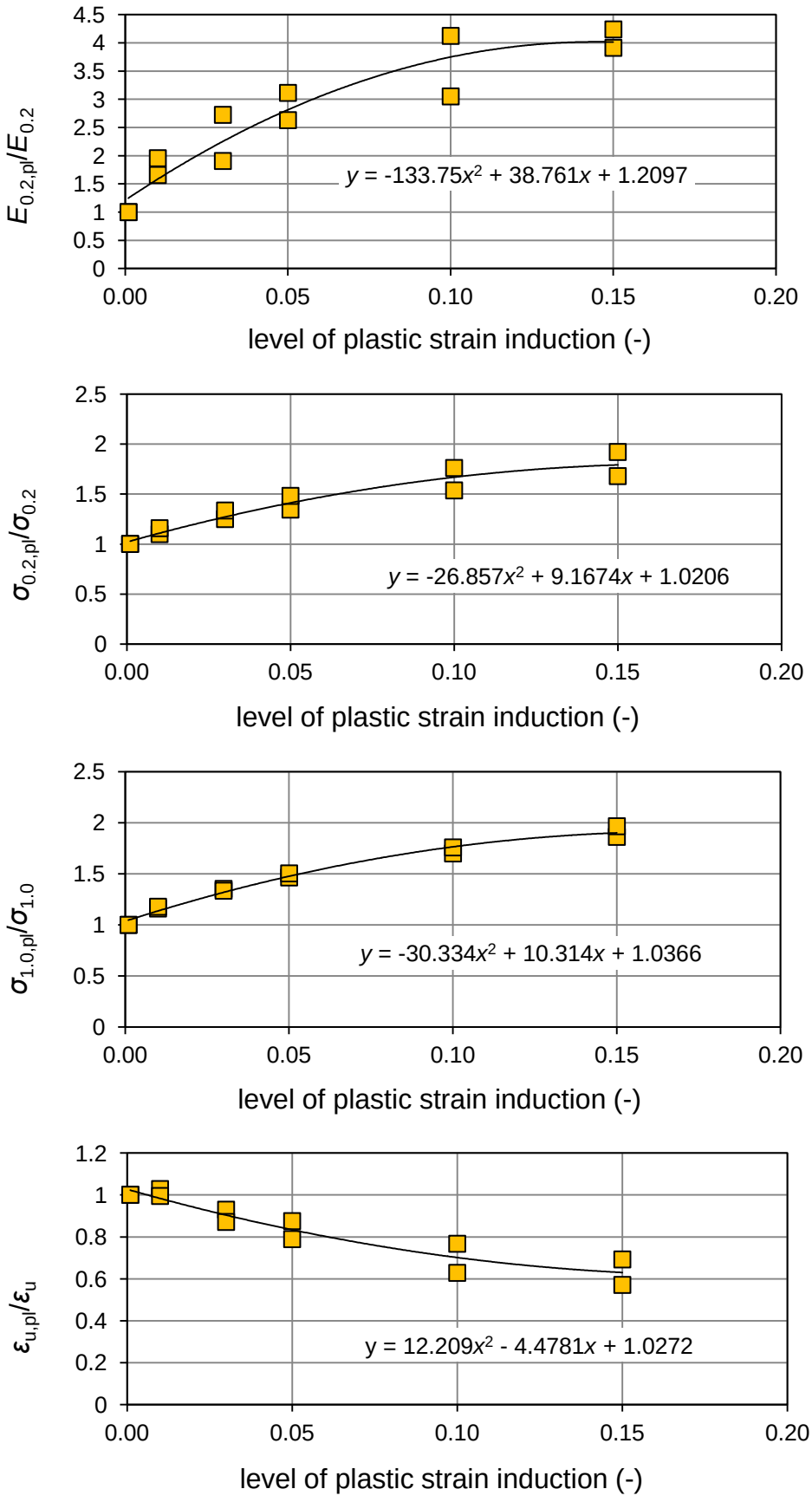

Figure 5.22 *Trends of the mechanical properties for the 1.4404 grade.*

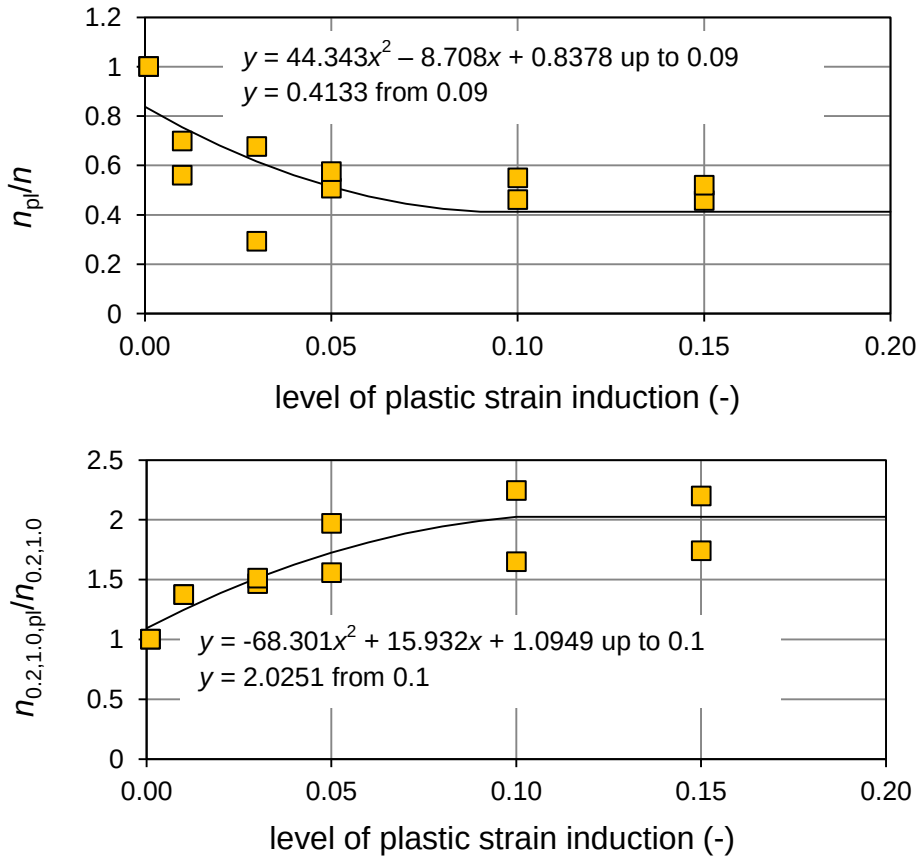

Figure 5.23 *Trends of the mechanical properties for the 1.4404 grade - follow up.*

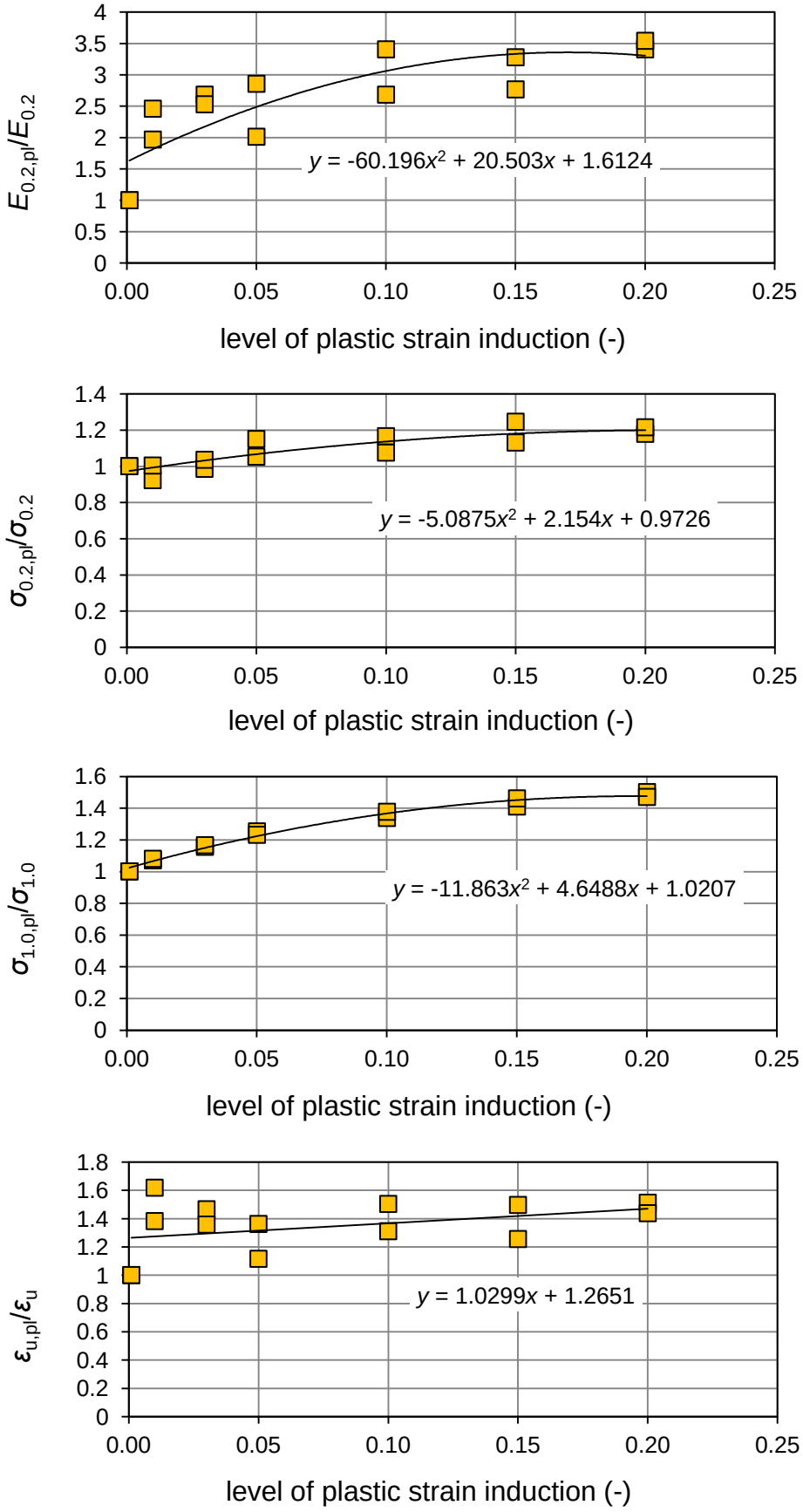

Figure 5.24 *Trends of the mechanical properties for the 1.4162 grade.*

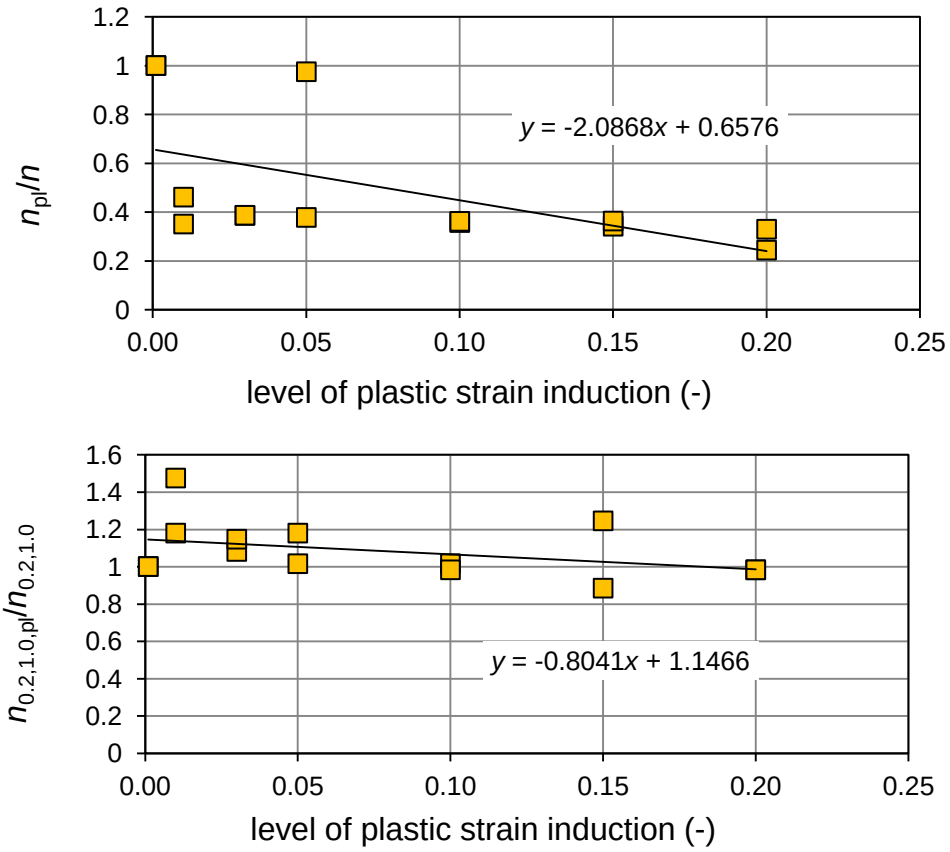

Figure 5.25 *Trends of the mechanical properties for the 1.4162 grade - follow up.*

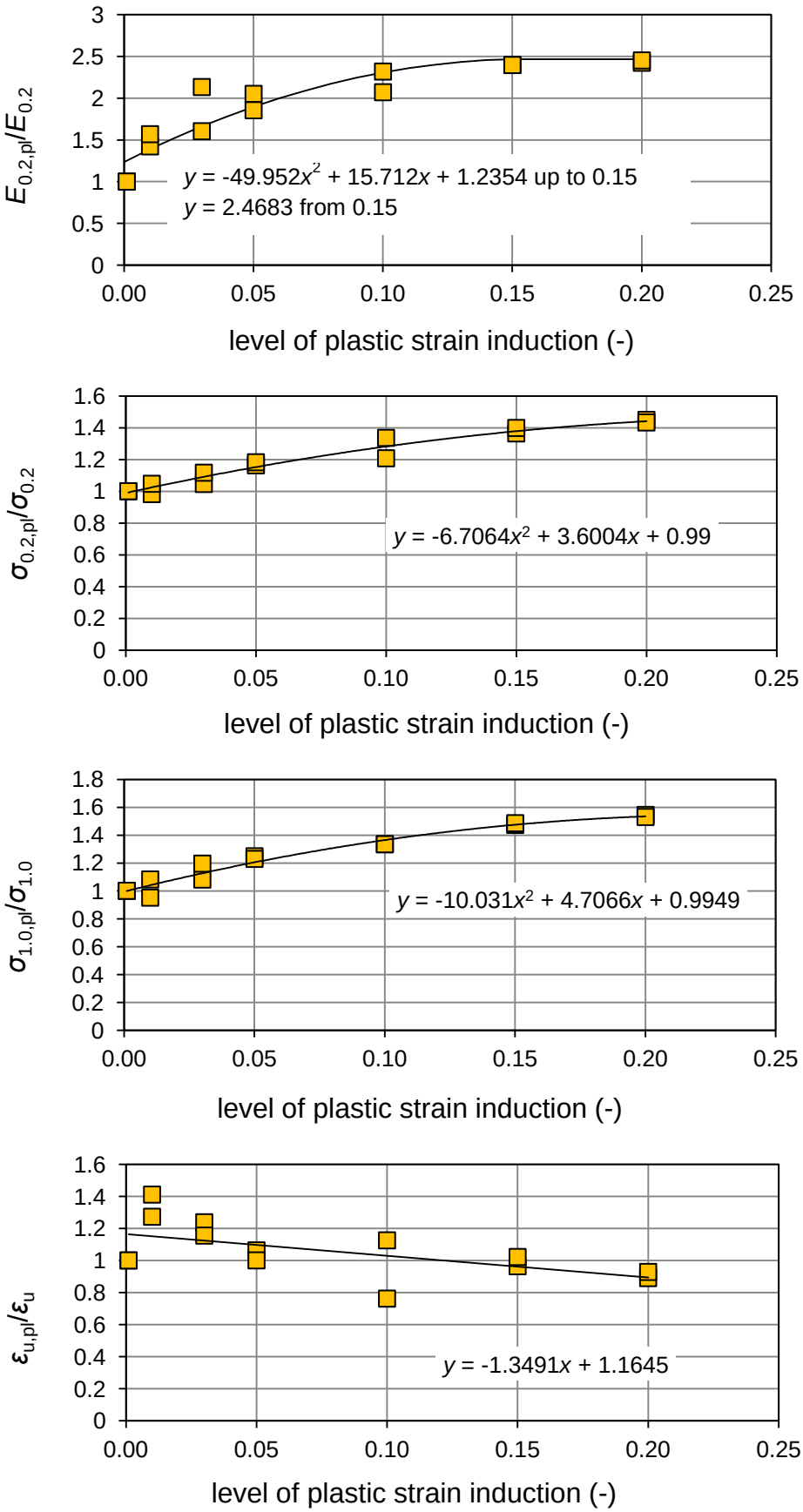

Figure 5.26 *Trends of the mechanical properties for the 1.4462 grade.*

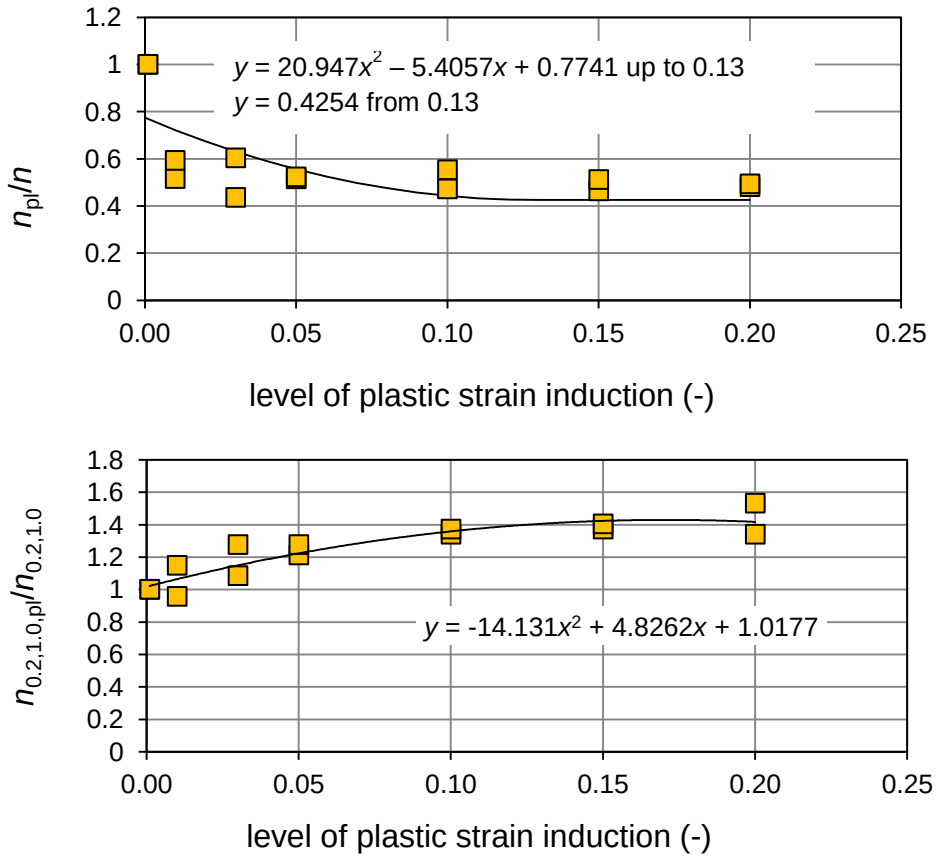

Figure 5.27 *Trends of the mechanical properties for the 1.4462 grade - follow up.*

Stress-strain determination is set by a stress increment for each layer across a thickness for a small increment of strain $\Delta\varepsilon = 10^{-4}$. The final curve is evaluated with 0.0001 strain precision as an average stress response of all layers. Partial isotropic behaviour including linear elastic part of the stress-strain response is implemented by a condition based on the residual stresses after the cold-forming. The material remains elastic until the actual stress reach the von Mises yield condition:

$$\sigma_i = \sqrt{\sigma_{x,i}^2 + \sigma_{z,i}^2 - \sigma_{x,i}\sigma_{z,i}} \leq \sqrt{\sigma_{x,pb}^2 + \sigma_{z,pb}^2 - \sigma_{x,pb}\sigma_{z,pb}} \tag{5.61}$$

where $\sigma_{x,i}$ and $\sigma_{z,i}$ is the instantaneous plan stresses,
$\sigma_{x,pb}$ and $\sigma_{z,pb}$ is the residual plan stresses after cold-bending.

As well as for the fabrication modelling, the further stress-strain response with particular plasticising is determined using the three stage material model (Eq. (3.23) - (3.25)). Stress-strain determination is set by a stress increment for each layer through a thickness for a small increment of strain $\Delta\varepsilon = 10^{-4}$ and expressed for *z*-direction.

5.4 Validation of the model

5.4.1 Comparison of the model with CTU section tests

The analytical model was compared with the section tests executed at CTU. The model is also suitable for a circular hollow section as the analytical procedure is able to solve CHS as well as flat faces and corners of SHS.

Following figures (Figure 5.28 - Figure 5.34) show the comparison of the modelled results with results of the measurement. In the figures there are curves resulting from the Maple model using assumed mechanical properties both for virgin material (marked 1.4404_MILL) and annealed material.

In case of CHS a mill certificate was not available.

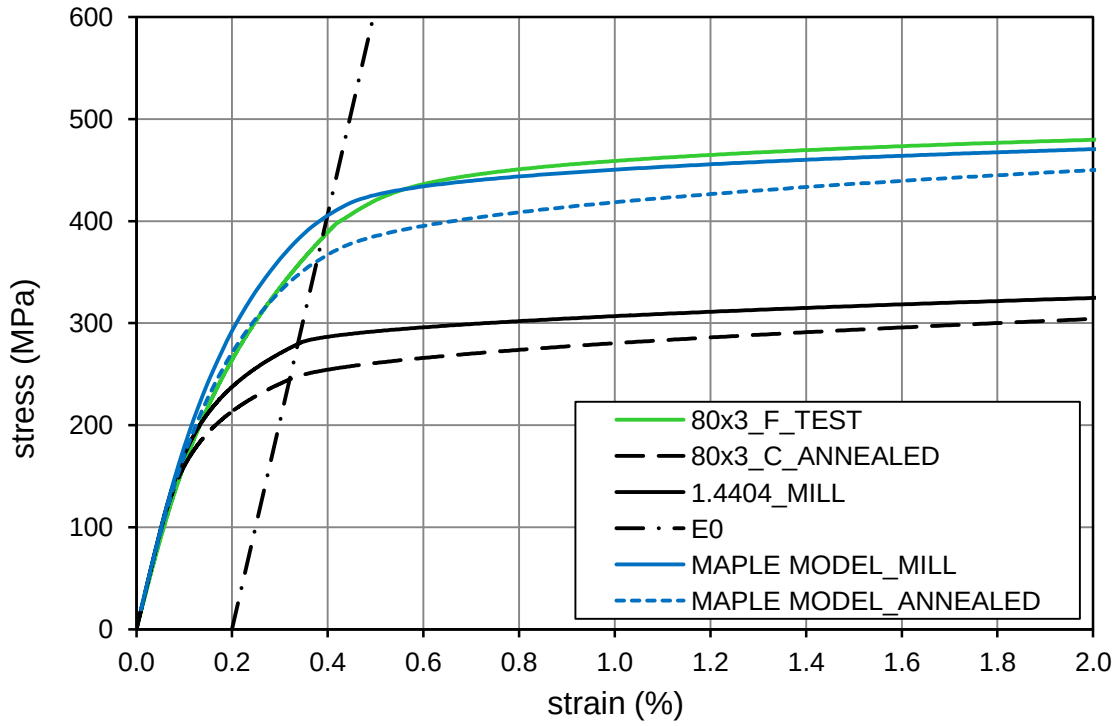

Figure 5.28 *Comparison of the predictive models for the flat face of the SHS 80x3.*

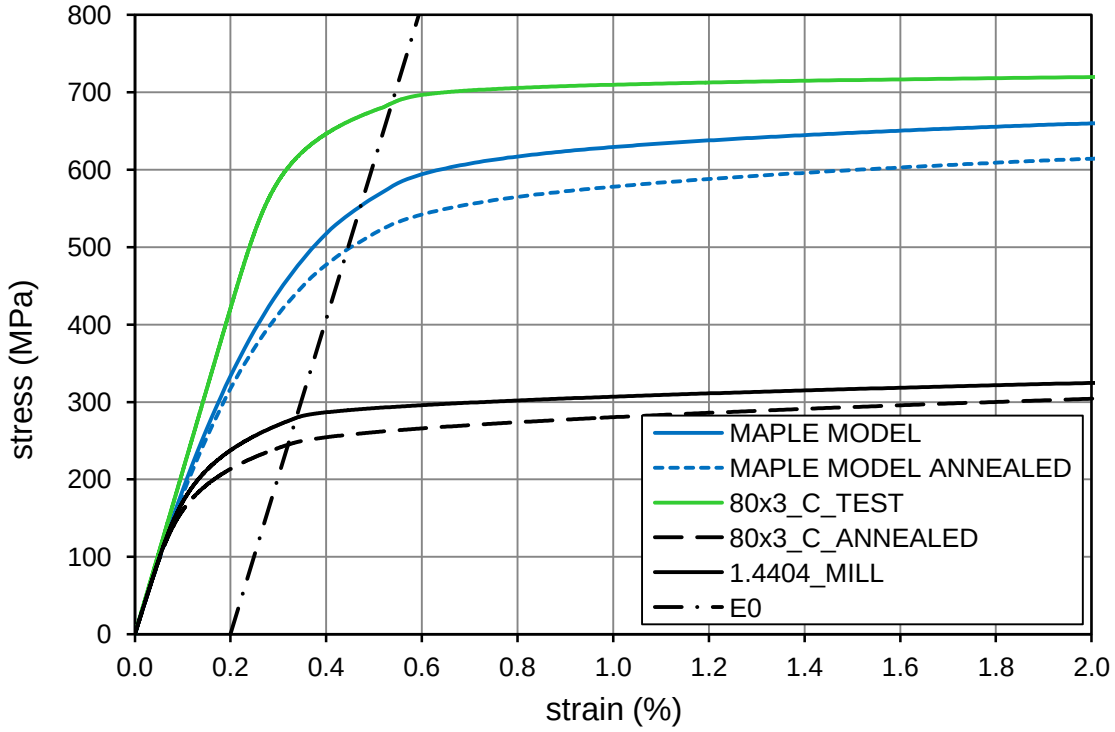

Figure 5.29 *Comparison of the predictive models for the corner of the SHS 80x3.*

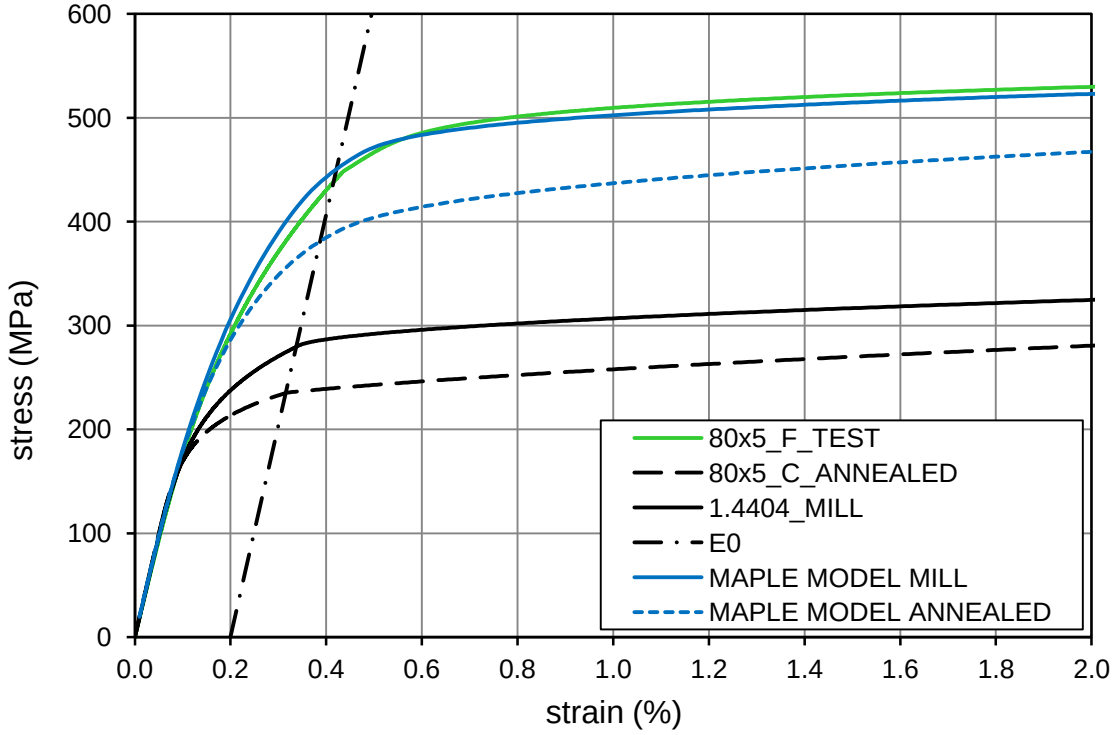

Figure 5.30 *Comparison of the predictive models for the flat face of the SHS 80x5.*

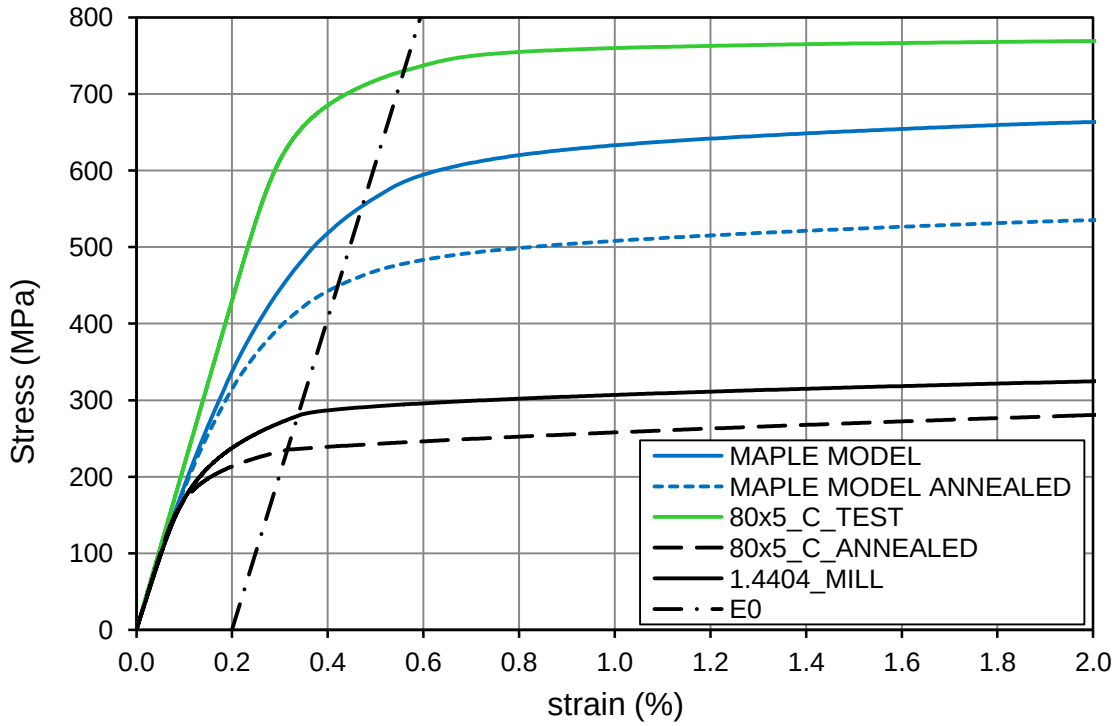

Figure 5.31 *Comparison of the predictive models for the corner of the SHS 80x5.*

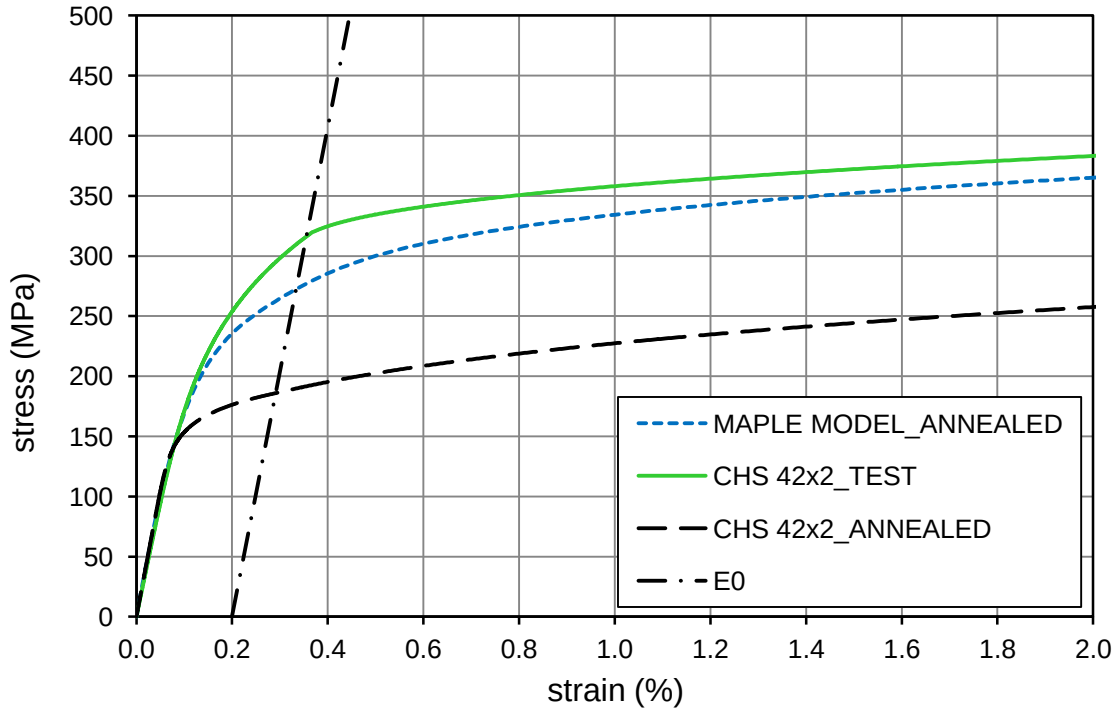

Figure 5.32 *Comparison of the predictive models for the CHS 42.4x2.*

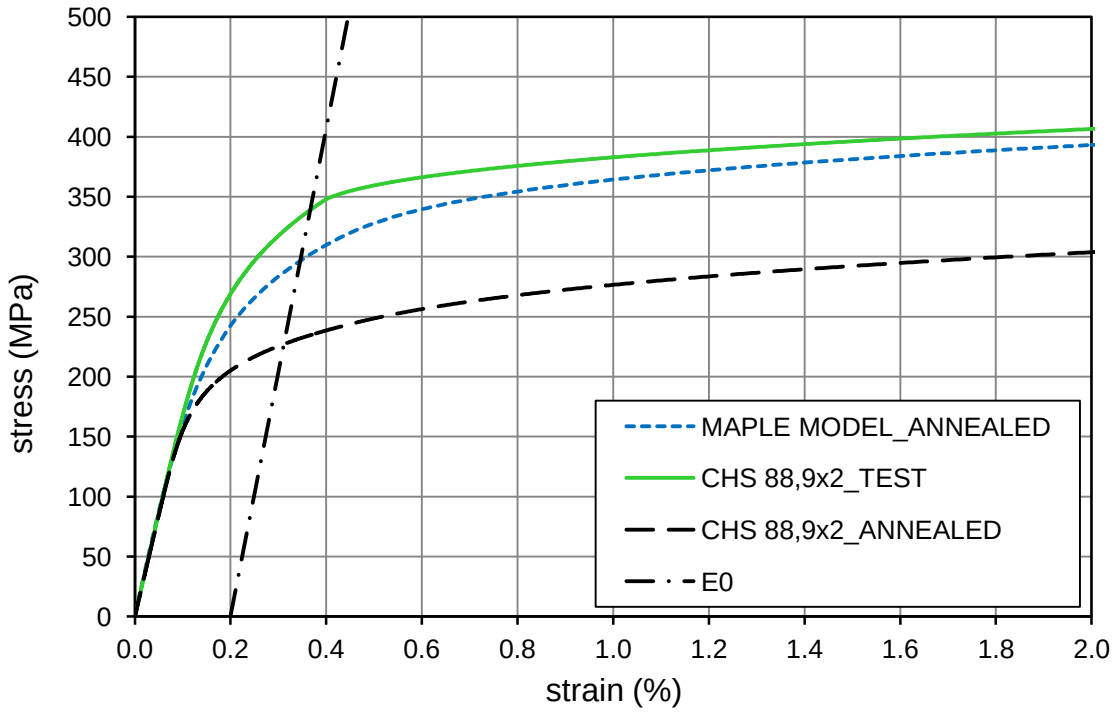

Figure 5.33 *Comparison of the predictive models for the CHS 88.9x2.*

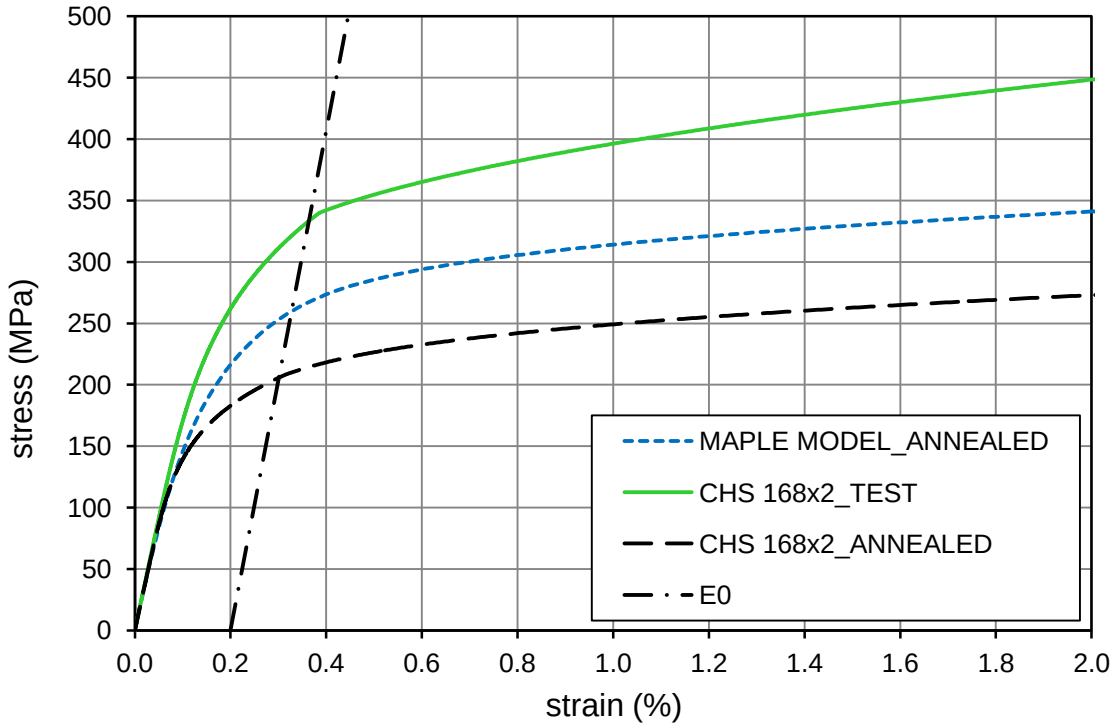

Figure 5.34 *Comparison of the predictive models for the CHS 168.3x2.*

There is need to mention the assumed process of fabrication is simplified significantly, thus the final results can be different (i.e. the model does not involve contact between a roll and a sheet that can cause further enhancement etc.). Nevertheless the figures above

show the model is also suitable for use in CHS properties modelling. The difference between the model and test curves is probably caused by unknown virgin material data. The annealed material used in the model may result in very conservative curves.

In the SHS cases there is closer agreement apparent for the flat faces than for the corners. The mill certificate is not often appropriate source of correct material properties. Thus, the model for annealed material is more suitable for use. For corners the model is rather conservative but still safe for use. The strength enhancement in corners reaches almost 300% representing very high level of cold-forming.

5.4.2 Comparison of the model with tests carried out at Imperial College

The Maple model for corners and flat faces was confronted with the recent extensive experimental programme conducted at Imperial College in London [47] containing 51 flat coupons, 28 corner coupons and 6 full section specimens made both of circular and rectangular hollows sections. This data set employs mill certificate for the sheet mechanical properties which sections were made of. However some tensile tests for corners and flat faces exhibit lower value for the 0.2% proof strength than in case of the mill certificate 0.2% proof strength. Hence these are not applicable for the confrontation due to lack of strength enhancement. Thus all other SHS cases were selected for the comparison as the most appropriate due to the identical or similar grades tested at Imperial College to those tested at CTU (see Chapter 4). Mechanical properties considered in the comparison are reported in Table 5.2. Geometrical properties considered in the Maple model are stated in Table 5.3. Other data are available in [47].

Cross-section		Material grade	E_0 (GPa)	$\sigma_{0.2,\text{mill}}$ (MPa)	$\sigma_{\text{u,mill}}$ (MPa)	n	$n'_{0.2,1.0}$
SHS	150×150×8	1.4404	195	302	605	5.2	3.6
SHS	100x100x5	1.4301	192	310	670	5.6	2.9
SHS	150x150x5	1.4301	192	289	621	5.6	2.9
SHS	100x100x5	1.4571	191	272	562	6.9	3.6
SHS	120x120x5	1.4571	191	268	584	6.9	3.6
SHS	30x30x2	1.4509	190	362	476	6.7	3.1
SHS	40x40x2	1.4509	190	362	476	6.7	3.1
SHS	50x50x2	1.4509	190	364	501	6.7	3.1
SHS	80x80x3	1.4003	199	324	467	8.4	2.5

Table 5.2 *Mechanical properties as stated in the mill certificates and considered in the study.*

Cross-section		Material grade	H (mm)	L (mm)	t -average (mm)	r_i -average (mm)	R_i - average
SHS	150×150×8	1.4404	150.01	150.51	7.76	10.39	90.72
SHS	100x100x5	1.4301	99.99	99.85	4.76	2.08	60.65
SHS	150x150x5	1.4301	149.82	149.88	5.00	6.68	92.21
SHS	100x100x5	1.4571	100.09	99.73	4.69	5.50	60.62
SHS	120x120x5	1.4571	120.30	120.14	4.64	5.79	73.58
SHS	30x30x2	1.4509	29.98	29.97	1.95	1.50	17.84
SHS	40x40x2	1.4509	40.07	40.02	2.02	1.75	24.21
SHS	50x50x2	1.4509	50.14	50.26	1.90	2.50	30.75
SHS	80x80x3	1.4003	79.75	79.74	2.80	3.86	48.98

Table 5.3 *Geometrical properties of the compared specimens.*

As 1.4571 and 1.4301 represent austenitic grades and 1.4509 a ferritic grade, corresponding trends functions for material properties were adopted from grade 1.4404 (for austenitic) and from grade 1.4003 (for ferritic).

The analytical model is confronted with the measured 0.2% proof strength of all investigated cross sections coupons mentioned above. Further figures show confrontation of the corner stress-strain behaviour following by the comparison of the stress-strain behaviour of flat faces. The corner test set-up contained two tensile tests of corners for each section. In case of the flat face the set-up consisted of three specimens for each section. Ferritic 1.4509 SHS were only tested in full section tests and flat faces tests due to their tiny dimensions for corner cutting. Thus in case of stress-strain curves an average recorded stress-strain response is plotted and compared to the analytic solution together with the curve for the material stated in the mill certificate. As it was stated above for bending radius greater than 10t it is possible to neglect the difference between true and nominal values of stress and strain. The section forming radius for flat faces is mostly greater and fulfils the condition. Hence the model for a flat face works with nominal values.

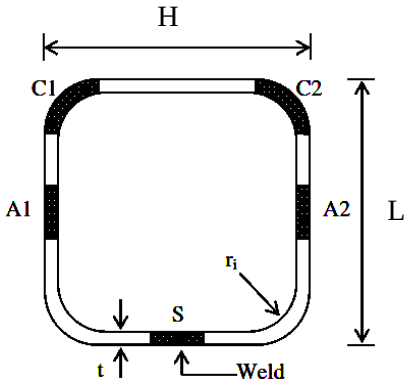

Figure 5.35 *Test set-up of the experimental programme conducted at Imperial College.*

Following figures (Figure 5.36 - Figure 5.39, Figure 5.41 - Figure 5.46) display comparison of the Maple model with the experimental data.

The first set of figures belongs to the corner properties whereas the second set represents comparison with the flat faces results.

Corners

Tests results exhibit a similar strength increase for both corner specimens allowing appropriate further evaluation due to the low scatter.

For selected specimens, there are plotted stress-strain responses according to the Maple model in comparison with the recorded stress-strain behaviour for evaluating the level of agreement.

It was observed the model for a corner is in relatively good agreement with the measured data up to the 2% strain. Thus all other curves (also for flat faces and full sections) are displayed up to this limit.

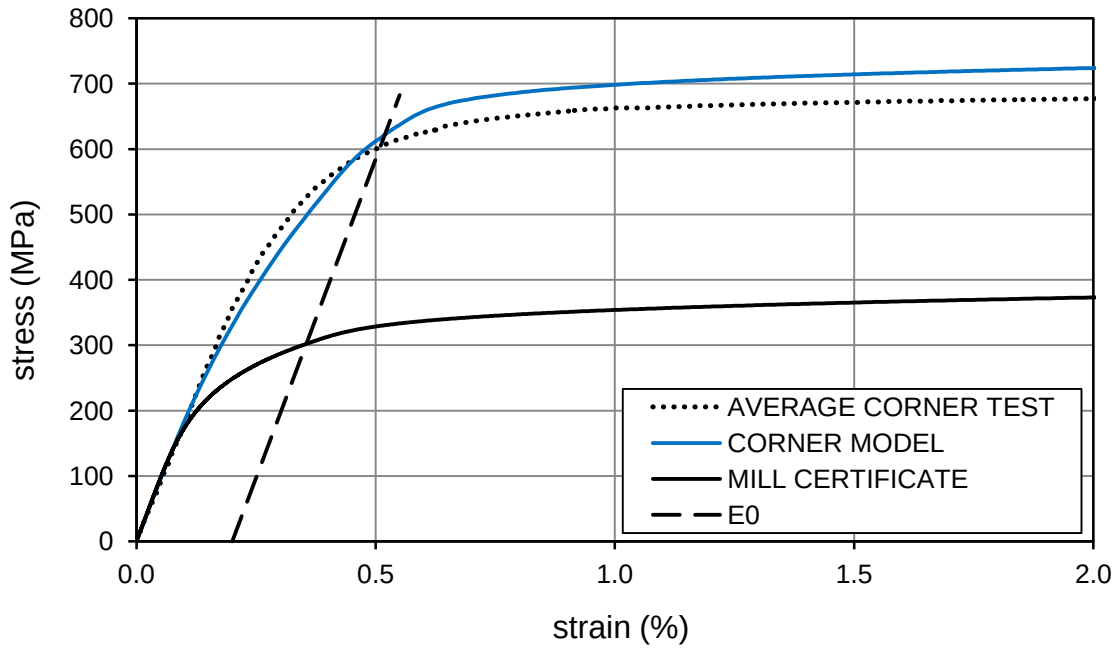

Figure 5.36 *Comparison of the modelled and measured stress-strain response for the corners from the 1.4404 SHS 150x150x8.*

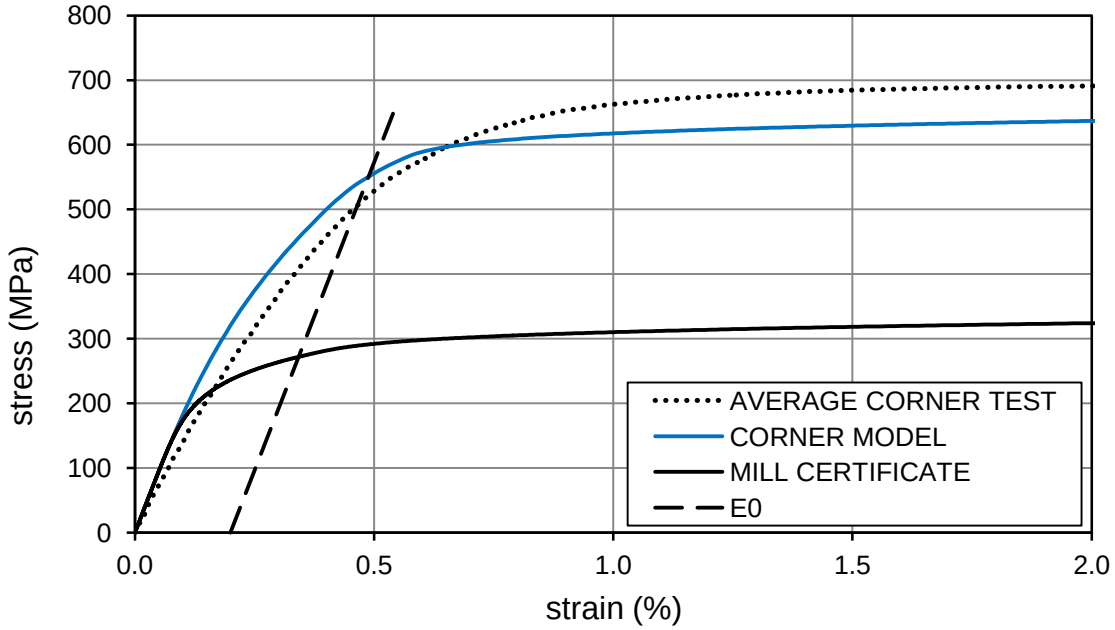

Figure 5.37 *Comparison of the modelled and measured stress-strain response for the corners from the1.4571 SHS 100x100x5.*

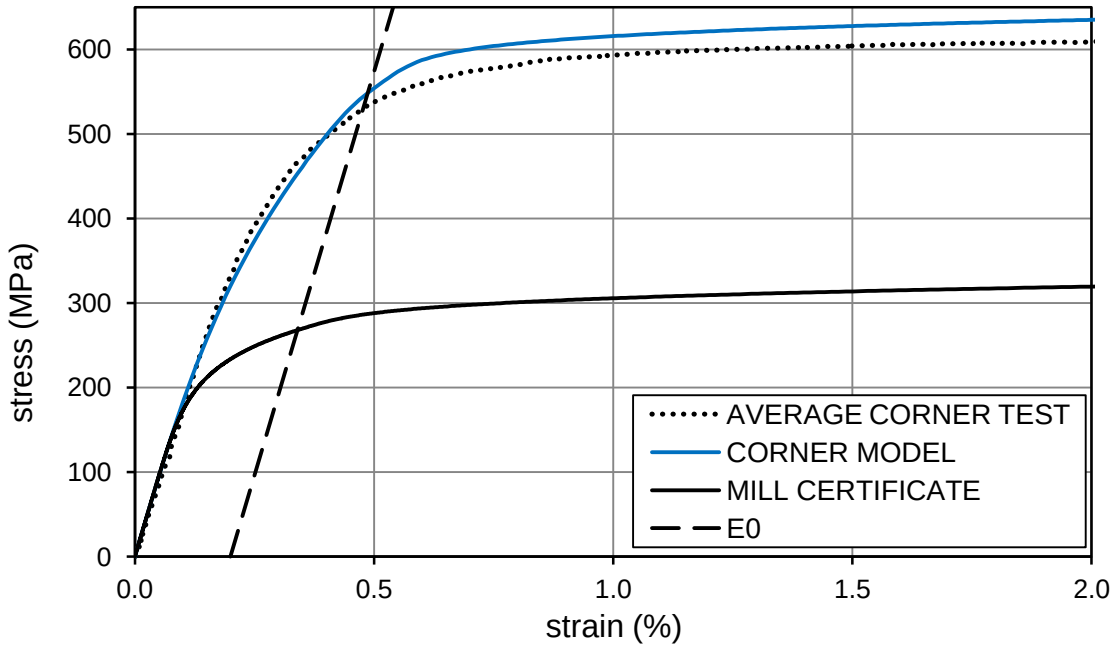

Figure 5.38 *Comparison of the modelled and measured stress-strain response for the corners from the 1.4571 SHS 120x120x5.*

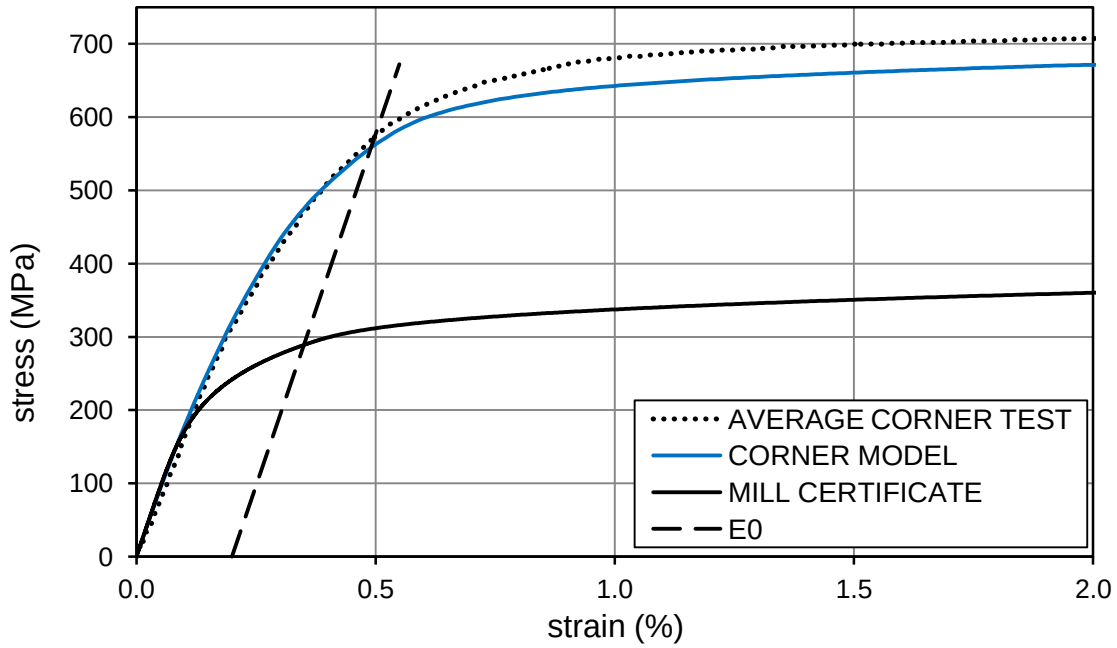

Figure 5.39 *Comparison of the modelled and measured stress-strain response for the corners from the 1.4301 SHS 150x150x5.*

The data provides very close agreement of the Maple model with the experimental data. The key question involves the mill declared properties that may be partially incorrect and cause differences in results as it was stated before.

Flat faces

Provided data refers to exclusion flat faces specimens cut out from the welded area (TEST S – denoted in figures) from further evaluation due to the significant strength increase difference between the welded areas and areas not affected by welding. It is also obvious that for all investigated SHS welded areas exhibit higher strength increase than other flat portions. Correct evaluation of the measured data is also more difficult due to the higher scatter. In case of 1.4571 SHS 120x120x5 there might have been some discrepancy of measuring process as there is considerable difference for flat faces not affected by welding. There is also a possibility of influencing the results by different fabricating routes. It should be noted rectangular hollow sections do not have to be always fabricated by making into a circular tube with subsequent forming into a final shape. Another possible fabricating way is making four cold-rolled corners directly and then welding edges of a sheet together. This is probably case of 1.4301 SHS 150x150x5 where the results of flat faces outside the welded area exhibit almost no strength increase. Also the dimension of 150 mm is commonly used limit for the change of the fabricating way.

As for corners, there are plotted stress-strain diagrams according to the calculation of the Maple model in comparison with the recorded stress-strain curve for evaluating the agreement level. However, for more clearance in the comparison of stress-strain diagrams there are used only coupons A1, A2 cut out from areas not affected by welding.

Due to the consistent approach, stress-strain responses are displayed up to 2% as it is depicted for corners results.

For the analytical model for flat faces there are introduced two ways of considering the plastic strain at the final state of flat faces. As the process of making corners and flattening the parts of faces is related to each other it is complicated to express particular effects on corner and flat faces individually. Also the mill certificate is not always appropriate source of the virgin material (the safe values of strength are obtainable from an annealed material test as it is stated before). Plotted model results are marked by "RS" and "CS" labels to differentiate the methods. Due to the planar analytical solution related to the previous expressions, two methods for evaluating induced plastic strain for material properties calculation are presented. Plastic strain induced is essential for new material properties providing. Hence "RS" denotes plastic strains during a process of bending into a circular tube with subsequent reverse bending into a flat part ("RS" model was used before in Section 5.4.1 as the primary model) whilst "CS" denotes final plastic strain for new properties resulting from the process of bending only into a circular hollow section (see Figure 5.40).

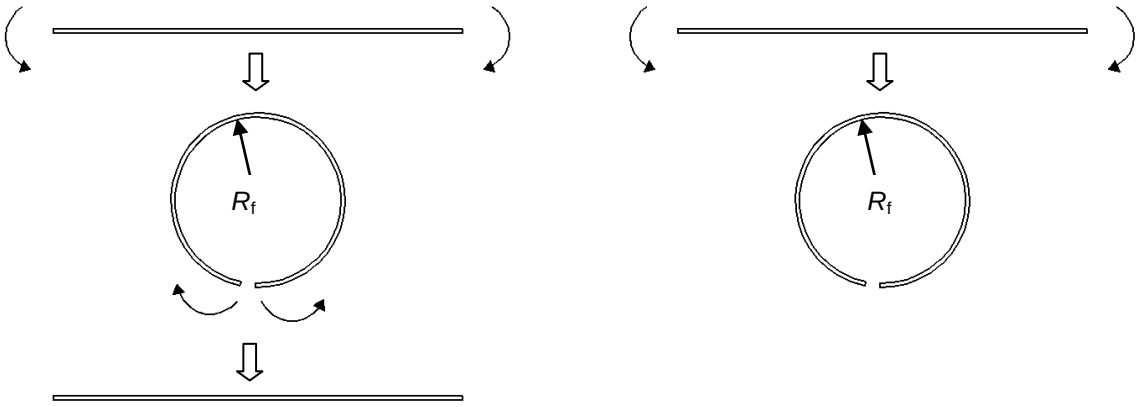

Figure 5.40 *Scheme of the methods for the flat faces fabrication modelling. Left figure represents "RS", right hand figure represent "CS".*

Model "RS" will provide higher values of induced plastic strain and therefore also higher strength enhancement. Next figures depict comparison of the modelled flat face 0.2% stress strain curves and test results.

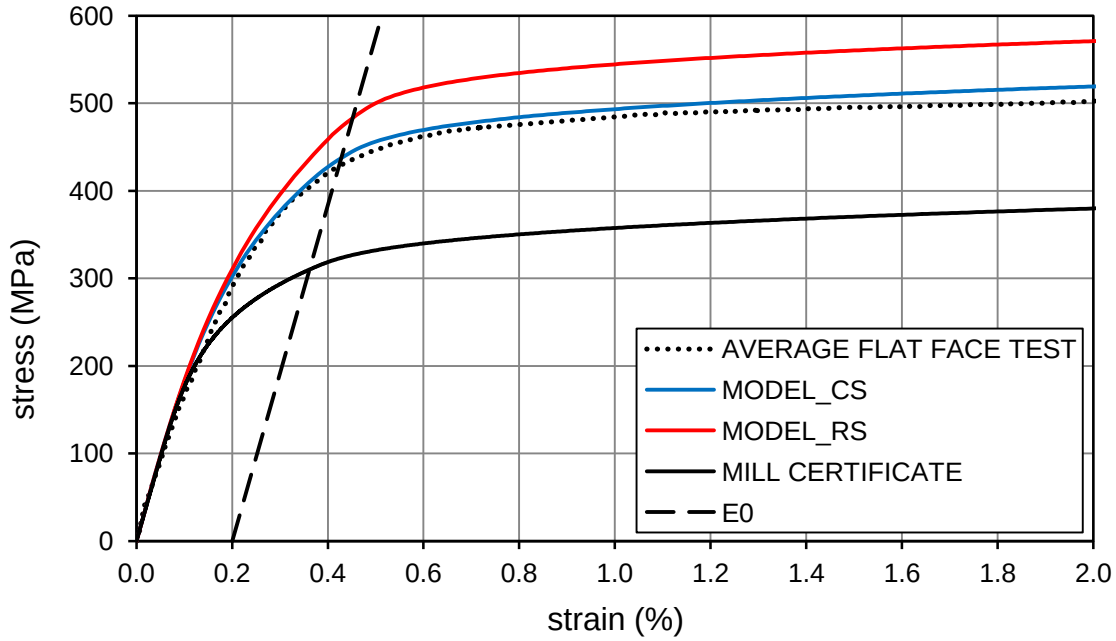

Figure 5.41 *Comparison of the modelled and measured stress-strain response for the flat faces from the 1.4301 SHS 100x100x5.*

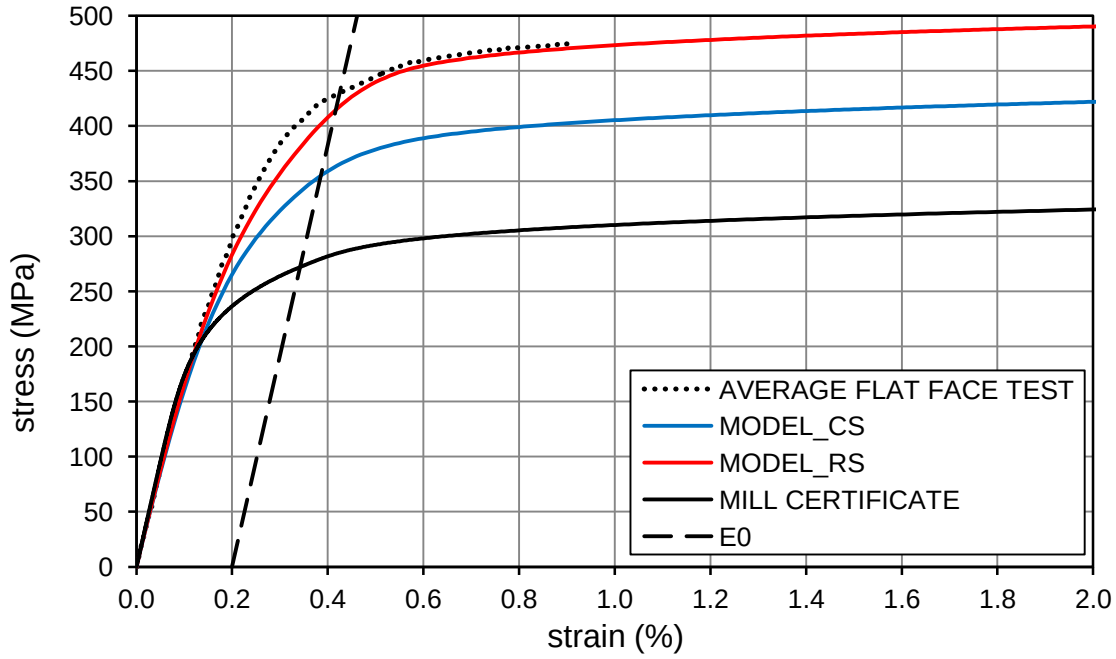

Figure 5.42 *Comparison of the modelled and measured stress-strain response for the flat faces from the 1.4571 SHS 100x100x5.*

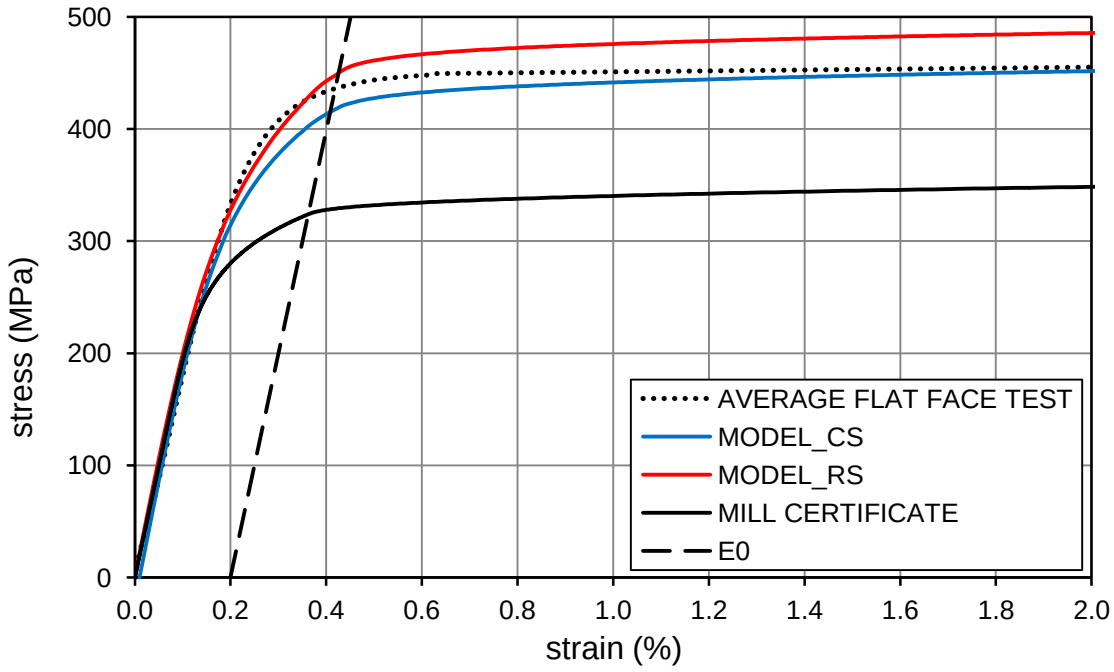

Figure 5.43 *Comparison of the modelled and measured stress-strain response for the flat faces from the 1.4003 SHS 80x80x3.*

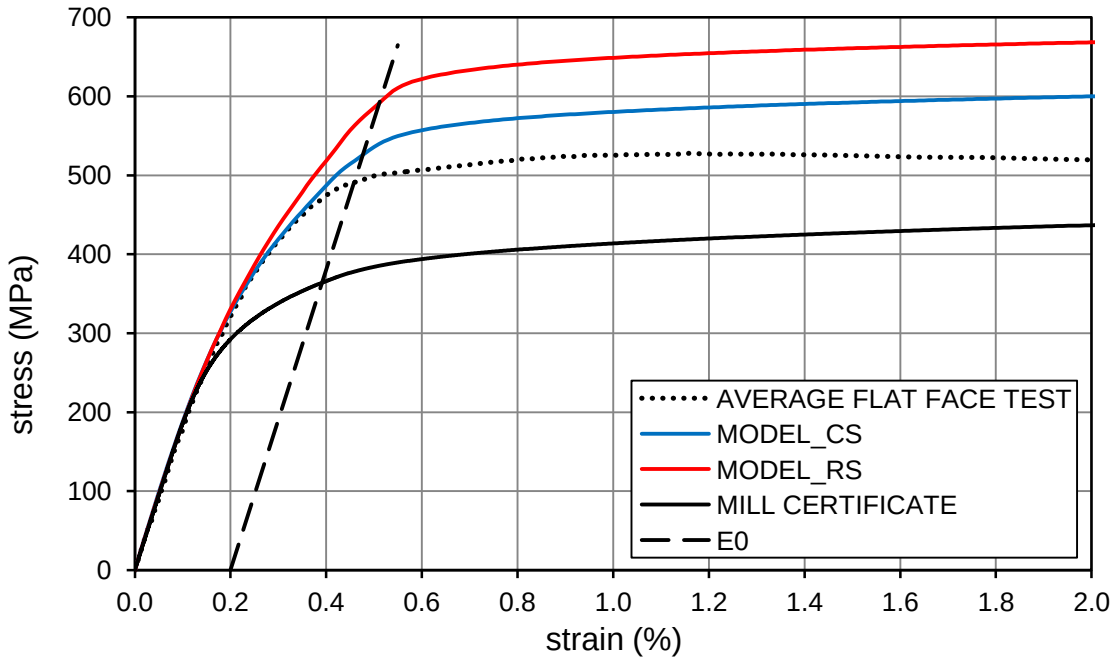

Figure 5.44 *Comparison of the modelled and measured stress-strain response for the flat faces from the 1.4509 SHS 30x30x2.*

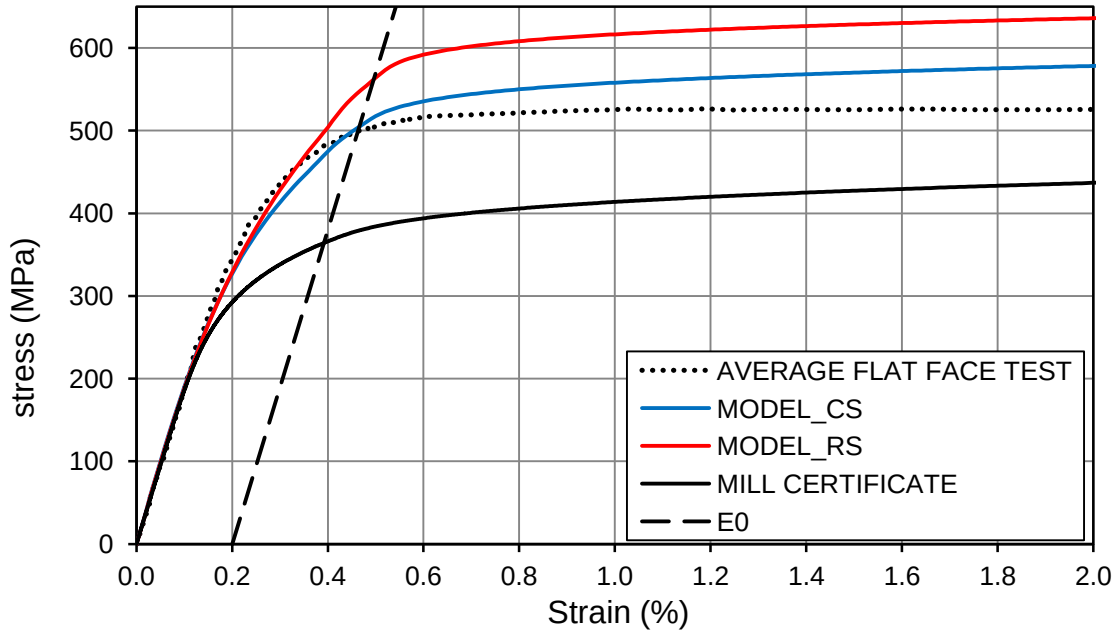

Figure 5.45 *Comparison of the modelled and measured stress-strain response for the flat faces from the 1.4509 SHS 40x40x2.*

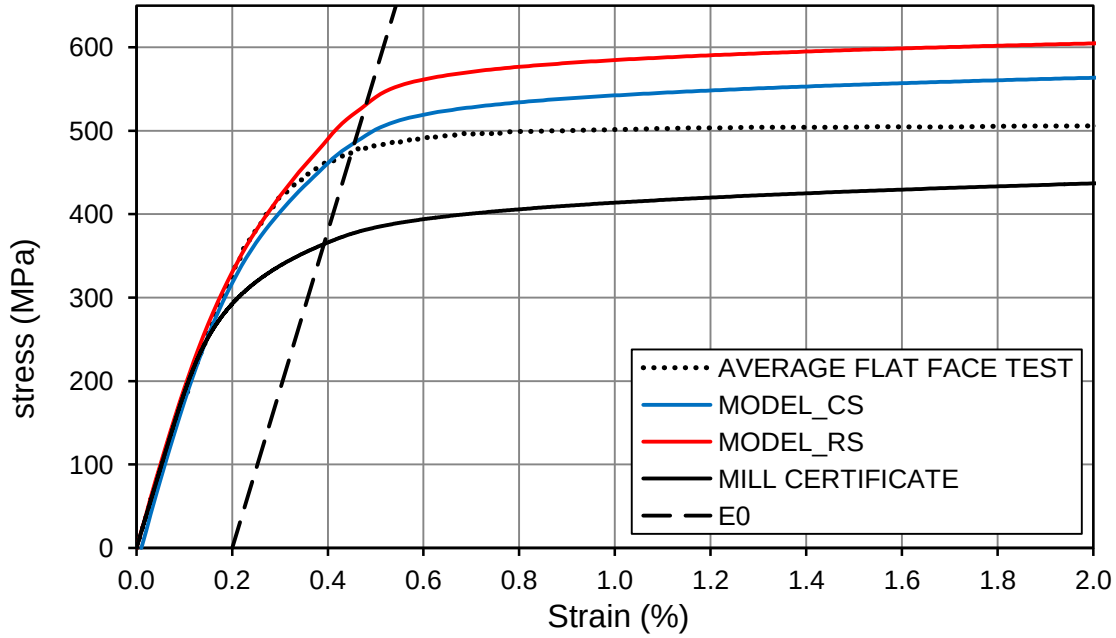

Figure 5.46 *Comparison of the modelled and measured stress-strain response for the flat faces from the 1.4509 SHS 50x50x2.*

Despite the fact that test results doesn't clearly match the "CS" nor the "RS" model, most cases rather indicate higher correlation with the "CS" model that gives lower values of the strength increase. The author also prefers this model as it gives safer prediction to structural calculations. Differences between the modelled response and the measured curve could be caused by a lot of circumstances. Modelled behaviour can be affected by incorrect material properties inputs due to lack of sufficient virgin material data with unknown real coiling and uncoiling radii. That could result in the difference between the model and the test data.

5.4.3 Comparison of the model with test results and recent predictive models

Following figures (Figure 5.54 - Figure 5.61) display comparison of the Maple model with the prediction methods and the experimental data.

The first set of figures belongs to the corner properties whereas the second set represents comparison with flat faces results.

Corners

For the corners test results with the particular inner radius to thickness ratio are plotted among the curves obtained from predictive formulas and the Maple model according to the varying r_i/t ratio (Figure 5.47 - Figure 5.52).

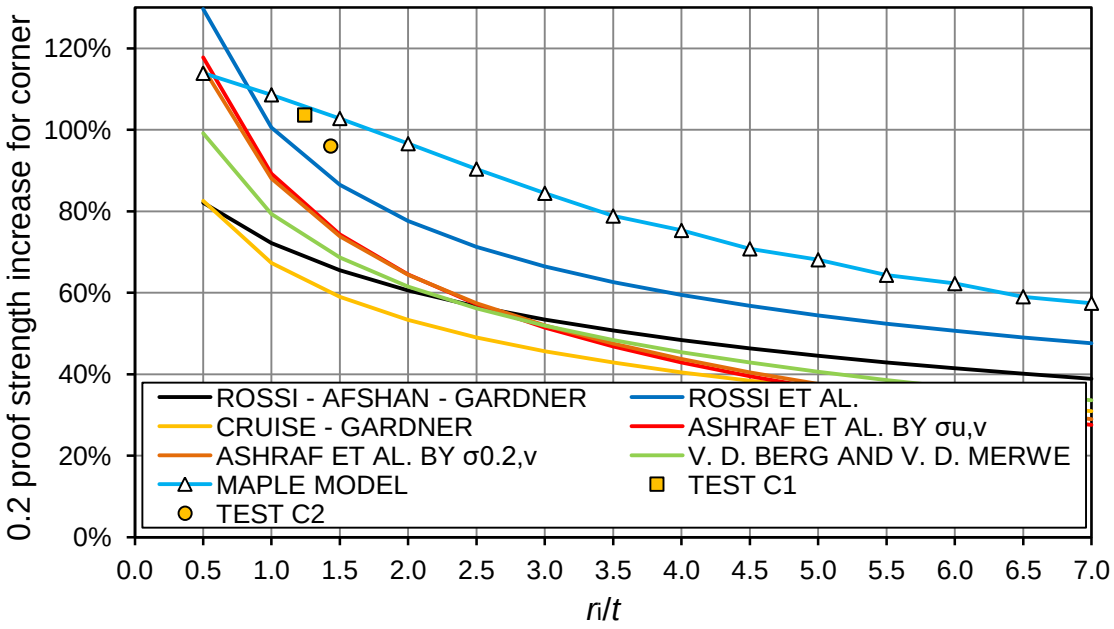

Figure 5.47 *Results of the corner tests in comparison with the Maple model and predictive methods for the SHS 150x150x8 made of 1.4404.*

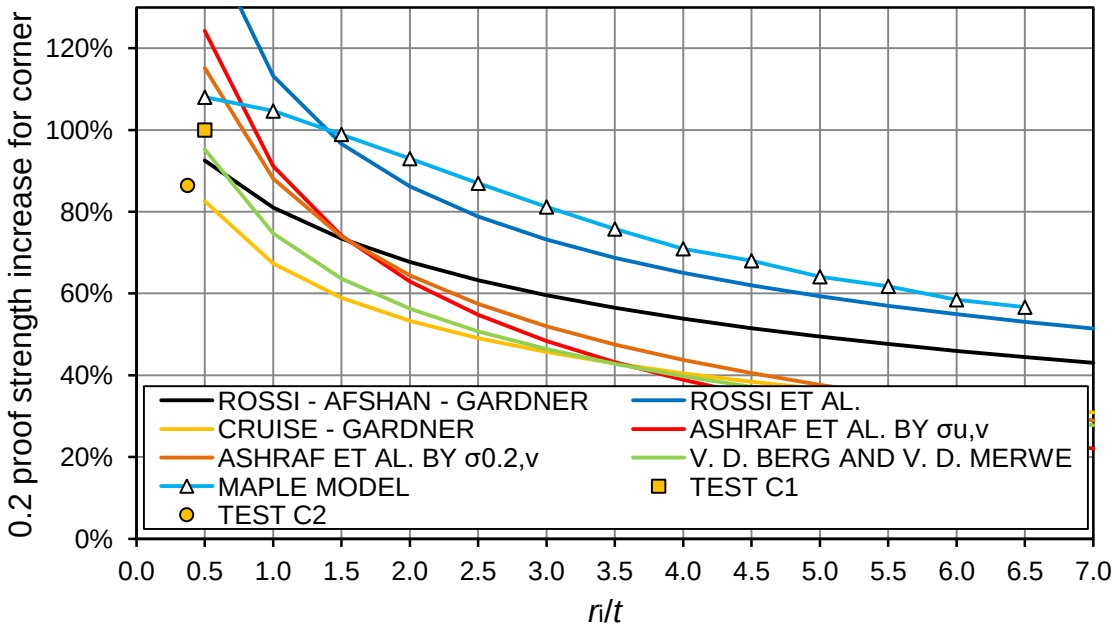

Figure 5.48 *Results of the corner tests in comparison with the Maple model and predictive methods for the SHS 100x100x5 made of 1.4301.*

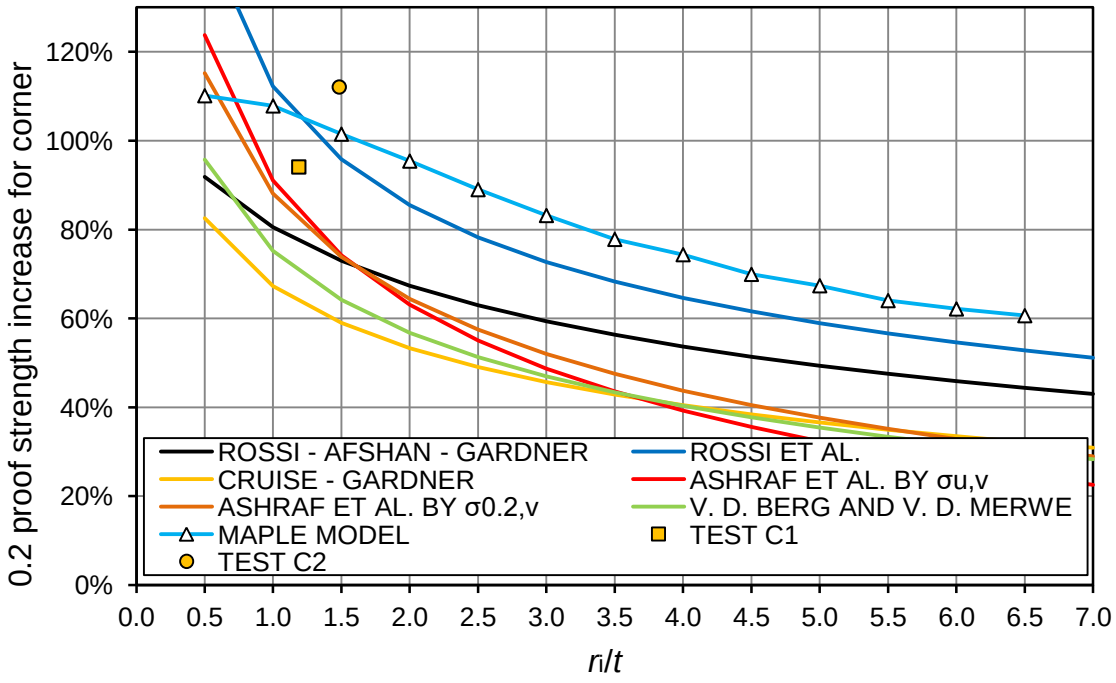

Figure 5.49 *Results of the corner tests in comparison with the Maple model and predictive methods for the SHS 150x150x5 made of 1.4301.*

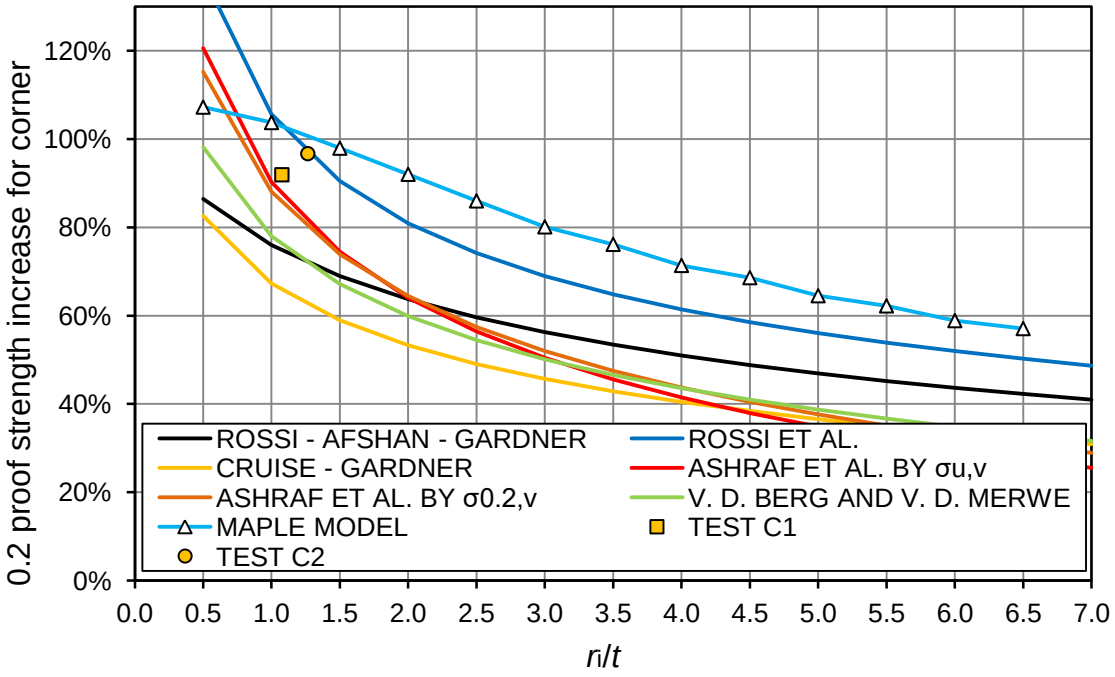

Figure 5.50 *Results of the corner tests in comparison with the Maple model and predictive methods for the SHS 100x100x5 made of 1.4571.*

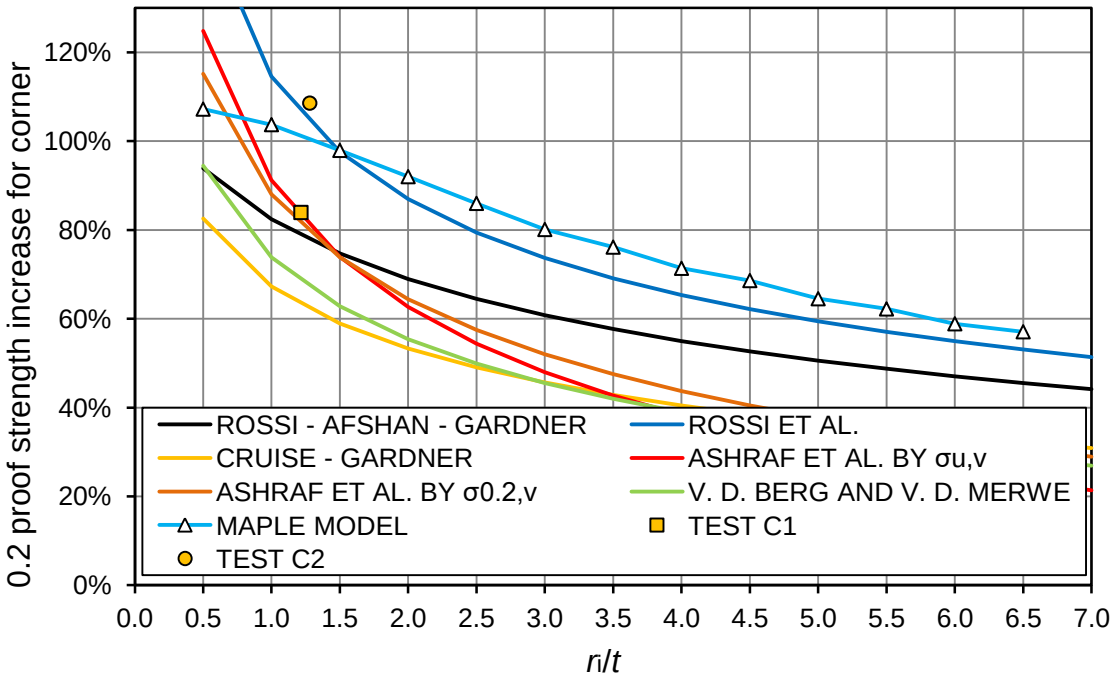

Figure 5.51 *Results of corner tests in comparison with the Maple model and predictive methods for the SHS 120x120x5 made of 1.4571.*

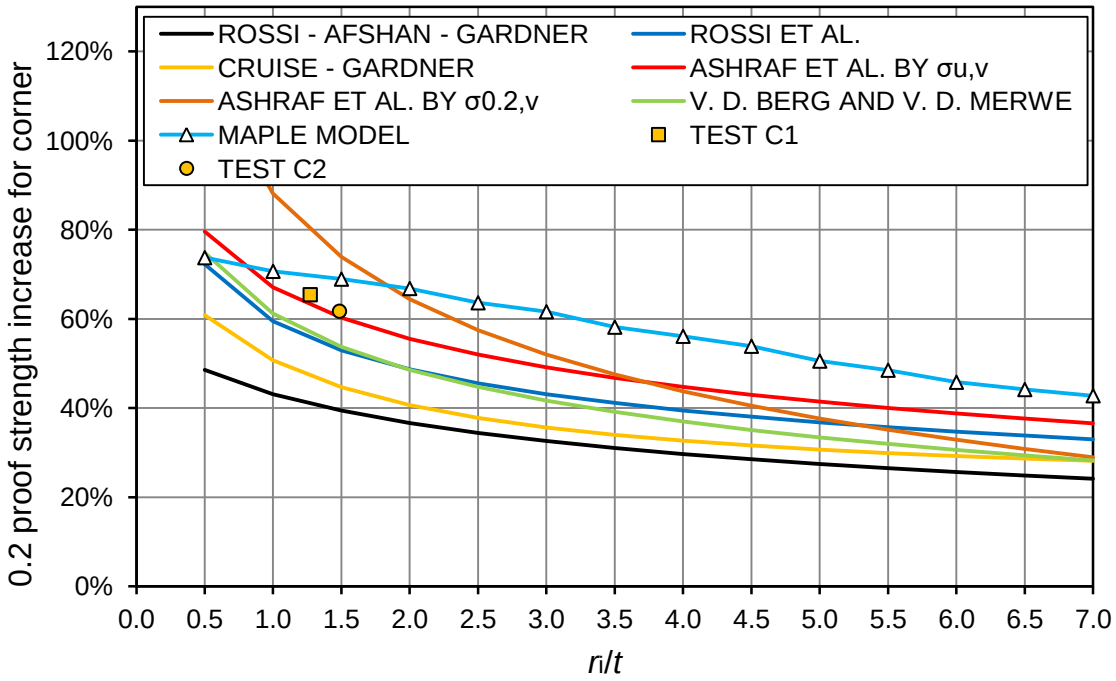

Figure 5.52 *Results of the corner tests in comparison with the Maple model and predictive methods for the SHS 80x80x3 made of 1.4003.*

Tests results exhibit a similar strength increase for both corner specimens.

Flat faces

Next figures (Figure 5.53 - Figure 5.61) show comparisons of the experimental data for the flat faces and other predictive methods with the proposed Maple model. As for the corners, firstly there are plotted records of the 0.2% proof strength increase for particular stainless steel grades with particular ratio R_f/t into the recent predictive and proposed curves.

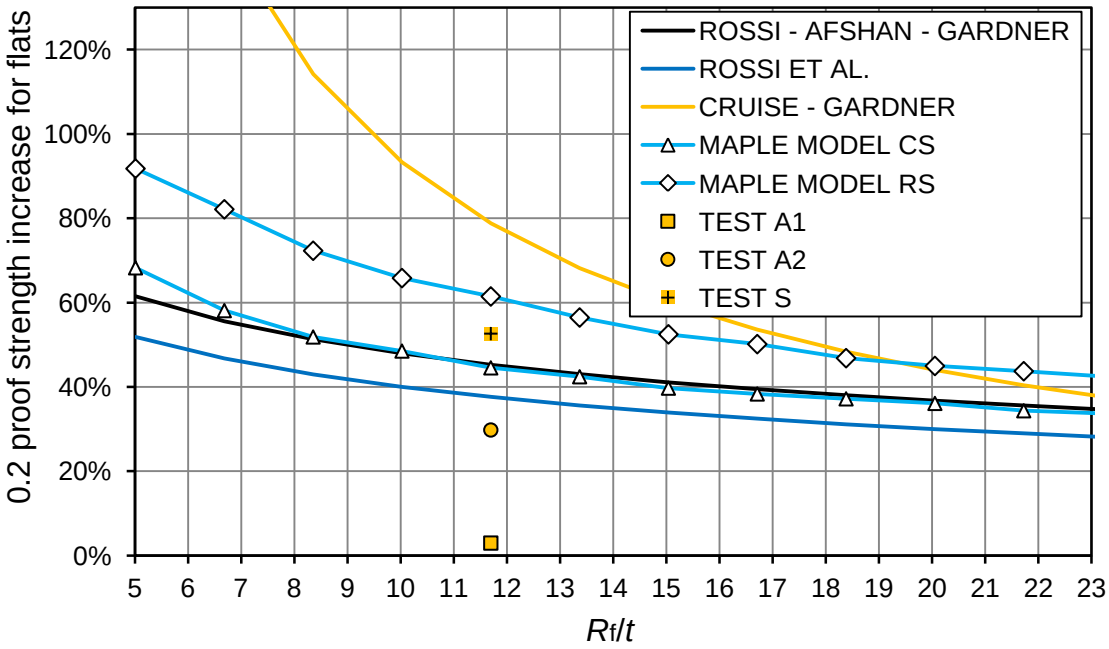

Figure 5.53 *Results of the flat faces tests in comparison with the Maple model and predictive methods for the SHS 150x150x8 made of 1.4404.*

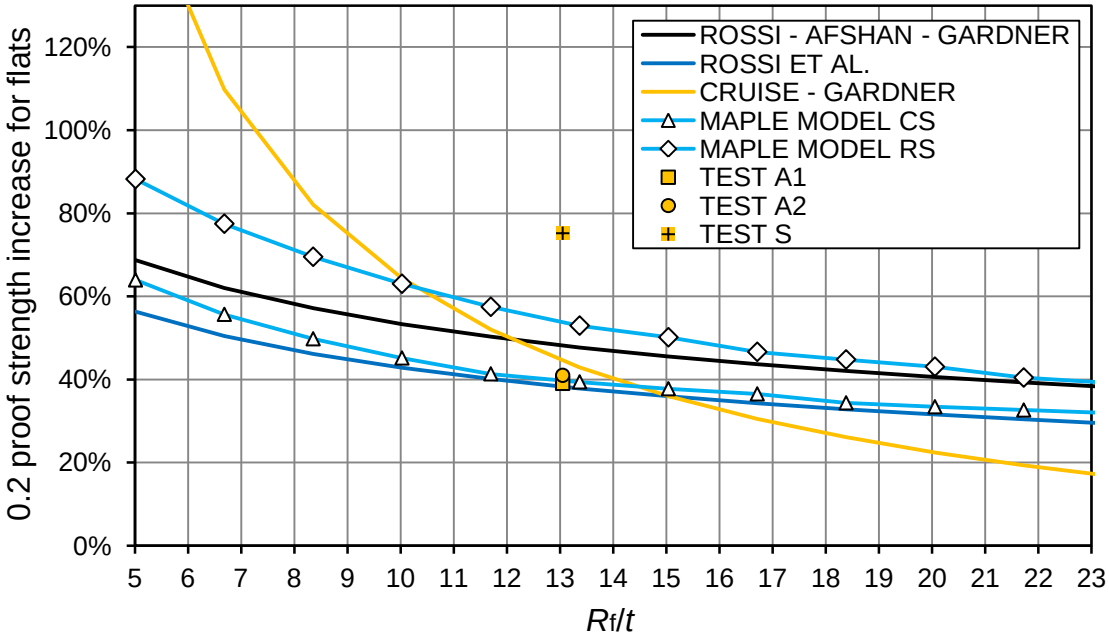

Figure 5.54 *Results of the flat face tests in comparison with the Maple model and predictive methods for the SHS 100x100x5 made of 1.4301.*

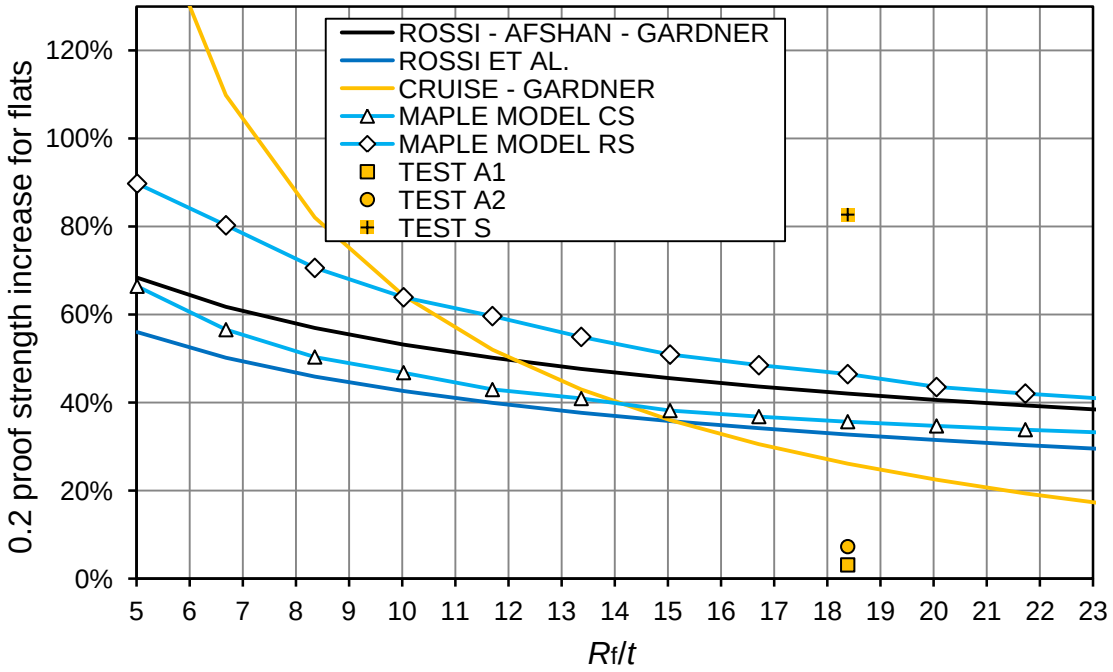

Figure 5.55 *Results of the flat face tests in comparison with the Maple model and predictive methods for the SHS 150x150x5 made of 1.4301.*

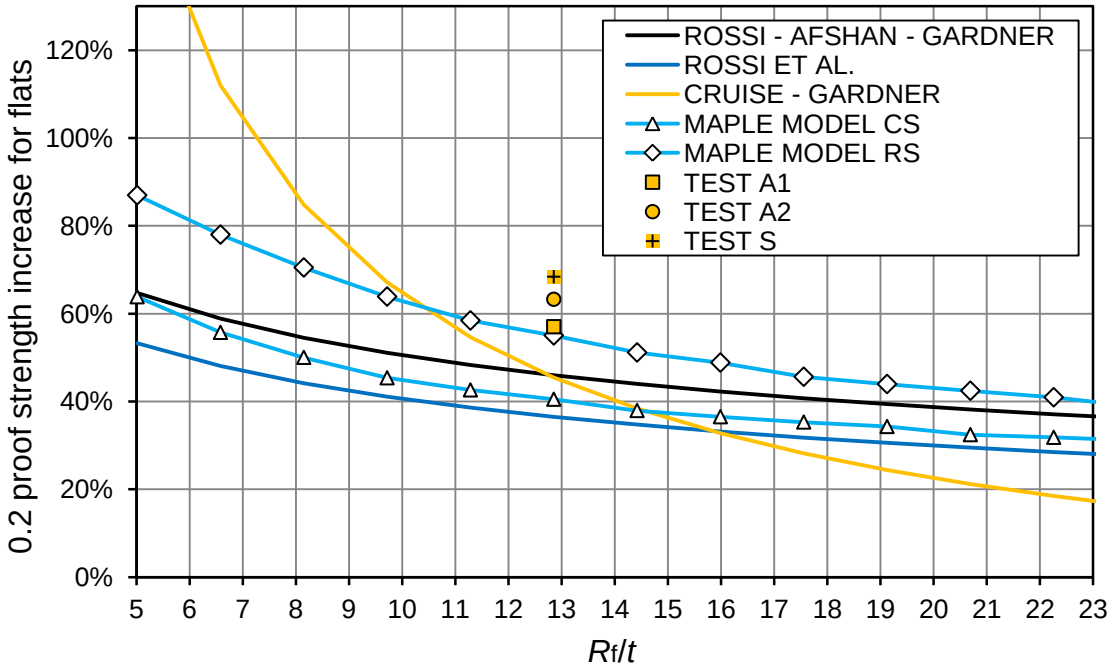

Figure 5.56 *Results of the flat face tests in comparison with the Maple model and predictive methods for the SHS 100x100x5 made of 1.4571*

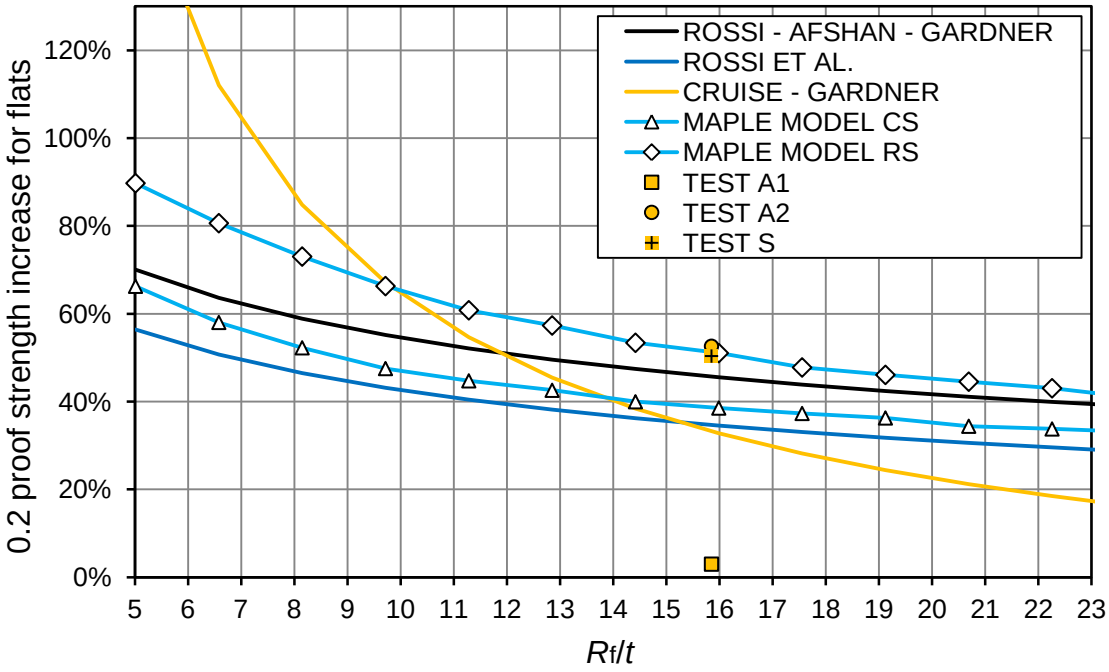

Figure 5.57 *Results of the flat face tests in comparison with the Maple model and predictive methods for the SHS 120x120x5 made of 1.4571*

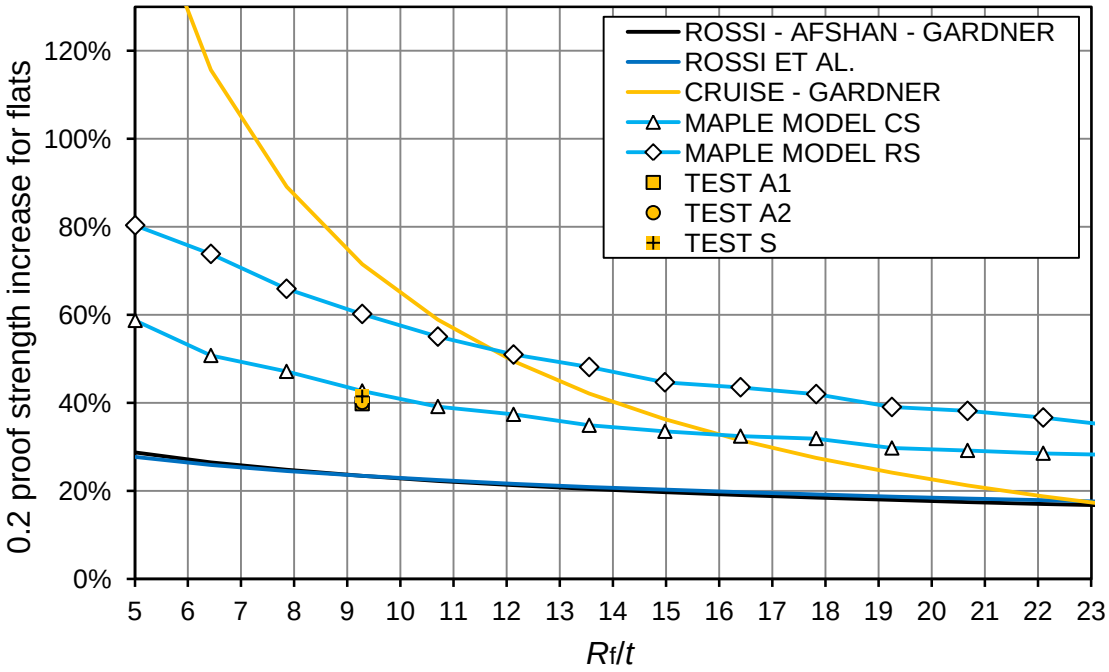

Figure 5.58 *Results of the flat face tests in comparison with the Maple model and predictive methods for the SHS 30x30x2 made of 1.4509.*

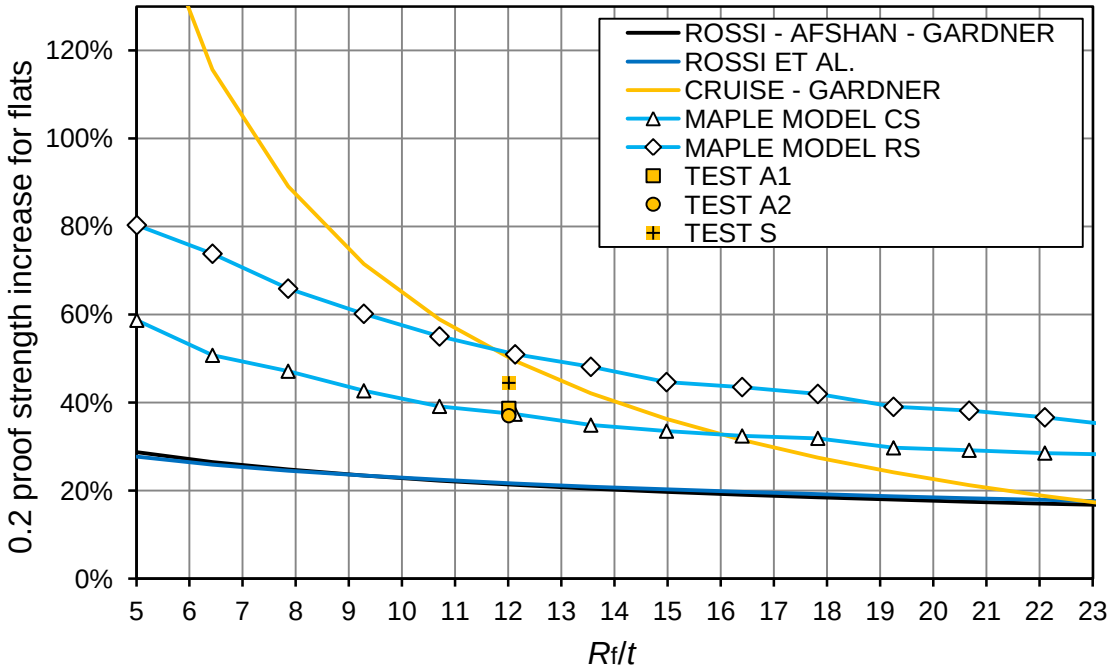

Figure 5.59 *Results of the flat face tests in comparison with the Maple model and predictive methods for the SHS 40x40x2 made of 1.4509.*

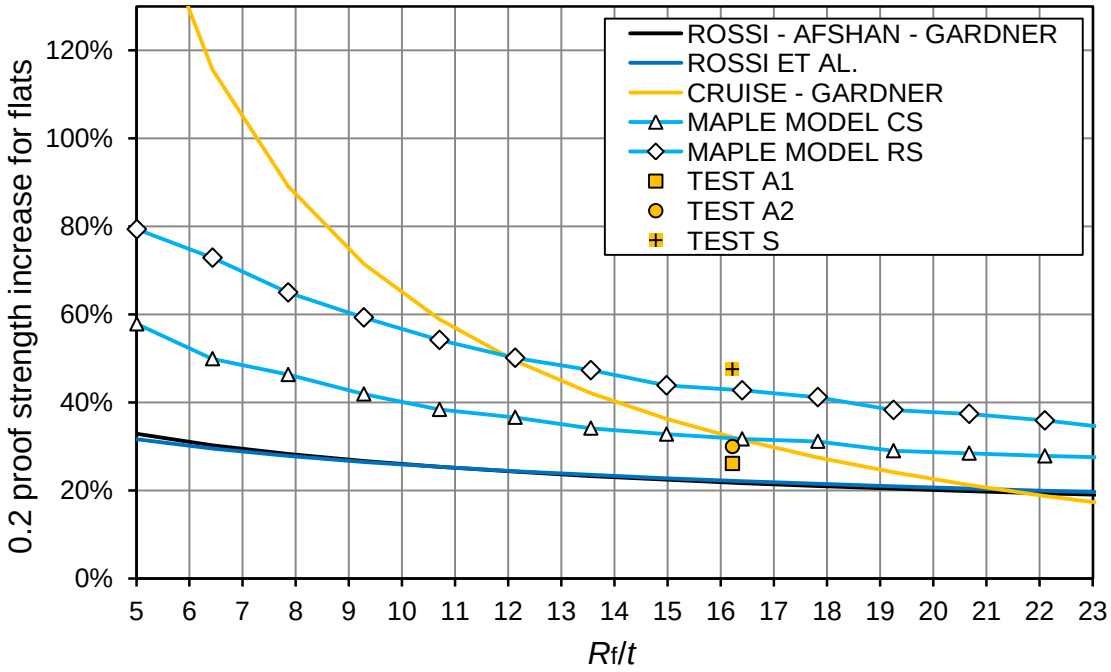

Figure 5.60 *Results of the flat face tests in comparison with the Maple model and predictive methods for the SHS 50x50x2 made of 1.4509.*

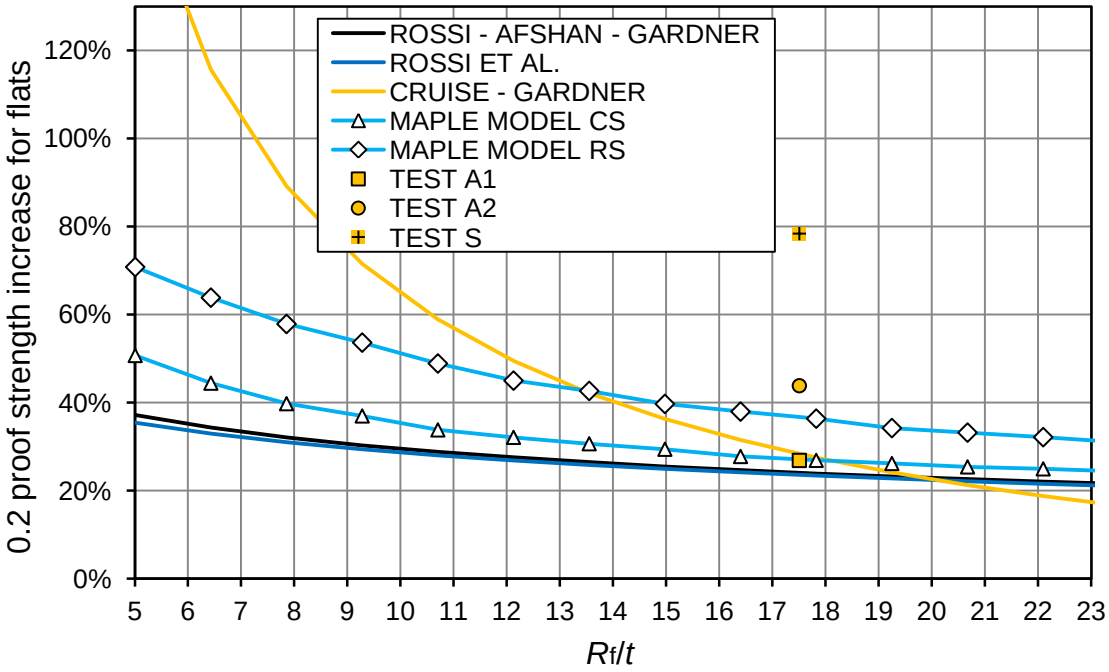

Figure 5.61 *Results of the flat face tests in comparison with the Maple model and predictive methods for the SHS 80x80x3 made of 1.4003.*

5.4.4 Comparison of the model with recent predictive methods

Following figures (Figure 5.62 -Figure 5.70) display a comparison of the recent predictive methods for corner and flat faces strength enhancement described in Chapter 3 – section 3.3 and the Maple model using experimental results gathered at CTU (see Chapter 4 – section 4.2 and 4.3). The first one (Figure 5.62) displays dependency of the 0.2% proof strength increase on the ultimate strength to the 0.2% proof strength ratio. Four values represent four tested grades (1.4404, 1.4003, 1.4162 and 1.4462). The nominal section serving for the prediction was set as SHS 100x4 with r_i/t = 1.5.

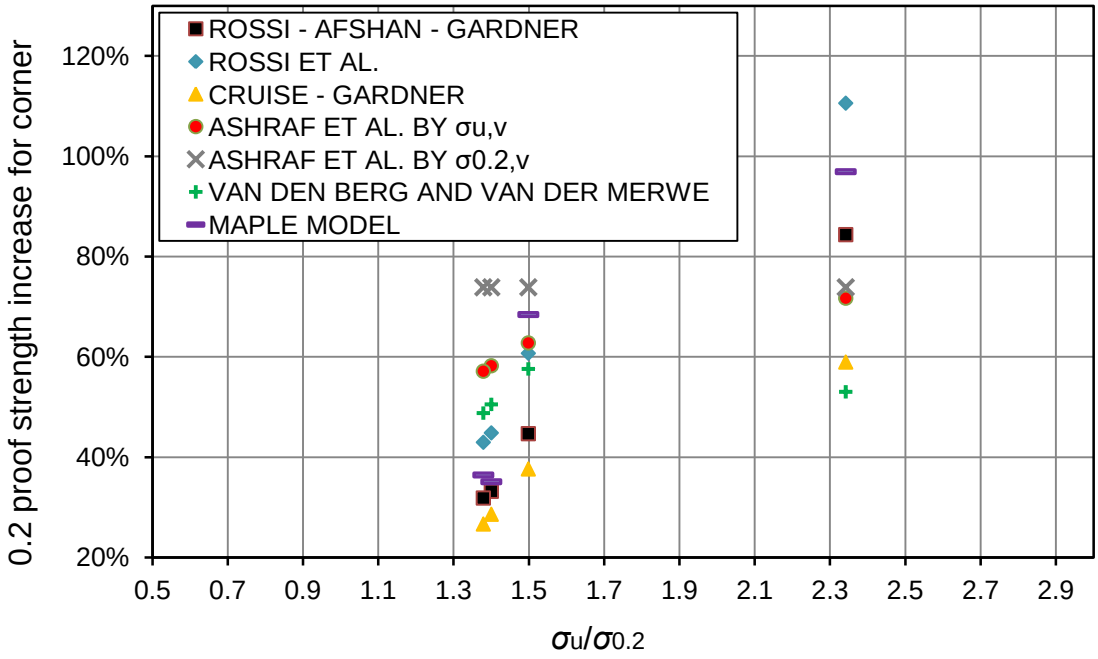

Figure 5.62 *Proof strength increase depending on the ratio between the 0.2% proof and ultimate strength for the tested grades.*

Most of the predictive formulas assume the effect of increasing strength enhancement joined to the increasing 0.2% proof to ultimate strength ratio. The maple model predicts similar behaviour except the case of the lean duplex and duplex grade. These grades are very close to themselves in their properties and the difference is caused by other material parameters and negligible in fact.

Corners

Next figures (Figure 5.63 - Figure 5.66) show comparison of the 0.2% proof strength predictive methods for these four tested grades according to the changing r_i/t ratio. Collected data of the r_i/t (see Appendix G) for cold-rolled and press-braked sections indicates the sufficient range of the ratio covering the majority of tested sections varies from 0.5 to 7. Therefore next figures are related to this range.

In case of the austenitic 1.4404 grade there is good agreement of the proposed model with the predictive relationship according to Rossi, Afshan and Gardner [8] with average difference of 9% and standard deviation of 4%. As austenitic grades are the most common for SHS fabrication the formula provides slightly lower and thus safe predictions and confirms results obtained from the Maple model.

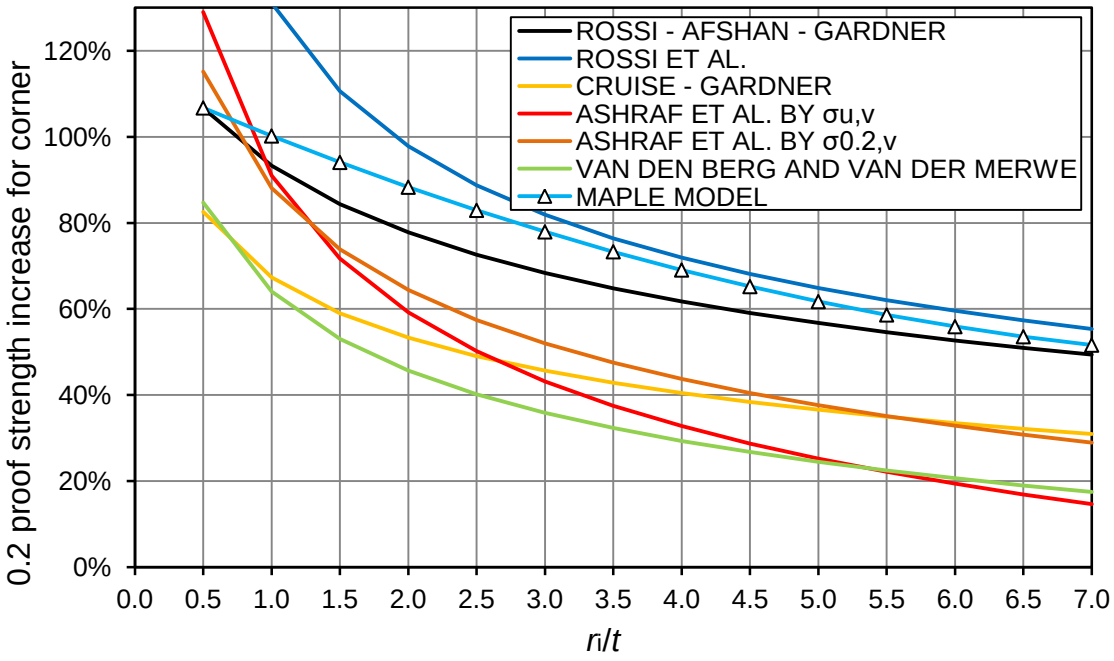

Figure 5.63 *0.2% proof strength increase for a corner depending on the inner radius to thickness ratio for the austenitic 1.4404 grade.*

In opposite to the austenitic grade, for other grades the Maple model does not sufficiently correspond with predictive relationships. In case of the r_i/t effect trend, the Maple model exhibits good accordance with the method proposed by Rossi, Afshan and Gardner [8]. This similarity occurs both for ferritic and lean duplex and duplex grades.

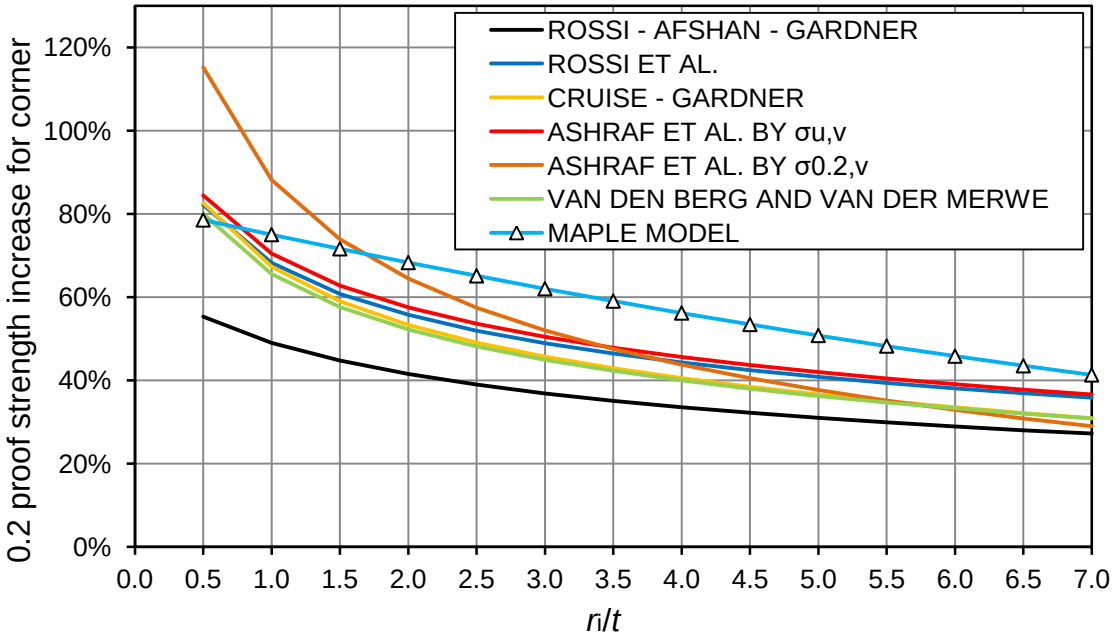

Figure 5.64 *0.2% proof strength increase for the corner depending on the inner radius to thickness ratio for the ferritic 1.4003 grade.*

The comparison of the predictive methods for ferritic grade 1.4003 shows lower differences between the Maple model and other formulas in opposite to the Rossi-Afshan-Gardner model. For lean duplex and duplex grades (1.4162, 1.4462) and common r_i/t ratios there is higher agreement of the Maple model with results according to Rossi-Afshan-Gardner relationship.

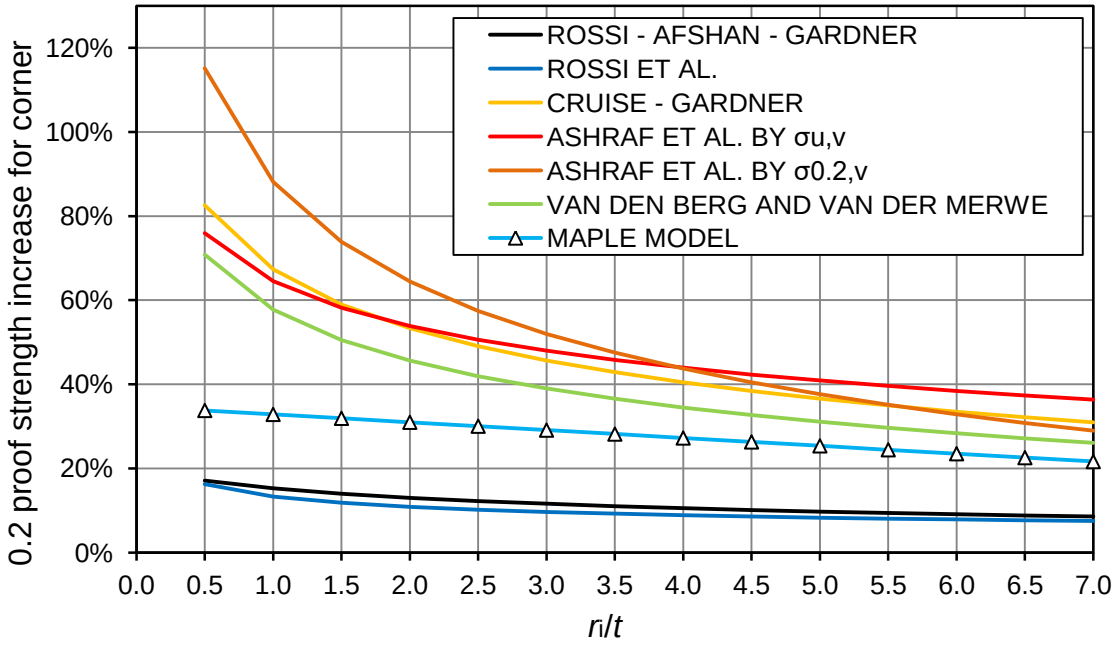

Figure 5.65 *0.2% proof strength increase for the corner depending on the inner radius to thickness ratio for the lean duplex 1.4162 grade.*

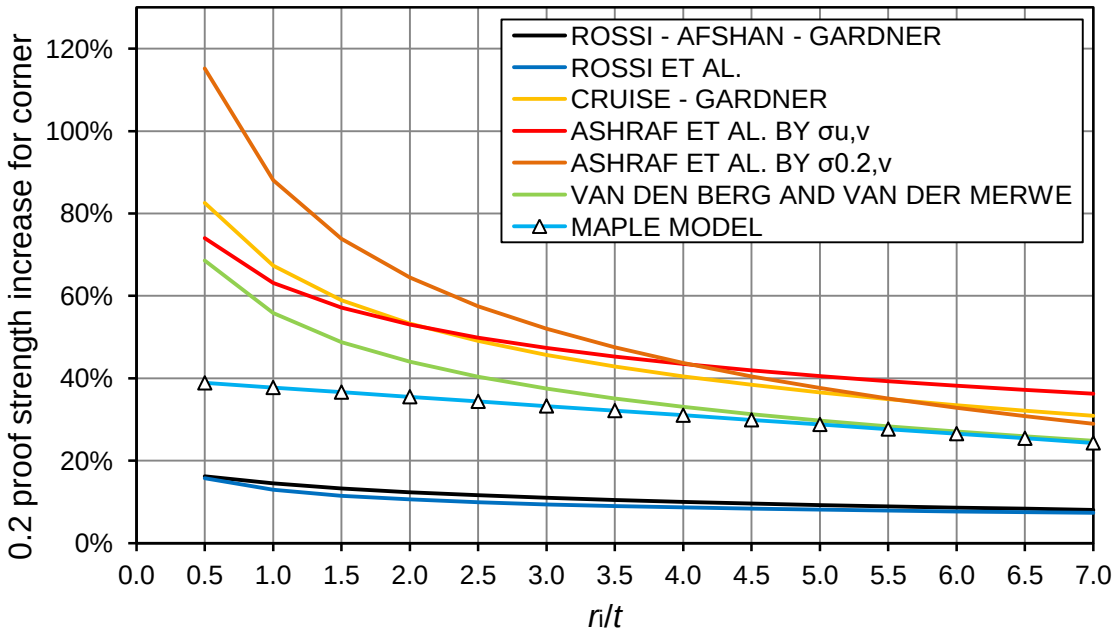

Figure 5.66 *Proof strength increase for the corner depending on the inner radius to thickness ratio for the duplex 1.4462 grade.*

The confrontation indicates the latest predictive Rossi-Afshan-Gardner proposal offer appropriate trend of strength increase dependency on r_i/t and good accordance for the austenitic grade. However for other stainless steel it could be modified.

Flat faces

Next figures (Figure 5.67 - Figure 5.70) depict comparison of the modelled flat face 0.2% proof strength and results according to the predictive methods (see Chapter 3 – section 3.3). Similar to the previous comparison for the corner there is displayed dependency of the 0.2% proof strength increase on the varying ratio between the flat face radius R_f to thickness - Eq. (5.60). Typically R_f/t varies from 10 to 20. For more convenient following figures involve range of R_f/t from 5 to 23.

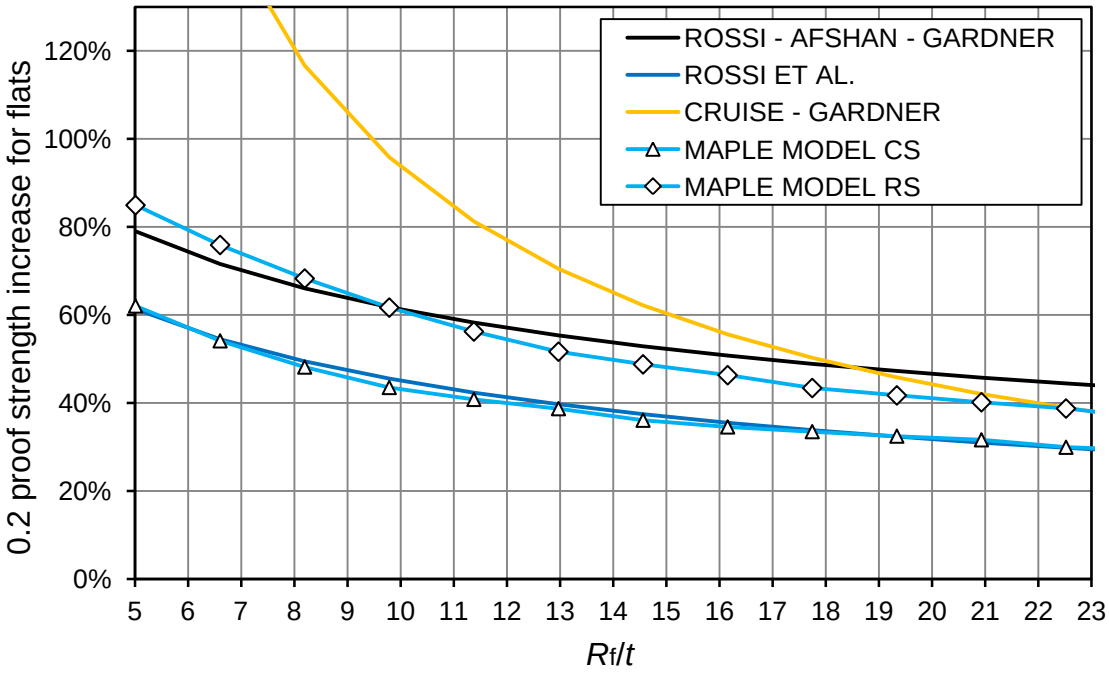

Figure 5.67 *0.2% proof strength increase for the flat face depending on the inner radius to thickness ratio for the austenitic 1.4404 grade.*

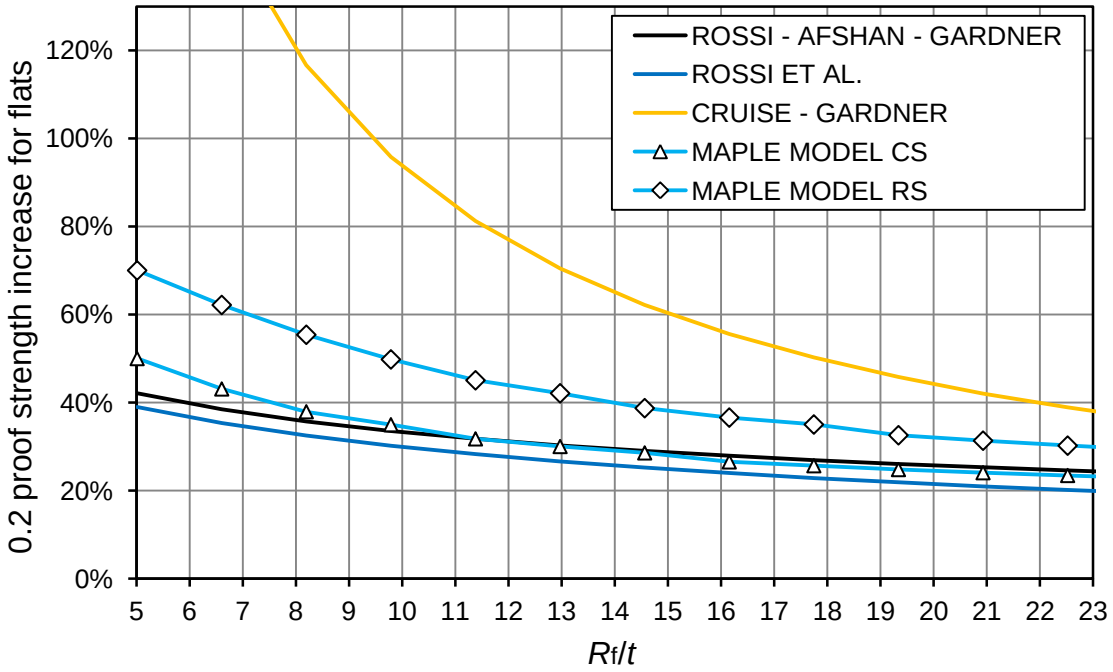

Figure 5.68 *0.2% proof strength increase for the flat face depending on the inner radius to thickness ratio for the ferritic 1.4003 grade.*

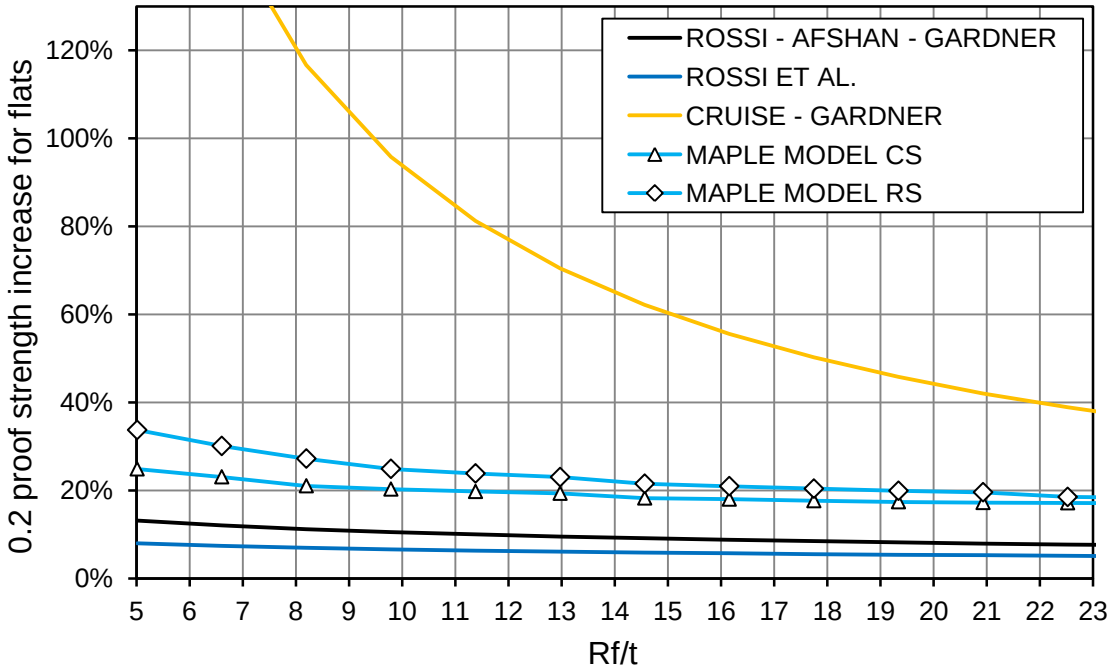

Figure 5.69 *0.2% proof strength increase for the flat face depending on the inner radius to thickness ratio for the lean duplex 1.4162 grade.*

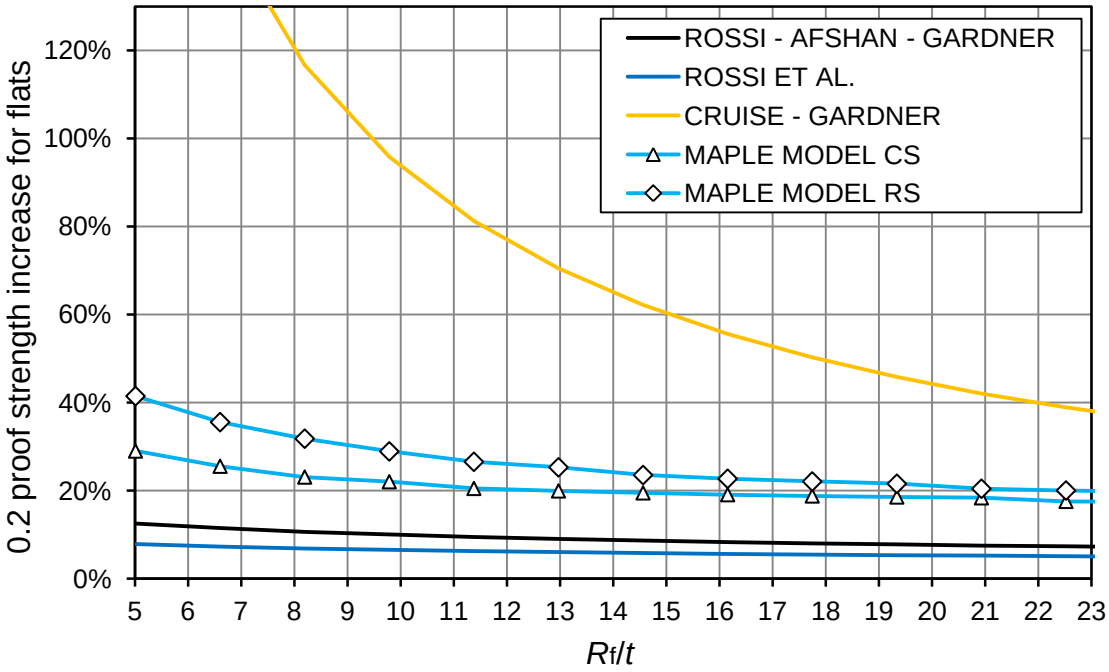

Figure 5.70 *0.2% proof strength increase for the flat face depending on the inner radius to thickness ratio for the duplex 1.4462 grade.*

The trend of the 0.2% proof strength dependency on R_f/t is close to the other models except the Cruise – Gardner´s which exhibits unlikely high values. The corner model and the flat face model exhibit higher strength increase for materials with higher ultimate strength to 0.2% proof strength ratio as well as other predictive methods do. Evaluation of the model based on the experimental investigations.

Finally the "CS" model is used for further evaluation and comparisons as a conservative solution, possibly compensating (in practise) many unknown parameters.

5.5 Stress-strain behaviour of SHS

Previously presented results of the full section testing at Imperial College allow evaluating the concept for full section curve establishment based on an averaged stress-strain description. As the Maple model output provides a stress increment for the strain increment of 0.0001 it is possible to perform the averaging by weighting as follows:

$$\sigma_{FS}=\frac{\sigma_F A_F+\sigma_C A_C}{A_G} \tag{5.62}$$

where

σ_{FS} denotes stress increment for a full section,
σ_F denotes stress increment for a flat face,
σ_C denotes stress increment for a corner,
A_G denotes a gross sectional area,
$A_F = A_G - A_C$, denotes an area of flat faces,
A_C denotes an area of corners.

Test set-up consisted of 2 tested specimens. Recorded stress-strain curves are compared with the modelled stress-strain responses.

In terms of the cold-rolling and its effect on section corners it has recently been considered that strength enhancement is possible to assume within the area of corner and also beyond this border by the distance of 2*t* on each side of the corner end due to the enhanced strength distributed along the corner area as it was stated above.

However for cold-rolled members the distribution of the increased proof strength is not uniform at all according to Cruise´s hardness tests indicating enhanced strength [4] (see Figure 5.18). The highest values occur at the junction of a corner area and a flat face. From this peak point the enhancement nearly linearly decreases both on the side of corner centre and on the side of the flat face. In contrast to press-braked sections this effect is probably caused by the last step of fabricating (if the manufacturing involves both making a circular tube and subsequent forming into a final shape). Forming into a rectangular section induces the largest plastic deformations exactly in this area. Thus the stress-strain behaviour could be more complex than the simple engineering idea of linear weighting of two separate particular portions by their areas. Nevertheless it is a simple solution easy to use. Therefore following figures show a comparison of the test data and model results both for assuming the extension of 2t and for assuming only the corner area as the area of enhanced corner properties. These curves create border lines which the final stress strain curve could be placed in.

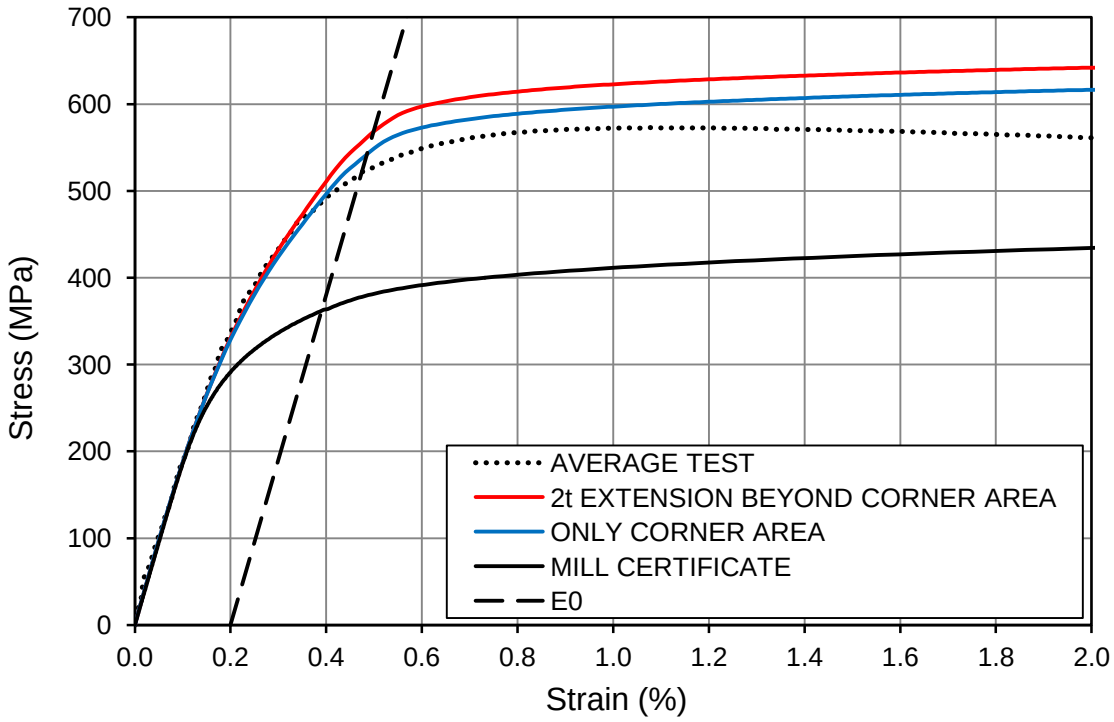

Figure 5.71 *Comparison of the modelled and measured stress-strain response for the full section - 1.4509 SHS 30x30x2.*

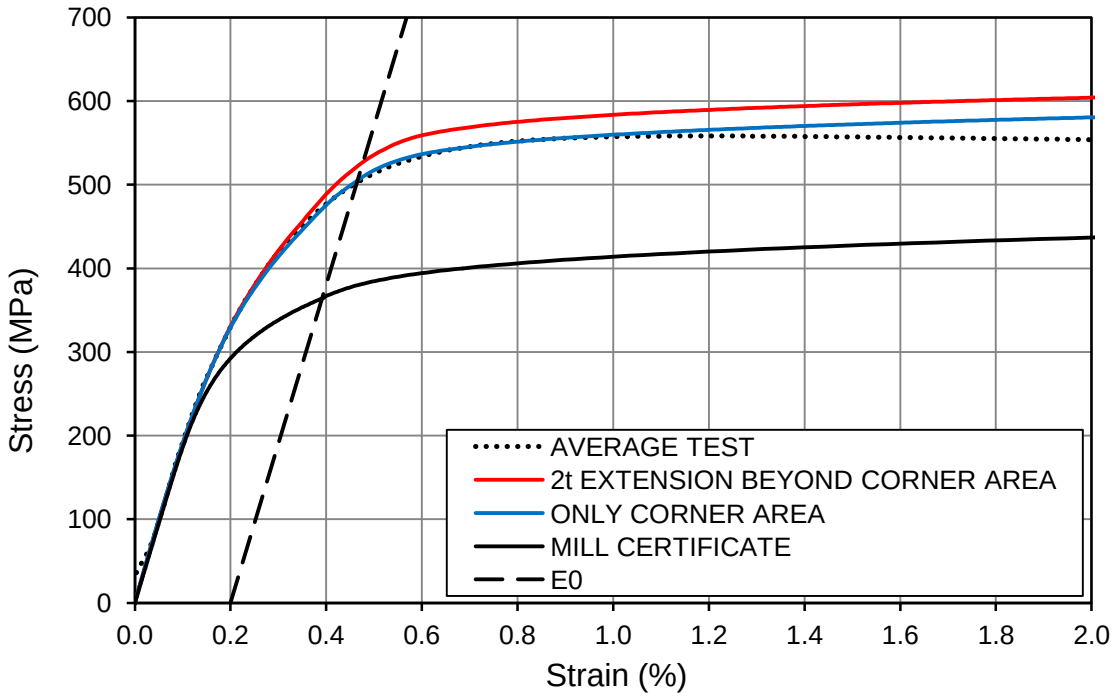

Figure 5.72 *Comparison of the modelled and measured stress-strain response for the full section - 1.4509 SHS 40x40x2.*

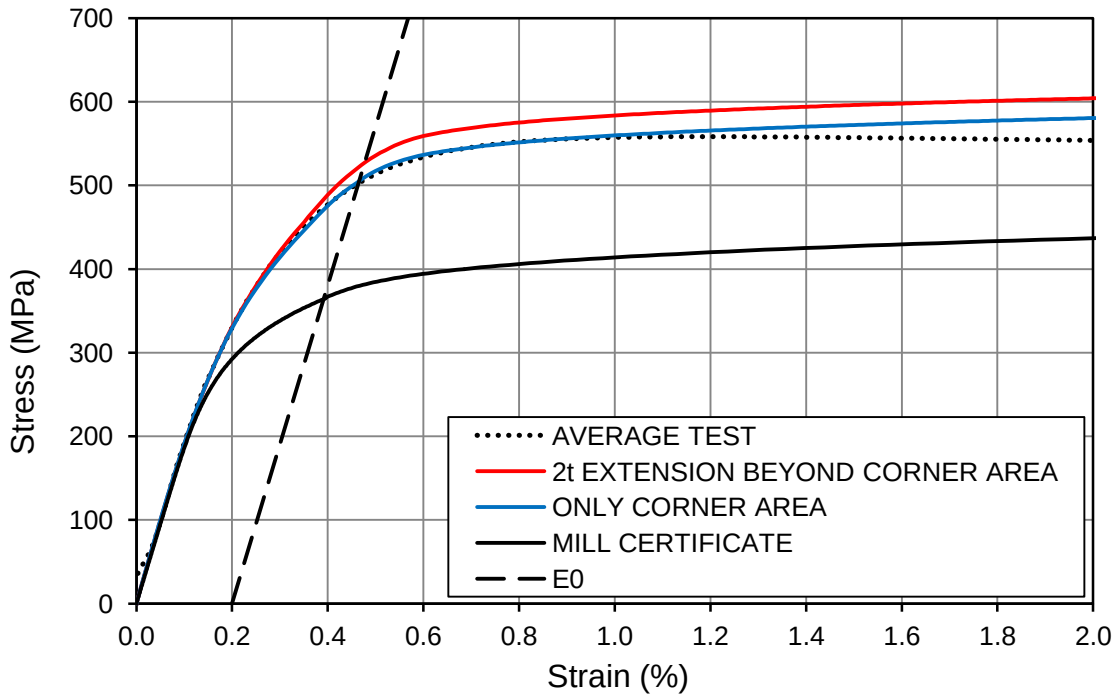

Figure 5.73 *Comparison of the modelled and measured stress-strain response for the full section - 1.4509 SHS 50x50x2.*

Figures above show good agreement of the proposed model with the test data. The model considering only pure corner matches the test data better with higher agreement of the 0.2% proof strength prediction. It also provides safer values for the 0.2% proof strength with small difference in comparison with the model of 2*t* extension. Another reason for better fitting of the model is due to thickness reducing within a cold-bending. The effect increases with a decreasing bending radius. According to Zhang and Yu [63] a reduction of sheet thickness reaches about 5% for the inner radius to thickness ratio $r_i/t = 1$. Hence the model assuming only pure corner area is used for further solutions.

5.6 Modification of the predictive model

As it was stated above the newest relevant relationship Rossi-Afshan-Gardner [8] for the enhanced 0.2% proof strength of corners and flat faces is appropriate for austenitic steel whilst for other grades it could be modified. The recent formulas consider a corner area with 2*t* extension beyond the geometrical boundary of a corner. The analytical solution described herein shows that a corner area should be assumed as the only pure bend. Comparison of the results obtained from tests conducted at CTU with the predictive model and the results obtained from the analytical solution compared with the predictive model confirmed the correct trend of the design formulas. Nevertheless the formula is based on a relation between values of the strain and stress at the 0.2% proof strength and ultimate strength. This relationship is suitable for materials with wide range of values between the 0.2% proof strength and ultimate strength, such as austenitic steel. For other grades it is possible to change the formulas by increasing the entire dependency by a correction factor related to the material properties and cover the higher 0.2% proof strength.

One of possible adjustment for non-austenitic steel grades is to simply employ ratio between the basic material properties $\sigma_{1.0}$ and $\sigma_{0.2}$. The predictive formula for the enhanced 0.2% proof strength of corners or flat faces without any safety factors can be set as:

$$\sigma_{\text{c or f,pred}} = p(\varepsilon_{\text{c or f}})^q \tag{5.63}$$

where

$$p = \frac{\sigma_{0.2,\text{mill}}}{\varepsilon_{\text{t},0.2}^{q}} \cdot \frac{\sigma_{1.0,\text{mill}}}{\sigma_{0.2,\text{mill}}} \tag{5.64}$$

$$q = \frac{\ln\left(\sigma_{0.2,\text{mill}}/\sigma_{\text{u,mill}}\right)}{\ln\left(\varepsilon_{\text{t},0.2}/\varepsilon_{\text{u}}\right)} \cdot \frac{\sigma_{0.2,\text{mill}}}{\sigma_{1.0,\text{mill}}} \tag{5.65}$$

Other essential parameters remain unchanged, see below.

$$\varepsilon_{\text{f,av}} = \left[(t/2)/R_{\text{coiling}}\right] + \left[(t/2)/R_{\text{f}}\right] \tag{3.82}$$

$$\varepsilon_{\text{c,av}} = 0.5\left[(t/2)/R_{\text{c}}\right] \tag{3.83}$$

$$R_{\text{f}} = \frac{b+h-2t}{\pi} \tag{3.84}$$

$$R_{\text{c}} = r_{\text{i}} + t/2 \tag{3.85}$$

$$\varepsilon_{\text{t},0.2} = 0.002 + \sigma_{0.2,\text{mill}}/\text{E}_0 \tag{3.88}$$

ε_{u} is the corresponding total strain at σ_{u},
R_{coiling} = 450 mm

The modified relationship is compared to the previous one with steel grades investigated at CTU (1.4003, 1.4162, 1.4462) to ensure the correctness of the approach. As one of recommendations related to this study states the corners should be considered

as the only pure bend area it implies the increased influence of flat faces. In terms of larger H/t dimension ratio of hollow sections it is important to be more accurate within enhanced strength prediction for flat faces than for corners. Following figures and tables display comparison between the Maple model and the modified and unchanged Rossi-Afshan-Gardner model related to the corner r_i/t ratio (minimal and maximal common ratios - r_i/t = 0.5, r_i/t = 2.0 respectively) and the dimension H/t ratio describing the effect for flat faces. Resulting full section strength increase is based on weighting according to Eq. (5.67). Comparison of the full section 0.2% proof strength evaluating by weighting of the stress-strain curves with weighting of the 0.2% proof strength for corners and flat faces shows that the difference of these two methods is negligible. Table below shows differences of the methods for the austenitic grade 1.4404 investigated at CTU with boundary limits for r_i/t and H/t ratios. Austenitic steel seems to be the best example for comparing due to the significant progress between the 0.2% proof strength and the ultimate strength as well as between the corresponding strains.

H (mm)	L (mm)	t (mm)	r_i (mm)	r_i/t	H/t	prediction difference (%)
68.0	68.0	4.0	2.00	0.50	17.00	0.42
140.0	140.0	4.0	2.00	0.50	35.00	0.73
68.0	68.0	4.0	8.00	2.00	17.00	5.28
140.0	140.0	4.0	8.00	2.00	35.00	3.38

Table 5.4 *Comparison of the weighting methods for the 0.2% proof strength determination.*

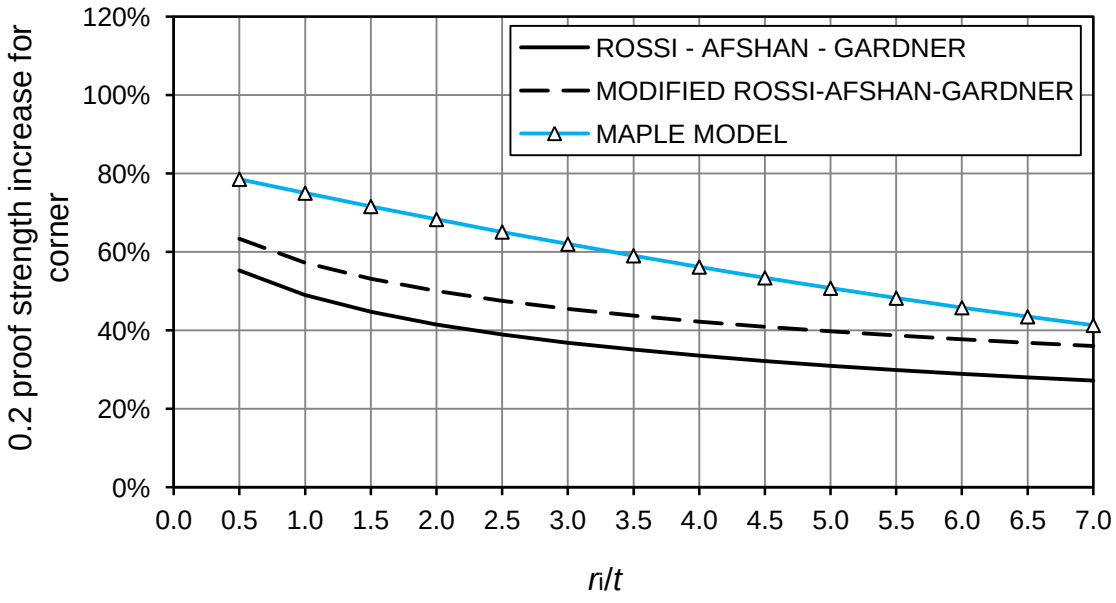

Figure 5.74 *Comparison of the predictive models for a corner of 1.4003.*

	R-A-G	MODIFIED R-A-G	MAPLE MODEL	R-A-G /MAPLE	M. R-A-G /MAPLE
r_i/t	$\sigma_{0.2,c,pred}$ (MPa)	$\sigma_{0.2,c,pred}$ (MPa)	$\sigma_{0.2,c,pred}$ (MPa)		
0.5	520.5	547.5	578.9	0.90	0.95
1.0	499.4	527.1	568.9	0.88	0.93
1.5	485.1	513.3	562.9	0.86	0.91
2.0	474.4	502.8	556.1	0.85	0.90
2.5	465.8	494.5	545.0	0.85	0.91
3.0	458.8	487.7	538.0	0.85	0.91
3.5	452.8	481.8	526.7	0.86	0.91
4.0	447.6	476.8	520.1	0.86	0.92
4.5	443.1	472.4	513.0	0.86	0.92
5.0	439.0	468.4	502.4	0.87	0.93
5.5	435.4	464.8	496.1	0.88	0.94
6.0	432.1	461.6	486.8	0.89	0.95
6.5	429.1	458.7	481.3	0.89	0.95
7.0	426.3	455.9	476.9	0.89	0.96
			MEAN	0.87	0.93
			SD	0.02	0.02

Table 5.5 *Comparison of the corner 0.2% proof strength for the ferritic 1.4003 grade.*

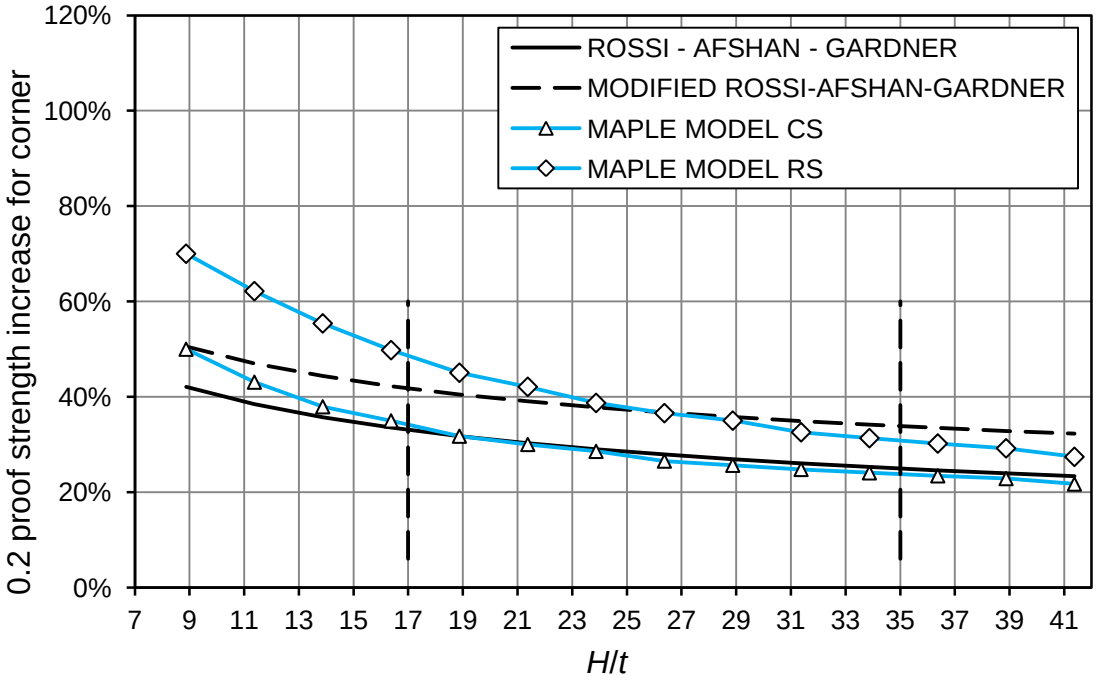

Figure 5.75 *Comparison of the predictive models for flat faces of 1.4003.*

r_i/t = 0.5; t = 4 mm		MODIFIED R-A-G					MAPLE MODEL	
H/t	A_g (mm^2)	A_c (mm^2)	A_f (mm^2)	$\sigma_{0.2,c,pred}$ (MPa)	$\sigma_{0.2,f,pred}$ (MPa)	$\sigma_{0.2,full,pred}$ (MPa)	$\sigma_{0.2,f,pred}$ (MPa)	M. R-A-G /MAPLE
8.9	476.5	100.5	376.0	547.5	504.7	513.7	502.8	1.00
11.4	636.5	100.5	536.0	547.5	492.8	501.4	479.6	1.03
13.9	796.5	100.5	696.0	547.5	483.8	491.9	462.3	1.05
16.4	956.5	100.5	856.0	547.5	476.8	484.2	452.4	1.05
18.9	1116.5	100.5	1016.0	547.5	471.0	477.9	441.6	1.07
21.4	1276.5	100.5	1176.0	547.5	466.1	472.5	435.8	1.07
23.9	1436.5	100.5	1336.0	547.5	461.9	467.9	431.0	1.07
26.4	1596.5	100.5	1496.0	547.5	458.3	463.9	424.1	1.08
28.9	1756.5	100.5	1656.0	547.5	455.1	460.4	421.2	1.08
31.4	1916.5	100.5	1816.0	547.5	452.3	457.3	418.3	1.08
33.9	2076.5	100.5	1976.0	547.5	449.7	454.4	415.9	1.08
36.4	2236.5	100.5	2136.0	547.5	447.4	451.9	413.8	1.08
38.9	2396.5	100.5	2296.0	547.5	445.3	449.6	411.8	1.08
41.4	2556.5	100.5	2456.0	547.5	443.4	447.5	408.0	1.09
						MEAN		1.07
						SD		0.02

Table 5.6 *Comparison of the flat face 0.2% proof strength for the ferritic 1.4003 grade with r_i/t = 0.5 according to the modified R-A-G relationship.*

r_i/t = 0.5; t = 4 mm		R-A-G					MAPLE MODEL		FULL SECTION
H/t	A_g (mm^2)	A_c (mm^2)	A_f (mm^2)	$\sigma_{0.2,c,pred}$ (MPa)	$\sigma_{0.2,f,pred}$ (MPa)	$\sigma_{0.2,full,pred}$ (MPa)	$\sigma_{0.2,f,pred}$ (MPa)	R-A-G /MAPLE	M. R-A-G /R-A-G
8.9	476.5	356.5	120.0	520.5	476.3	509.3	502.8	0.95	1.01
11.4	636.5	356.5	280.0	520.5	464.0	495.6	479.6	0.97	1.01
13.9	796.5	356.5	440.0	520.5	454.8	484.2	462.3	0.98	1.02
16.4	956.5	356.5	600.0	520.5	447.6	474.7	452.4	0.99	1.02
18.9	1116.5	356.5	760.0	520.5	441.7	466.8	441.6	1.00	1.02
21.4	1276.5	356.5	920.0	520.5	436.7	460.1	435.8	1.00	1.03
23.9	1436.5	356.5	1080.0	520.5	432.4	454.3	431.0	1.00	1.03
26.4	1596.5	356.5	1240.0	520.5	428.7	449.2	424.1	1.01	1.03
28.9	1756.5	356.5	1400.0	520.5	425.4	444.7	421.2	1.01	1.04
31.4	1916.5	356.5	1560.0	520.5	422.5	440.7	418.3	1.01	1.04
33.9	2076.5	356.5	1720.0	520.5	419.9	437.2	415.9	1.01	1.04
36.4	2236.5	356.5	1880.0	520.5	417.6	434.0	413.8	1.01	1.04
38.9	2396.5	356.5	2040.0	520.5	415.4	431.1	411.8	1.01	1.04
41.4	2556.5	356.5	2200.0	520.5	413.5	428.4	408.0	1.01	1.04
						MEAN		1.00	1.03
						SD		0.02	0.01

Table 5.7 *Comparison of the flat face 0.2% proof strength for the ferritic 1.4003 grade with r_i/t = 0.5 and the ratio between predictive strength for a full section according to the modified and unchanged R-A-G relationship.*

In terms of the ferritic grade, the formula gives relatively low enhancement for corners. However it is suggested to be more conservative due to the limited ductility of ferritic grades. In case of flat faces the curve should by located under the "RS" Maple model representing the reverse bending of a face from a circular hollow section to a flat portion at least. In some comparison the curve is above, nevertheless for the most common ratios of H/t the differences are negligible. In the tables for flat faces there are stated values obtained by the "CS" model although the direct relation to which of model ("CS" or "RS") is correct was not proved. Therefore slightly higher values might not be important difficulty. Undoubtedly the "CS" model is more conservative. The ratio comparing the full section strength according to the modified and unchanged model shows mean increase of only 3% for r_i/t =0.5, 5% for r_i/t =2.0 respectively.

r_i/t = 2; t = 4 mm		MODIFIED R-A-G				
H/t	A_g (mm^2)	A_c (mm^2)	A_f (mm^2)	$\sigma_{0.2,c,pred}$ (MPa)	$\sigma_{0.2,f,pred}$ (MPa)	$\sigma_{0.2,full,pred}$ (MPa)
8.9	435.3	251.3	184.0	502.8	504.7	503.6
11.4	595.3	251.3	344.0	502.8	492.8	497.0
13.9	755.3	251.3	504.0	502.8	483.8	490.2
16.4	915.3	251.3	664.0	502.8	476.8	483.9
18.9	1075.3	251.3	824.0	502.8	471.0	478.4
21.4	1235.3	251.3	984.0	502.8	466.1	473.6
23.9	1395.3	251.3	1144.0	502.8	461.9	469.3
26.4	1555.3	251.3	1304.0	502.8	458.3	465.5
28.9	1715.3	251.3	1464.0	502.8	455.1	462.1
31.4	1875.3	251.3	1624.0	502.8	452.3	459.0
33.9	2035.3	251.3	1784.0	502.8	449.7	456.3
36.4	2195.3	251.3	1944.0	502.8	447.4	453.7
38.9	2355.3	251.3	2104.0	502.8	445.3	451.4
41.4	2515.3	251.3	2264.0	502.8	443.4	449.3

Table 5.8 *Predictive 0.2% proof strength for the ferritic 1.4003 grade with r_i/t = 2.0 according to the modified R-A-G relationship.*

r_i/t = 2; t = 4 mm		R-A-G					FULL SECTION
H/t	A_g (mm^2)	A_c (mm^2)	A_f (mm^2)	$\sigma_{0.2,c,pred}$ (MPa)	$\sigma_{0.2,f,pred}$ (MPa)	$\sigma_{0.2,full,pred}$ (MPa)	M. R-A-G /R-A-G
8.9	435.3	435.3	0.0	474.4	476.3	474.4	1.06
11.4	595.3	507.3	88.0	474.4	464.0	472.8	1.05
13.9	755.3	507.3	248.0	474.4	454.8	467.9	1.05
16.4	915.3	507.3	408.0	474.4	447.6	462.4	1.05
18.9	1075.3	507.3	568.0	474.4	441.7	457.1	1.05
21.4	1235.3	507.3	728.0	474.4	436.7	452.1	1.05
23.9	1395.3	507.3	888.0	474.4	432.4	447.7	1.05
26.4	1555.3	507.3	1048.0	474.4	428.7	443.6	1.05
28.9	1715.3	507.3	1208.0	474.4	425.4	439.9	1.05
31.4	1875.3	507.3	1368.0	474.4	422.5	436.6	1.05
33.9	2035.3	507.3	1528.0	474.4	419.9	433.5	1.05
36.4	2195.3	507.3	1688.0	474.4	417.6	430.7	1.05
38.9	2355.3	507.3	1848.0	474.4	415.4	428.1	1.05
41.4	2515.3	507.3	2008.0	474.4	413.5	425.8	1.06
						MEAN	1.05
						SD	0.00

Table 5.9 *0.2% proof strength for the ferritic 1.4003 grade with r_i/t = 2.0 and the ratio between predictive strength for a full section according to the modified and unchanged R-A-G relationship.*

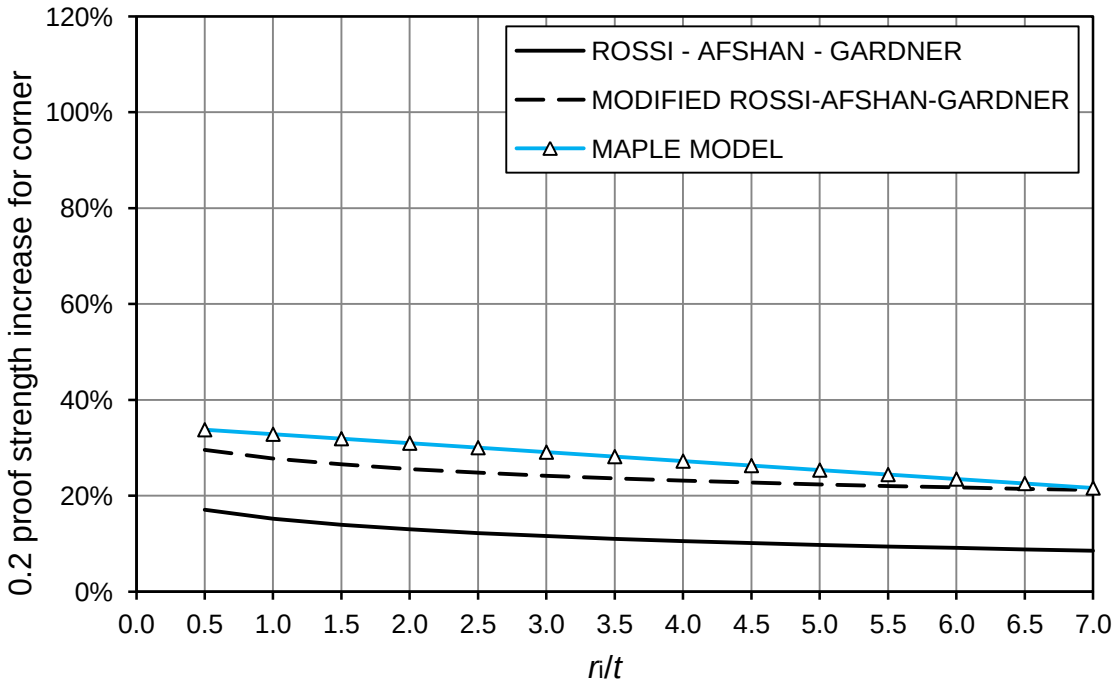

Figure 5.76 *Comparison of the predictive models for a corner of 1.4162.*

	R-A-G	MODIFIED R-A-G	MAPLE MODEL	R-A-G /MAPLE	M. R-A-G /MAPLE
r_i/t	$\sigma_{0.2,c,pred}$ (MPa)	$\sigma_{0.2,c,pred}$ (MPa)	$\sigma_{0.2,c,pred}$ (MPa)		
0.5	648.5	717.9	742.6	0.87	0.97
1.0	638.4	708.0	739.0	0.86	0.96
1.5	631.4	701.0	729.8	0.87	0.96
2.0	626.0	695.8	726.0	0.86	0.96
2.5	621.7	691.5	721.5	0.86	0.96
3.0	618.2	688.0	712.1	0.87	0.97
3.5	615.1	685.0	707.9	0.87	0.97
4.0	612.5	682.4	704.2	0.87	0.97
4.5	610.1	680.0	700.6	0.87	0.97
5.0	608.0	678.0	691.6	0.88	0.98
5.5	606.1	676.1	688.3	0.88	0.98
6.0	604.4	674.4	685.3	0.88	0.98
6.5	602.8	672.8	682.7	0.88	0.99
7.0	601.4	671.4	675.0	0.89	0.99
			MEAN	0.87	0.97
			SD	0.01	0.01

Table 5.10 *Comparison of the corner 0.2% proof strength for the lean duplex 1.4162 grade.*

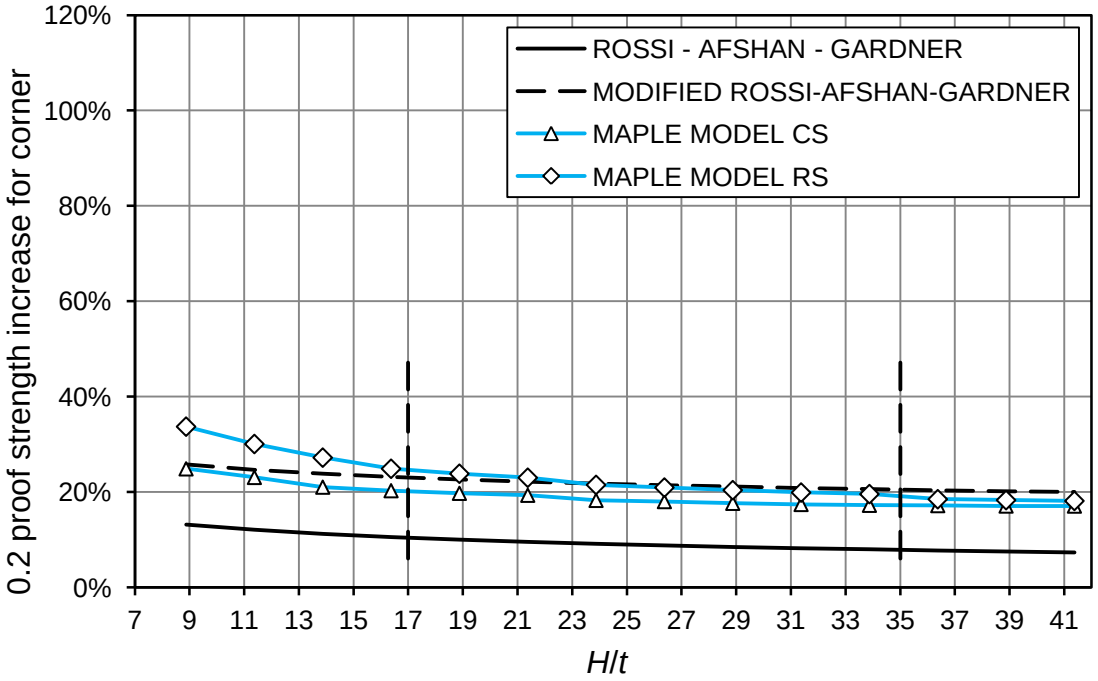

Figure 5.77 *Comparison of the predictive models for flat faces of 1.4162.*

r_i/t = 0.5; t = 4 mm		MODIFIED R-A-G					MAPLE MODEL	
H/t	A_g (mm^2)	A_c (mm^2)	A_f (mm^2)	$\sigma_{0.2,c,pred}$ (MPa)	$\sigma_{0.2,f,pred}$ (MPa)	$\sigma_{0.2,full,pred}$ (MPa)	$\sigma_{0.2,f,pred}$ (MPa)	M. R-A-G /MAPLE
8.9	476.5	100.5	376.0	717.9	696.7	701.2	691.8	1.01
11.4	636.5	100.5	536.0	717.9	690.6	694.9	681.8	1.01
13.9	796.5	100.5	696.0	717.9	686.0	690.0	670.6	1.02
16.4	956.5	100.5	856.0	717.9	682.3	686.1	666.4	1.02
18.9	1116.5	100.5	1016.0	717.9	679.3	682.8	663.4	1.02
21.4	1276.5	100.5	1176.0	717.9	676.8	680.0	661.1	1.02
23.9	1436.5	100.5	1336.0	717.9	674.6	677.6	655.2	1.03
26.4	1596.5	100.5	1496.0	717.9	672.6	675.5	653.8	1.03
28.9	1756.5	100.5	1656.0	717.9	670.9	673.6	651.8	1.03
31.4	1916.5	100.5	1816.0	717.9	669.4	672.0	650.4	1.03
33.9	2076.5	100.5	1976.0	717.9	668.1	670.5	649.5	1.03
36.4	2236.5	100.5	2136.0	717.9	666.9	669.1	649.1	1.03
38.9	2396.5	100.5	2296.0	717.9	665.7	667.9	648.6	1.03
41.4	2556.5	100.5	2456.0	717.9	664.7	666.8	648.6	1.02
						MEAN		1.02
						SD		0.01

Table 5.11 *Comparison of the flat face 0.2% proof strength for the lean duplex 1.4162 grade with r_i/t = 0.5 according to the modified R-A-G relationship.*

r_i/t = 0.5; t = 4 mm		R-A-G					MAPLE MODEL		FULL SECTION
H/t	A_g (mm^2)	A_c (mm^2)	A_f (mm^2)	$\sigma_{0.2,c,pred}$ (MPa)	$\sigma_{0.2,f,pred}$ (MPa)	$\sigma_{0.2,full,pred}$ (MPa)	$\sigma_{0.2,f,pred}$ (MPa)	R-A-G /MAPLE	M. R-A-G /R-A-G
8.9	476.5	356.5	120.0	648.5	627.0	643.1	691.8	0.91	1.09
11.4	636.5	356.5	280.0	648.5	620.8	636.4	681.8	0.91	1.09
13.9	796.5	356.5	440.0	648.5	616.2	630.7	670.6	0.92	1.09
16.4	956.5	356.5	600.0	648.5	612.5	625.9	666.4	0.92	1.10
18.9	1116.5	356.5	760.0	648.5	609.4	621.9	663.4	0.92	1.10
21.4	1276.5	356.5	920.0	648.5	606.8	618.5	661.1	0.92	1.10
23.9	1436.5	356.5	1080.0	648.5	604.6	615.5	655.2	0.92	1.10
26.4	1596.5	356.5	1240.0	648.5	602.7	612.9	653.8	0.92	1.10
28.9	1756.5	356.5	1400.0	648.5	600.9	610.6	651.8	0.92	1.10
31.4	1916.5	356.5	1560.0	648.5	599.4	608.6	650.4	0.92	1.10
33.9	2076.5	356.5	1720.0	648.5	598.0	606.7	649.5	0.92	1.11
36.4	2236.5	356.5	1880.0	648.5	596.8	605.1	649.1	0.92	1.11
38.9	2396.5	356.5	2040.0	648.5	595.7	603.5	648.6	0.92	1.11
41.4	2556.5	356.5	2200.0	648.5	594.6	602.2	648.6	0.92	1.11
						MEAN		0.92	1.10
						SD		0.00	0.01

Table 5.12 *Comparison of the flat face 0.2% proof strength for the lean duplex 1.4162 grade with r_i/t = 0.5 and the ratio between the predictive strength for a full section according to modified and unchanged R-A-G relationship.*

The modified R-A-G relationship is closer to the modelled properties and gives higher values of the 0.2% proof strength for a full section by approximately 10%. Despite the decrease of corner areas the new formula gives higher enhanced strength.

r_i/t = 2; t = 4 mm		MODIFIED R-A-G				
H/t	A_g (mm^2)	A_c (mm^2)	A_f (mm^2)	$\sigma_{0.2,c,pred}$ (MPa)	$\sigma_{0.2,f,pred}$ (MPa)	$\sigma_{0.2,full,pred}$ (MPa)
8.9	435.3	251.3	184.0	695.8	696.7	696.2
11.4	595.3	251.3	344.0	695.8	690.6	692.8
13.9	755.3	251.3	504.0	695.8	686.0	689.3
16.4	915.3	251.3	664.0	695.8	682.3	686.0
18.9	1075.3	251.3	824.0	695.8	679.3	683.2
21.4	1235.3	251.3	984.0	695.8	676.8	680.6
23.9	1395.3	251.3	1144.0	695.8	674.6	678.4
26.4	1555.3	251.3	1304.0	695.8	672.6	676.4
28.9	1715.3	251.3	1464.0	695.8	670.9	674.6
31.4	1875.3	251.3	1624.0	695.8	669.4	673.0
33.9	2035.3	251.3	1784.0	695.8	668.1	671.5
36.4	2195.3	251.3	1944.0	695.8	666.9	670.2
38.9	2355.3	251.3	2104.0	695.8	665.7	668.9
41.4	2515.3	251.3	2264.0	695.8	664.7	667.8

Table 5.13 *Predictive 0.2% proof strength for the lean duplex 1.4162 grade with r_i/t = 2.0 according to the modified R-A-G relationship.*

r_i/t = 2; t = 4 mm		R-A-G					FULL SECTION
H/t	A_g (mm^2)	A_c (mm^2)	A_f (mm^2)	$\sigma_{0.2,c,pred}$ (MPa)	$\sigma_{0.2,f,pred}$ (MPa)	$\sigma_{0.2,full,pred}$ (MPa)	M. R-A-G /R-A-G
8.9	435.3	435.3	0.0	626.0	627.0	626.0	1.11
11.4	595.3	507.3	88.0	626.0	620.8	625.3	1.11
13.9	755.3	507.3	248.0	626.0	616.2	622.8	1.11
16.4	915.3	507.3	408.0	626.0	612.5	620.0	1.11
18.9	1075.3	507.3	568.0	626.0	609.4	617.2	1.11
21.4	1235.3	507.3	728.0	626.0	606.8	614.7	1.11
23.9	1395.3	507.3	888.0	626.0	604.6	612.4	1.11
26.4	1555.3	507.3	1048.0	626.0	602.7	610.3	1.11
28.9	1715.3	507.3	1208.0	626.0	600.9	608.4	1.11
31.4	1875.3	507.3	1368.0	626.0	599.4	606.6	1.11
33.9	2035.3	507.3	1528.0	626.0	598.0	605.0	1.11
36.4	2195.3	507.3	1688.0	626.0	596.8	603.6	1.11
38.9	2355.3	507.3	1848.0	626.0	595.7	602.2	1.11
41.4	2515.3	507.3	2008.0	626.0	594.6	601.0	1.11
						MEAN	1.11
						SD	0.00

Table 5.14 *0.2% proof strength for the lean duplex 1.4162 grade with r_i/t = 2.0 and the ratio between the predictive strength for a full section according to modified and unchanged R-A-G relationship.*

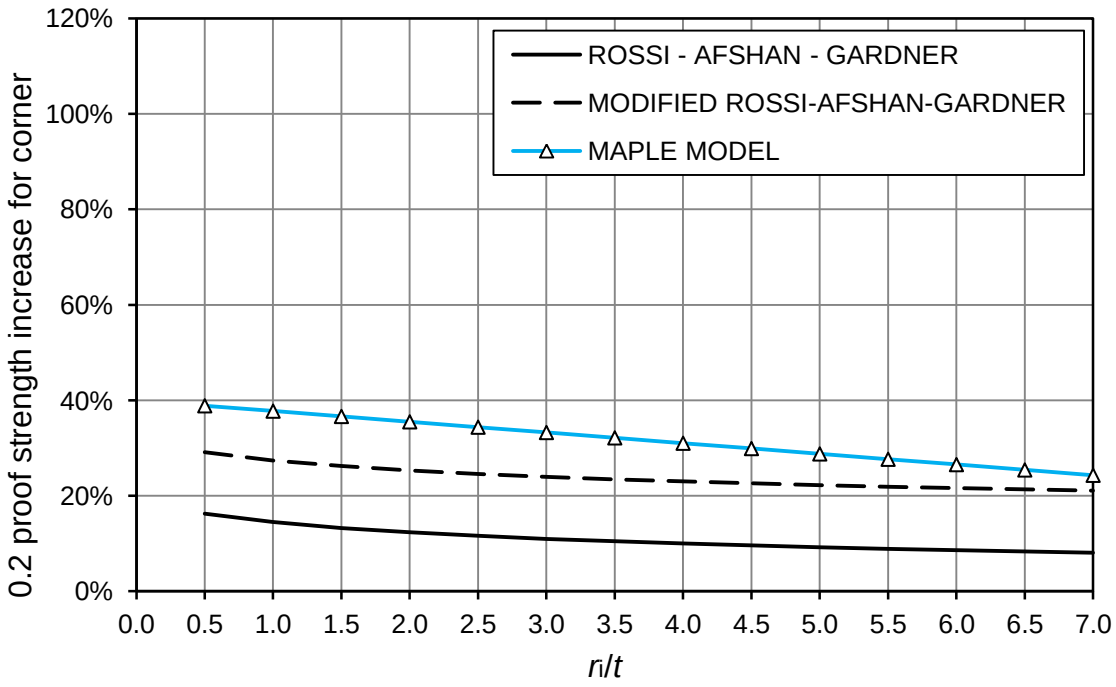

Figure 5.78 *Comparison of the predictive models for a corner of 1.4462.*

	R-A-G	MODIFIED R-A-G	MAPLE MODEL	R-A-G /MAPLE	M. R-A-G /MAPLE
r_i/t	$\sigma_{0.2,c,pred}$ (MPa)	$\sigma_{0.2,c,pred}$ (MPa)	$\sigma_{0.2,c,pred}$ (MPa)		
0.5	719.3	799.2	859.4	0.84	0.93
1.0	708.5	788.5	855.2	0.83	0.92
1.5	701.0	781.1	844.4	0.83	0.93
2.0	695.2	775.5	840.1	0.83	0.92
2.5	690.6	770.9	834.1	0.83	0.92
3.0	686.8	767.2	823.3	0.83	0.93
3.5	683.6	764.0	817.8	0.84	0.93
4.0	680.7	761.1	806.7	0.84	0.94
4.5	678.2	758.7	801.9	0.85	0.95
5.0	676.0	756.5	796.7	0.85	0.95
5.5	674.0	754.5	786.4	0.86	0.96
6.0	672.1	752.6	782.2	0.86	0.96
6.5	670.5	751.0	777.9	0.86	0.97
7.0	668.9	749.4	774.2	0.86	0.97
			MEAN	0.84	0.94
			SD	0.02	0.02

Table 5.15 *Comparison of the corner 0.2% proof strength for the duplex 1.4462 grade.*

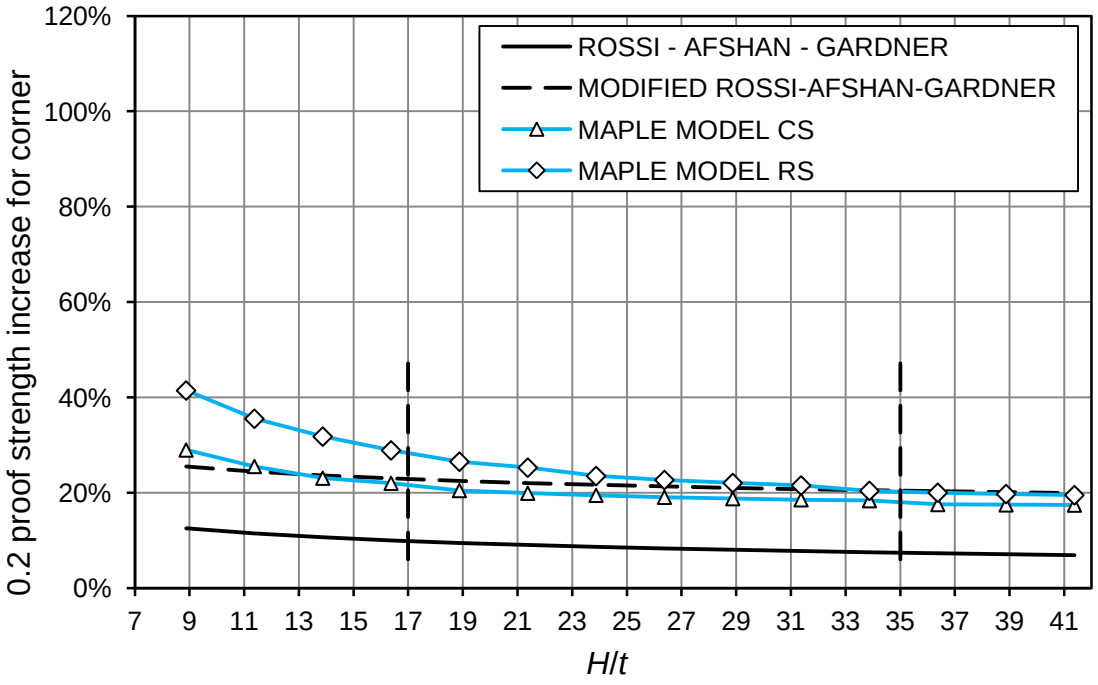

Figure 5.79 *Comparison of the predictive models for flat faces of 1.4462.*

r_i/t = 0.5; t = 4 mm		MODIFIED R-A-G					MAPLE MODEL	
H/t	A_g (mm^2)	A_c (mm^2)	A_f (mm^2)	$\sigma_{0.2,c,pred}$ (MPa)	$\sigma_{0.2,f,pred}$ (MPa)	$\sigma_{0.2,full,pred}$ (MPa)	$\sigma_{0.2,f,pred}$ (MPa)	M. R-A-G /MAPLE
8.9	476.5	100.5	376.0	799.2	776.5	781.3	798.2	0.97
11.4	636.5	100.5	536.0	799.2	770.0	774.6	776.9	0.99
13.9	796.5	100.5	696.0	799.2	765.1	769.4	761.6	1.00
16.4	956.5	100.5	856.0	799.2	761.1	765.1	755.1	1.01
18.9	1116.5	100.5	1016.0	799.2	757.9	761.6	745.6	1.02
21.4	1276.5	100.5	1176.0	799.2	755.2	758.6	742.1	1.02
23.9	1436.5	100.5	1336.0	799.2	752.8	756.1	739.4	1.02
26.4	1596.5	100.5	1496.0	799.2	750.8	753.8	736.9	1.02
28.9	1756.5	100.5	1656.0	799.2	749.0	751.8	735.1	1.02
31.4	1916.5	100.5	1816.0	799.2	747.4	750.1	733.6	1.02
33.9	2076.5	100.5	1976.0	799.2	745.9	748.5	732.5	1.02
36.4	2236.5	100.5	2136.0	799.2	744.6	747.0	727.4	1.02
38.9	2396.5	100.5	2296.0	799.2	743.4	745.7	727.0	1.02
41.4	2556.5	100.5	2456.0	799.2	742.3	744.5	726.7	1.02
						MEAN		1.01
						SD		0.01

Table 5.16 *Comparison of the flat face 0.2% proof strength for the duplex 1.4462 grade with r_i/t = 0.5 according to the modified R-A-G relationship.*

r_i/t = 0.5; t = 4 mm		R-A-G					MAPLE MODEL		FULL SECTION
H/t	A_g (mm^2)	A_c (mm^2)	A_f (mm^2)	$\sigma_{0.2,c,pred}$ (MPa)	$\sigma_{0.2,f,pred}$ (MPa)	$\sigma_{0.2,full,pred}$ (MPa)	$\sigma_{0.2,f,pred}$ (MPa)	R-A-G /MAPLE	M. R-A-G /R-A-G
8.9	476.5	356.5	120.0	719.3	696.3	713.5	798.2	0.87	1.10
11.4	636.5	356.5	280.0	719.3	689.7	706.3	776.9	0.89	1.10
13.9	796.5	356.5	440.0	719.3	684.7	700.2	761.6	0.90	1.10
16.4	956.5	356.5	600.0	719.3	680.7	695.1	755.1	0.90	1.10
18.9	1116.5	356.5	760.0	719.3	677.4	690.8	745.6	0.91	1.10
21.4	1276.5	356.5	920.0	719.3	674.7	687.1	742.1	0.91	1.10
23.9	1436.5	356.5	1080.0	719.3	672.3	684.0	739.4	0.91	1.11
26.4	1596.5	356.5	1240.0	719.3	670.3	681.2	736.9	0.91	1.11
28.9	1756.5	356.5	1400.0	719.3	668.4	678.8	735.1	0.91	1.11
31.4	1916.5	356.5	1560.0	719.3	666.8	676.6	733.6	0.91	1.11
33.9	2076.5	356.5	1720.0	719.3	665.3	674.6	732.5	0.91	1.11
36.4	2236.5	356.5	1880.0	719.3	664.0	672.8	727.4	0.91	1.11
38.9	2396.5	356.5	2040.0	719.3	662.8	671.2	727.0	0.91	1.11
41.4	2556.5	356.5	2200.0	719.3	661.7	669.7	726.7	0.91	1.11
						MEAN		0.90	1.10
						SD		0.01	0.01

Table 5.17 *Comparison of the flat face 0.2% proof strength for the duplex 1.4462 grade with r_i/t = 0.5 and the ratio between the predictive strength for a full section according to the modified and unchanged R-A-G relationship.*

As well as for the lean duplex grade (also for the duplex grade), the modified R-A-G relationship is closer to the modelled properties and gives higher values of the 0.2% proof strength for a full section by approximately 10%.

r_i/t = 2; t = 4 mm		MODIFIED R-A-G				
H/t	A_g (mm^2)	A_c (mm^2)	A_f (mm^2)	$\sigma_{0.2,c,pred}$ (MPa)	$\sigma_{0.2,f,pred}$ (MPa)	$\sigma_{0.2,full,pred}$ (MPa)
8.9	435.3	251.3	184.0	775.5	776.5	775.9
11.4	595.3	251.3	344.0	775.5	770.0	772.3
13.9	755.3	251.3	504.0	775.5	765.1	768.5
16.4	915.3	251.3	664.0	775.5	761.1	765.1
18.9	1075.3	251.3	824.0	775.5	757.9	762.0
21.4	1235.3	251.3	984.0	775.5	755.2	759.3
23.9	1395.3	251.3	1144.0	775.5	752.8	756.9
26.4	1555.3	251.3	1304.0	775.5	750.8	754.8
28.9	1715.3	251.3	1464.0	775.5	749.0	752.9
31.4	1875.3	251.3	1624.0	775.5	747.4	751.1
33.9	2035.3	251.3	1784.0	775.5	745.9	749.6
36.4	2195.3	251.3	1944.0	775.5	744.6	748.1
38.9	2355.3	251.3	2104.0	775.5	743.4	746.8
41.4	2515.3	251.3	2264.0	775.5	742.3	745.6

Table 5.18 *Predictive 0.2% proof strength for the duplex 1.4462 grade with r_i/t = 2.0 according to the modified R-A-G relationship.*

$r_i/t = 2$; $t = 4$ mm		R-A-G					FULL SECTION
H/t	A_g (mm^2)	A_c (mm^2)	A_f (mm^2)	$\sigma_{0.2,c,pred}$ (MPa)	$\sigma_{0.2,f,pred}$ (MPa)	$\sigma_{0.2,full,pred}$ (MPa)	M. R-A-G /R-A-G
8.9	435.3	435.3	0.0	695.2	696.3	695.2	1.12
11.4	595.3	507.3	88.0	695.2	689.7	694.4	1.11
13.9	755.3	507.3	248.0	695.2	684.7	691.8	1.11
16.4	915.3	507.3	408.0	695.2	680.7	688.8	1.11
18.9	1075.3	507.3	568.0	695.2	677.4	685.8	1.11
21.4	1235.3	507.3	728.0	695.2	674.7	683.1	1.11
23.9	1395.3	507.3	888.0	695.2	672.3	680.7	1.11
26.4	1555.3	507.3	1048.0	695.2	670.3	678.4	1.11
28.9	1715.3	507.3	1208.0	695.2	668.4	676.4	1.11
31.4	1875.3	507.3	1368.0	695.2	666.8	674.5	1.11
33.9	2035.3	507.3	1528.0	695.2	665.3	672.8	1.11
36.4	2195.3	507.3	1688.0	695.2	664.0	671.2	1.11
38.9	2355.3	507.3	1848.0	695.2	662.8	669.8	1.12
41.4	2515.3	507.3	2008.0	695.2	661.7	668.5	1.12
						MEAN	1.11
						SD	0.00

Table 5.19 *0.2% proof strength for the duplex 1.4462 grade with r_i/t = 2.0 and the ratio between the predictive strength for a full section according to the modified and unchanged R-A-G relationship – follow up.*

Modified formulas for the 0.2% proof strength enhancement stated above give a prediction of final mechanical properties by increase up to 11%. Despite the lower corner area considered it results in increase for all non-austenitic grades. Standard deviation is low and does not significantly differ from the unchanged relationship due to the close shape of the mathematical expression. Due to the assumption of the only pure bend area representing enhanced corner properties the resulting 0.2% proof strength for a full section of austenitic is lower than in case of the unchanged R-A-G expression. Particularly for the investigated 1.4404 grade, the maximal difference (assuming r_i/t = 0.5 or 2.0) is only 3% due to the significant influence of flat faces. That means there is no important decrease of overall enhancement for a member by using the reduced corner area.

5.7 Ductility of a full section

Uniaxial test results in Chapter 3 indicate simple dependency of ductility decrease on plastic strain induced during the cold-forming. Plastic strain evaluating for a flat face and a corner according to the previous Maple modelling allows establishing overall ductility decrease for a whole section by averaging values of all layers. Ductility of a full section ε_{full} can be given by weighting as:

$$\varepsilon_{full} = \varepsilon_v - \varepsilon_s \tag{5.66}$$

where ε_v is ductility of a virgin material,
ε_s is average plastic strain induced within fabricating given by:

$$\varepsilon_s = \frac{\varepsilon_c A_F + \varepsilon_f A_C}{A_G} \tag{5.67}$$

where ε_c is a mean value of plastic strain for a corner,
ε_f is a mean value of plastic strain for a flat part.

As the simplest way for assuming of plastic strain distribution is the linear one. The mean value of plastic strain for a corner can be determined by thickness t and inner radius r_i as:

$$\varepsilon_c = 0.5 \left(\frac{t/2}{r_i + t/2} \right) \tag{5.68}$$

Figure 5.80 shows that for common geometric properties of cold-rolled section corners, the decrease can reach 10% at least.

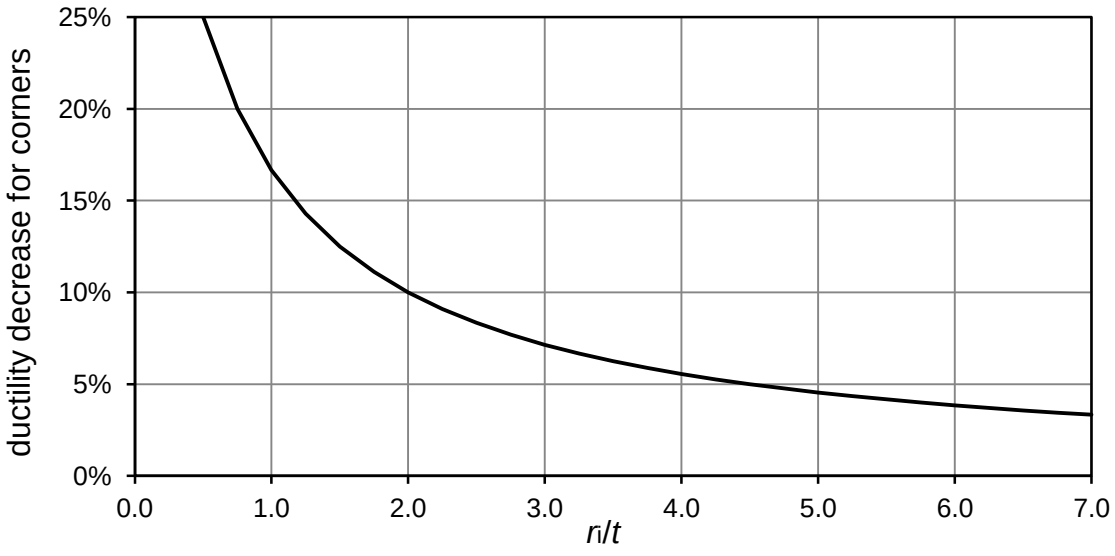

Figure 5.80 *Mean ductility decrease for corners depending on the r_i/t ratio.*

Similarly for a flat face there can be established a mean value of plastic strain regarding the influence of coiling-uncoiling process with making a circular tube and reverse bending into a flat face as:

$$\varepsilon_f = \left(\frac{t/2}{R_{coiling}}\right) + \left(\frac{t/2}{\frac{H+L-2t}{\pi}}\right) \qquad \text{with } R_{coiling} = 450 \text{ mm} \qquad (5.69)$$

For flat faces the ratio $R_f/t = (H+L-2t)/(\pi t)$ typically varies between values of 10 and 20. In terms of the H/t ratio (if $H=L$) the range of typical values is from 17 to 35.

Figure 5.81 displays that typical decrease for flat faces lies between 3% or 6%. It is evident that the higher B/t ratio is, the lower decrease of ductility of a full section will occur not because of only the lower ductility decrease in flat faces but also due to the higher influence of the flat faces areas. Figure 5.82 displays the decrease of ductility for a full section depending on the B/t ratio with minimal and maximal common r_i/t ratios (namely - $r_i/t = 0.5$, $r_i/t = 2.0$ respectively). It shows the total ductility decrease for full sections varies between 3% and 11%. That can importantly affect material demands for structural members, especially for ferrtic grades (ductility decrease is slightly higher than for others). For austenitic and duplex grades (including lean duplex) the decrease might be not important in case of minimal required ductility, because the ductility of a virgin material usually exceeds 30%.

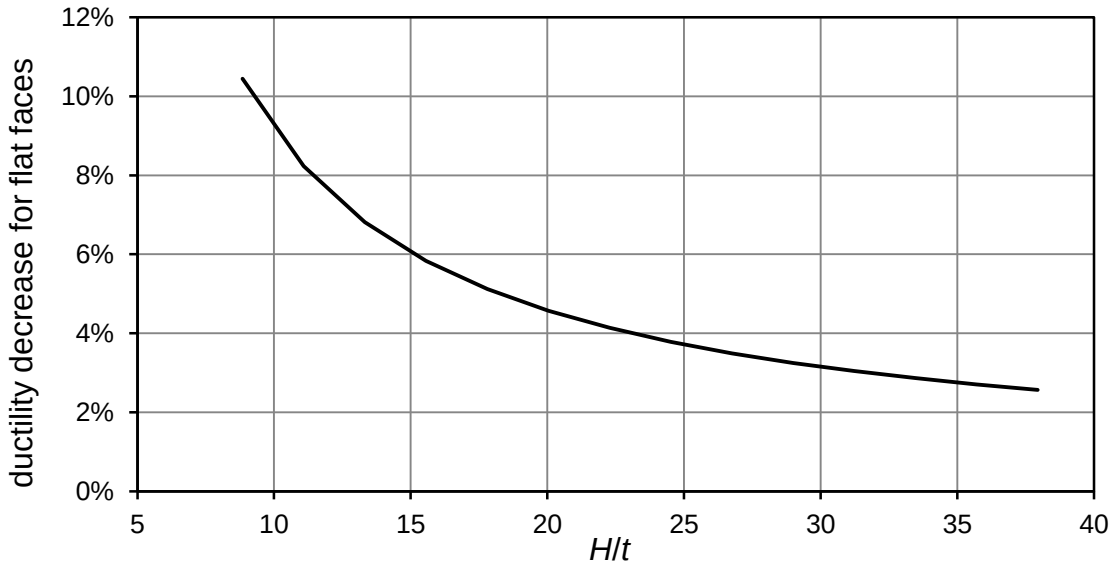

Figure 5.81 *Mean ductility decrease for flat faces depending on the H/t ratio.*

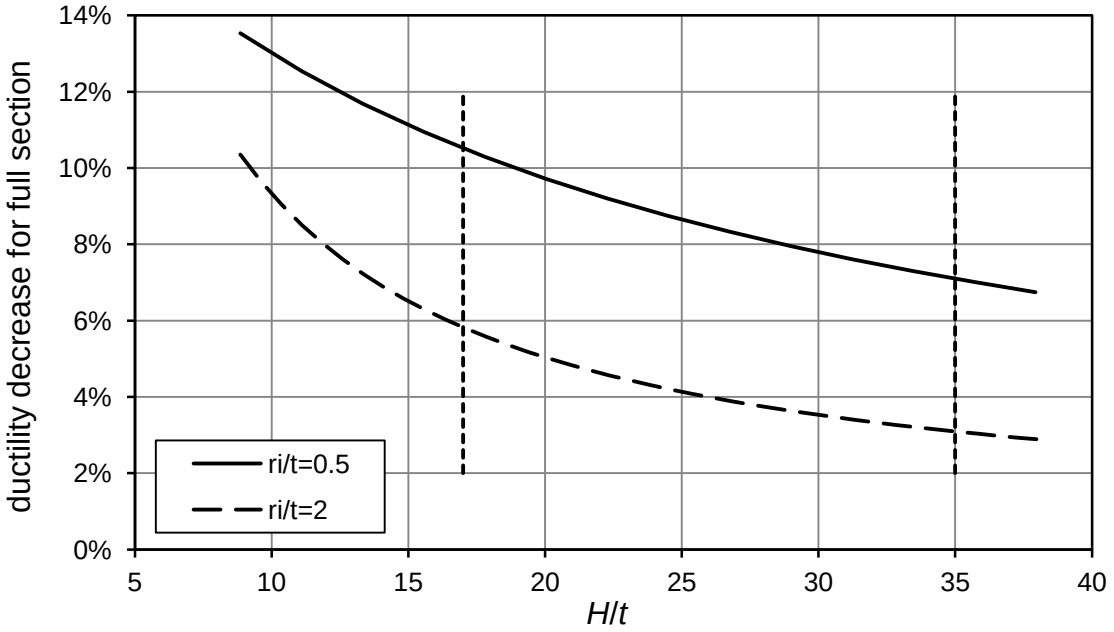

Figure 5.82 *Mean ductility decrease for a full section depending on the H/t ratio.*

As plastic strain across the thickness is not uniform and also not the same for a corner and a flat face it should be noted that the real ductility of a section is probably slightly lower than ε_{full}. Nevertheless ε_{full} can serve as an upper limit for the ductility determining. Figure 5.83 displays a recorded stress-strain response for the full section made of the ferritic steel 1.4509. Despite unknown ductility of the virgin material it could be assumed it was higher than the measured value about only 6% that represents very low level of ductility. Similar cases can be problematic in terms of plastic design and should be carefully considered in specific structural applications according to particular conditions.

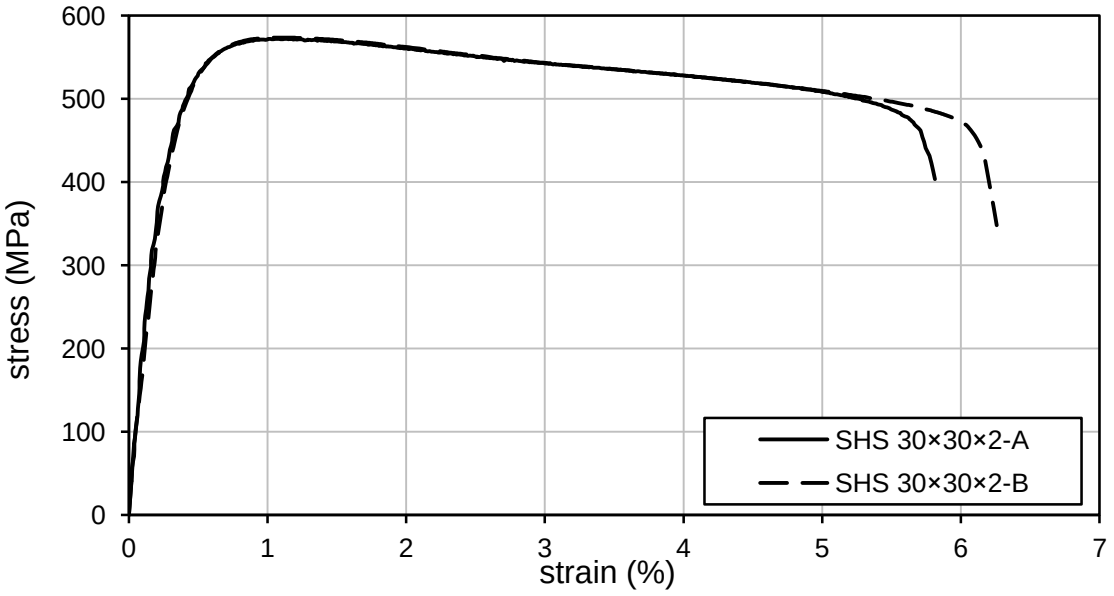

Figure 5.83 *Recorded stress-strain curve for two full section specimens of the 1.4509 SHS 30x30x2 measured at Imperial College* [47].

5.8 Stress-strain response of cold-formed sections

Results of the experimental programme stated in Chapter 3 indicate the Ramberg-Osgood parameter of non-linearity *n* decreases with increasing plastic strain induced within the cold-working. Plastic straining develops changes in microstructure of an original material that cause different stress-strain behaviour of a newly made material. As the Maple model considers the thickness divided into several layers, layers near to the surfaces exhibit more rounded stress-strain response up to the increased 0.2% proof strength than the layers near to the central core. Within the summation of contribution of each layer the final state represents an average value of the nonlinearity parameter *n* arisen from stress-strain diagrams different across the thickness of the investigated parts of sections. The principle is depicted in Figure 5.84. The stress-strain curve for the layer nearer to the central core and neutral surface with lower level of plastic strain induced exhibits a less rounded loading response and lower 0.2% proof strength than the layer, nearer to the surface with larger plastic strain induced exhibiting a more rounded loading response and also higher 0.2% proof strength. The resulting stress strain diagram arisen from summation of these curves mainly lies within the area defined by these responses with intermediate values of the 0.2% proof strength and parameter of nonlinearity. In case of cold-rolled sections it means the final stress-strain curve should be more rounded due to the significant level of plastic strain induction during the fabrication process. The lower parameter of nonlinearity affects especially calculation of deflections that would be higher in contrast to the calculation with the nonlinearity parameter of the virgin material. In addition, it could affect also the buckling resistance of structural members due to the reduced tangential modulus.

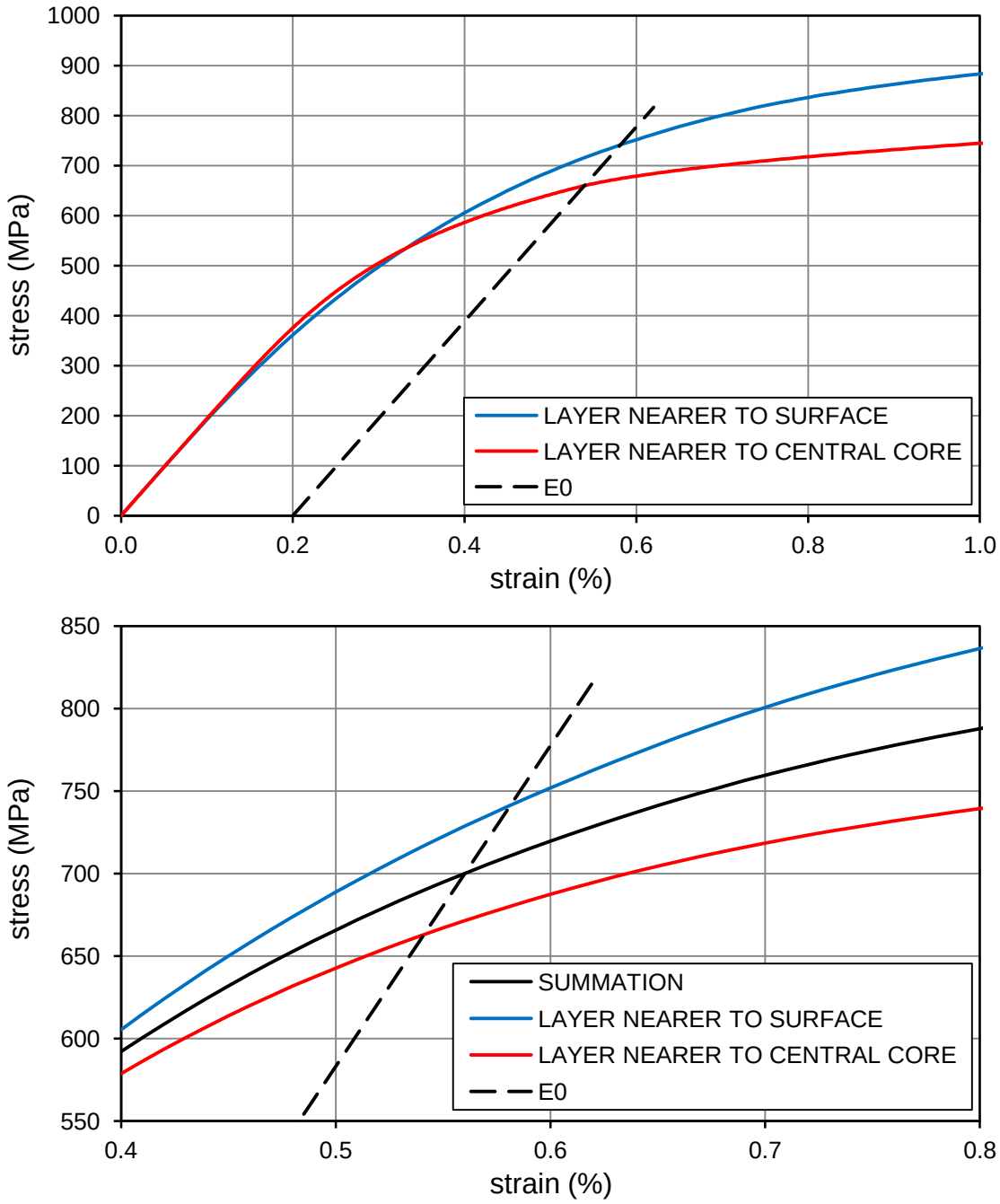

Figure 5.84 *Stress-strain curves demonstrating different layers across the thickness according to their location related to the neutral surface. Lower figure displays a detail of the upper figure.*

Following figures display change of nonlinearity parameter n related to the original parameter of nonlinearity n both for flat faces (n_i/n) and corners (n_c/n) by means of results of stainless steel grades investigated at CTU (their trends describing n according to the increasing level of plastic strain induction).

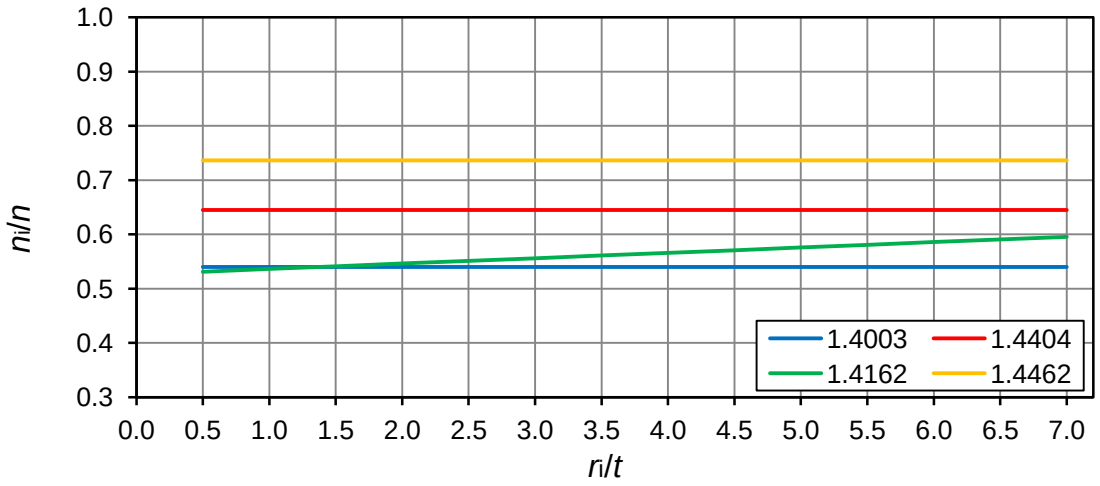

Figure 5.85 *Parameter of nonlinearity n depending on the inner radius to thickness ratio for corners.*

Figure 5.85 shows that except the lean duplex 1.4162 grade there is no change of the nonlinearity depending on the r_i/t ratio. However, in case of the 1.4162 grade the dependency is negligible. For all corners the new material nonlinearity is reduced by a different rate and remains constant. It is given by high level of plastic straining which the constant reduced nonlinearity is defined for (see section 5.3). The lowest values reach only 55% of original ones and the highest values reach 75% of original values that means significant decrease.

As the influence on the corner material remains constant, the most important effect for section material nonlinearity is generated by the influence on flat faces. Figure below displays almost linearly increasing dependency of the parameter *n* on the outer dimension to thickness ratio for all grades. Even, except the lean duplex steel, the slope of the curves is almost the same.

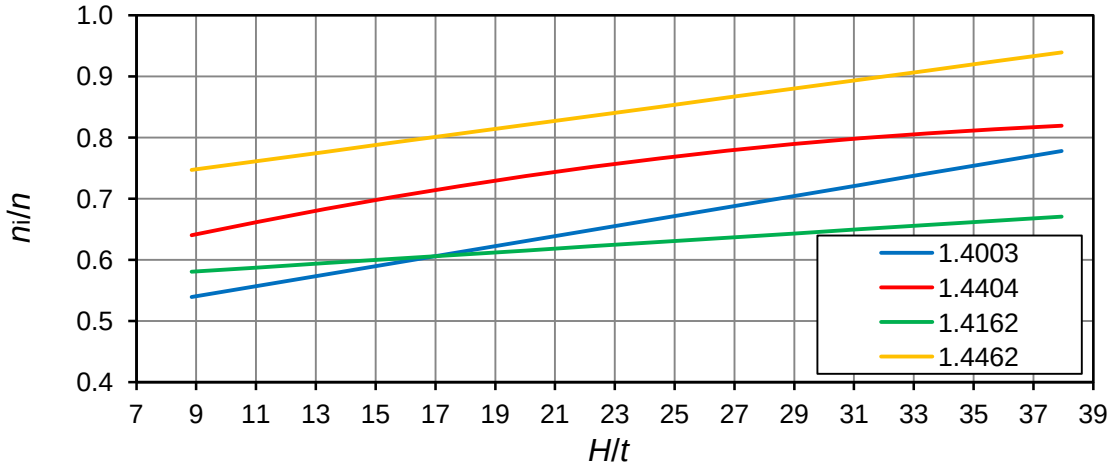

Figure 5.86 *Parameter of nonlinearity n depending on the H/t ratio for flat faces*

.

As for the ductility it is possible to determine a new parameter of nonlinearity for a full section by weighting contribution of corners and flat faces by their areas according to Eq. (5.67) with negligible difference between this summing and the real stress-strain

curve. The resulting parameter of nonlinearity depending on the *H/t* ratio is displayed in Figure 5.87 and Figure 5.88 with common borders for the ratio lying between 17 and 35. For the lean duplex grade, the decrease in the corner is for most common $r_i/t \in (0.5, 2.0)$ almost the same and thus it is not much pronounced.

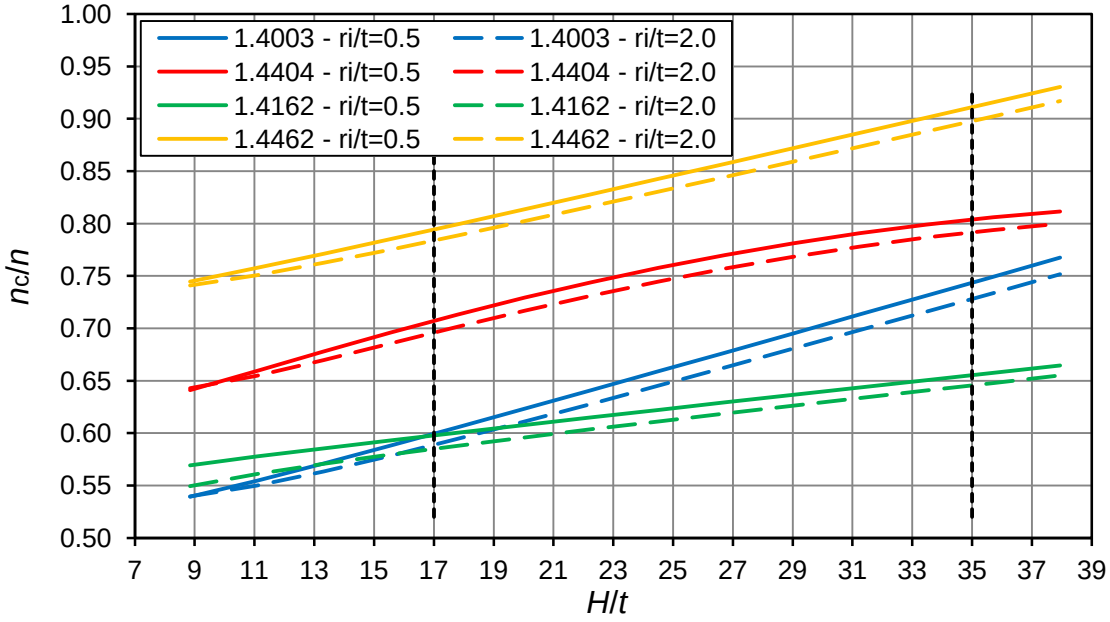

Figure 5.87 *Parameter of nonlinearity n related to the property of virgin material depending on the H/t ratio for full sections.*

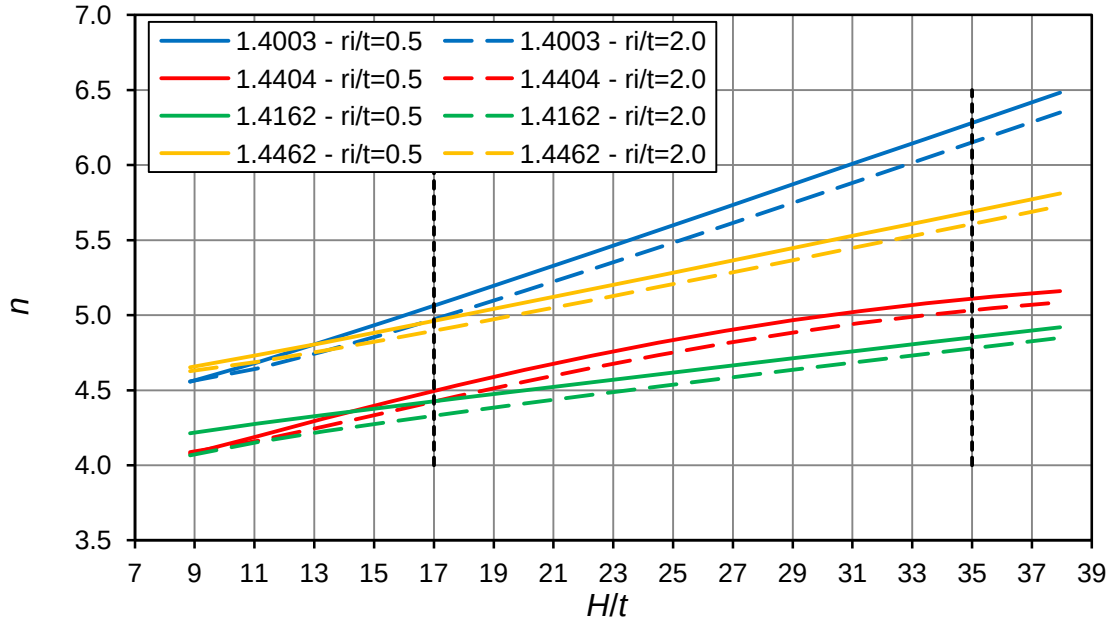

Figure 5.88 *Parameter of nonlinearity n depending on H/t ratio for full sections*

The figures above show the parameter of nonlinearity for a full section lies in the range of 60% - 90% in relation to the virgin material property of the investigated grades. Previous figures also confirm the lowest decrease of the parameter is observed for the

duplex steel, following by the austenitic grade. The highest decrease is exhibited by the ferritic and lean duplex grades. Most of the investigated cases also show the nonlinearity parameter *n* does not go under value of 4.5 and does not exceed value of 6.5.

As the data does not involve sufficient values for statistical evaluation, a conservative relationship determining the parameter of nonlinearity of cold-formed SHS n_c given by the lowest curve obtained from the analytical solution depending on the dimension to thickness ratio is expressed as:

$$n_c = 0.0035(H/t)+0.523 \tag{5.70}$$

In terms of safety, lower values of nonlinearity parameter result in increased values of deflection at the same stress level. That means more safe prediction of deflection within structural design. When detailed calculation of members including direct computing of stability issues with imperfections is required, the results obtained will provide a conservative result. As well as for deflection, the more accurate calculation of *n* might precise results.

As well as for basic parameter of nonlinearity *n*, global effect for compound Ramber-Osgood parameter $n_{0.2,1.0}$ can be shown in Figure 5.89. It could be expected that stress and strain will usually not exceed values for the 0.2% proof strength in case of structural members made of cold-formed section. Hence the second parameter of non-linearity is not as important. Its influence would be especially employed in finite elements modelling of joints and connections or buckling tasks or when using the Continuous Strength method. It is apparent that except the ferritic grade the increase is not such important although higher $n_{0.2,1.0}$ leads to increased strains at higher strain ranges.

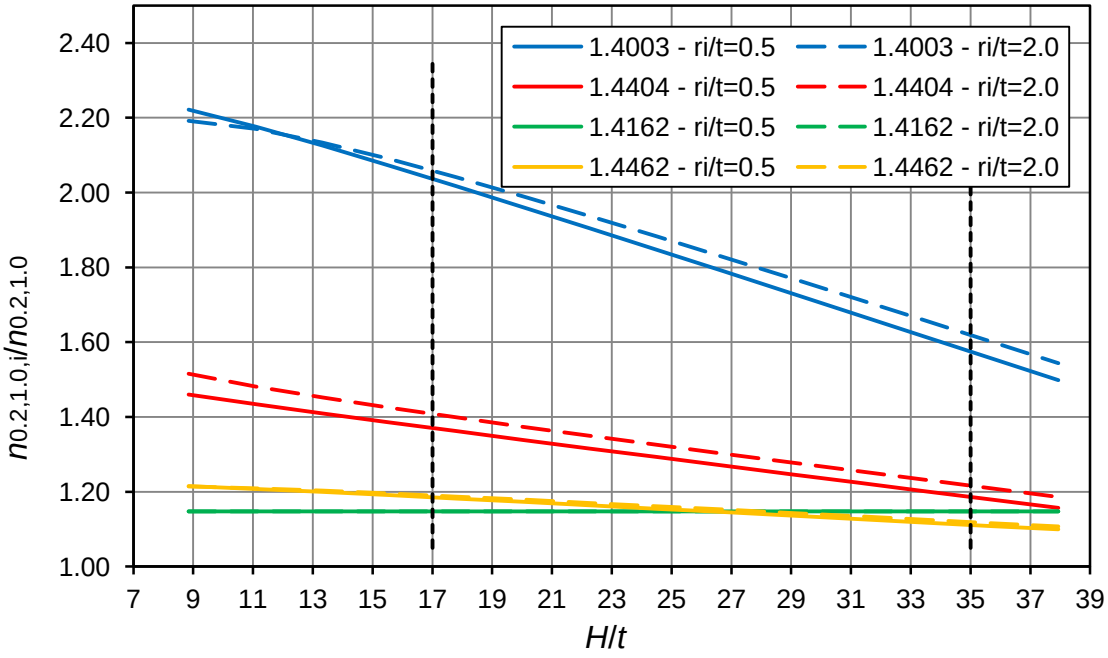

Figure 5.89 *Parameter of nonlinearity $n_{0.2,1.0}$ for full sections depending on the H/t ratio.*

5.9 Determination of ultimate strength

Ultimate stress is one of the essential properties describing a structural element. In terms of material demands for structural purposes, the European design code requires ultimate stress to yield stress ratio f_u/f_y (for stainless steel - $\sigma_u/\sigma_{0.2}$) to be 1.10 at least to provide sufficient ability of possible overloading. Full section tests performed at Imperial College [47] demonstrate the point of ultimate strength lies close to the "yield" point. Another demand requiring the strain at the ultimate stress ε_u to be higher than $15x\varepsilon_y$, the strain at the yield stress (in case of stainless steel $\varepsilon_{0.2}$), might not be satisfied. Figure 5.90 displays full section tests for the SHS 30x30x2 made of the ferritic grade 1.4509. Other figures depict square hollow sections of the same material tested along with this one. Following figures display stress strain curves for the whole section of SHS 40x40x2, SHS 50x50x2 and SHS 30x30x2 again.

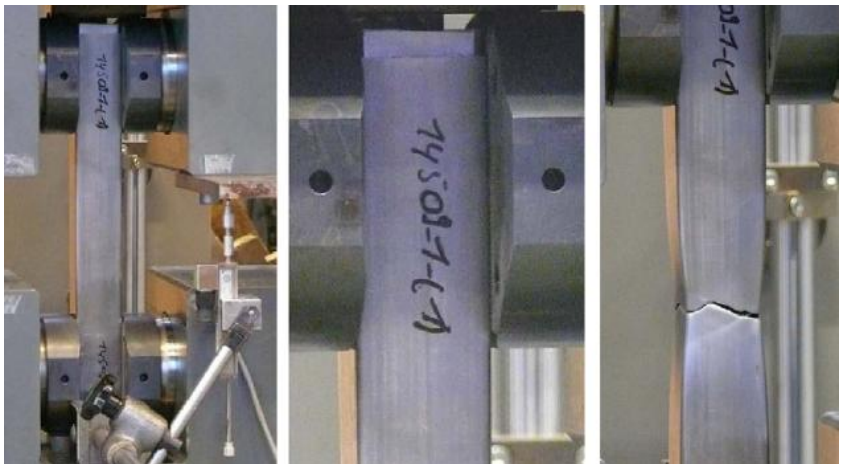

Figure 5.90 *Test set-up at Imperial College* [47].

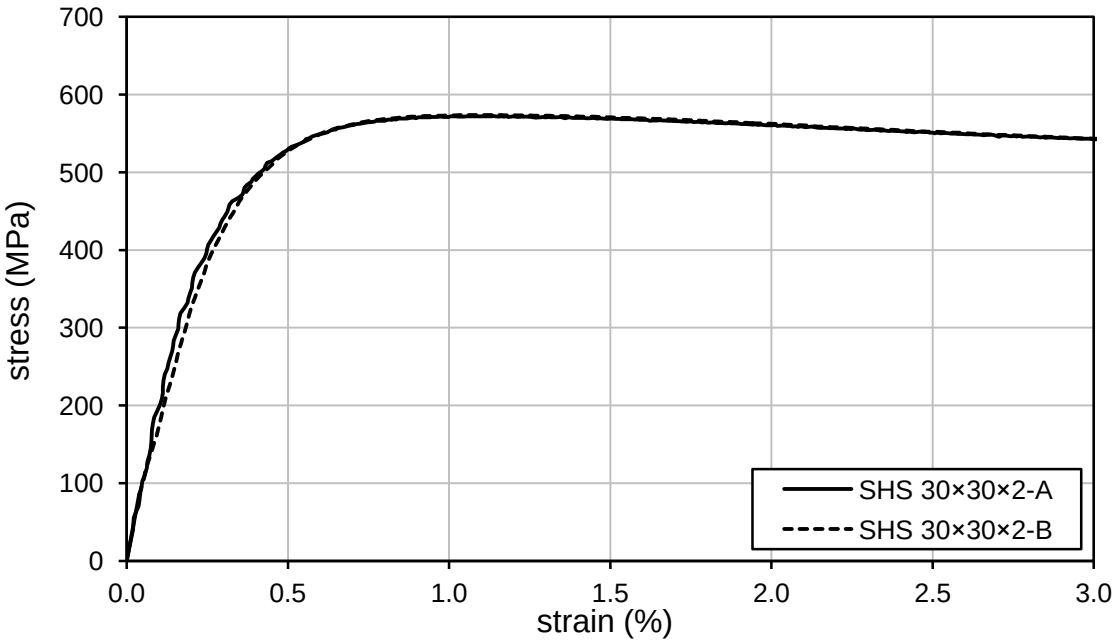

Figure 5.91 *Recorded stress-strain curve for two full section specimens of the 1.4509 SHS 30x30x2 measured at Imperial College* [47].

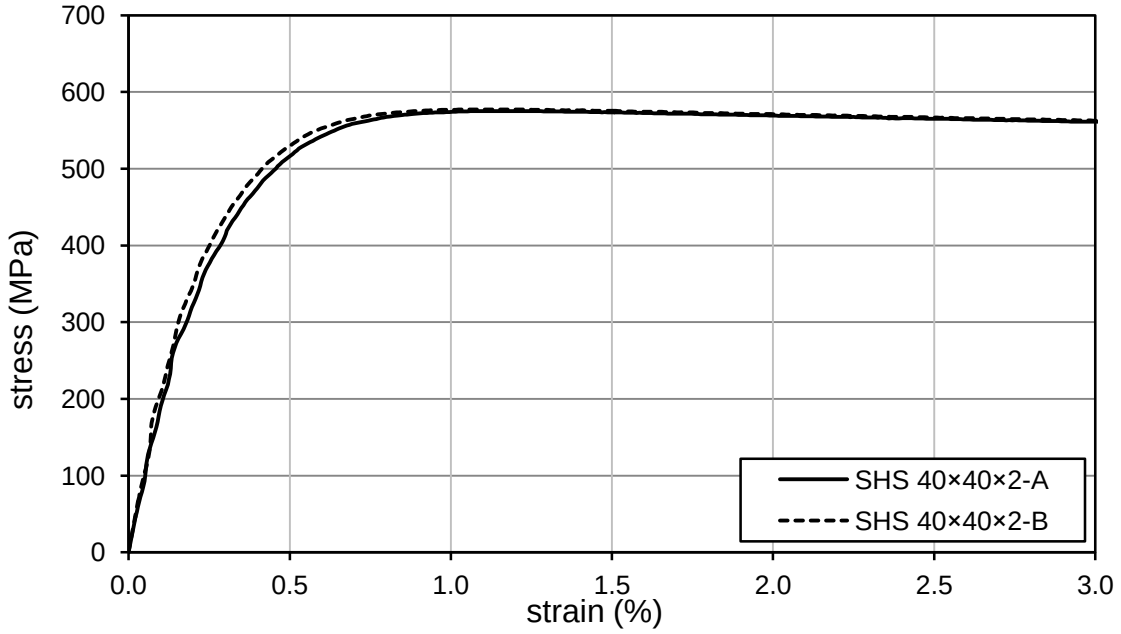

Figure 5.92 *Recorded stress-strain curve for two full section specimens of the 1.4509 SHS 40x40x2 measured at Imperial College* [47].

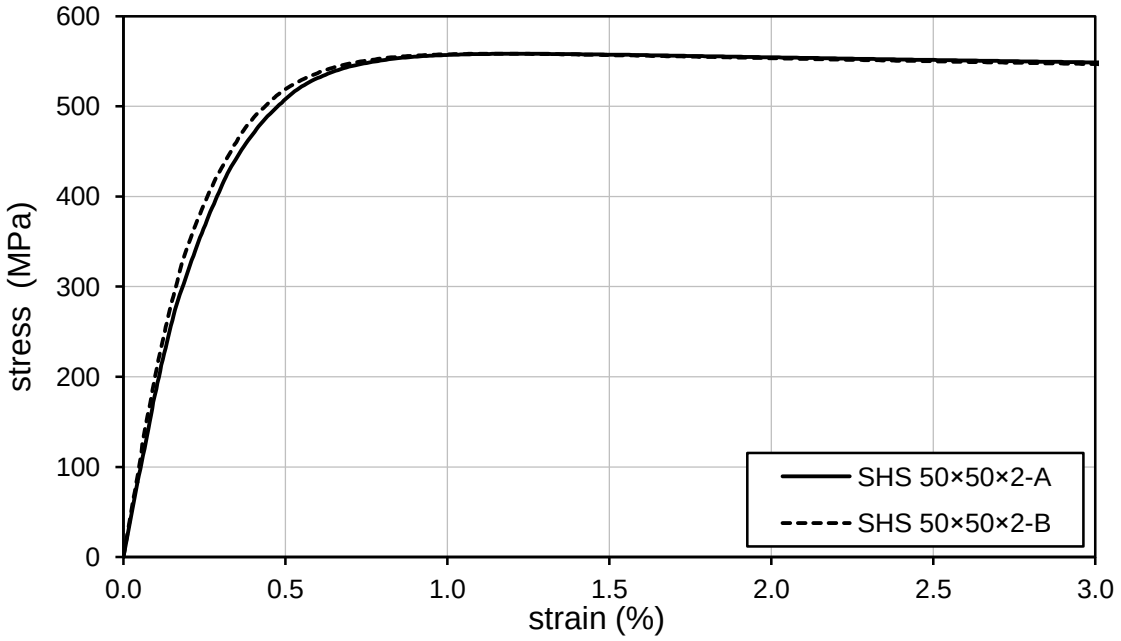

Figure 5.93 *Recorded stress-strain curve for two full section specimens of the 1.4509 SHS 50x50x2 measured at Imperial College* [47].

Test results indicate the maximal stress reached during the full section testing is similar to the value of the 1.0% proof stress. Maximal difference between the ultimate strength and the 1.0% proof strength obtained from these tests is 0.3%. Especially for SHS 30x30x2 there is big amount of plastic straining induced both for corner and flat faces. The effect of short range between strain at the 0.2% proof strength and strain at the ultimate strength or large plastic plateau with nearly no strength increase is probably

given by the specific ferritic steel grade and also by acting of corners and flat portions together that may exhibit this stress-strain response. A part of a section with nearly perfect yield plateau is shown in Figure 5.94 displaying the record of a tensile test conducted at Imperial College.

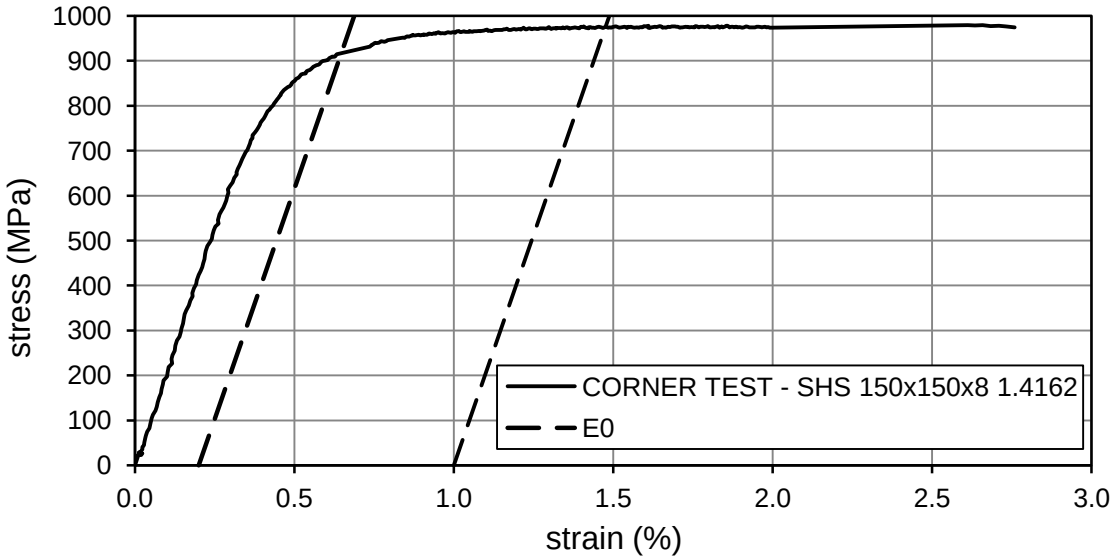

Figure 5.94 *Recorded stress-strain curve from a corner tensile test.* [47]

While full section acts as one unit, each part exhibits different stress-strain behaviour as it is depicted in Figure 4.39 and Figure 4.40. The behaviour of corners under loading can exhibit decreasing stage after reaching the ultimate strength near the 0.2% proof strength, especially for ferritic grades. Such behaviour is caused by engineering form of stress and strain expression. In case of true values, the stage after reaching the 0.2% proof strength exhibits increasing or at least constant trend. For materials with the more "clear" 0.2% proof strength boundary (high values of nonlinearity parameter n) and lower ratios of $\varepsilon_{0.2}/\varepsilon_u$, resulting behaviour performed by summing particular effects of sections portions may be influenced more by corners. It can be expected that for sections with larger ratios of H/t and for steel with larger ratios of $\varepsilon_u/\varepsilon_{0.2}$ the ultimate strength should be evaluated for higher proof strength than for the 1.0% plastic strain. Nevertheless, the 1% proof strength seems to be a safe and conservative estimation. Thus where there is lack of information about the material properties, the 1.0% proof strength of a full section $\sigma_{1.0,full}$ can be assumed as very conservative value as supplement for the ultimate strength $\sigma_{s,full}$:

$$\sigma_{s,full} = \sigma_{1.0,full} \tag{5.71}$$

A parametric study based on the Maple model performed for stainless steel grades investigated at CTU determined both the 0.2% proof strength and the 1.0% proof strength for flat faces and corners. Evaluated values are summarized in following tables together with the 1.0% proof strength to the 0.2% proof strength ratio. For each grade, the table contains minimal values of the ratios. In case of the corners, there is specified a minimum for the range of common inner radii (see Appendix G), i.e. for $r_i/t \leq 2.0$. For the flat faces, the minimum is set for the most common range of the H/t ratio lying

between 17 and 35. The corner and flat face values are used for further specification of the full section strength as representatives.

r_i/t	$\sigma_{0.2,c}$ (MPa)	$\sigma_{1.0,c}$ (MPa)	$\sigma_{1.0,c}/\sigma_{0.2,c}$	H/t	$\sigma_{0.2,f}$ (MPa)	$\sigma_{1.0,f}$ (MPa)	$\sigma_{1.0,f}/\sigma_{0.2,f}$
0.50	562.91	673.40	1.20	8.85	488.26	572.43	1.17
1.00	552.98	661.40	1.20	11.09	467.89	545.53	1.17
1.50	547.31	652.62	1.19	13.33	452.79	526.19	1.16
2.00	540.52	640.22	1.18	15.56	443.76	512.42	1.15
2.50	530.12	629.64	1.19	17.80	433.49	501.77	1.16
3.00	523.63	618.01	1.18	20.04	427.98	493.87	1.15
3.50	512.43	607.52	1.19	22.28	423.29	487.06	1.15
4.00	505.78	594.35	1.18	24.51	419.24	481.27	1.15
4.50	498.55	584.03	1.17	26.75	413.90	477.26	1.15
5.00	487.74	573.41	1.18	28.99	411.05	473.23	1.15
5.50	481.13	564.17	1.17	31.23	408.79	469.69	1.15
6.00	472.38	556.03	1.18	33.46	406.25	466.83	1.15
6.50	467.06	548.74	1.17	35.70	404.82	464.22	1.15
7.00	462.55	542.96	1.17	37.94	402.88	461.95	1.15
MINIMUM FOR $r_i/t \leq 2$			1.18	MINIMUM FOR $H/t \leq 35$			1.15

Table 5.20 *Ratio of the 1.0% proof stress to the 0.2% proof strength for the ferritic 1.4003 grade.*

r_i/t	$\sigma_{0.2,c}$ (MPa)	$\sigma_{1.0,c}$ (MPa)	$\sigma_{1.0,c}/\sigma_{0.2,c}$	H/t	$\sigma_{0.2,f}$ (MPa)	$\sigma_{1.0,f}$ (MPa)	$\sigma_{1.0,f}/\sigma_{0.2,f}$
0.50	552.27	661.19	1.20	8.85	434.42	517.52	1.19
1.00	537.16	643.78	1.20	11.09	413.18	491.44	1.19
1.50	521.08	626.10	1.20	13.33	397.22	472.85	1.19
2.00	509.45	608.13	1.19	15.56	384.77	459.08	1.19
2.50	493.07	589.53	1.20	17.80	377.50	448.39	1.19
3.00	476.62	570.86	1.20	20.04	371.87	440.52	1.18
3.50	461.75	554.27	1.20	22.28	364.82	434.50	1.19
4.00	452.44	540.17	1.19	24.51	360.72	428.42	1.19
4.50	440.50	528.12	1.20	26.75	357.87	424.49	1.19
5.00	433.54	517.56	1.19	28.99	355.14	420.75	1.18
5.50	423.78	508.56	1.20	31.23	352.88	417.67	1.18
6.00	418.35	500.24	1.20	33.46	348.36	414.81	1.19
6.50	413.59	493.31	1.19	35.70	346.52	412.27	1.19
7.00	405.77	486.53	1.20	37.94	344.98	409.75	1.19
MINIMUM FOR $r_i/t \leq 2$			1.19	MINIMUM FOR $H/t \leq 35$			1.18

Table 5.21 *Ratio of the 1.0% proof stress to the 0.2% proof strength for the austenitic 1.4404 grade.*

r_i/t	$\sigma_{0.2,c}$ (MPa)	$\sigma_{1.0,c}$ (MPa)	$\sigma_{1.0,c}/\sigma_{0.2,c}$	H/t	$\sigma_{0.2,f}$ (MPa)	$\sigma_{1.0,f}$ (MPa)	$\sigma_{1.0,f}/\sigma_{0.2,f}$
0.50	749.30	966.74	1.29	8.85	691.82	869.05	1.26
1.00	744.45	954.87	1.28	11.09	681.84	842.47	1.24
1.50	729.76	934.07	1.28	13.33	670.56	824.12	1.23
2.00	726.00	925.15	1.27	15.56	666.44	810.63	1.22
2.50	721.47	915.44	1.27	17.80	663.40	800.84	1.21
3.00	712.11	906.65	1.27	20.04	661.13	792.47	1.20
3.50	707.90	897.33	1.27	22.28	655.18	786.66	1.20
4.00	704.24	888.26	1.26	24.51	653.78	781.43	1.20
4.50	700.59	879.72	1.26	26.75	651.77	776.29	1.19
5.00	691.58	870.32	1.26	28.99	650.45	772.60	1.19
5.50	688.29	862.21	1.25	31.23	649.49	769.35	1.18
6.00	685.32	853.99	1.25	33.46	649.11	766.97	1.18
6.50	682.65	847.20	1.24	35.70	648.61	764.59	1.18
7.00	674.99	841.06	1.25	37.94	648.55	762.70	1.18
MINIMUM FOR $r_i/t \leq 2$			1.27	MINIMUM FOR $H/t \leq 35$			1.18

Table 5.22 *Ratio of the 1.0% proof stress to the 0.2% proof strength for the lean duplex 1.4162 grade.*

r_i/t	$\sigma_{0.2,c}$ (MPa)	$\sigma_{1.0,c}$ (MPa)	$\sigma_{1.0,c}/\sigma_{0.2,c}$	H/t	$\sigma_{0.2,f}$ (MPa)	$\sigma_{1.0,f}$ (MPa)	$\sigma_{1.0,f}/\sigma_{0.2,f}$
0.50	876.54	1050.90	1.20	8.85	798.21	950.39	1.19
1.00	864.06	1039.18	1.20	11.09	776.85	919.66	1.18
1.50	844.43	1014.79	1.20	13.33	761.64	898.69	1.18
2.00	840.09	1007.81	1.20	15.56	755.06	884.01	1.17
2.50	834.15	997.18	1.20	17.80	745.62	873.01	1.17
3.00	823.29	988.07	1.20	20.04	742.13	864.25	1.16
3.50	817.83	978.88	1.20	22.28	739.38	857.24	1.16
4.00	806.73	968.96	1.20	24.51	736.87	850.59	1.15
4.50	801.86	960.56	1.20	26.75	735.05	845.86	1.15
5.00	796.69	950.54	1.19	28.99	733.63	841.95	1.15
5.50	786.43	942.03	1.20	31.23	732.46	838.64	1.14
6.00	782.17	933.62	1.19	33.46	727.43	835.67	1.15
6.50	777.91	925.52	1.19	35.70	727.01	832.80	1.15
7.00	774.21	918.57	1.19	37.94	726.70	830.74	1.14
MINIMUM FOR $r_i/t \leq 2$			1.20	MINIMUM FOR $H/t \leq 35$			1.15

Table 5.23 *Ratio of the 1.0% proof stress to the 0.2% proof strength for the duplex 1.4462 grade.*

As for parameter of nonlinearity n it is possible to determine the ratio $\sigma_{1.0,full}/\sigma_{0.2,full}$ by means of weighting the contribution of the corners and flat faces by their areas according to Eq. (5.67) with negligible difference to the real stress-strain response of a

full section. Influence of the corner area related to the gross sectional area is plotted in Figure 5.95. Corner area mostly represents 5% - 25% of a gross area of a section.

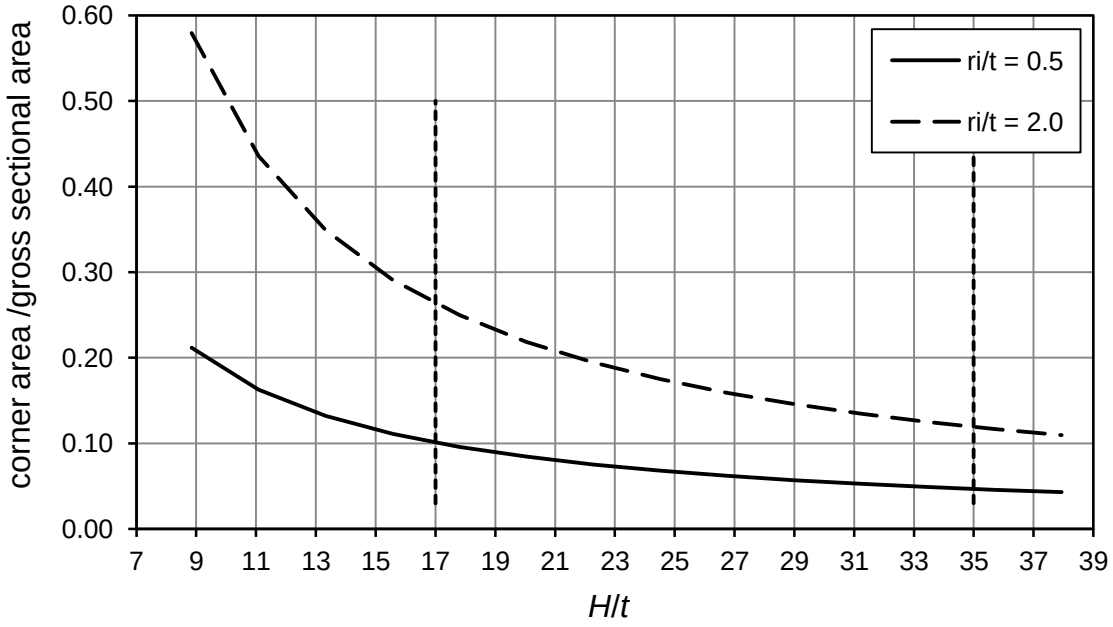

Figure 5.95 *Contribution of the corners related to the gross sectional area for the bordering values of the inner radius.*

Similarly to the previous establishing of material parameters, the weighting according to areas of particular portions enables to plot the overall 1.0% proof strength related to the 0.2% proof strength of a full section. Figure 5.96 displays all investigated grades regarding the H/t ratio. Within summing the corner influence remains constant whilst contribution of the flat faces depends both on the H/t ratio and the area of flat faces. Plotted values indicate the minimal $\sigma_{1.0,full}/\sigma_{0.2,full}$ ratio to be 1.15 and maximum to be 1.22. The austenitic grade 1.4404 exhibits almost constant trend equal to 1.18. The ferritic 1.4003 and duplex 1.4462 grades exhibit slightly decreasing trend with negligible differences between the boundary lines (H/t = 17 and 35). The most decreasing trend belongs to the lean duplex 1.4162 grade. Because the differences of the curves are not much significant it is possible to conservatively estimate the 1.0% proof strength of a full section $\sigma_{1.0,full}$ by the same value for all grades as:

$$\sigma_{1.0,full} = 1.15 \cdot \sigma_{0.2,full} \tag{5.72}$$

It should be noted that for austenitic steel it is very conservative estimation with high level of safety. For other grades with lower values of ductility and relatively flat stress-strain curve in a higher strain range it could be an adequate relationship.

Finally cold-formed stainless steel sections fulfil the demand for the structural material requiring the $\sigma_u/\sigma_{0.2}$ ratio to be higher than 1.10 and allow partial overloading of a structure. However as it was stated above, for the non-austenitic (especially ferritic) grades the conditions for ductility determining or the $\varepsilon_u/\varepsilon_{0.2}$ ratio could be limiting in terms of plastic design. Thus within designing of cold-formed hollow sections with enhanced strength properties it would be better to use the elastic calculus together with the elastic design to avoid this issue. This problem is worth further investigation.

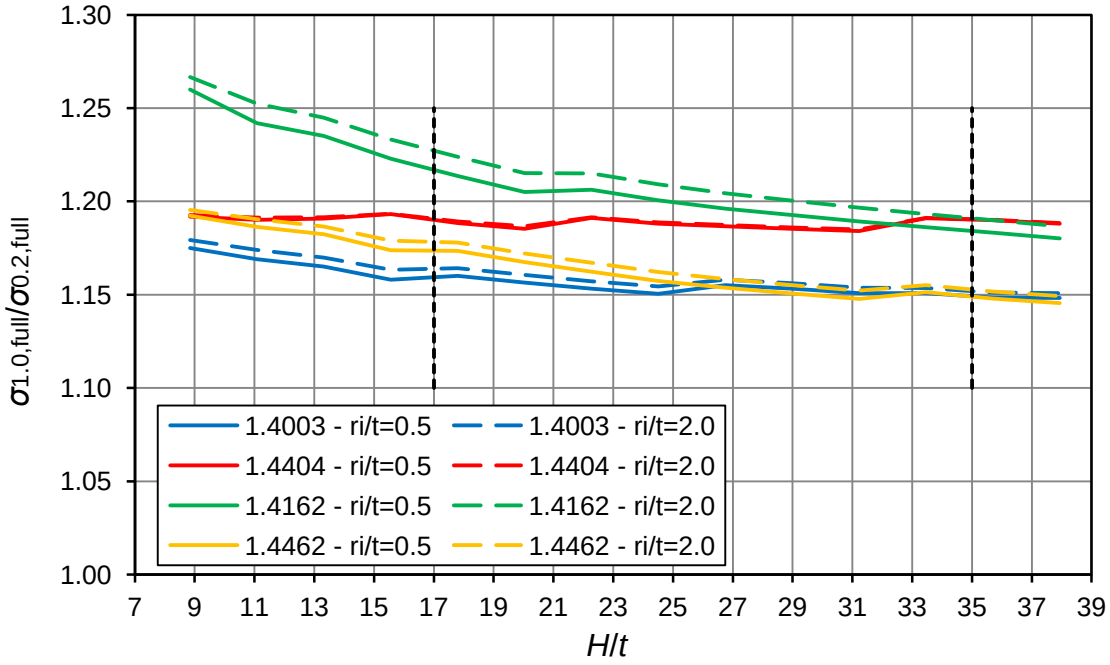

Figure 5.96 *Overall 1.0% proof strength to the 0.2% strength ratio depending on the H/t ratio.*

Chapter 6

Conclusions

6.1 Project summary

The thesis presented herein consists of three main parts. The first describes the material as such, routes of fabrication of the particular stainless steel products, mechanical properties and the cold-forming effect on the section strength. The most relevant and recent research and design approaches are also stated as a base for further comparisons and results. The second part is focused on the experimental programme conducted at CTU in Prague focused on material tensile testing of four grades of stainless steel representing the most common families used for structural members, i.e. austenitic (1.4404), ferritic (1.4003), lean duplex (1.4162) and duplex (1.4462). All flat coupons and specimens were made of a cold-rolled sheet. The programme involved, except the basic determination of the mechanical properties, uniaxial cold-forming of the specimens serving for further evaluations and the analytical part. All coupons were tested with a couple of strain gauges for covering the initial part of the stress-strain response. A mechanical extensometer served for covering higher strain ranges. All tests were conducted using strain-control. The shape of the coupons and the entire testing procedure was conducted in accordance with EN ISO 6892-1 [57]. Following section presents summation of performed tests.

Experimental part of the thesis contains:

1) Execution of the tensile tests with the material parameters analysis for the stainless steel grades: 1.4404 (austenitic), 1.4003 (ferritic), 1.4462 (duplex) and 1.4162 (lean duplex) in two options:

    - Cold-rolled sheet test in the direction parallel as well as transverse to the rolling direction.

2) Plastic strain induction of cold-rolled sheet in four options:

    - Sample cut out parallel to the rolling direction and strain induced parallel to the subsequent tensile test.

    - Sample cut out parallel to the rolling direction and strain induced transverse to the subsequent tensile test.

    - Sample cut out transverse to the rolling direction and strain induced parallel to the subsequent tensile test.

    - Sample cut out transverse to the rolling direction and strain induced transverse to the subsequent tensile test.

      Levels of plastic deformation varied in sufficient range: 1%, 3%, 5%, 10%, 15% and 20% or 50% (the last one for austenitic only).

The test programme containing 160 coupons was executed and its results presented. Outputs stated in Chapter 4 were focused on the strength enhancement of the cold-formed specimens, change of properties determining the stress-strain behaviour such as the parameters of nonlinearity, initial modulus of elasticity or ductility related to the level of the plastic strain induction.

The third part of the thesis solves the analytical expression for the fabrication route describing a cold-bent part of sections. The fabrication route for cold-rolled box sections usually involves coiling and uncoiling of a sheet with subsequent circular section making and further forming it into a square or rectangular hollow section. The analytical model employs Quach´s equations [24] for plastic strain induction establishing during the fabrication process and the mathematical program Maple to process a lot of data including iteration steps for final state evaluating. As the plastic strain distribution across the thickness is known it is possible to divide the thickness into several layers and match each layer with specific properties obtained from experimental testing and referring to a particular cold-formed material. The Maple model is divided into the corner model and the flat face model. Finally there can be generated a new stress-strain curve for the cold-formed portion of a section.

On the basis of this new stress-strain behaviour, it is possible to determine enhanced strength and material nonlinearity. With respect to the results of the experimental program, it is also possible to determine ductility decrease. For other comparisons and statements there were used results from tests conducted at Imperial College London. The extensive testing programme involved tests of the corners and flat faces of the box

sections and the full section tests as well and served for further comparisons. Therefore it is possible to determine properties of a full cold-formed square and circular hollow section.

6.2 Contributions and recommendations

This research has shown the significant change of the stress-strain behaviour of structural hollow sections compared to its virgin material stress-strain response. Thus it is important to use the correct material properties for insuring the correct and more effective structural design.

The most relevant general observations and recommendations can be summarized as follows:

1) A cold-rolled stainless sheet exhibits higher 0.2% proof strength for the direction transverse to the rolling, whereas if a member is subjected to the uniaxial cold-forming, it tends to exhibit higher 0.2% proof strength in the direction parallel to the previous forming.

2) Ductility of a hollow section compared to the virgin material property can be decreased by more than 10%. Especially for ferritic grades the structural design should carefully consider lower resistance to straining with all consequences such as plastic redistribution of internal forces in structure or plasticisation of a section.

3) It is possible to assume the initial modulus of elasticity by the same value for virgin material as well as for cold-formed one.

4) True value of the ultimate strength remains constant for unformed material as well as for a cold-formed element.

5) The Ramberg-Osgood parameter of non-linearity decreases with increasing level of plastic strain induction. Overall it means higher deflections and in fact also decreased buckling resistance.

6) Ultimate tensile strength could be conservatively assumed as 1.15 multiple of the full section enhanced 0.2% proof strength.

7) Experimental results of full sections stated herein are closer to the assumption of enhanced corner area determined as a pure geometrical bend without any extension on each side.

8) The most recent predictive model for the 0.2% proof strength of box hollow sections published by Rossi, Afshan and Gardner [8] was slightly modified for non-austenitic grades in terms of providing higher predictive values. Nevertheless, this research has confirmed that predictive strengths obtained from this expression are safe and applicable for other purposes.

   The confirmation of the predictive model correctness is valuable in terms of different methods used to obtain similar results providing a good proof.

9) Comparison of (especially European) recent available cross-section shown following data:

   If the inner radius to thickness ratio was unknown, it would be possible to assume it with sufficient reliability as 6.9 for press-braked sections and 1.7 for cold-rolled sections (in comparison with the only European valid standard for the enhanced 0.2% proof strength – British National Annex for EN 1993-1-4 [50] specifying the value of 2.0).

Chapter 7

Future work

During the experimental programme and work on this study more other areas of investigations that could be beneficial for the issue emerged. One of the areas that deserve attention could be demands for classification of sections. As stainless steel loses the ability of creating plastic zones with sufficient deformation capacity due to cold-forming it could result in change of classification rules. In term of results described herein it would be appropriate to conduct further testing focused on other grades of stainless steel or other types of structural section with different fabricating routes. Especially more full section tensile tests would be suitable to perform for obtaining a more precise design method. Extension of conclusions for CHS and RHS would be favourable approach how to use the current investigation. As the study deals with the analytical solution for cold-formed stainless steel structural sections another solution could be also based on finite element modelling in terms of namely residual stresses and plastic strain evaluating. For the key issue of material hardening it is possible to employ advanced models such as multiple surface complex models etc. However such solution usually requires a lot of inputs and demanding calculation that spend too much time particularly in engineering tasks. This chapter presents future experiments that are in progress at CTU.

Experimental planned programme is aimed on obtaining more test results that could contribute to get more precise design methods. Testing programme consists of set of compressive tests. Hot-rolled plate made of austenitic grade 1.4404 should be analysed in compression to evaluate anisotropy effect and differences of material properties between cold-rolled and hot-rolled sheet (see Figure 7.1). There are also planned tests with plastic strain induction according to Chapter 4 for compressive loading. For this purposes a device for a compression test was also designed. A specimen could be clamped into the device to prevent any instability. Side slots serve for attaching strain gauges or extensometer (see Figure 7.2).

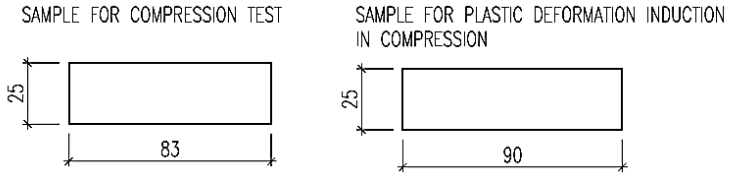

Figure 7.1 *Specimens made of hot rolled sheet for compressive and tensile test*

.

Figure 7.2 *The device for compression test.*

Analytical and experimental results can provide required data to cover complete behaviour including the Bauschinger effect and other phenomena. In terms of cold-working, when parts of section are subjected to tension and compression as well, the resulting state of the cross-section and its behaviour during acting in structures can differ from current assumptions. Knowledge of the full stress-strain behaviour both for tension, compression and bending can result in new complex rules for designing with new limits and borders for particular cold-formed members or at least confirm the currently adopted simplifications.

References

1. **Křivý, V., Urban, V. and Kubzová, M.** Thickness of Corrosion Layers on Typical Surfaces of Weathering Steel Bridges. *Procedia Engineering.* 2016, Vol. 142, pp. 56-62.
2. *Design Manual for Structural Stainless Steel - Commentary.* s.l. : The Steel Construction Institute, Euro Inox. 2003.
3. **Tylek, I. and Kuchta, K.** Mechanical properties of structural stainless steels. *Technical transactions.* 4-B, 2014, pp. 60-80.
4. **Cruise, Rachel B.** *The influence of production route on the response of structural stainless steel members.* PhD thesis. London : Imperial College London, 2007.
5. *Design Manual for Structural Stainless Steel Third Edition.* s.l. : The Steel Construction Institute, Euro Inox. 2006.
6. **Baddoo, N. R.** *A comparison of structural stainless steel standards.* s.l. : The Steel Construction Institute, 2003.
7. **Ganping Shu, Baofeng Zheng and Xiaoming Shen.** Experimental and Theoretical Study on the Behavior of Cold-formed Stainless Steel Stub Columns. *International Journal of Steel Structures.* 13, 2013, pp. 141-153.
8. **Rossi, B., Afshan, S. and Gardner, L.** Strength enhancements in cold-formed structural sections - Part II: Predictive models. *Journal of Constructional Steel Research.* 2013, Vol. 83, pp. 189-196.
9. **Rasmussen, K. J.R., et al.** Numerical modelling of stainless steel plates in compression. *Journal of Constructional Steel Research.* 59, 2003, pp. 1345–1362.
10. **Gozzi, J.** *Plastic Behaviour of Steel: Experimental study and modelling.* Luleå : Luleå University of Technology, 2004.
11. **Jirásek, M. and Bažant, Z., P.** *Inelastic analysis of structures.* s.l. : John Wiley & Sons, 2001.
12. **Granlund, J.** *Structural Steel Plasticity - Experimental study and theoretical modelling.* Doctoral thesis. Luleå : Luleå University of Technology, 1997.
13. **Olsson, A.** *Stainless steel plasticity – material modelling and structural applications.* PhD. thesis. Luleå : Department of Civil and Mining Engineering, Luleå University of Technology, 2001.
14. **Hill, R.** *The mathematical theory of plasticity.* Oxford : Oxford University Press, 1998.
15. **Rossi, B., Degée, H. and Pascon, F.** Enhanced mechanical properties after cold process of fabrication of non-linear metallic profiles. *Thin-Walled Structures.* 47, 2009, pp. 1575-1589.
16. EN 1993-1-4. *Eurocode 3: Design of steel structures - Part 1-4: General rules - Supplementary rules for stainless steels.* Brussels : CEN, 2006.
17. **Holmquist, J. L. and Nadai, A.** A Theoretical and Experimental Approach to the Problem of Collapse of Deep-Well Casing. *Drilling and Production Practice.* 1939, pp. 392-420.
18. **Ramberg, W. and Osgood, W.R.** *Description of stress-strain curves by three parametrs.* s.l. : National Advisory Comittee for Aeronautics, 1943. Technical Node No. 902.

19. **Hill, H.N.** *Determination of stress-strain relations from the offset yield strength values.* Washington : National Advisory Committee for Aeronautics, Technical Note No. 927, 1944.
20. **Mirambell, E. and Real, E.** On the calculation of deflections in structural stainless steel beams. *Journal of Constructional Steel Research.* 54, 2000, pp. 109–133.
21. **Gardner, L. a Nethercot, D.** Numerical modelling of stainless steel structural components – A consistent approach. *Journal of Structural Engineering.* Vol. 130, 2004, stránky 1586–1601.
22. **MacDonald, M, Rhodes, J and GT., Taylor.** Mechanical properties of stainless steel lipped channels. *Proceedings, 15th International Specialty Conference on Coldformed Steel Structures. University of Missouri-Rolla.* 2000, pp. 673–686.
23. **Rasmussen, K. J. R.** Full-range stress-strain curves for stainless steel alloys. *Journal of Constructional Steel Research.* 59, 2003, pp. 47-61.
24. **Korvink, S. A., Van den Berg, G. J. and Van der Merwe, P.** Web crippling of stainless steel cold-formed beams. *Journal of Constructional Steel Research.* 34, 1995, pp. 225-248.
25. **Quach, W.M.** *Residual stresses in cold-formed steel sections and their effect on column behaviour.* PhD Thesis. Hong Kong : The Hong Kong Polytechnic University, 2005.
26. **Abdella, K.** Inversion of a full-range stress–strain relation for stainless steel alloys. *International Journal of Non-Linear Mechanics.* Vol. 41, 2006, stránky 456-463.
27. **Arrayago, I., Real, E. and Mirambell, E.** *Constitutive equations for stainless steels: experimental tests and new proposal.* s.l. : Proceedings of the Fifth International Conference on Structural Engineering, Mechanics & Computation, 2013. pp. 1435-1440.
28. **Hradil, P., et al.** Generalized multistage mechanical model for non linear metallic materials. *Thin-Walled Structures.* 63, 2013, pp. 63-69.
29. **Huang, Y. and Young, B.** Material properties of cold-formed lean duplex stainless steel sections. *Thin-Walled Structures.* 54, 2012, pp. 72-81.
30. **Xing-Qiang Wang, Zhong Tao, Tian-Yi Song and Lin-Hai Han.** Stress–strain model of austenitic stainless steel after exposure to elevated temperatures. *Journal of Constructional Steel Research.* 99, 2014, pp. 129-139.
31. **Píchal, R. and Macháček, J.** Buckling and Post-buckling of Prestressed Stainless Steel Stayed Columns. *Procedia Engineering.* 2017, Vol. 172, pp. 875-882.
32. **Karren, K. W.** Corner Properties of cold-formed steel shapes. *ASCE Proceedings.* 1967, pp. 401-432 .
33. **Belica, M.** *Vývoj tenkostenných profilov tvarovaných za studena.* Výzkumná zpráva E-7-22-2/1. Košice : VSŽ Košice, 1969.
34. **Cruise, Rachel B. and Gardner, L.** Strength enhancements induced during cold forming of stainless steel sections. *Journal of Constructional Steel Research 64.* 2008, pp. 1310–1316.
35. **Karren, K. W. a G., Winter.** Effect of cold-forming on light-gage steel members. *ASCE Proceedings.* Vol. 93, 1967.
36. EN 1993-1-3. *Eurocode 3: Design of steel structures - Part 1-3: General rules - Supplementary rules for cold-formed members and sheeting.* Brussels : CEN, 2008.
37. **Abdel-Rahman, N. and Sivakumaran, K.S.** Material properties models for analysis of cold-formed steel members. *Journal of Structural Engineering.* 1997, Vol. 123, pp. 1135–1143.
38. **Gardner, L. and Nethercot, D.** Experiments on stainless steel hollow sections – Part 1: Material and cross-sectional behaviour. *Journal of Constructional Steel Research.* 61, 2004, pp. 1291–1318.

39. **Ashraf, M., Gardner, L. and Nethercot, D. A.** Numerical modelling of stainless steel open sections. *Proceedings of the Fourth European Conference on Steel and Composite Structures – Eurosteel, Maastricht, Netherlands.* 2005, pp. 197-204.
40. **Van den Berg, GJ and Van der Merwe, P.** Prediction of corner mechanical properties for stainless steels due to cold forming. *Proceedings of the eleventh international specialty conference on cold-formed steel structures.* 1992, pp. 571–586.
41. **Ashraf, M., Gardner, L. and Nethercot, D. A.** Strength enhancement of the corner regions of stainless steel cross-sections. *Journal of Constructional Steel Research.* 61, 2005, pp. 37–52.
42. **Gardner, L.** *A new approach to structural stainless steel design.* PhD thesis. London : Imperial College London, 2002.
43. **Jandera, M.** *Residual stresses in stainless steel box sections.* Ph.D. thesis. Prague : Faculty of Civil Engineering,Czech Technical University in Prague, 2009.
44. **Rossi, B. and Jaspart, J.P.** Enhanced proof strength after cold process of fabrication of non-linear metallic profiles—Comparison of two predictive models for hollow sections. *Tubular Structures.* XIII, 2010, pp. 397–402.
45. **Rossi, B., Boman, R. and Degée, H.** Effects of the roll forming process on the mechanical properties of thin-walled sections made from non linear metallic materials. *Proceedings Thin-Walled Structures conference.* Vol. 2, 2011, pp. 633-640.
46. **Abdella, K.** An explicit stress formulation for stainless steel applicable in tension and. *Journal of Constructional Steel Research.* Vol. 63, 2007, pp. 326-331.
47. **Afshan, S., Rossi, B. and Gardner, L.** Strength enhancements in cold-formed structural sections - Part I: Material testing. *Journal of Constructional Steel Research.* 2013, Vol. 83, pp. 177-188.
48. **Moen, C.D., Igusa, T. and Schafer, B.W.** Prediction of residual stresses and strains in cold-formed steel members. *Thin-walled structures.* 46, 2008, pp. 1274-1289.
49. **Arrayago, I., Real, E. and Gardner, L.** Description of stress–strain curves for stainless steel alloys. *Materials and Design.* 2015, Vol. 87, pp. 540–552.
50. NA to BS EN 1993-1-4 UK National Annex to Eurocode 3. *Design of steel structures. General rules. Supplementary rules for stainless steels.* 2006.
51. **Hlaváček, V.** *Navrhování tenkostěnných ocelových konstrukcí – Komentář a příklady k ČSN 73 1402.* Praha : Vydavatelství Úřadu pro normalizaci a měření, 1976. p. 216 (in Czech).
52. **Weng, C., C. and White, R., N.** Ressidual stresses in cold-bent thick steel plates. *Journal of structural engineering.* 1990, Vol. 116, pp. 24-39.
53. **Rossi, B., Habraken, A-M. and Pascon, F.** *On The Evaluation Of The Through Thickness Residual Stresses Distribution Of Cold Formed Profiles.* Zaragoza : AIP Conference Proceedings, 2007. pp. 570-577. Vol. 907.
54. EN 10088-1. *Stainless steels - Part 1: List of stainless steels.* Brussels : CEN, 2005.
55. EN 10088-2. *Stainless steels - Part 2: Technical delivery conditions for sheet/plate and strip of corrosion resisting steels for general purpose.* Brussels : CEN, 2005.
56. **Gardner, L., Taljab, A. and Baddoo, N. R.** Structural design of high-strength austenitic stainless steel. *Thin-Walled Structures.* 44, 2006, pp. 517–528.
57. EN ISO 6892-1. *Metallic materials - Tensile testing - Part 1: Method of test at room temperature.* Brussels : CEN, 2009.
58. SEP 1235. *Determination of the modulus of elasticity on steels by tensile testing at room temperature.* Düsseldorf : Verlag Stahleisen GmbH, 2012.
59. **Howlader, M.,K., Mařík, J. and Jandera, M.** Cold-Forming Effect on Stainless Steel Sections. *International Journal of Steel Structures.* 16, 2016, pp. 317-332.
60. **Yu, T., X. and Zhang, L., C.** *Plastic Bending: Theory and applications.* New Jersey : World Scientific Publishing Co., 1996.

61. **Bock, M., Gardner, L. and Real, E.** Material and local buckling response of ferritic stainless steel sections. *Thin-Walled Structures 89.* 2015, pp. 131-141.
62. **Hradil, P., Talja, A. and VTT Technical Research Centre of Finland, Espoo, Finland.** Investigating the role of gradual yielding in stainless steel columns and beams by virtual testing. *The Fifth International Conference on Structural Engineering, Mechanics and Computation.* 2013.
63. **Zhang, L., C. and Yu, T., X.** A refined theory of elastic-plastic pure bending of wide plates. *Journal of Peking University.* 24, 1988, pp. 65-72.
64. **Coetzee, J., S., Van den Berg, G., J. and Van der Merwe, P.** The effect of work hardening and residual stresses due to cold-work of forming on the strength of cold-formed stainless steel lipped channel section. *Proceedings of the tenth international specialty conference on cold-formed steel structures.* 1990, pp. 143-162.
65. **Lecce, M. and Rasmussen, K., J., R.** Distortional buckling of cold-formed stainless steel sections: finite-element modeling and design. *Journal of Structural Engineering.* 132(4), 2006, pp. 505-514.
66. **Rasmussen, K., J., R. and Hancock, G., J.** Design of cold-formed stainless steel tubular members. I: Columns. *Journal of the Structural Engineering.* 119(8), 1993, pp. 2349-2367.
67. **Gardner, L. and Talja, A.** *WP2: Structural hollow sections. ECSC project: structural design of cold-worked austenitic stainless steel.* The Steel Construction Institute : 2003.

Appendix A

Maple model for coiling

units [N, mm, MPa]

Material and geometrical characteristics

---

material

```
> E[0] :=195.4e3:
nu := 0.3:
sigma[y0] := 0.001: ##sigma[y0]>0.0001##
sigma[0.2] :=205;
sigma[1.0] := .542*sigma[0.2]/n[0]+1.072*sigma[0.2]; formula - Quach
found by analysing tension coupon test data
sigma[ult]:=520;
epsilon[ult] := min(1-sigma[.2]/sigma[ult],0.6);
n[0]:=7.5;
E[0.2] := E[0]/(1+0.002*n[0]*E[0]/sigma[0.2]); formula-Rasmussen
n[0.2,1.0] := 12.225*E[.2]*sigma[1.0]/(E[0]*sigma[0.2])+1.037; formula
- Quach found by analysing tension coupon test data
e[0.2]:=sigma[0.2]/E[0]; formula-Rasmussen
B[0]:=0.018+e[0.2]*((E[0]/E[0.2])-1); formula-Quach
A[0]:=B[0]/(0.008+e[0.2]*(sigma[1.0]/sigma[0.2]-1)*(1-E[0]/E[0.2]));
formula-Quach
sigma[2.0]:=(1+(sigma[1.0]/sigma[0.2]-
1)*(A[0]^(1/n[0.2,1.0])))/(1+e[0.2]*(E[0]/E[0.2]-
1)*(sigma[1.0]/sigma[0.2]-
1)*A[0]^(1/n[0.2,1.0])/(n[0.2,1.0]*B[0]))*sigma[0.2]; formula-Quach
epsilon[2.0]:= (sigma[2.0]/E[0])+0.02;
b[0]:=(sigma[ult]*(1+epsilon[ult])-
sigma[2.0]*(1+epsilon[2.0]))/(epsilon[ult]-epsilon[2.0]); formula-
Quach
a[0]:=sigma[2.0]*(1+epsilon[2.0])-b[0]*epsilon[2.0]; formula-Quach
t := 2;
```

coiling curvature

```
> Kappa[c] := 1/(250);
```

For Coiling

```
>
> i:=-1:
for y from (t/2) by (-t/30) while y > 0 do

i:=i+1:
axy[i]:=y:
####coiling
epsilon[z,cy] := sigma[y0]*(1-nu^2)/(E[0]*sqrt(1-nu+nu^2)):
epsilon[z,c] := Kappa[c]*y:
if epsilon[z,cy] < epsilon[z,c] then
e := 0:
sigma[c] := sigma[y0]:
omega[c] := nu:
```

```
for s from sigma[y0] by 0.5 to sigma[ult] while abs(e) <
abs(epsilon[z,c]-epsilon[z,cy]) do
ds := s - sigma[c]:
if s <= sigma[0.2] then
eps:= X/(E[0])+0.002*(X/(sigma[0.2]))^n[0]:
else if s <= sigma[2.0] then
eps:=(X-sigma[0.2])/(E[0.2])+(0.008+(sigma[1.0]-sigma[0.2])*((1/E[0])-
(1/E[0.2])))*((X-sigma[0.2])/(sigma[1.0]-
sigma[0.2]))^n[0.2,1.0]+(sigma[0.2])/(E[0])+0.002:
else
eps:=(X-a[0])/(b[0]-X):
end if:
end if:
dH:=((diff(eps,X))-(1/E[0]))^(-1):
Omega[c] := (4*nu*(subs(X=s,dH))*(1-omega[c]+omega[c]^2)-E[0]*(2-
omega[c])*(2*omega[c]-1))/(E[0]*(2*omega[c]-1)^2+4*(subs(X=s,dH))*(1-
omega[c]+omega[c]^2)):
dom[c] := (2*(1-omega[c]+omega[c]^2)*(Omega[c]-omega[c]))/(s*((2-
omega[c])+Omega[c]*(2*omega[c]-1)))*ds:
omega[c] := omega[c] + dom[c]:
de :=  subs(X=omega[c],(((1-2*X)^2-2*nu*(1-2*X)*(2-X)+(2-
X)^2)*s)/(2*E[0]*(1-2*X)*(1-X+X^2)^(3/2)))*dom[c] + subs(X=s,((1-
omega[c]^2)*(1-2*nu))/(E[0]*(1-2*omega[c])*sqrt(1-
omega[c]+omega[c]^2)))*ds;
e:= de + e:
sigma[c] := s:
end do:
sigma[z,c,i] := sigma[c]/sqrt(1-omega[c]+omega[c]^2):
sigma[x,c,i] := omega[c]*sigma[c]/sqrt(1-omega[c]+omega[c]^2):
else
sigma[z,c,i] := E[0]*epsilon[z,c]/(1-nu^2):
sigma[x,c,i] := nu*E[0]*epsilon[z,c]/(1-nu^2):
omega[c] := nu:
end if:
epsilon[c,pl,i]:=e-s/E[0]:
end do:
```

using simmetry for whole thickness data

```
> axy[15]:=0:
sigma[c,15]:=sigma[y0]:
sigma[z,c,15]:=sigma[y0]*(1-nu^2)/(E[0]):
sigma[x,c,15]:=sigma[y0]*(1-nu^2)/(E[0]*nu):
epsilon[c,pl,15]:=0:

> for i from 0 by 1 to 14 do
axy[30-i]:= -axy[i]:
sigma[c,30-i]:= sigma[c,i]:
sigma[z,c,30-i]:=-sigma[z,c,i]:
sigma[x,c,30-i]:=-sigma[x,c,i]:
epsilon[c,pl,30-i]:= epsilon[c,pl,i]:
end do:
```

Appendix B

Maple model for coiling and uncoiling

units [N, mm, MPa]

Material and geometrical characteristics

---

material

```
> E[0] :=195.4e3:
nu := 0.3:
sigma[y0] := 0.001: ##sigma[y0]>0.0001##
sigma[0.2] :=205;
sigma[1.0] := .542*sigma[0.2]/n[0]+1.072*sigma[0.2]; formula - Quach
found by analysing tension coupon test data
sigma[ult]:=520;
epsilon[ult] := min(1-sigma[.2]/sigma[ult],0.6);
n[0]:=7.5;
E[0.2] := E[0]/(1+0.002*n[0]*E[0]/sigma[0.2]); formula-Rasmussen
n[0.2,1.0] := 12.225*E[.2]*sigma[1.0]/(E[0]*sigma[0.2])+1.037; formula
- Quach found by analysing tension coupon test data
e[0.2]:=sigma[0.2]/E[0]; formula-Rasmussen
B[0]:=0.018+e[0.2]*((E[0]/E[0.2])-1); formula-Quach
A[0]:=B[0]/(0.008+e[0.2]*(sigma[1.0]/sigma[0.2]-1)*(1-E[0]/E[0.2]));
formula-Quach
sigma[2.0]:=(1+(sigma[1.0]/sigma[0.2]-
1)*(A[0]^(1/n[0.2,1.0])))/(1+e[0.2]*(E[0]/E[0.2]-
1)*(sigma[1.0]/sigma[0.2]-
1)*A[0]^(1/n[0.2,1.0])/(n[0.2,1.0]*B[0]))*sigma[0.2]; formula-Quach
epsilon[2.0]:= (sigma[2.0]/E[0])+0.02;
b[0]:=(sigma[ult]*(1+epsilon[ult])-
sigma[2.0]*(1+epsilon[2.0]))/(epsilon[ult]-epsilon[2.0]);formula-Quach
a[0]:=sigma[2.0]*(1+epsilon[2.0])-b[0]*epsilon[2.0]; formula-Quach
t := 2;
```

coiling curvature

```
> Kappa[c] := 1/(250);
```

F O R M I N G P R O C E S S

---

loop for coiling and uncoiling (small strain condition)

```
> i:=-1:
for y from (t/2) by (-t/30) while y > 0 do
i:=i+1:
axy[i]:=y:
####coiling
epsilon[z,cy] := sigma[y0]*(1-nu^2)/(E[0]*sqrt(1-nu+nu^2)):
epsilon[z,c] := Kappa[c]*y:
if epsilon[z,cy] < epsilon[z,c] then
e := 0:
sigma[c] := sigma[y0]:
```

```
omega[c] := nu:
for s from sigma[y0] by 0.5 to sigma[ult] while abs(e) <
abs(epsilon[z,c]-epsilon[z,cy]) do
ds := s - sigma[c]:
if s <= sigma[0.2] then
eps:= X/(E[0])+0.002*(X/(sigma[0.2]))^n[0]:
else if s <= sigma[2.0] then
eps:=(X-sigma[0.2])/(E[0.2])+(0.008+(sigma[1.0]-sigma[0.2])*((1/E[0])-
(1/E[0.2])))*((X-sigma[0.2])/(sigma[1.0]-
sigma[0.2]))^n[0.2,1.0]+(sigma[0.2])/(E[0])+0.002:
else
eps:=(X-a[0])/(b[0]-X):
end if:
end if:
dH:=((diff(eps,X))-(1/E[0]))^(-1):
Omega[c] := (4*nu*(subs(X=s,dH))*(1-omega[c]+omega[c]^2)-E[0]*(2-
omega[c])*(2*omega[c]-1))/(E[0]*(2*omega[c]-1)^2+4*(subs(X=s,dH))*(1-
omega[c]+omega[c]^2)):
dom[c] := (2*(1-omega[c]+omega[c]^2)*(Omega[c]-omega[c]))/(s*((2-
omega[c])+Omega[c]*(2*omega[c]-1)))*ds:
omega[c] := omega[c] + dom[c]:
de :=  subs(X=omega[c],(((1-2*X)^2-2*nu*(1-2*X)*(2-X)+(2-
X)^2)*s)/(2*E[0]*(1-2*X)*(1-X+X^2)^(3/2)))*dom[c] + subs(X=s,((1-
omega[c]^2)*(1-2*nu))/(E[0]*(1-2*omega[c])*sqrt(1-
omega[c]+omega[c]^2)))*ds;
e:= de + e:
sigma[c] := s:
end do:
sigma[z,c,i] := sigma[c]/sqrt(1-omega[c]+omega[c]^2):
sigma[x,c,i] := omega[c]*sigma[c]/sqrt(1-omega[c]+omega[c]^2):
else
sigma[z,c,i] := E[0]*epsilon[z,c]/(1-nu^2):
sigma[x,c,i] := nu*E[0]*epsilon[z,c]/(1-nu^2):
omega[c] := nu:
end if:
epsilon[c,pl,i]:=e-s/E[0]:
#####uncoiling including flatening
Kappa[u] := -Kappa[c]:
Kappa[uy]:=-(sigma[c]*(1-nu^2)*(2-nu+(2*nu-1)*omega[c]))/(E[0]*y*(1-
nu+nu^2)*sqrt((1-omega[c]+omega[c]^2))):
epsilon[z,uy] := (Kappa[c]+Kappa[uy])*y:
epsilon[z,r] := 0:
if abs(Kappa[uy]) < abs(Kappa[u]) then
omega[uy] := ((1-nu^2)*omega[c]-nu*(2-nu))/((1-2*nu)*omega[c]-(1-
nu^2)):
sigma[u]:= sigma[c]:
omega[u]:= omega[uy]:
e:=0:
for s from sigma[u] by 0.5 to sigma[ult] while abs(e) <
abs(epsilon[z,uy]) do
ds := s - sigma[u]:
if s <= sigma[0.2] then
eps:= X/(E[0])+0.002*(X/(sigma[0.2]))^n[0]:
else if s <= sigma[2.0] then
eps:=(X-sigma[0.2])/(E[0.2])+(0.008+(sigma[1.0]-sigma[0.2])*((1/E[0])-
(1/E[0.2])))*((X-sigma[0.2])/(sigma[1.0]-
sigma[0.2]))^n[0.2,1.0]+(sigma[0.2])/(E[0])+0.002:
else
eps:=(X-a[0])/(b[0]-X):
end if:
end if:
dH:=((diff(eps,X))-(1/E[0]))^(-1):
```

```
Omega[u] := (4*nu*(subs(X=s,dH))*(1-omega[u]+omega[u]^2)-E[0]*(2-
omega[u])*(2*omega[u]-1))/(E[0]*(2*omega[u]-1)^2+4*(subs(X=s,dH))*(1-
omega[u]+omega[u]^2)):
dom[u] := (2*(1-omega[u]+omega[u]^2)*(Omega[u]-omega[u]))/(s*((2-
omega[u])+Omega[u]*(2*omega[u]-1)))*ds:
omega[u] := omega[u] + dom[u]:
de :=  subs(X=omega[u],(((1-2*X)^2-2*nu*(1-2*X)*(2-X)+(2-
X)^2)*s)/(2*E[0]*(1-2*X)*(1-X+X^2)^(3/2)))*dom[u] + subs(X=s,((1-
omega[u]^2)*(1-2*nu))/(E[0]*(1-2*omega[u])*sqrt(1-
omega[u]+omega[u]^2)))*ds;
e:= de + e:
sigma[u] := s:
end do:
sigma[z,r,i] := - sigma[u]/sqrt(1-omega[u]+omega[u]^2):
sigma[x,r,i] := - omega[u]*sigma[u]/sqrt(1-omega[u]+omega[u]^2):
epsilon[i]:=e:
epsilon[u,pl,i]:=e-(s-sigma[c])/E[0]:
epsilon[r,pl,i]:=epsilon[u,pl,i]+epsilon[c,pl,i]:
else
sigma[z,u,i] := E[0]*Kappa[u]*y/(1-nu^2):
sigma[x,u,i] := nu*E[0]*Kappa[u]*y/(1-nu^2):
sigma[z,r,i] := sigma[z,c,i]+sigma[z,u,i]:
sigma[x,r,i] := sigma[x,c,i]+sigma[x,u,i]:
omega[u,i]:= sigma[x,r,i]/sigma[z,r,i]:
sigma[u,i]:= sigma[c]:
s:=sigma[c]:
epsilon[i]:=Kappa[u]*y:
epsilon[u,pl,i]:=0:
epsilon[r,pl,i]:=epsilon[u,pl,i]+epsilon[c,pl,i]:
end if:
end do:
```

using simmetry for whole thickness data

```
> axy[15]:=0:
sigma[u,15]:=sigma[y0]:
sigma[z,r,15]:=sigma[y0]*(1-nu^2)/(E[0]):
sigma[x,r,15]:=sigma[y0]*(1-nu^2)/(E[0]*nu):
epsilon[r,pl,15]:=0:

> for i from 0 by 1 to 14 do
axy[30-i]:= -axy[i]:
sigma[u,30-i]:= sigma[u,i]:
sigma[z,r,30-i]:=-sigma[z,r,i]:
sigma[x,r,30-i]:=-sigma[x,r,i]:
epsilon[r,pl,30-i]:= epsilon[r,pl,i]:
end do:
```

Appendix C

Maple model for cold-bending

C.1 Model in nominal values

units [N, mm, MPa]

```
---------------------------------------
Material and geometrical characteristics
---------------------------------------
material
> E[0] :=195.4e3:
nu := 0.3:
sigma[y0] := 0.001: ##sigma[y0]>0.0001##
sigma[0.2] :=205;
sigma[1.0] := .542*sigma[0.2]/n[0]+1.072*sigma[0.2]; formula - Quach
found by analysing tension coupon test data
sigma[ult]:=520;
epsilon[ult] := min(1-sigma[.2]/sigma[ult],0.6);
n[0]:=7.5;
E[0.2] := E[0]/(1+0.002*n[0]*E[0]/sigma[0.2]); formula-Rasmussen
n[0.2,1.0] := 12.225*E[.2]*sigma[1.0]/(E[0]*sigma[0.2])+1.037; formula
- Quach found by analysing tension coupon test data
e[0.2]:=sigma[0.2]/E[0]; formula-Rasmussen
B[0]:=0.018+e[0.2]*((E[0]/E[0.2])-1); formula-Quach
A[0]:=B[0]/(0.008+e[0.2]*(sigma[1.0]/sigma[0.2]-1)*(1-E[0]/E[0.2]));
formula-Quach
sigma[2.0]:=(1+(sigma[1.0]/sigma[0.2]-
1)*(A[0]^(1/n[0.2,1.0])))/(1+e[0.2]*(E[0]/E[0.2]-
1)*(sigma[1.0]/sigma[0.2]-
1)*A[0]^(1/n[0.2,1.0])/(n[0.2,1.0]*B[0]))*sigma[0.2]; formula-Quach
epsilon[2.0]:= (sigma[2.0]/E[0])+0.02;
b[0]:=(sigma[ult]*(1+epsilon[ult])-
sigma[2.0]*(1+epsilon[2.0]))/(epsilon[ult]-epsilon[2.0]); formula-
Quach
a[0]:=sigma[2.0]*(1+epsilon[2.0])-b[0]*epsilon[2.0]; formula-Quach
t := 2;


>
coiling curvature
> Kappa[c] := 1/(450);
circling or bending radius
ri:=4*t:
radius :=ri+t/2;
Kappa[cs]:= 1/radius;


---------------------------------
F O R M I N G   P R O C E S S
---------------------------------
loop for coiling and uncoiling  (small strain condition)
> i:=-1:
for y from (t/2) by (-t/30) while y > 0 do
i:=i+1:
```

```
axy[i]:=y:

####coiling
epsilon[z,cy] := sigma[y0]*(1-nu^2)/(E[0]*sqrt(1-nu+nu^2)):
epsilon[z,c] := Kappa[c]*y:
if epsilon[z,cy] < epsilon[z,c] then
e := 0:
sigma[c] := sigma[y0]:
omega[c] := nu:
for s from sigma[y0] by 0.5 to sigma[ult] while abs(e) <
abs(epsilon[z,c]-epsilon[z,cy]) do
ds := s - sigma[c]:
if s <= sigma[0.2] then
eps:= X/(E[0])+0.002*(X/(sigma[0.2]))^n[0]:
else if s <= sigma[2.0] then
eps:=(X-sigma[0.2])/(E[0.2])+(0.008+(sigma[1.0]-sigma[0.2])*((1/E[0])-
(1/E[0.2])))*((X-sigma[0.2])/(sigma[1.0]-
sigma[0.2]))^n[0.2,1.0]+(sigma[0.2])/(E[0])+0.002:
else
eps:=(X-a[0])/(b[0]-X):
end if:
end if:
dH:=((diff(eps,X))-(1/E[0]))^(-1):
Omega[c] := (4*nu*(subs(X=s,dH))*(1-omega[c]+omega[c]^2)-E[0]*(2-
omega[c])*(2*omega[c]-1))/(E[0]*(2*omega[c]-1)^2+4*(subs(X=s,dH))*(1-
omega[c]+omega[c]^2)):
dom[c] := (2*(1-omega[c]+omega[c]^2)*(Omega[c]-omega[c]))/(s*((2-
omega[c])+Omega[c]*(2*omega[c]-1)))*ds:
omega[c] := omega[c] + dom[c]:
de :=  subs(X=omega[c],(((1-2*X)^2-2*nu*(1-2*X)*(2-X)+(2-
X)^2)*s)/(2*E[0]*(1-2*X)*(1-X+X^2)^(3/2)))*dom[c] + subs(X=s,((1-
omega[c]^2)*(1-2*nu))/(E[0]*(1-2*omega[c])*sqrt(1-
omega[c]+omega[c]^2)))*ds;
e:= de + e:
sigma[c] := s:
end do:
sigma[z,c] := sigma[c]/sqrt(1-omega[c]+omega[c]^2):
sigma[x,c] := omega[c]*sigma[c]/sqrt(1-omega[c]+omega[c]^2):
else
sigma[z,c] := E[0]*epsilon[z,c]/(1-nu^2):
sigma[x,c] := nu*E[0]*epsilon[z,c]/(1-nu^2):
omega[c] := nu:
end if:
epsilon[c,pl,i]:=e-s/E[0]:
#####uncoiling including flatening
Kappa[u] := -Kappa[c]:
Kappa[uy]:=-(sigma[c]*(1-nu^2)*(2-nu+(2*nu-1)*omega[c]))/(E[0]*y*(1-
nu+nu^2)*sqrt((1-omega[c]+omega[c]^2))):
epsilon[z,uy] := (Kappa[c]+Kappa[uy])*y:
epsilon[z,r] := 0:
if abs(Kappa[uy]) < abs(Kappa[u]) then
omega[uy] := ((1-nu^2)*omega[c]-nu*(2-nu))/((1-2*nu)*omega[c]-(1-
nu^2)):
sigma[u]:= sigma[c]:
omega[u]:= omega[uy]:
e:=0:
for s from sigma[u] by 0.5 to sigma[ult] while abs(e) <
abs(epsilon[z,uy] + epsilon[z,r] ) do
ds := s - sigma[u]:
if s <= sigma[0.2] then
eps:= X/(E[0])+0.002*(X/(sigma[0.2]))^n[0]:
else if s <= sigma[2.0] then
```

```
eps:=(X-sigma[0.2])/(E[0.2])+(0.008+(sigma[1.0]-sigma[0.2])*((1/E[0])-
(1/E[0.2])))*((X-sigma[0.2])/(sigma[1.0]-
sigma[0.2]))^n[0.2,1.0]+(sigma[0.2])/(E[0])+0.002:
else
eps:=(X-a[0])/(b[0]-X):
end if:
end if:
dH:=((diff(eps,X))-(1/E[0]))^(-1):
Omega[u] := (4*nu*(subs(X=s,dH))*(1-omega[u]+omega[u]^2)-E[0]*(2-
omega[u])*(2*omega[u]-1))/(E[0]*(2*omega[u]-1)^2+4*(subs(X=s,dH))*(1-
omega[u]+omega[u]^2)):
dom[u] := (2*(1-omega[u]+omega[u]^2)*(Omega[u]-omega[u]))/(s*((2-
omega[u])+Omega[u]*(2*omega[u]-1)))*ds:
omega[u] := omega[u] + dom[u]:
de:=  subs(X=omega[u],(((1-2*X)^2-2*nu*(1-2*X)*(2-X)+(2-
X)^2)*s)/(2*E[0]*(1-2*X)*(1-X+X^2)^(3/2)))*dom[u] + subs(X=s,((1-
omega[u]^2)*(1-2*nu))/(E[0]*(1-2*omega[u])*sqrt(1-
omega[u]+omega[u]^2)))*ds;
e:= de + e:
sigma[u]:=s:
end do:
sigma[u,i]:= sigma[u]:
sigma[z,r,i] := - sigma[u]/sqrt(1-omega[u]+omega[u]^2):
sigma[x,r,i] := - omega[u]*sigma[u]/sqrt(1-omega[u]+omega[u]^2):
epsilon[i]:=e:
epsilon[u,pl,i]:=e-(s-sigma[c])/E[0]:
epsilon[r,pl,i]:=epsilon[u,pl,i]+epsilon[c,pl,i]:
else
sigma[z,u] := E[0]*Kappa[u]*y/(1-nu^2):
sigma[x,u] := nu*E[0]*Kappa[u]*y/(1-nu^2):
sigma[z,r,i] := sigma[z,c]+sigma[z,u]:
sigma[x,r,i] := sigma[x,c]+sigma[x,u]:
omega[u,i]:= sigma[x,r,i]/sigma[z,r,i]:
sigma[u,i]:= sigma[c]:
s:=sigma[c]:
epsilon[i]:=Kappa[u]*y:
epsilon[u,pl,i]:=0:
epsilon[r,pl,i]:=epsilon[u,pl,i]+epsilon[c,pl,i]:
end if:
end do:
```

using simmetry for whole thickness data

```
> axy[15]:=0:
sigma[us,15]:=sigma[y0]:
sigma[z,r,15]:=sigma[y0]*(1-nu^2)/(E[0]):
sigma[x,r,15]:=sigma[y0]*(1-nu^2)/(E[0]*nu):
epsilon[r,pl,15]:=0:
sigma[u,15]:=sigma[y0]:
> for i from 0 by 1 to 29 do
axy[30-i]:= -axy[i]:
sigma[u,30-i]:= sigma[u,i]:
sigma[z,r,30-i]:= -sigma[z,r,i]:
sigma[x,r,30-i]:= -sigma[x,r,i]:
epsilon[r,pl,30-i]:= epsilon[r,pl,i]:
end do:
```

bending to the corner radius (x-axis bending)

```
> q[x]:=1:
for shift from 0.001 by 0.001 while q[x] > 0.25 do
for i from 0 by 1 to 30 do
y:= axy[i]:
epsilon[x,cs,i]:= ln(1+(shift-y)/(1/Kappa[cs]-shift)):
epsilon[x,csy,i]:= sigma[u,i]*(1-nu^2)/(E[0]*sqrt(1-nu+nu^2)):
```

```
if abs(epsilon[x,csy,i])<abs(epsilon[x,cs,i])then
e:= 0:
sigma[z,cs,i]:= sigma[z,r,i] + nu*E[0]*epsilon[x,csy,i]/(1-nu^2):
sigma[x,cs,i]:= sigma[x,r,i] + E[0]*epsilon[x,csy,i]/(1-nu^2):
omega[cs] := sigma[z,cs,i]/sigma[x,cs,i]:
sigma[cs]:=sigma[u,i]:
for s from sigma[u,i] by 1 to sigma[ult] while abs(e)
<(abs(epsilon[x,cs,i]-epsilon[x,csy,i])) do
ds:= s-sigma[cs]:
if s <= sigma[0.2] then
eps:= X/(E[0])+0.002*(X/(sigma[0.2]))^n[0]:
else if s <= sigma[2.0] then
eps:=(X-sigma[0.2])/(E[0.2])+(0.008+(sigma[1.0]-sigma[0.2])*((1/E[0])-
(1/E[0.2])))*((X-sigma[0.2])/(sigma[1.0]-
sigma[0.2]))^n[0.2,1.0]+(sigma[0.2])/(E[0])+0.002:
else
eps:=(X-a[0])/(b[0]+X):
end if:
end if:
dH:=((diff(eps,X))-(1/E[0]))^(-1):
Omega[cs]:= (4*nu*(subs(X=s,dH))*(1-omega[cs]+omega[cs]^2)-E[0]*(2-
omega[cs])*(2*omega[cs]-1))/(E[0]*(2*omega[cs]-
1)^2+4*(subs(X=s,dH))*(1-omega[cs]+omega[cs]^2)):
dom[cs]:=((2*(1-omega[cs]+omega[cs]^2)*(Omega[cs]-omega[cs]))/(s*((2-
omega[cs])+Omega[cs]*(2*omega[cs]-1))))*ds:
omega[cs]:= omega[cs] + dom[cs]:
de:= subs(X=omega[cs],(((1-2*X)^2-2*nu*(1-2*X)*(2-X)+(2-
X)^2)*s)/(2*E[0]*(1-2*X)*(1-X+X^2)^(3/2)))*dom[cs] + subs(X=s,((1-
omega[cs]^2)*(1-2*nu))/(E[0]*(1-2*omega[cs])*sqrt(1-
omega[cs]+omega[cs]^2)))*ds:
e:= de + e:
sigma[cs]:=s:
end do:
if y>= shift then
sigma[z,cs,i]:= -omega[cs]*sigma[cs]/sqrt(1-omega[cs]+omega[cs]^2):
sigma[x,cs,i]:= -sigma[cs]/sqrt(1-omega[cs]+omega[cs]^2):
else
sigma[z,cs,i]:= omega[cs]*sigma[cs]/sqrt(1-omega[cs]+omega[cs]^2):
sigma[x,cs,i]:= sigma[cs]/sqrt(1-omega[cs]+omega[cs]^2):
end if:
sigma[cs,i]:= s:
omega[cs,i]:=omega[cs]:
epsilon[cs,pl,i]:=e-s/E[0]:
else
sigma[z,cs,i]:= sigma[z,r,i] + nu*E[0]*epsilon[x,cs,i]/(1-nu^2):
sigma[x,cs,i]:= sigma[x,r,i] + E[0]*epsilon[x,cs,i]/(1-nu^2):
sigma[cs,i]:= sigma[u,i]:
omega[cs,i]:= sigma[z,cs,i]/sigma[x,cs,i]:
epsilon[cs,pl,i] := 0:
end if:
end do:
#### membrane residual stress
q[x]:= 0:
for i from 0 by 1 to 29 do
q[x]:= q[x]-(sigma[x,cs,i+1]+sigma[x,cs,i] )/2*(axy[i]-axy[i+1]):
end do:
q[x]:=q[x]/t;
end do:
q[x];
shift;
```

C.2 Model in true values

units [N, mm, MPa]

Material and geometrical characteristics
---
material

```
> E[0] :=195.4e3:
nu := 0.3:
sigma[y0] := 0.001: ##sigma[y0]>0.0001##
sigma[0.2] :=205;
sigma[1.0] := .542*sigma[0.2]/n[0]+1.072*sigma[0.2]; formula - Quach
found by analysing tension coupon test data
sigma[ult]:=520;
epsilon[ult] := min(1-sigma[.2]/sigma[ult],0.6);
n[0]:=7.5;
E[0.2] := E[0]/(1+0.002*n[0]*E[0]/sigma[0.2]); formula-Rasmussen
n[0.2,1.0] := 12.225*E[.2]*sigma[1.0]/(E[0]*sigma[0.2])+1.037; formula
- Quach found by analysing tension coupon test data
e[0.2]:=sigma[0.2]/E[0]; formula-Rasmussen
B[0]:=0.018+e[0.2]*((E[0]/E[0.2])-1); formula-Quach
A[0]:=B[0]/(0.008+e[0.2]*(sigma[1.0]/sigma[0.2]-1)*(1-E[0]/E[0.2]));
formula-Quach
sigma[2.0]:=(1+(sigma[1.0]/sigma[0.2]-
1)*(A[0]^(1/n[0.2,1.0])))/(1+e[0.2]*(E[0]/E[0.2]-
1)*(sigma[1.0]/sigma[0.2]-
1)*A[0]^(1/n[0.2,1.0])/(n[0.2,1.0]*B[0]))*sigma[0.2]; formula-Quach
epsilon[2.0]:= (sigma[2.0]/E[0])+0.02;
b[0]:=(sigma[ult]*(1+epsilon[ult])-
sigma[2.0]*(1+epsilon[2.0]))/(epsilon[ult]-epsilon[2.0]); formula-
Quach
a[0]:=sigma[2.0]*(1+epsilon[2.0])-b[0]*epsilon[2.0]; formula-Quach
t := 2;

>
```

coiling curvature

```
> Kappa[c] := 1/(450);
```

circling or bending radius

```
ri:=4*t:
radius :=ri+t/2;
Kappa[cs]:= 1/radius;
```

F O R M I N G P R O C E S S
---
loop for coiling and uncoiling (small strain condition)

```
> i:=-1:
for y from (t/2) by (-t/30) while y > 0 do
i:=i+1:
axy[i]:=y:
####coiling
epsilon[z,cy] := sigma[y0]*(1-nu^2)/(E[0]*sqrt(1-nu+nu^2)):
epsilon[z,c] := Kappa[c]*y:
if epsilon[z,cy] < epsilon[z,c] then
e := 0:
sigma[c] := sigma[y0]:
omega[c] := nu:
for s from sigma[y0] by 0.5 to sigma[ult] while abs(e) <
abs(epsilon[z,c]-epsilon[z,cy]) do
ds := s - sigma[c]:
```

```
if s <= sigma[0.2] then
eps:= X/(E[0])+0.002*(X/(sigma[0.2]))^n[0]:
else if s <= sigma[2.0] then
eps:=(X-sigma[0.2])/(E[0.2])+(0.008+(sigma[1.0]-sigma[0.2])*((1/E[0])-
(1/E[0.2])))*((X-sigma[0.2])/(sigma[1.0]-
sigma[0.2]))^n[0.2,1.0]+(sigma[0.2])/(E[0])+0.002:
else
eps:=(X-a[0])/(b[0]-X):
end if:
end if:
dH:=((diff(eps,X))-(1/E[0]))^(-1):
Omega[c] := (4*nu*(subs(X=s,dH))*(1-omega[c]+omega[c]^2)-E[0]*(2-
omega[c])*(2*omega[c]-1))/(E[0]*(2*omega[c]-1)^2+4*(subs(X=s,dH))*(1-
omega[c]+omega[c]^2)):
dom[c] := (2*(1-omega[c]+omega[c]^2)*(Omega[c]-omega[c]))/(s*((2-
omega[c])+Omega[c]*(2*omega[c]-1))*ds:
omega[c] := omega[c] + dom[c]:
de :=  subs(X=omega[c],(((1-2*X)^2-2*nu*(1-2*X)*(2-X)+(2-
X)^2)*s)/(2*E[0]*(1-2*X)*(1-X+X^2)^(3/2)))*dom[c] + subs(X=s,((1-
omega[c]^2)*(1-2*nu))/(E[0]*(1-2*omega[c])*sqrt(1-
omega[c]+omega[c]^2)))*ds;
e:= de + e:
sigma[c] := s:
end do:
sigma[z,c] := sigma[c]/sqrt(1-omega[c]+omega[c]^2):
sigma[x,c] := omega[c]*sigma[c]/sqrt(1-omega[c]+omega[c]^2):
else
sigma[z,c] := E[0]*epsilon[z,c]/(1-nu^2):
sigma[x,c] := nu*E[0]*epsilon[z,c]/(1-nu^2):
omega[c] := nu:
end if:
epsilon[c,pl,i]:=e-s/E[0]:
#####uncoiling including flatening
Kappa[u] := -Kappa[c]:
Kappa[uy]:=-(sigma[c]*(1-nu^2)*(2-nu+(2*nu-1)*omega[c]))/(E[0]*y*(1-
nu+nu^2)*sqrt((1-omega[c]+omega[c]^2))):
epsilon[z,uy] := (Kappa[c]+Kappa[uy])*y:
epsilon[z,r] := 0:
if abs(Kappa[uy]) < abs(Kappa[u]) then
omega[uy] := ((1-nu^2)*omega[c]-nu*(2-nu))/((1-2*nu)*omega[c]-(1-
nu^2)):
sigma[u]:= sigma[c]:
omega[u]:= omega[uy]:
e:=0:
for s from sigma[u] by 0.5 to sigma[ult] while abs(e) <
abs(epsilon[z,uy] + epsilon[z,r] ) do
ds := s - sigma[u]:
if s <= sigma[0.2] then
eps:= X/(E[0])+0.002*(X/(sigma[0.2]))^n[0]:
else if s <= sigma[2.0] then
eps:=(X-sigma[0.2])/(E[0.2])+(0.008+(sigma[1.0]-sigma[0.2])*((1/E[0])-
(1/E[0.2])))*((X-sigma[0.2])/(sigma[1.0]-
sigma[0.2]))^n[0.2,1.0]+(sigma[0.2])/(E[0])+0.002:
else
eps:=(X-a[0])/(b[0]-X):
end if:
end if:
dH:=((diff(eps,X))-(1/E[0]))^(-1):
Omega[u] := (4*nu*(subs(X=s,dH))*(1-omega[u]+omega[u]^2)-E[0]*(2-
omega[u])*(2*omega[u]-1))/(E[0]*(2*omega[u]-1)^2+4*(subs(X=s,dH))*(1-
omega[u]+omega[u]^2)):
```

```
dom[u] := (2*(1-omega[u]+omega[u]^2)*(Omega[u]-omega[u]))/(s*((2-
omega[u])+Omega[u]*(2*omega[u]-1)))*ds:
omega[u] := omega[u] + dom[u]:
de:=  subs(X=omega[u],(((1-2*X)^2-2*nu*(1-2*X)*(2-X)+(2-
X)^2)*s)/(2*E[0]*(1-2*X)*(1-X+X^2)^(3/2)))*dom[u] + subs(X=s,((1-
omega[u]^2)*(1-2*nu))/(E[0]*(1-2*omega[u])*sqrt(1-
omega[u]+omega[u]^2)))*ds;
e:= de + e:
sigma[u]:=s:
end do:
sigma[u,i]:= sigma[u]:
sigma[z,r,i] := - sigma[u]/sqrt(1-omega[u]+omega[u]^2):
sigma[x,r,i] := - omega[u]*sigma[u]/sqrt(1-omega[u]+omega[u]^2):
epsilon[i]:=e:
epsilon[u,pl,i]:=e-(s-sigma[c])/E[0]:
epsilon[r,pl,i]:=epsilon[u,pl,i]+epsilon[c,pl,i]:
else
sigma[z,u] := E[0]*Kappa[u]*y/(1-nu^2):
sigma[x,u] := nu*E[0]*Kappa[u]*y/(1-nu^2):
sigma[z,r,i] := sigma[z,c]+sigma[z,u]:
sigma[x,r,i] := sigma[x,c]+sigma[x,u]:
omega[u,i]:= sigma[x,r,i]/sigma[z,r,i]:
sigma[u,i]:= sigma[c]:
s:=sigma[c]:
epsilon[i]:=Kappa[u]*y:
epsilon[u,pl,i]:=0:
epsilon[r,pl,i]:=epsilon[u,pl,i]+epsilon[c,pl,i]:
end if:
end do:
```

using simmetry for whole thickness data

```
> axy[15]:=0:
sigma[us,15]:=sigma[y0]:
sigma[z,r,15]:=sigma[y0]*(1-nu^2)/(E[0]):
sigma[x,r,15]:=sigma[y0]*(1-nu^2)/(E[0]*nu):
epsilon[r,pl,15]:=0:
sigma[u,15]:=sigma[y0]:
> for i from 0 by 1 to 29 do
axy[30-i]:= -axy[i]:
sigma[u,30-i]:= sigma[u,i]:
sigma[z,r,30-i]:= -sigma[z,r,i]:
sigma[x,r,30-i]:= -sigma[x,r,i]:
epsilon[r,pl,30-i]:= epsilon[r,pl,i]:
end do:
```

bending to the corner radius (x-axis bending)

```
> q[x]:=1:
for shift from 0.001 by 0.001 while q[x] > 0.25 do
for i from 0 by 1 to 30 do
y:= axy[i]:
epsilon[x,cs,i]:= ln(1+(shift-y)/(1/Kappa[cs]-shift)):
epsilon[x,csy,i]:= sigma[u,i]*(1-nu^2)/(E[0]*sqrt(1-nu+nu^2)):
if abs(epsilon[x,csy,i])<abs(epsilon[x,cs,i])then
e:= 0:
sigma[z,cs,i]:= sigma[z,r,i] + nu*E[0]*epsilon[x,csy,i]/(1-nu^2):
sigma[x,cs,i]:= sigma[x,r,i] + E[0]*epsilon[x,csy,i]/(1-nu^2):
omega[cs] := sigma[z,cs,i]/sigma[x,cs,i]:
sigma[cs]:=sigma[u,i]:
for s from sigma[u,i] by 1 to sigma[ult] while abs(e)
<(abs(epsilon[x,cs,i]-epsilon[x,csy,i])) do
ds:= s-sigma[cs]:
if s <= sigma[0.2] then
eps:= X/(E[0])+0.002*(X/(sigma[0.2]))^n[0]:
```

```
dt:=ds+ds*((2*X/E[0])+0.002*(n[0]+1)*(X/sigma[0.2])^n[0]):
else if s <= sigma[2.0] then
eps:=(X-sigma[0.2])/(E[0.2])+(0.008+(sigma[1.0]-sigma[0.2])*((1/E[0])-
(1/E[0.2])))*((X-sigma[0.2])/(sigma[1.0]-
sigma[0.2]))^n[0.2,1.0]+(sigma[0.2])/(E[0])+0.002:
dt:=ds+ds*(((sigma[0.2])/(E[0]))+0.002+((2*X-
sigma[0.2])/E[0.2])+((((n[0.2,1.0]+1)*X)-
sigma[0.2]))*(0.008+(sigma[1.0]-sigma[0.2])*((1/E[0])-
(1/E[0.2])))*((X-sigma[0.2])^(n[0.2,1.0]-1)/(sigma[1.0]-
sigma[0.2])^n[0.2,1.0])):
else
eps:=(X-a[0])/(b[0]-X):
dt:=ds+ds*(((2*X-a[0])*(b[0]-X)+X*(X-a[0]))/(b[0]-X)^2):
end if:
end if:
dH:=(((diff(eps,X))/((1+eps)*((1+eps)+X*((diff(eps,X))))))-
(1/E[0]))^(-1):
Omega[cs]:= (4*nu*(subs(X=s,dH))*(1-omega[cs]+omega[cs]^2)-E[0]*(2-
omega[cs])*(2*omega[cs]-1))/(E[0]*(2*omega[cs]-
1)^2+4*(subs(X=s,dH))*(1-omega[cs]+omega[cs]^2)):
dom[cs]:=((2*(1-omega[cs]+omega[cs]^2)*(Omega[cs]-omega[cs]))/(s*((2-
omega[cs])+Omega[cs]*(2*omega[cs]-1))))*(subs(X=s,dt)):
omega[cs]:= omega[cs] + dom[cs]:
de:= subs(X=omega[cs],(((1-2*X)^2-2*nu*(1-2*X)*(2-X)+(2-
X)^2)*s)/(2*E[0]*(1-2*X)*(1-X+X^2)^(3/2)))*dom[cs] + subs(X=s,((1-
omega[cs]^2)*(1-2*nu))/(E[0]*(1-2*omega[cs])*sqrt(1-
omega[cs]+omega[cs]^2)))*ds:
e:= de + e:
sigma[cs]:=s:
end do:
if y>= shift then
sigma[z,cs,i]:= -omega[cs]*sigma[cs]/sqrt(1-omega[cs]+omega[cs]^2):
sigma[x,cs,i]:= -sigma[cs]/sqrt(1-omega[cs]+omega[cs]^2):
else
sigma[z,cs,i]:= omega[cs]*sigma[cs]/sqrt(1-omega[cs]+omega[cs]^2):
sigma[x,cs,i]:= sigma[cs]/sqrt(1-omega[cs]+omega[cs]^2):
end if:
sigma[cs,i]:= s:
omega[cs,i]:=omega[cs]:
epsilon[cs,pl,i]:=ln(1+e)-(s*(1+e)/E[0]):
else
sigma[z,cs,i]:= sigma[z,r,i] + nu*E[0]*epsilon[x,cs,i]/(1-nu^2):
sigma[x,cs,i]:= sigma[x,r,i] + E[0]*epsilon[x,cs]/(1-nu^2):
sigma[cs,i]:= sigma[u,i]:
omega[cs,i]:= sigma[z,cs,i]/sigma[x,cs,i]:
epsilon[cs,pl,i] := 0:
end if:
end do:
#### membrane residual stress
q[x]:= 0:
for i from 0 by 1 to 29 do
q[x]:= q[x]-(sigma[x,cs,i+1]+sigma[x,cs,i] )/2*(axy[i]-axy[i+1]):
end do:
q[x]:=q[x]/t;
end do:
q[x];
shift;
```

Appendix D

Maple model for cold-bending including springback of a carbon steel thick sheet

```
----------------------------------------
Material and geometrical characteristics
----------------------------------------
material
> E[0]:=203.9e3;
nu:= 0.28;
sigma[0.2]:=593.2;
sigma[ult]:=737.9;
epsilon[ult]:=1-sigma[0.2]/sigma[ult];
E[n]:=(sigma[ult]-sigma[0.2])/(epsilon[ult]-(sigma[0.2]/E[0]));
t:=25.4;

circling or bending radius
ri:=5.5*t:
radius :=ri+t/2;
Kappa[cs]:= 1/radius;

F O R M I N G  P R O C E S S
loop for cold bending
> i:=-1:
for y from (t/2) by (-t/20)while abs(y)<=(t/2) do
i:=i+1:
axy[i]:=y:
end do:

bending to the corner radius (x-axis bending)
> q[x]:=1:
for shift from 0.001 by 0.001 while abs(q[x]) > 0.9 do
for i from 0 by 1 to 20 do
y:= axy[i]:
epsilon[x,cs,i] := ln(1+(shift-y)/(1/Kappa[cs]-shift)):
epsilon[x,csy,i] := sigma[0.2]*(1-nu^2)/(E[0]*sqrt(1-nu+nu^2)):
if abs(epsilon[x,csy,i])<abs(epsilon[x,cs,i]) then
e:= 0:
sigma[z,cs,i]:=nu*E[0]*epsilon[x,csy,i]/(1-nu^2):
sigma[x,cs,i] :=E[0]*epsilon[x,csy,i]/(1-nu^2):
omega[cs] :=nu:
sigma[cs]:=sigma[0.2]:
for s from sigma[0.2] by 1 to sigma[ult] while abs(e)
<(abs(epsilon[x,cs,i]-epsilon[x,csy,i])) do
ds:= s-sigma[cs]:
eps:=(sigma[0.2]/E[0])+((X-sigma[0.2])/E[n]):
dH:=(E[0]*E[n])/(E[0]-E[n]):
Omega[cs]:=(4*nu*dH*(1-omega[cs]+omega[cs]^2)-E[0]*(2-
omega[cs])*(2*omega[cs]-1))/(E[0]*(2*omega[cs]-1)^2+4*dH*(1-
omega[cs]+omega[cs]^2)):
```

```
dom[cs]:=((2*(1-omega[cs]+omega[cs]^2)*(Omega[cs]-omega[cs]))/(s*((2-
omega[cs])+Omega[cs]*(2*omega[cs]-1))))*ds:
omega[cs]:= omega[cs] + dom[cs]:
de:=subs(X=omega[cs],(((1-2*X)^2-2*nu*(1-2*X)*(2-X)+(2-
X)^2)*s)/(2*E[0]*(1-2*X)*(1-X+X^2)^(3/2)))*dom[cs]+subs(X=s,((1-
omega[cs]^2)*(1-2*nu))/(E[0]*(1-2*omega[cs])*sqrt(1-
omega[cs]+omega[cs]^2)))*ds:
e:= de + e:
sigma[cs]:=s:
end do:
if y>= shift then
sigma[z,cs,i]:= -omega[cs]*sigma[cs]/sqrt(1-omega[cs]+omega[cs]^2):
sigma[x,cs,i]:= -sigma[cs]/sqrt(1-omega[cs]+omega[cs]^2):
else
sigma[z,cs,i]:= omega[cs]*sigma[cs]/sqrt(1-omega[cs]+omega[cs]^2):
sigma[x,cs,i]:= sigma[cs]/sqrt(1-omega[cs]+omega[cs]^2):
end if:
sigma[cs,i]:=s:
omega[cs,i]:=omega[cs]:
epsilon[cs,pl,i]:=(s-sigma[0.2])*((E[0]-E[n])/(E[0]*E[n])):
else
sigma[z,cs,i]:=nu*E[0]*epsilon[x,cs,i]/(1-nu^2):
sigma[x,cs,i]:= E[0]*epsilon[x,cs,i]/(1-nu^2):
sigma[cs,i]:= sigma[0.2]:
omega[cs,i]:= sigma[z,cs,i]/sigma[x,cs,i]:
epsilon[cs,pl,i] := 0:
end if:
end do:
#### membrane residual stress
q[x]:= 0:
for i from 0 by 1 to 19 do
q[x]:= q[x]-(sigma[x,cs,i+1]+sigma[x,cs,i] )/2*(axy[i]-axy[i+1]):
end do:
q[x]:=q[x]/t;
end do:
q[x];
shift;

####Spring back
M[t]:=0:
for i from 0 by 1 to 20 do
if i=0 then
M[i]:=(sigma[x,cs,i]*axy[i]*t/20)/2:
elif i=26 then
M[i]:=(sigma[x,cs,i]*axy[i]*t/20)/2:
else
M[i]:=sigma[x,cs,i]*axy[i]*t/20:
end if:
M[t]:=M[t]+M[i]:
end do:
Iy:=1*t^3/12:
###Final stress(including spring back)
for i from 0 by 1 to 20 do
epsilon[x,sb,i]:= M[t]*axy[i]/(Iy*E[0]):
sigma[x,sb,i]:=epsilon[x,sb,i]*E[0]:
sigma[z,sb,i]:=nu*epsilon[x,sb,i]*E[0]:
sigma[z,pb,i]:=sigma[z,cs,i]-sigma[z,sb,i]:
sigma[x,pb,i]:=sigma[x,cs,i]-sigma[x,sb,i]:
end do:
```

Appendix E

Maple model for corner cold-bending including springback with stress-strain curve

```
----------------------------------------
Material and geometrical characteristics
----------------------------------------
material
> E[0] :=190e3:
nu := 0.3:
sigma[y0] := 0.001: ##sigma[y0]>0.0001##
sigma[0.2] :=364;
sigma[ult]:=501;
n[0]:=6.7;
epsilon[ult] := min(1-sigma[.2]/sigma[ult],0.6);
sigma[1.0] := 0.542*sigma[0.2]/n[0]+1.072*sigma[0.2]; formula - Quach
found by analysing tension coupon test data
E[0.2] := E[0]/(1+0.002*n[0]*E[0]/sigma[0.2]); formula-Rasmussen
n[0.2,1.0] := 3.1;
t := 1.9;

e[0.2]:=sigma[0.2]/E[0]; formula-Rasmussen
B[0]:=0.018+e[0.2]*((E[0]/E[0.2])-1); formula-Quach
A[0]:=B[0]/(0.008+e[0.2]*(sigma[1.0]/sigma[0.2]-1)*(1-E[0]/E[0.2]));
formula-Quach
sigma[2.0]:=(1+(sigma[1.0]/sigma[0.2]-
1)*(A[0]^(1/n[0.2,1.0])))/(1+e[0.2]*(E[0]/E[0.2]-
1)*(sigma[1.0]/sigma[0.2]-
1)*A[0]^(1/n[0.2,1.0])/(n[0.2,1.0]*B[0]))*sigma[0.2]; formula-Quach
epsilon[2.0]:= (sigma[2.0]/E[0])+0.02;
b[0]:=(sigma[ult]*(1+epsilon[ult])-
sigma[2.0]*(1+epsilon[2.0]))/(epsilon[ult]-epsilon[2.0]); formula-
Quach
a[0]:=sigma[2.0]*(1+epsilon[2.0])-b[0]*epsilon[2.0]; formula-Quach
>
coiling curvature
> Kappa[c] := 1/(450);
circling or bending radius
ri:=2.5:
radius :=ri+t/2;
Kappa[cs]:= 1/radius;
---------------------------------
F O R M I N G   P R O C E S S
---------------------------------
loop for coiling and uncoiling  (small strain condition)
> i:=-1:
for y from (t/2) by (-t/10) while y > 0 do
i:=i+1:
axy[i]:=y:
####coiling
epsilon[z,cy] := sigma[y0]*(1-nu^2)/(E[0]*sqrt(1-nu+nu^2)):
```

```
epsilon[z,c] := Kappa[c]*y:
if epsilon[z,cy] < epsilon[z,c] then
e := 0:
sigma[c] := sigma[y0]:
omega[c] := nu:
omega[last]:=omega[c]:
for s from sigma[y0] by 0.5 to sigma[ult] while abs(e) <
abs(epsilon[z,c]-epsilon[z,cy]) do
ds := s - sigma[c]:
if s <= sigma[0.2] then
eps:= X/(E[0])+0.002*(X/(sigma[0.2]))^n[0]:
else if s <= sigma[2.0] then
eps:=(X-sigma[0.2])/(E[0.2])+(0.008+(sigma[1.0]-sigma[0.2])*((1/E[0])-
(1/E[0.2])))*((X-sigma[0.2])/(sigma[1.0]-
sigma[0.2]))^n[0.2,1.0]+(sigma[0.2])/(E[0])+0.002:
else
eps:=(X-a[0])/(b[0]-X):
end if:
end if:
dH:=((diff(eps,X))-(1/E[0]))^(-1):
Omega[c] := (4*nu*(subs(X=s,dH))*(1-omega[c]+omega[c]^2)-E[0]*(2-
omega[c])*(2*omega[c]-1))/(E[0]*(2*omega[c]-1)^2+4*(subs(X=s,dH))*(1-
omega[c]+omega[c]^2)):
dom[c] := (2*(1-omega[c]+omega[c]^2)*(Omega[c]-omega[c]))/(s*((2-
omega[c])+Omega[c]*(2*omega[c]-1)))*ds:
omega[c] := omega[c] + dom[c]:
de :=  subs(X=omega[c],(((1-2*X)^2-2*nu*(1-2*X)*(2-X)+(2-
X)^2)*s)/(2*E[0]*(1-2*X)*(1-X+X^2)^(3/2)))*dom[c] + subs(X=s,((1-
omega[c]^2)*(1-2*nu))/(E[0]*(1-2*omega[c])*sqrt(1-
omega[c]+omega[c]^2)))*ds;
e:= de + e:
sigma[c] := s:
end do:
sigma[z,c] := sigma[c]/sqrt(1-omega[c]+omega[c]^2):
sigma[x,c] := omega[c]*sigma[c]/sqrt(1-omega[c]+omega[c]^2):
else
sigma[z,c] := E[0]*epsilon[z,c]/(1-nu^2):
sigma[x,c] := nu*E[0]*epsilon[z,c]/(1-nu^2):
omega[c] := nu:
end if:
epsilon[c,pl,i]:=e-s/E[0]:
#####uncoiling including flatening
Kappa[u] := -Kappa[c]:
Kappa[uy]:=-(sigma[c]*(1-nu^2)*(2-nu+(2*nu-1)*omega[c]))/(E[0]*y*(1-
nu+nu^2)*sqrt((1-omega[c]+omega[c]^2))):
epsilon[z,uy] := (Kappa[c]+Kappa[uy])*y:
epsilon[z,r] := 0:
if abs(Kappa[uy]) < abs(Kappa[u]) then
omega[uy] := ((1-nu^2)*omega[c]-nu*(2-nu))/((1-2*nu)*omega[c]-(1-
nu^2)):
omega[last]:= omega[uy]:
sigma[u]:= sigma[c]:
omega[u]:= omega[uy]:
e:=0:
for s from sigma[u] by 0.5 to sigma[ult] while abs(e) <
abs(epsilon[z,uy] + epsilon[z,r] ) do
ds := s - sigma[u]:
if s <= sigma[0.2] then
eps:= X/(E[0])+0.002*(X/(sigma[0.2]))^n[0]:
else if s <= sigma[2.0] then
```

```
eps:=(X-sigma[0.2])/(E[0.2])+(0.008+(sigma[1.0]-sigma[0.2])*((1/E[0])-
(1/E[0.2])))*((X-sigma[0.2])/(sigma[1.0]-
sigma[0.2]))^n[0.2,1.0]+(sigma[0.2])/(E[0])+0.002:
else
eps:=(X-a[0])/(b[0]-X):
end if:
end if:
dH:=((diff(eps,X))-(1/E[0]))^(-1):
Omega[u] := (4*nu*(subs(X=s,dH))*(1-omega[u]+omega[u]^2)-E[0]*(2-
omega[u])*(2*omega[u]-1))/(E[0]*(2*omega[u]-1)^2+4*(subs(X=s,dH))*(1-
omega[u]+omega[u]^2)):
dom[u] := (2*(1-omega[u]+omega[u]^2)*(Omega[u]-omega[u]))/(s*((2-
omega[u])+Omega[u]*(2*omega[u]-1)))*ds:
omega[u] := omega[u] + dom[u]:
de:=  subs(X=omega[u],(((1-2*X)^2-2*nu*(1-2*X)*(2-X)+(2-
X)^2)*s)/(2*E[0]*(1-2*X)*(1-X+X^2)^(3/2)))*dom[u] + subs(X=s,((1-
omega[u]^2)*(1-2*nu))/(E[0]*(1-2*omega[u])*sqrt(1-
omega[u]+omega[u]^2)))*ds;
e:= de + e:
sigma[u]:=s:
end do:
sigma[u,i]:= sigma[u]:
sigma[z,r,i] := - sigma[u]/sqrt(1-omega[u]+omega[u]^2):
sigma[x,r,i] := - omega[u]*sigma[u]/sqrt(1-omega[u]+omega[u]^2):
epsilon[i]:=e:
epsilon[u,pl,i]:=e-(s-sigma[c])/E[0]:
epsilon[r,pl,i]:=epsilon[u,pl,i]+epsilon[c,pl,i]:
else
sigma[z,u] := E[0]*Kappa[u]*y/(1-nu^2):
sigma[x,u] := nu*E[0]*Kappa[u]*y/(1-nu^2):
sigma[z,r,i] := sigma[z,c]+sigma[z,u]:
sigma[x,r,i] := sigma[x,c]+sigma[x,u]:
omega[u,i]:= sigma[x,r,i]/sigma[z,r,i]:
sigma[u,i]:= sigma[c]:
s:=sigma[c]:
epsilon[i]:=Kappa[u]*y:
epsilon[u,pl,i]:=0:
epsilon[r,pl,i]:=epsilon[u,pl,i]+epsilon[c,pl,i]:
end if:
end do:
```

using simmetry for whole thickness data

```
> axy[5]:=0:
sigma[us,5]:=sigma[y0]:
sigma[z,r,5]:=sigma[y0]*(1-nu^2)/(E[0]):
sigma[x,r,5]:=sigma[y0]*(1-nu^2)/(E[0]*nu):
epsilon[r,pl,5]:=0:
sigma[u,5]:=sigma[y0]:
> for i from 0 by 1 to 4 do
axy[10-i]:= -axy[i]:
sigma[u,10-i]:= sigma[u,i]:
sigma[z,r,10-i]:= -sigma[z,r,i]:
sigma[x,r,10-i]:= -sigma[x,r,i]:
epsilon[r,pl,10-i]:= epsilon[r,pl,i]:
end do:
```

bending to the corner radius (x-axis bending)

```
> q[x]:=5:
for shift from 0.001 by 0.001 while abs(q[x]) >4.9 do
for i from 0 by 1 to 10 do
y:= axy[i]:
epsilon[x,cs,i]:= ln(1+(shift-y)/(1/Kappa[cs]-shift)):
epsilon[x,csy,i]:= sigma[u,i]*(1-nu^2)/(E[0]*sqrt(1-nu+nu^2)):
```

```
if abs(epsilon[x,csy,i])<abs(epsilon[x,cs,i])then
e:= 0:
sigma[z,cs,i]:= sigma[z,r,i] + nu*E[0]*epsilon[x,csy,i]/(1-nu^2):
sigma[x,cs,i]:= sigma[x,r,i] + E[0]*epsilon[x,csy,i]/(1-nu^2):
omega[cs] := sigma[z,cs,i]/sigma[x,cs,i]:
sigma[cs]:=sigma[u,i]:
for s from sigma[u,i] by 1 to sigma[ult] while abs(e)
<(abs(epsilon[x,cs,i]-epsilon[x,csy,i])) do
ds:= s-sigma[cs]:
if s <= sigma[0.2] then
eps:= X/(E[0])+0.002*(X/(sigma[0.2]))^n[0]:
dt:=ds+ds*((2*X/E[0])+0.002*(n[0]+1)*(X/sigma[0.2])^n[0]):
else if s <= sigma[2.0] then
eps:=(X-sigma[0.2])/(E[0.2])+(0.008+(sigma[1.0]-sigma[0.2])*((1/E[0])-
(1/E[0.2])))*((X-sigma[0.2])/(sigma[1.0]-
sigma[0.2]))^n[0.2,1.0]+(sigma[0.2])/(E[0])+0.002:
dt:=ds+ds*(((sigma[0.2])/(E[0]))+0.002+((2*X-
sigma[0.2])/E[0.2])+((((n[0.2,1.0]+1)*X)-
sigma[0.2]))*(0.008+(sigma[1.0]-sigma[0.2])*((1/E[0])-
(1/E[0.2])))*((X-sigma[0.2])^(n[0.2,1.0]-1)/(sigma[1.0]-
sigma[0.2])^n[0.2,1.0])):
else
eps:=(X-a[0])/(b[0]-X):
dt:=ds+ds*(((2*X-a[0])*(b[0]-X)+X*(X-a[0]))/(b[0]-X)^2):
end if:
end if:
dH:=(((diff(eps,X))/((1+eps)*((1+eps)+X*((diff(eps,X))))))-
(1/E[0]))^(-1):
Omega[cs]:= (4*nu*(subs(X=s,dH))*(1-omega[cs]+omega[cs]^2)-E[0]*(2-
omega[cs])*(2*omega[cs]-1))/(E[0]*(2*omega[cs]-
1)^2+4*(subs(X=s,dH))*(1-omega[cs]+omega[cs]^2)):
dom[cs]:=((2*(1-omega[cs]+omega[cs]^2)*(Omega[cs]-omega[cs]))/(s*((2-
omega[cs])+Omega[cs]*(2*omega[cs]-1))))*(subs(X=s,dt)):
omega[cs]:= omega[cs] + dom[cs]:
de:= subs(X=omega[cs],(((1-2*X)^2-2*nu*(1-2*X)*(2-X)+(2-
X)^2)*s)/(2*E[0]*(1-2*X)*(1-X+X^2)^(3/2)))*dom[cs] + subs(X=s,((1-
omega[cs]^2)*(1-2*nu))/(E[0]*(1-2*omega[cs])*sqrt(1-
omega[cs]+omega[cs]^2)))*ds:
e:= de + e:
sigma[cs]:=s:
end do:
if y>= shift then
sigma[z,cs,i]:= -omega[cs]*sigma[cs]/sqrt(1-omega[cs]+omega[cs]^2):
sigma[x,cs,i]:= -sigma[cs]/sqrt(1-omega[cs]+omega[cs]^2):
else
sigma[z,cs,i]:= omega[cs]*sigma[cs]/sqrt(1-omega[cs]+omega[cs]^2):
sigma[x,cs,i]:= sigma[cs]/sqrt(1-omega[cs]+omega[cs]^2):
end if:
sigma[cs,i]:= s:
omega[cs,i]:=omega[cs]:
epsilon[cs,pl,i]:=ln(1+e)-(s*(1+e)/E[0]):
else
sigma[z,cs,i]:= sigma[z,r,i] + nu*E[0]*epsilon[x,cs,i]/(1-nu^2):
sigma[x,cs,i]:= sigma[x,r,i] + E[0]*epsilon[x,cs]/(1-nu^2):
sigma[cs,i]:= sigma[u,i]:
omega[cs,i]:= sigma[z,cs,i]/sigma[x,cs,i]:
epsilon[cs,pl,i] := 0:
end if:
end do:
#### membrane residual stress
q[x]:= 0:
for i from 0 by 1 to 9 do
```

```
q[x]:= q[x]-(sigma[x,cs,i+1]+sigma[x,cs,i] )/2*(axy[i]-axy[i+1]):
end do:
q[x]:=q[x]/t;
end do:
q[x];
shift;
####Spring back
M[t]:=0:
for i from 0 by 1 to 10 do
if i=0 then
M[i]:=(sigma[x,cs,i]*axy[i]*t/10)/2:
elif i=10 then
M[i]:=(sigma[x,cs,i]*axy[i]*t/10)/2:
else
M[i]:=sigma[x,cs,i]*axy[i]*t/10:
end if:
M[t]:=M[t]+M[i]:
end do:
Iy:=1*t^3/12:
###Final stress(including spring back)
for i from 0 by 1 to 10 do
epsilon[x,sb,i]:= M[t]*axy[i]/(Iy*E[0]):
sigma[x,sb,i]:=epsilon[x,sb,i]*E[0]:
sigma[z,sb,i]:=nu*epsilon[x,sb,i]*E[0]:
sigma[z,pb,i]:=sigma[z,cs,i]-sigma[z,sb,i]:
sigma[x,pb,i]:=sigma[x,cs,i]-sigma[x,sb,i]:
end do:
```

Stress strain diagram after press breaking in longitudinal direction

```
> for i from 0 by 1 to 10 do
sigma[z,i]:=sigma[x,pb,i];
sigma[x,i]:=sigma[z,pb,i];
sigma[i]:= sqrt(sigma[x,pb,i]^2+sigma[z,pb,i]^2-
sigma[x,pb,i]*sigma[z,pb,i]);
sigma[rs,i]:= sqrt(sigma[x,pb,i]^2+sigma[z,pb,i]^2-
sigma[x,pb,i]*sigma[z,pb,i]);
omega[i]:=sigma[z,i]/sigma[x,i];
end do:
> precise:= 0.0001;
beginning:= 0;
de:= 1e-5;
e:=0:
ss[z] := 0:
ss[x] := 0:
ss[av] := 0:
for i from 0 by 1 to 10 do

E[0,pl,i] :=E[0]:
nu :=0.3:
sigma[0.2,pl,i]:= (-
26.857*epsilon[cs,pl,i]^2+9.1674*epsilon[cs,pl,i]+1.0206)*sigma[0.2]:
sigma[1.0,pl,i]:= (-
30.334*epsilon[cs,pl,i]^2+10.314*epsilon[cs,pl,i]+1.0366)*sigma[1.0]:
sigma[ult,pl,i]:= sigma[ult]:
epsilon[ult,pl,i]:= (12.209*epsilon[cs,pl,i]^2-
4.4781*epsilon[cs,pl,i]+1.00272)*epsilon[ult]:

if abs(epsilon[cs,pl,i]) <= 0.09 then
n[0,pl,i]:= (44.343*epsilon[cs,pl,i]^2-
8.708*epsilon[cs,pl,i]+0.8378)*n[0]:
else n[0,pl,i]:= 0.4133*n[0]:
end if:
```

```
E[0.2,pl,i]:= (-
133.75*epsilon[cs,pl,i]^2+38.761*epsilon[cs,pl,i]+1.2097)*E[0.2]:

if abs(epsilon[cs,pl,i]) <= 0.1 then
n[0.2,1.0,pl,i]:= (-
68.301*epsilon[cs,pl,i]^2+15.932*epsilon[cs,pl,i]+1.0949)*n[0.2,1.0]:
else n[0.2,1.0,pl,i]:=2.0251*n[0.2,1.0]:
end if:
epsilon[max,pl,i]:= (44.343*epsilon[cs,pl,i]^2-
8.708*epsilon[cs,pl,i]+0.8378)*epsilon[max]:

e[0.2,pl,i]:=sigma[0.2,pl,i]/E[0,pl,i]:
B[0,pl,i]:=0.018+e[0.2,pl,i]*((E[0,pl,i]/E[0.2,pl,i])-1):
A[0,pl,i]:=B[0,pl,i]/(0.008+e[0.2,pl,i]*(sigma[1.0,pl,i]/sigma[0.2,pl,
i]-1)*(1-E[0,pl,i]/E[0.2,pl,i])):
sigma[2.0,pl,i]:=sigma[0.2,pl,i]+(sigma[1.0,pl,i]-
sigma[0.2,pl,i])*(A[0,pl,i]^(1/n[0.2,1.0,pl,i]))*(1-((1/E[0.2,pl,i]-
1/E[0,pl,i])*sigma[0.2,pl,i])/B[0,pl,i])^(1/n[0.2,1.0,pl,i]):
epsilon[2.0,pl,i]:= (sigma[2.0,pl,i]/E[0,pl,i])+0.02:
b[0,pl,i]:=(sigma[ult,pl,i]*(1+epsilon[ult,pl,i])-
sigma[2.0,pl,i]*(1+epsilon[2.0,pl,i]))/(epsilon[ult,pl,i]-
epsilon[2.0,pl,i]):
a[0,pl,i]:=sigma[2.0,pl,i]*(1+epsilon[2.0,pl,i])-
b[0,pl,i]*epsilon[2.0,pl,i]:
end do:
for e from de by de while e <0.05 do
for i from 0 by 1 to 10 do
if sigma[i] < sigma[rs,i] then
dsigma[x] :=  E[0,pl,i] / (1-nu^2)*de:
dsigma[z] := nu *E[0,pl,i]/(1-nu^2)* de:
else
if sigma[i] <= sigma[0.2,pl,i] then
eps:= X/(E[0,pl,i])+0.002*(X/(sigma[0.2,pl,i]))^n[0,pl,i]:
else
if sigma[i] <= sigma[2.0,pl,i] then
eps:=(X-sigma[0.2,pl,i])/(E[0.2,pl,i])+(0.008+(sigma[1.0,pl,i]-
sigma[0.2,pl,i])*((1/E[0,pl,i])-(1/E[0.2,pl,i])))*((X-
sigma[0.2,pl,i])/(sigma[1.0,pl,i]-
sigma[0.2,pl,i]))^n[0.2,1.0,pl,i]+(sigma[0.2,pl,i])/(E[0,pl,i])+0.002:
else
eps:=(X-a[0,pl,i])/(b[0,pl,i]-X):
end if:
end if:
dH:=subs(X=sigma[i],((diff(eps,X))-(1/E[0,pl,i]))^(-1));
depsilon[x]:= de;
dsigma[z]:= E[0,pl,i]*(4/9*nu*sigma[i]^2*dH/E[0,pl,i]-(2/3*sigma[z,i]-
1/3*sigma[x,i])*(2/3*sigma[x,i]-
1/3*sigma[z,i]))*depsilon[x]/(4/9*sigma[i]^2*dH*(1-
nu^2)/E[0,pl,i]+(2/3*sigma[z,i]-1/3*sigma[x,i])^2+(2/3*sigma[x,i]-
1/3*sigma[z,i])^2+2*nu*(2/3*sigma[z,i]-
1/3*sigma[x,i])*(2/3*sigma[x,i]-1/3*sigma[z,i]));
dsigma[x]:= E[0,pl,i]*((2/3*sigma[z,i]-
1/3*sigma[x,i])^2+4/9*sigma[i]^2*dH/E[0,pl,i])*depsilon[x]/(4/9*sigma[
i]^2*dH*(1-nu^2)/E[0,pl,i]+(2/3*sigma[z,i]-
1/3*sigma[x,i])^2+(2/3*sigma[x,i]-
1/3*sigma[z,i])^2+2*nu*(2/3*sigma[z,i]-
1/3*sigma[x,i])*(2/3*sigma[x,i]-1/3*sigma[z,i]));
end if;
if i = 0 then
ss[x]:= ss[x] + 0.5 * dsigma[x];
ss[z]:= ss[z] + 0.5 * dsigma[z];
ss[av]:= ss[av] + 0.5 * dsig[i]:
```

```
elif i = 10 then
ss[x]:= ss[x] + 0.5 * dsigma[x];
ss[z]:= ss[z] + 0.5 * dsigma[z];
ss[av]:= ss[av] + 0.5 * dsig[i]:
else
ss[x]:= ss[x] + dsigma[x];
ss[z]:= ss[z] + dsigma[z];
ss[av]:= ss[av] + dsig[i]:
end if:
sigma[x,i]:= sigma[x,i] + dsigma[x];
sigma[z,i]:= sigma[z,i] + dsigma[z];
omega[i]:=sigma[z,i]/sigma[x,i];
dsig[i]:= abs(sqrt(sigma[x,i]^2+sigma[z,i]^2-sigma[z,i]*sigma[x,i]) -
sigma[i]);
sigma[i]:= max(sqrt(sigma[x,i]^2+sigma[z,i]^2-
sigma[z,i]*sigma[x,i]),sigma[i]);
end do:
sigma[yield]:= sqrt((ss[z]/10)^2+(ss[x]/10)^2-(ss[x]/10)*(ss[z]/10)):
for ep from 1 to 500 by 1 do
if (e-beginning)=ep*precise then
sigma[ep,plot]:=(ss[x]/10):
epsilon[ep,plot]:=e:
end if:
end do:
end do:
sigma[x,yield]:=sigma[yield]:
epsilon[yield,pl]:= e-sigma[yield]/E[0,pl,i];
ss[x]:= ss[x]/10;
ss[z]:= ss[z]/10;
sqrt(ss[z]^2+ss[x]^2-ss[z]*ss[x]);
sigma[ep,plot];
epsilon[ep,plot];
sigma[100,plot];
epsilon[100,plot];
```

Appendix F

Maple model for flat face cold-bending including springback with stress-strain curve

MODEL CS

units [N, mm, MPa]

Material and geometrical characteristics

---

material

```
> E[0] :=191e3:
nu := 0.3:
sigma[y0] := 0.001: ##sigma[y0]>0.0001##
sigma[0.2] :=268;
sigma[ult]:=584;
n[0]:=6.9;
epsilon[ult] := min(1-sigma[.2]/sigma[ult],0.6);
sigma[1.0] := 0.542*sigma[0.2]/n[0]+1.072*sigma[0.2]; formula - Quach
found by analysing tension coupon test data
E[0.2] := E[0]/(1+0.002*n[0]*E[0]/sigma[0.2]); formula-Rasmussen
n[0.2,1.0] := 3.6;
t := 4.64;

e[0.2]:=sigma[0.2]/E[0]; formula-Rasmussen
B[0]:=0.018+e[0.2]*((E[0]/E[0.2])-1); formula-Quach
A[0]:=B[0]/(0.008+e[0.2]*(sigma[1.0]/sigma[0.2]-1)*(1-E[0]/E[0.2]));
formula-Quach
sigma[2.0]:=(1+(sigma[1.0]/sigma[0.2]-
1)*(A[0]^(1/n[0.2,1.0])))/(1+e[0.2]*(E[0]/E[0.2]-
1)*(sigma[1.0]/sigma[0.2]-
1)*A[0]^(1/n[0.2,1.0])/(n[0.2,1.0]*B[0]))*sigma[0.2]; formula-Quach
epsilon[2.0]:= (sigma[2.0]/E[0])+0.02;
b[0]:=(sigma[ult]*(1+epsilon[ult])-
sigma[2.0]*(1+epsilon[2.0]))/(epsilon[ult]-epsilon[2.0]); formula-
Quach
a[0]:=sigma[2.0]*(1+epsilon[2.0])-b[0]*epsilon[2.0]; formula-Quach
```

coiling curvature

```
> Kappa[c] := 1/(450);
```

circling or bending radius

```
ri:=73.58:
radius :=ri+t/2;
Kappa[cs]:= 1/radius;
```

F O R M I N G P R O C E S S
---
loop for coiling and uncoiling (small strain condition)

```
> i:=-1:
for y from (t/2) by (-t/10) while y > 0 do
i:=i+1:
axy[i]:=y:
####coiling
epsilon[z,cy]:= sigma[y0]*(1-nu^2)/(E[0]*sqrt(1-nu+nu^2)):
epsilon[z,c]:= Kappa[c]*y:
if epsilon[z,cy] < epsilon[z,c] then
e := 0:
sigma[c]:= sigma[y0]:
omega[c]:= nu:

for s from sigma[y0] by 0.5 to sigma[ult] while abs(e)
<abs(epsilon[z,c]-epsilon[z,cy]) do
ds:= s-sigma[c]:
if s <= sigma[0.2] then
eps:= X/(E[0])+0.002*(X/(sigma[0.2]))^n[0]:
else if s <= sigma[2.0] then
eps:=(X-sigma[0.2])/(E[0.2])+(0.008+(sigma[1.0]-sigma[0.2])*((1/E[0])-
(1/E[0.2])))*((X-sigma[0.2])/(sigma[1.0]-
sigma[0.2]))^n[0.2,1.0]+(sigma[0.2])/(E[0])+0.002:
else
eps:=(X-a[0])/(b[0]-X):
end if:
end if:
dH:=((diff(eps,X))-(1/E[0]))^(-1):
Omega[c] := (4*nu*(subs(X=s,dH))*(1-omega[c]+omega[c]^2)-E[0]*(2-
omega[c])*(2*omega[c]-1))/(E[0]*(2*omega[c]-1)^2+4*(subs(X=s,dH))*(1-
omega[c]+omega[c]^2)):
dom[c] := (2*(1-omega[c]+omega[c]^2)*(Omega[c]-omega[c]))/(s*((2-
omega[c])+Omega[c]*(2*omega[c]-1)))*ds:
omega[c] := omega[c] + dom[c]:
de :=  subs(X=omega[c],(((1-2*X)^2-2*nu*(1-2*X)*(2-X)+(2-
X)^2)*s)/(2*E[0]*(1-2*X)*(1-X+X^2)^(3/2)))*dom[c] + subs(X=s,((1-
omega[c]^2)*(1-2*nu))/(E[0]*(1-2*omega[c])*sqrt(1-
omega[c]+omega[c]^2)))*ds;
e:= de + e:
sigma[c] := s:
end do:
sigma[z,c] := sigma[c]/sqrt(1-omega[c]+omega[c]^2):
sigma[x,c] := omega[c]*sigma[c]/sqrt(1-omega[c]+omega[c]^2):
else
sigma[z,c] := E[0]*epsilon[z,c]/(1-nu^2):
sigma[x,c] := nu*E[0]*epsilon[z,c]/(1-nu^2):
omega[c] := nu:
end if:
epsilon[c,pl]:=e-s/E[0]:
#####uncoiling including flatening
Kappa[u] := -Kappa[c]:
Kappa[uy]:=-(sigma[c]*(1-nu^2)*(2-nu+(2*nu-1)*omega[c]))/(E[0]*y*(1-
nu+nu^2)*sqrt((1-omega[c]+omega[c]^2))):
epsilon[z,uy] := (Kappa[c]+Kappa[uy])*y:
epsilon[z,r] := 0:
if abs(Kappa[uy]) < abs(Kappa[u]) then
omega[uy] := ((1-nu^2)*omega[c]-nu*(2-nu))/((1-2*nu)*omega[c]-(1-
nu^2)):

sigma[u]:= sigma[c]:
```

```
omega[u]:= omega[uy]:
e:=0:
for s from sigma[u] by 0.5 to sigma[ult] while abs(e) <
abs(epsilon[z,uy] + epsilon[z,r] ) do
ds := s - sigma[u]:
if s <= sigma[0.2] then
eps:= X/(E[0])+0.002*(X/(sigma[0.2]))^n[0]:
else if s <= sigma[2.0] then
eps:=(X-sigma[0.2])/(E[0.2])+(0.008+(sigma[1.0]-sigma[0.2])*((1/E[0])-
(1/E[0.2])))*((X-sigma[0.2])/(sigma[1.0]-
sigma[0.2]))^n[0.2,1.0]+(sigma[0.2])/(E[0])+0.002:
else
eps:=(X-a[0])/(b[0]-X):
end if:
end if:
dH:=((diff(eps,X))-(1/E[0]))^(-1):
Omega[u] := (4*nu*(subs(X=s,dH))*(1-omega[u]+omega[u]^2)-E[0]*(2-
omega[u])*(2*omega[u]-1))/(E[0]*(2*omega[u]-1)^2+4*(subs(X=s,dH))*(1-
omega[u]+omega[u]^2)):
dom[u] := (2*(1-omega[u]+omega[u]^2)*(Omega[u]-omega[u]))/(s*((2-
omega[u])+Omega[u]*(2*omega[u]-1)))*ds:
omega[u] := omega[u] + dom[u]:
de :=  subs(X=omega[u],(((1-2*X)^2-2*nu*(1-2*X)*(2-X)+(2-
X)^2)*s)/(2*E[0]*(1-2*X)*(1-X+X^2)^(3/2)))*dom[u] + subs(X=s,((1-
omega[u]^2)*(1-2*nu))/(E[0]*(1-2*omega[u])*sqrt(1-
omega[u]+omega[u]^2)))*ds;
e:= de + e:
sigma[u] := s:
end do:
sigma[u,i]:= sigma[u]:
sigma[z,r,i]:= - sigma[u]/sqrt(1-omega[u]+omega[u]^2):
sigma[x,r,i]:= - omega[u]*sigma[u]/sqrt(1-omega[u]+omega[u]^2):
else
sigma[z,u]:= E[0]*Kappa[u]*y/(1-nu^2):
sigma[x,u]:= nu*E[0]*Kappa[u]*y/(1-nu^2):
sigma[z,r,i] := sigma[z,c]+sigma[z,u]:
sigma[x,r,i] := sigma[x,c]+sigma[x,u]:
omega[u,i]:= sigma[x,r,i]/sigma[z,r,i]:
sigma[u,i]:=sigma[c]:
s:=sigma[c]:
end if:
epsilon[u,pl]:=e-(s-sigma[c])/E[0]:
epsilon[r,pl,i]:=epsilon[u,pl]+epsilon[c,pl]:
#####bending for making circle (x-axis bending)
epsilon[x,csy]:= sigma[u,i]*(1-nu^2)/(E[0]*sqrt(1-nu+nu^2)):
epsilon[x,cs]:= Kappa[cs]*y:
if epsilon[x,csy] < epsilon[x,cs] then
e := 0:
sigma[cs]:= sigma[u,i]:
omega[cs]:= nu:

for s from sigma[u,i] by 0.5 to sigma[ult] while abs(e)
<abs(epsilon[x,cs]-epsilon[x,csy]) do
ds:= s-sigma[cs]:
if s <= sigma[0.2] then
eps:= X/(E[0])+0.002*(X/(sigma[0.2]))^n[0]:
else if s <= sigma[2.0] then
eps:=(X-sigma[0.2])/(E[0.2])+(0.008+(sigma[1.0]-sigma[0.2])*((1/E[0])-
(1/E[0.2])))*((X-sigma[0.2])/(sigma[1.0]-
sigma[0.2]))^n[0.2,1.0]+(sigma[0.2])/(E[0])+0.002:
else
eps:=(X-a[0])/(b[0]-X):
```

```
end if:
end if:
dH:=((diff(eps,X))-(1/E[0]))^(-1):
Omega[cs]:= (4*nu*(subs(X=s,dH))*(1-omega[cs]+omega[cs]^2)-E[0]*(2-
omega[cs])*(2*omega[cs]-1))/(E[0]*(2*omega[cs]-
1)^2+4*(subs(X=s,dH))*(1-omega[cs]+omega[cs]^2)):
dom[cs]:=((2*(1-omega[cs]+omega[cs]^2)*(Omega[cs]-omega[cs]))/(s*((2-
omega[cs])+Omega[cs]*(2*omega[cs]-1))))*ds:
omega[cs]:= omega[cs] + dom[cs]:
de:= subs(X=omega[cs],(((1-2*X)^2-2*nu*(1-2*X)*(2-X)+(2-
X)^2)*s)/(2*E[0]*(1-2*X)*(1-X+X^2)^(3/2)))*dom[cs] + subs(X=s,((1-
omega[cs]^2)*(1-2*nu))/(E[0]*(1-2*omega[cs])*sqrt(1-
omega[cs]+omega[cs]^2)))*ds:
e:= de + e:
sigma[cs]:= s:
end do:
sigma[z,cs,i] := sigma[z,r,i]+ omega[cs]*sigma[cs]/sqrt(1-
omega[cs]+omega[cs]^2):
sigma[x,cs,i] := sigma[x,r,i]+sigma[cs]/sqrt(1-omega[cs]+omega[cs]^2):
else
sigma[z,cs,i]:= sigma[z,r,i]+nu*E[0]*epsilon[x,cs]/(1-nu^2):
sigma[x,cs,i]:= sigma[x,r,i]+E[0]*epsilon[x,cs]/(1-nu^2):
omega[cs] := sigma[z,cs,i]/sigma[x,cs,i]:
end if:
epsilon[cs,pl,i]:=e-s/E[0]:

######Uncoiling for final shape
Kappa[us] := -Kappa[cs]:
Kappa[usy]:=-(sigma[cs]*(1-nu^2)*(2-nu+(2*nu-
1)*omega[cs]))/(E[0]*y*(1-nu+nu^2)*sqrt((1-omega[cs]+omega[cs]^2))):
epsilon[x,usy] := (Kappa[cs]+Kappa[usy])*y:
epsilon[x,rs] := 0:
if abs(Kappa[usy]) < abs(Kappa[us]) then
omega[usy] := ((1-nu^2)*omega[cs]-nu*(2-nu))/((1-2*nu)*omega[cs]-(1-
nu^2)):

sigma[us]:= sigma[cs]:
omega[us]:= omega[usy]:
e:=0:
for s from sigma[us] by 0.5 to sigma[ult] while abs(e) <
abs(epsilon[x,usy] + epsilon[x,rs]) do
ds := s-sigma[us]:
if s <= sigma[0.2] then
eps:= X/(E[0])+0.002*(X/(sigma[0.2]))^n[0]:
else if s <= sigma[2.0] then
eps:=(X-sigma[0.2])/(E[0.2])+(0.008+(sigma[1.0]-sigma[0.2])*((1/E[0])-
(1/E[0.2])))*((X-sigma[0.2])/(sigma[1.0]-
sigma[0.2]))^n[0.2,1.0]+(sigma[0.2])/(E[0])+0.002:
else
eps:=(X-a[0])/(b[0]-X):
end if:
end if:
dH:=((diff(eps,X))-(1/E[0]))^(-1):
Omega[us] := (4*nu*(subs(X=s,dH))*(1-omega[us]+omega[us]^2)-E[0]*(2-
omega[us])*(2*omega[us]-1))/(E[0]*(2*omega[us]-
1)^2+4*(subs(X=s,dH))*(1-omega[us]+omega[us]^2)):
dom[us] := (2*(1-omega[us]+omega[us]^2)*(Omega[us]-omega[us]))/(s*((2-
omega[us])+Omega[us]*(2*omega[us]-1)))*ds:
omega[us] := omega[us] + dom[us]:
de := subs(X=omega[us],(((1-2*X)^2-2*nu*(1-2*X)*(2-X)+(2-
X)^2)*s)/(2*E[0]*(1-2*X)*(1-X+X^2)^(3/2)))*dom[us] + subs(X=s,((1-
```

```
omega[us]^2)*(1-2*nu))/(E[0]*(1-2*omega[us])*sqrt(1-
omega[us]+omega[us]^2)))*ds;
e:= de + e:
sigma[us]:=s:
end do:
sigma[us,i]:= sigma[us]:
sigma[z,rs,i]:= - omega[us]*sigma[us]/sqrt(1-omega[us]+omega[us]^2):
sigma[x,rs,i] := - sigma[us]/sqrt(1-omega[us]+omega[us]^2):
epsilon[i]:=e:
epsilon[us,pl,i]:=e-(s-sigma[cs])/E[0]:
epsilon[rs,pl,i]:=epsilon[us,pl,i]+epsilon[cs,pl,i]:
else
sigma[z,us,i] :=nu*E[0]*Kappa[us]*y/(1-nu^2):
sigma[x,us,i] := E[0]*Kappa[us]*y/(1-nu^2):
sigma[z,rs,i] := sigma[z,cs,i]+sigma[z,us,i]:
sigma[x,rs,i] := sigma[x,cs,i]+sigma[x,us,i]:
omega[us,i]:= sigma[x,rs,i]/sigma[z,rs,i]:
sigma[us,i]:= sigma[cs]:
sigma[cs]:=s:
epsilon[i]:=Kappa[us]*y:
epsilon[us,pl,i]:=0:
epsilon[rs,pl,i]:=epsilon[us,pl,i]+epsilon[cs,pl,i]:
end if:
end do:
```

using simmetry for whole thickness data

```
> axy[5]:=0:
sigma[us,5]:=sigma[y0]:
sigma[z,rs,5]:=sigma[y0]*(1-nu^2)/(E[0]):
sigma[x,rs,5]:=sigma[y0]*(1-nu^2)/(E[0]*nu):
epsilon[rs,pl,5]:=0:
sigma[cs,5]:=sigma[y0]:
sigma[z,cs,5]:=sigma[y0]*(1-nu^2)/(E[0]*nu):
sigma[x,cs,5]:=sigma[y0]*(1-nu^2)/(E[0]):
epsilon[cs,pl,5]:=0:

> for i from 0 by 1 to 4 do
axy[10-i]:= -axy[i]:
sigma[us,10-i]:= sigma[us,i]:
sigma[z,rs,10-i]:= -sigma[z,rs,i]:
sigma[x,rs,10-i]:= -sigma[x,rs,i]:
epsilon[rs,pl,10-i]:= epsilon[rs,pl,i]:
sigma[cs,10-i]:= sigma[cs,i]:
sigma[z,cs,10-i]:= -sigma[z,cs,i]:
sigma[x,cs,10-i]:= -sigma[x,cs,i]:
epsilon[cs,pl,10-i]:= epsilon[cs,pl,i]:
end do:

####Spring back
M[t]:=0:
for i from 0 by 1 to 10 do
if i=0 then
M[i]:=(sigma[x,rs,i]*axy[i]*t/10)/2:
elif i=10 then
M[i]:=(sigma[x,rs,i]*axy[i]*t/10)/2:
else
M[i]:=sigma[x,rs,i]*axy[i]*t/10:
end if:
M[t]:=M[t]+M[i]:
end do:
Iy:=1*t^3/12:
###Final stress(including spring back)
```

```
for i from 0 by 1 to 10 do
epsilon[x,sb,i]:= M[t]*axy[i]/(Iy*E[0]):
sigma[x,sb,i]:=epsilon[x,sb,i]*E[0]:
sigma[z,sb,i]:=nu*epsilon[x,sb,i]*E[0]:
sigma[z,pb,i]:=sigma[z,rs,i]-sigma[z,sb,i]:
sigma[x,pb,i]:=sigma[x,rs,i]-sigma[x,sb,i]:
end do:
```

Stress strain diagram after press breaking in longitudinal direction

```
> for i from 0 by 1 to 10 do
sigma[z,i]:=sigma[x,pb,i];
sigma[x,i]:=sigma[z,pb,i];
sigma[i]:= sqrt(sigma[x,pb,i]^2+sigma[z,pb,i]^2-
sigma[x,pb,i]*sigma[z,pb,i]);
sigma[rs,i]:= sqrt(sigma[x,pb,i]^2+sigma[z,pb,i]^2-
sigma[x,pb,i]*sigma[z,pb,i]);
omega[i]:=sigma[z,i]/sigma[x,i];
end do:
> precise:= 0.0001;
beginning:= 0;
de:= 1e-5;
e:=0:
ss[z] := 0:
ss[x] := 0:
ss[av] := 0:
for i from 0 by 1 to 10 do

E[0,pl,i] :=E[0]:
nu :=0.3:
sigma[0.2,pl,i]:= (-
26.857*epsilon[cs,pl,i]^2+9.1674*epsilon[cs,pl,i]+1.0206)*sigma[0.2]:
sigma[1.0,pl,i]:= (-
30.334*epsilon[cs,pl,i]^2+10.314*epsilon[cs,pl,i]+1.0366)*sigma[1.0]:
sigma[ult,pl,i]:= sigma[ult]:
epsilon[ult,pl,i]:= (12.209*epsilon[cs,pl,i]^2-
4.4781*epsilon[cs,pl,i]+1.00272)*epsilon[ult]:

if abs(epsilon[cs,pl,i]) <= 0.09 then
n[0,pl,i]:= (44.343*epsilon[cs,pl,i]^2-
8.708*epsilon[cs,pl,i]+0.8378)*n[0]:
else n[0,pl,i]:= 0.4133*n[0]:
end if:
E[0.2,pl,i]:= (-
133.75*epsilon[cs,pl,i]^2+38.761*epsilon[cs,pl,i]+1.2097)*E[0.2]:

if abs(epsilon[cs,pl,i]) <= 0.1 then
n[0.2,1.0,pl,i]:= (-
68.301*epsilon[cs,pl,i]^2+15.932*epsilon[cs,pl,i]+1.0949)*n[0.2,1.0]:
else n[0.2,1.0,pl,i]:=2.0251*n[0.2,1.0]:
end if:
epsilon[max,pl,i]:= (44.343*epsilon[cs,pl,i]^2-
8.708*epsilon[cs,pl,i]+0.8378)*epsilon[max]:

e[0.2,pl,i]:=sigma[0.2,pl,i]/E[0,pl,i]:
B[0,pl,i]:=0.018+e[0.2,pl,i]*((E[0,pl,i]/E[0.2,pl,i])-1):
A[0,pl,i]:=B[0,pl,i]/(0.008+e[0.2,pl,i]*(sigma[1.0,pl,i]/sigma[0.2,pl,
i]-1)*(1-E[0,pl,i]/E[0.2,pl,i])):
sigma[2.0,pl,i]:=sigma[0.2,pl,i]+(sigma[1.0,pl,i]-
sigma[0.2,pl,i])*(A[0,pl,i]^(1/n[0.2,1.0,pl,i]))*(1-((1/E[0.2,pl,i]-
1/E[0,pl,i])*sigma[0.2,pl,i])/B[0,pl,i])^(1/n[0.2,1.0,pl,i]):
epsilon[2.0,pl,i]:= (sigma[2.0,pl,i]/E[0,pl,i])+0.02:
```

```
b[0,pl,i]:=(sigma[ult,pl,i]*(1+epsilon[ult,pl,i])-
sigma[2.0,pl,i]*(1+epsilon[2.0,pl,i]))/(epsilon[ult,pl,i]-
epsilon[2.0,pl,i]):
a[0,pl,i]:=sigma[2.0,pl,i]*(1+epsilon[2.0,pl,i])-
b[0,pl,i]*epsilon[2.0,pl,i]:
end do:
for e from de by de while e <0.05 do
for i from 0 by 1 to 10 do
if sigma[i] < sigma[rs,i] then
dsigma[x] :=  E[0,pl,i] / (1-nu^2)*de:
dsigma[z] := nu *E[0,pl,i]/(1-nu^2)* de:
else
if sigma[i] <= sigma[0.2,pl,i] then
eps:= X/(E[0,pl,i])+0.002*(X/(sigma[0.2,pl,i]))^n[0,pl,i]:
else
if sigma[i] <= sigma[2.0,pl,i] then
eps:=(X-sigma[0.2,pl,i])/(E[0.2,pl,i])+(0.008+(sigma[1.0,pl,i]-
sigma[0.2,pl,i])*((1/E[0,pl,i])-(1/E[0.2,pl,i])))*((X-
sigma[0.2,pl,i])/(sigma[1.0,pl,i]-
sigma[0.2,pl,i]))^n[0.2,1.0,pl,i]+(sigma[0.2,pl,i])/(E[0,pl,i])+0.002:
else
eps:=(X-a[0,pl,i])/(b[0,pl,i]-X):
end if:
end if:
dH:=subs(X=sigma[i],((diff(eps,X))-(1/E[0,pl,i]))^(-1));
depsilon[x]:= de;
dsigma[z]:= E[0,pl,i]*(4/9*nu*sigma[i]^2*dH/E[0,pl,i]-(2/3*sigma[z,i]-
1/3*sigma[x,i])*(2/3*sigma[x,i]-
1/3*sigma[z,i]))*depsilon[x]/(4/9*sigma[i]^2*dH*(1-
nu^2)/E[0,pl,i]+(2/3*sigma[z,i]-1/3*sigma[x,i])^2+(2/3*sigma[x,i]-
1/3*sigma[z,i])^2+2*nu*(2/3*sigma[z,i]-
1/3*sigma[x,i])*(2/3*sigma[x,i]-1/3*sigma[z,i]));
dsigma[x]:= E[0,pl,i]*((2/3*sigma[z,i]-
1/3*sigma[x,i])^2+4/9*sigma[i]^2*dH/E[0,pl,i])*depsilon[x]/(4/9*sigma[
i]^2*dH*(1-nu^2)/E[0,pl,i]+(2/3*sigma[z,i]-
1/3*sigma[x,i])^2+(2/3*sigma[x,i]-
1/3*sigma[z,i])^2+2*nu*(2/3*sigma[z,i]-
1/3*sigma[x,i])*(2/3*sigma[x,i]-1/3*sigma[z,i]));
end if;
if i = 0 then
ss[x]:= ss[x] + 0.5 * dsigma[x];
ss[z]:= ss[z] + 0.5 * dsigma[z];
ss[av]:= ss[av] + 0.5 * dsig[i]:
elif i = 10 then
ss[x]:= ss[x] + 0.5 * dsigma[x];
ss[z]:= ss[z] + 0.5 * dsigma[z];
ss[av]:= ss[av] + 0.5 * dsig[i]:
else
ss[x]:= ss[x] + dsigma[x];
ss[z]:= ss[z] + dsigma[z];
ss[av]:= ss[av] + dsig[i]:
end if:
sigma[x,i]:= sigma[x,i] + dsigma[x];
sigma[z,i]:= sigma[z,i] + dsigma[z];
omega[i]:=sigma[z,i]/sigma[x,i];
dsig[i]:= abs(sqrt(sigma[x,i]^2+sigma[z,i]^2-sigma[z,i]*sigma[x,i]) -
sigma[i]);
sigma[i]:= max(sqrt(sigma[x,i]^2+sigma[z,i]^2-
sigma[z,i]*sigma[x,i]),sigma[i]);
end do:
sigma[yield]:= sqrt((ss[z]/10)^2+(ss[x]/10)^2-(ss[x]/10)*(ss[z]/10)):
for ep from 1 to 500 by 1 do
```

```
if (e-beginning)=ep*precise then
sigma[ep,plot]:=(ss[x]/10):
epsilon[ep,plot]:=e:
end if:
end do:
end do:
sigma[x,yield]:=sigma[yield]:
epsilon[yield,pl]:= e-sigma[yield]/E[0,pl,i];
ss[x]:= ss[x]/10;
ss[z]:= ss[z]/10;
sqrt(ss[z]^2+ss[x]^2-ss[z]*ss[x]);
sigma[ep,plot];
epsilon[ep,plot];
sigma[100,plot];
epsilon[100,plot];
```

MODEL RS

units [N, mm, MPa]

Material and geometrical characteristics

---

material

```
> E[0] :=191e3:
nu := 0.3:
sigma[y0] := 0.001: ##sigma[y0]>0.0001##
sigma[0.2] :=268;
sigma[ult]:=584;
n[0]:=6.9;
epsilon[ult] := min(1-sigma[.2]/sigma[ult],0.6);
sigma[1.0] := 0.542*sigma[0.2]/n[0]+1.072*sigma[0.2]; formula - Quach
found by analysing tension coupon test data
E[0.2] := E[0]/(1+0.002*n[0]*E[0]/sigma[0.2]); formula-Rasmussen
n[0.2,1.0] := 3.6;
t := 4.64;

e[0.2]:=sigma[0.2]/E[0]; formula-Rasmussen
B[0]:=0.018+e[0.2]*((E[0]/E[0.2])-1); formula-Quach
A[0]:=B[0]/(0.008+e[0.2]*(sigma[1.0]/sigma[0.2]-1)*(1-E[0]/E[0.2]));
formula-Quach
sigma[2.0]:=sigma[0.2]+(sigma[1.0]-
sigma[0.2])*(A[0]^(1/n[0.2,1.0]))*(1-((1/E[0.2]-
1/E[0])*sigma[0.2])/B[0])^(1/n[0.2,1.0]); formula-Quach
epsilon[2.0]:= (sigma[2.0]/E[0])+0.02;
b[0]:=(sigma[ult]*(1+epsilon[ult])-
sigma[2.0]*(1+epsilon[2.0]))/(epsilon[ult]-epsilon[2.0]);      formula-
Quach
a[0]:=sigma[2.0]*(1+epsilon[2.0])-b[0]*epsilon[2.0]; formula-Quach
```

coiling curvature

```
> Kappa[c] := 1/(450);
```

circling or bending radius

```
>
w1:=0:
w2:=0:
ri:=73.58:
radius :=ri+t/2;
Kappa[cs]:= 1/radius;
```

FORMING PROCESS

---

loop for coiling and uncoiling (small strain condition)

```
> i:=-1:
for y from (t/2) by (-t/10) while y > 0 do
i:=i+1:
axy[i]:=y:
####coiling
epsilon[z,cy]:= sigma[y0]*(1-nu^2)/(E[0]*sqrt(1-nu+nu^2)):
epsilon[z,c]:= Kappa[c]*y:
if epsilon[z,cy] < epsilon[z,c] then
e := 0:
sigma[c]:= sigma[y0]:
```

```
omega[c]:= nu:

for s from sigma[y0] by 0.5 to sigma[ult] while abs(e)
<abs(epsilon[z,c]-epsilon[z,cy]) do
ds:= s-sigma[c]:
if s <= sigma[0.2] then
eps:= X/(E[0])+0.002*(X/(sigma[0.2]))^n[0]:
else if s <= sigma[2.0] then
eps:=(X-sigma[0.2])/(E[0.2])+(0.008+(sigma[1.0]-sigma[0.2])*((1/E[0])-
(1/E[0.2])))*((X-sigma[0.2])/(sigma[1.0]-
sigma[0.2]))^n[0.2,1.0]+(sigma[0.2])/(E[0])+0.002:
else
eps:=(X-a[0])/(b[0]-X):
end if:
end if:
dH:=((diff(eps,X))-(1/E[0]))^(-1):
Omega[c]    :=    (4*nu*(subs(X=s,dH))*(1-omega[c]+omega[c]^2)-E[0]*(2-
omega[c])*(2*omega[c]-1))/(E[0]*(2*omega[c]-1)^2+4*(subs(X=s,dH))*(1-
omega[c]+omega[c]^2)):
dom[c]    :=    (2*(1-omega[c]+omega[c]^2)*(Omega[c]-omega[c]))/(s*((2-
omega[c])+Omega[c]*(2*omega[c]-1)))*ds:
omega[c] := omega[c] + dom[c]:
de      :=           subs(X=omega[c],(((1-2*X)^2-2*nu*(1-2*X)*(2-X)+(2-
X)^2)*s)/(2*E[0]*(1-2*X)*(1-X+X^2)^(3/2)))*dom[c]    +    subs(X=s,((1-
omega[c]^2)*(1-2*nu))/(E[0]*(1-2*omega[c])*sqrt(1-
omega[c]+omega[c]^2)))*ds;
e:= de + e:
sigma[c] := s:
end do:
sigma[z,c] := sigma[c]/sqrt(1-omega[c]+omega[c]^2):
sigma[x,c] := omega[c]*sigma[c]/sqrt(1-omega[c]+omega[c]^2):
else
sigma[z,c] := E[0]*epsilon[z,c]/(1-nu^2):
sigma[x,c] := nu*E[0]*epsilon[z,c]/(1-nu^2):
omega[c] := nu:
end if:
epsilon[c,pl]:=e-s/E[0]:
#####uncoiling including flatening
Kappa[u] := -Kappa[c]:
Kappa[uy]:=-(sigma[c]*(1-nu^2)*(2-nu+(2*nu-1)*omega[c]))/(E[0]*y*(1-
nu+nu^2)*sqrt((1-omega[c]+omega[c]^2))):
epsilon[z,uy] := (Kappa[c]+Kappa[uy])*y:
epsilon[z,r] := 0:
if abs(Kappa[uy]) < abs(Kappa[u]) then
omega[uy]    :=    ((1-nu^2)*omega[c]-nu*(2-nu))/((1-2*nu)*omega[c]-(1-
nu^2)):

sigma[u]:= sigma[c]:
omega[u]:= omega[uy]:
e:=0:
for s from sigma[u] by 0.5 to sigma[ult] while abs(e) <
abs(epsilon[z,uy] + epsilon[z,r] ) do
ds := s - sigma[u]:
if s <= sigma[0.2] then
eps:= X/(E[0])+0.002*(X/(sigma[0.2]))^n[0]:
else if s <= sigma[2.0] then
eps:=(X-sigma[0.2])/(E[0.2])+(0.008+(sigma[1.0]-sigma[0.2])*((1/E[0])-
(1/E[0.2])))*((X-sigma[0.2])/(sigma[1.0]-
sigma[0.2]))^n[0.2,1.0]+(sigma[0.2])/(E[0])+0.002:
else
eps:=(X-a[0])/(b[0]-X):
end if:
```

```
end if:
dH:=((diff(eps,X))-(1/E[0]))^(-1):
Omega[u]    :=    (4*nu*(subs(X=s,dH))*(1-omega[u]+omega[u]^2)-E[0]*(2-
omega[u])*(2*omega[u]-1))/(E[0]*(2*omega[u]-1)^2+4*(subs(X=s,dH))*(1-
omega[u]+omega[u]^2)):
dom[u]    :=    (2*(1-omega[u]+omega[u]^2)*(Omega[u]-omega[u]))/(s*((2-
omega[u])+Omega[u]*(2*omega[u]-1)))*ds:
omega[u] := omega[u] + dom[u]:
de     :=          subs(X=omega[u],(((1-2*X)^2-2*nu*(1-2*X)*(2-X)+(2-
X)^2)*s)/(2*E[0]*(1-2*X)*(1-X+X^2)^(3/2)))*dom[u]    +    subs(X=s,((1-
omega[u]^2)*(1-2*nu))/(E[0]*(1-2*omega[u])*sqrt(1-
omega[u]+omega[u]^2)))*ds;
e:= de + e:
sigma[u] := s:
end do:
sigma[u,i]:= sigma[u]:
sigma[z,r,i]:= - sigma[u]/sqrt(1-omega[u]+omega[u]^2):
sigma[x,r,i]:= - omega[u]*sigma[u]/sqrt(1-omega[u]+omega[u]^2):
else
sigma[z,u]:= E[0]*Kappa[u]*y/(1-nu^2):
sigma[x,u]:= nu*E[0]*Kappa[u]*y/(1-nu^2):
sigma[z,r,i] := sigma[z,c]+sigma[z,u]:
sigma[x,r,i] := sigma[x,c]+sigma[x,u]:
omega[u,i]:= sigma[x,r,i]/sigma[z,r,i]:
sigma[u,i]:=sigma[c]:
s:=sigma[c]:
end if:
epsilon[u,pl]:=e-(s-sigma[c])/E[0]:
epsilon[r,pl,i]:=epsilon[u,pl]+epsilon[c,pl]:
#####bending for making circle (x-axis bending)
epsilon[x,csy]:= sigma[u,i]*(1-nu^2)/(E[0]*sqrt(1-nu+nu^2)):
epsilon[x,cs]:= Kappa[cs]*y:
if epsilon[x,csy] < epsilon[x,cs] then
e := 0:
sigma[cs]:= sigma[u,i]:
omega[cs]:= nu:

for   s   from   sigma[u,i]   by   0.5   to   sigma[ult]   while   abs(e)
<abs(epsilon[x,cs]-epsilon[x,csy]) do
ds:= s-sigma[cs]:
if s <= sigma[0.2] then
eps:= X/(E[0])+0.002*(X/(sigma[0.2]))^n[0]:
else if s <= sigma[2.0] then
eps:=(X-sigma[0.2])/(E[0.2])+(0.008+(sigma[1.0]-sigma[0.2])*((1/E[0])-
(1/E[0.2])))*((X-sigma[0.2])/(sigma[1.0]-
sigma[0.2]))^n[0.2,1.0]+(sigma[0.2])/(E[0])+0.002:
else
eps:=(X-a[0])/(b[0]-X):
end if:
end if:
dH:=((diff(eps,X))-(1/E[0]))^(-1):
Omega[cs]:=     (4*nu*(subs(X=s,dH))*(1-omega[cs]+omega[cs]^2)-E[0]*(2-
omega[cs])*(2*omega[cs]-1))/(E[0]*(2*omega[cs]-
1)^2+4*(subs(X=s,dH))*(1-omega[cs]+omega[cs]^2)):
dom[cs]:=((2*(1-omega[cs]+omega[cs]^2)*(Omega[cs]-omega[cs]))/(s*((2-
omega[cs])+Omega[cs]*(2*omega[cs]-1))))*ds:
omega[cs]:= omega[cs] + dom[cs]:
de:=                subs(X=omega[cs],(((1-2*X)^2-2*nu*(1-2*X)*(2-X)+(2-
X)^2)*s)/(2*E[0]*(1-2*X)*(1-X+X^2)^(3/2)))*dom[cs]    +    subs(X=s,((1-
omega[cs]^2)*(1-2*nu))/(E[0]*(1-2*omega[cs])*sqrt(1-
omega[cs]+omega[cs]^2)))*ds:
e:= de + e:
```

```
sigma[cs]:= s:
end do:
sigma[z,cs,i]      :=      sigma[z,r,i]+      omega[cs]*sigma[cs]/sqrt(1-
omega[cs]+omega[cs]^2):
sigma[x,cs,i] := sigma[x,r,i]+sigma[cs]/sqrt(1-omega[cs]+omega[cs]^2):
else
sigma[z,cs,i]:= sigma[z,r,i]+nu*E[0]*epsilon[x,cs]/(1-nu^2):
sigma[x,cs,i]:= sigma[x,r,i]+E[0]*epsilon[x,cs]/(1-nu^2):
omega[cs] := sigma[z,cs,i]/sigma[x,cs,i]:
end if:
epsilon[cs,pl,i]:=e-s/E[0]:

######Uncoiling for final shape
Kappa[us] := -Kappa[cs]:
Kappa[usy]:=-(sigma[cs]*(1-nu^2)*(2-nu+(2*nu-
1)*omega[cs]))/(E[0]*y*(1-nu+nu^2)*sqrt((1-omega[cs]+omega[cs]^2))):
epsilon[x,usy] := (Kappa[cs]+Kappa[usy])*y:
epsilon[x,rs] := 0:
if abs(Kappa[usy]) < abs(Kappa[us]) then
omega[usy]   :=   ((1-nu^2)*omega[cs]-nu*(2-nu))/((1-2*nu)*omega[cs]-(1-
nu^2)):

sigma[us]:= sigma[cs]:
omega[us]:= omega[usy]:
e:=0:
for   s   from   sigma[us]   by   0.5   to   sigma[ult]   while   abs(e)   <
abs(epsilon[x,usy] + epsilon[x,rs]) do
ds := s-sigma[us]:
if s <= sigma[0.2] then
eps:= X/(E[0])+0.002*(X/(sigma[0.2]))^n[0]:
else if s <= sigma[2.0] then
eps:=(X-sigma[0.2])/(E[0.2])+(0.008+(sigma[1.0]-sigma[0.2])*((1/E[0])-
(1/E[0.2])))*((X-sigma[0.2])/(sigma[1.0]-
sigma[0.2]))^n[0.2,1.0]+(sigma[0.2])/(E[0])+0.002:
else
eps:=(X-a[0])/(b[0]-X):
end if:
end if:
dH:=((diff(eps,X))-(1/E[0]))^(-1):
Omega[us]   :=   (4*nu*(subs(X=s,dH))*(1-omega[us]+omega[us]^2)-E[0]*(2-
omega[us])*(2*omega[us]-1))/(E[0]*(2*omega[us]-
1)^2+4*(subs(X=s,dH))*(1-omega[us]+omega[us]^2)):
dom[us] := (2*(1-omega[us]+omega[us]^2)*(Omega[us]-omega[us]))/(s*((2-
omega[us])+Omega[us]*(2*omega[us]-1)))*ds:
omega[us] := omega[us] + dom[us]:
de        :=        subs(X=omega[us],(((1-2*X)^2-2*nu*(1-2*X)*(2-X)+(2-
X)^2)*s)/(2*E[0]*(1-2*X)*(1-X+X^2)^(3/2)))*dom[us]    +    subs(X=s,((1-
omega[us]^2)*(1-2*nu))/(E[0]*(1-2*omega[us])*sqrt(1-
omega[us]+omega[us]^2)))*ds;
e:= de + e:
sigma[us]:=s:
end do:
sigma[us,i]:= sigma[us]:
sigma[z,rs,i]:= - omega[us]*sigma[us]/sqrt(1-omega[us]+omega[us]^2):
sigma[x,rs,i] := - sigma[us]/sqrt(1-omega[us]+omega[us]^2):
epsilon[i]:=e:
epsilon[us,pl,i]:=e-(s-sigma[cs])/E[0]:
epsilon[rs,pl,i]:=epsilon[us,pl,i]+epsilon[cs,pl,i]:
else
sigma[z,us,i] :=nu*E[0]*Kappa[us]*y/(1-nu^2):
sigma[x,us,i] := E[0]*Kappa[us]*y/(1-nu^2):
sigma[z,rs,i] := sigma[z,cs,i]+sigma[z,us,i]:
```

```
sigma[x,rs,i] := sigma[x,cs,i]+sigma[x,us,i]:
omega[us,i]:= sigma[x,rs,i]/sigma[z,rs,i]:
sigma[us,i]:= sigma[cs]:
sigma[cs]:=s:
epsilon[i]:=Kappa[us]*y:
epsilon[us,pl,i]:=0:
epsilon[rs,pl,i]:=epsilon[us,pl,i]+epsilon[cs,pl,i]:
end if:
end do:
```

using simmetry for whole thickness data

```
> axy[5]:=0:
sigma[us,5]:=sigma[y0]:
sigma[z,rs,5]:=sigma[y0]*(1-nu^2)/(E[0]):
sigma[x,rs,5]:=sigma[y0]*(1-nu^2)/(E[0]*nu):
epsilon[rs,pl,5]:=0:
sigma[cs,5]:=sigma[y0]:
sigma[z,cs,5]:=sigma[y0]*(1-nu^2)/(E[0]*nu):
sigma[x,cs,5]:=sigma[y0]*(1-nu^2)/(E[0]):
epsilon[cs,pl,5]:=0:

> for i from 0 by 1 to 4 do
axy[10-i]:= -axy[i]:
sigma[us,10-i]:= sigma[us,i]:
sigma[z,rs,10-i]:= -sigma[z,rs,i]:
sigma[x,rs,10-i]:= -sigma[x,rs,i]:
epsilon[rs,pl,10-i]:= epsilon[rs,pl,i]:
sigma[cs,10-i]:= sigma[cs,i]:
sigma[z,cs,10-i]:= -sigma[z,cs,i]:
sigma[x,cs,10-i]:= -sigma[x,cs,i]:
epsilon[cs,pl,10-i]:= epsilon[cs,pl,i]:
end do:

####Spring back
M[t]:=0:
for i from 0 by 1 to 10 do
if i=0 then
M[i]:=(sigma[x,rs,i]*axy[i]*t/10)/2:
elif i=10 then
M[i]:=(sigma[x,rs,i]*axy[i]*t/10)/2:
else
M[i]:=sigma[x,rs,i]*axy[i]*t/10:
end if:
M[t]:=M[t]+M[i]:
end do:
Iy:=1*t^3/12:
###Final stress(including spring back)
for i from 0 by 1 to 10 do
epsilon[x,sb,i]:= M[t]*axy[i]/(Iy*E[0]):
sigma[x,sb,i]:=epsilon[x,sb,i]*E[0]:
sigma[z,sb,i]:=nu*epsilon[x,sb,i]*E[0]:
sigma[z,pb,i]:=sigma[z,rs,i]-sigma[z,sb,i]:
sigma[x,pb,i]:=sigma[x,rs,i]-sigma[x,sb,i]:
end do:
```

Stress strain diagram after press breaking in longitudinal direction

```
> for i from 0 by 1 to 10 do
sigma[z,i]:=sigma[x,pb,i];
sigma[x,i]:=sigma[z,pb,i];
sigma[i]:=                          sqrt(sigma[x,pb,i]^2+sigma[z,pb,i]^2-
sigma[x,pb,i]*sigma[z,pb,i]);
```

```
sigma[rs,i]:=                    sqrt(sigma[x,pb,i]^2+sigma[z,pb,i]^2-
sigma[x,pb,i]*sigma[z,pb,i]);
omega[i]:=sigma[z,i]/sigma[x,i];
end do:
> precise:= 0.0001;
beginning:= 0;
de:= 1e-5;
e:=0:
ss[z] := 0:
ss[x] := 0:
ss[av] := 0:
for i from 0 by 1 to 10 do

E[0,pl,i] :=E[0]:
nu :=0.3:
sigma[0.2,pl,i]:=                                                    (-
26.857*epsilon[rs,pl,i]^2+9.1674*epsilon[rs,pl,i]+1.0206)*sigma[0.2]:
sigma[1.0,pl,i]:=                                                    (-
30.334*epsilon[rs,pl,i]^2+10.314*epsilon[rs,pl,i]+1.0366)*sigma[1.0]:
sigma[ult,pl,i]:= sigma[ult]:
epsilon[ult,pl,i]:=                        (12.209*epsilon[rs,pl,i]^2-
4.4781*epsilon[rs,pl,i]+1.00272)*epsilon[ult]:
n[0,pl,i]:=                                (44.343*epsilon[rs,pl,i]^2-
8.708*epsilon[rs,pl,i]+0.8378)*n[0]:
E[0.2,pl,i]:=                                                        (-
133.75*epsilon[rs,pl,i]^2+38.761*epsilon[rs,pl,i]+1.2097)*E[0.2]:
n[0.2,1.0,pl,i]:=                                                    (-
68.301*epsilon[rs,pl,i]^2+15.932*epsilon[rs,pl,i]+1.0949)*n[0.2,1.0]:
epsilon[max,pl,i]:=                        (44.343*epsilon[rs,pl,i]^2-
8.708*epsilon[rs,pl,i]+0.8378)*epsilon[max]:

e[0.2,pl,i]:=sigma[0.2,pl,i]/E[0,pl,i]:
B[0,pl,i]:=0.018+e[0.2,pl,i]*((E[0,pl,i]/E[0.2,pl,i])-1):
A[0,pl,i]:=B[0,pl,i]/(0.008+e[0.2,pl,i]*(sigma[1.0,pl,i]/sigma[0.2,pl,
i]-1)*(1-E[0,pl,i]/E[0.2,pl,i])):
sigma[2.0,pl,i]:=sigma[0.2,pl,i]+(sigma[1.0,pl,i]-
sigma[0.2,pl,i])*(A[0,pl,i]^(1/n[0.2,1.0,pl,i]))*(1-((1/E[0.2,pl,i]-
1/E[0,pl,i])*sigma[0.2,pl,i])/B[0,pl,i])^(1/n[0.2,1.0,pl,i]):
epsilon[2.0,pl,i]:= (sigma[2.0,pl,i]/E[0,pl,i])+0.02:
b[0,pl,i]:=(sigma[ult,pl,i]*(1+epsilon[ult,pl,i])-
sigma[2.0,pl,i]*(1+epsilon[2.0,pl,i]))/(epsilon[ult,pl,i]-
epsilon[2.0,pl,i]):
a[0,pl,i]:=sigma[2.0,pl,i]*(1+epsilon[2.0,pl,i])-
b[0,pl,i]*epsilon[2.0,pl,i]:
end do:
for e from de by de while e <0.3 do
for i from 0 by 1 to 10 do
if sigma[i] < sigma[rs,i] then
dsigma[x] :=  E[0,pl,i] / (1-nu^2)*de:
dsigma[z] := nu *E[0,pl,i]/(1-nu^2)* de:
else
if sigma[i] <= sigma[0.2,pl,i] then
eps:= X/(E[0,pl,i])+0.002*(X/(sigma[0.2,pl,i]))^n[0,pl,i]:
else
if sigma[i] <= sigma[2.0,pl,i] then
eps:=(X-sigma[0.2,pl,i])/(E[0.2,pl,i])+(0.008+(sigma[1.0,pl,i]-
sigma[0.2,pl,i])*((1/E[0,pl,i])-(1/E[0.2,pl,i])))*((X-
sigma[0.2,pl,i])/(sigma[1.0,pl,i]-
sigma[0.2,pl,i]))^n[0.2,1.0,pl,i]+(sigma[0.2,pl,i])/(E[0,pl,i])+0.002:
else
eps:=(X-a[0,pl,i])/(b[0,pl,i]-X):
end if:
```

```
end if:
dH:=subs(X=sigma[i],((diff(eps,X))-(1/E[0,pl,i]))^(-1));
depsilon[x]:= de;
dsigma[z]:=  E[0,pl,i]*(4/9*nu*sigma[i]^2*dH/E[0,pl,i]-(2/3*sigma[z,i]-
1/3*sigma[x,i])*(2/3*sigma[x,i]-
1/3*sigma[z,i]))*depsilon[x]/(4/9*sigma[i]^2*dH*(1-
nu^2)/E[0,pl,i]+(2/3*sigma[z,i]-1/3*sigma[x,i])^2+(2/3*sigma[x,i]-
1/3*sigma[z,i])^2+2*nu*(2/3*sigma[z,i]-
1/3*sigma[x,i])*(2/3*sigma[x,i]-1/3*sigma[z,i]));
dsigma[x]:=                                  E[0,pl,i]*((2/3*sigma[z,i]-
1/3*sigma[x,i])^2+4/9*sigma[i]^2*dH/E[0,pl,i])*depsilon[x]/(4/9*sigma[
i]^2*dH*(1-nu^2)/E[0,pl,i]+(2/3*sigma[z,i]-
1/3*sigma[x,i])^2+(2/3*sigma[x,i]-
1/3*sigma[z,i])^2+2*nu*(2/3*sigma[z,i]-
1/3*sigma[x,i])*(2/3*sigma[x,i]-1/3*sigma[z,i]));
end if;
if i = 0 then
ss[x]:= ss[x] + 0.5 * dsigma[x];
ss[z]:= ss[z] + 0.5 * dsigma[z];
ss[av]:= ss[av] + 0.5 * dsig[i]:
elif i = 10 then
ss[x]:= ss[x] + 0.5 * dsigma[x];
ss[z]:= ss[z] + 0.5 * dsigma[z];
ss[av]:= ss[av] + 0.5 * dsig[i]:
else
ss[x]:= ss[x] + dsigma[x];
ss[z]:= ss[z] + dsigma[z];
ss[av]:= ss[av] + dsig[i]:
end if:
sigma[x,i]:= sigma[x,i] + dsigma[x];
sigma[z,i]:= sigma[z,i] + dsigma[z];
omega[i]:=sigma[z,i]/sigma[x,i];
dsig[i]:=  abs(sqrt(sigma[x,i]^2+sigma[z,i]^2-sigma[z,i]*sigma[x,i])  -
sigma[i]);
sigma[i]:=                            max(sqrt(sigma[x,i]^2+sigma[z,i]^2-
sigma[z,i]*sigma[x,i]),sigma[i]);
end do:
sigma[yield]:= sqrt((ss[z]/10)^2+(ss[x]/10)^2-(ss[x]/10)*(ss[z]/10)):
for ep from 1 to 3000 by 1 do
if (e-beginning)=ep*precise then
sigma[ep,plot]:=(ss[x]/10):
epsilon[ep,plot]:=e:
end if:
end do:
end do:
sigma[x,yield]:=sigma[yield]:
epsilon[yield,pl]:= e-sigma[yield]/E[0,pl,i];
ss[x]:= ss[x]/10;
ss[z]:= ss[z]/10;
sqrt(ss[z]^2+ss[x]^2-ss[z]*ss[x]);
sigma[ep,plot];
epsilon[ep,plot];
sigma[100,plot];
epsilon[100,plot];
```

Appendix G

Collected data of corner radii

Press-braked sections					
Published by	Material grade	r_i/t	Published by	Material grade	r_i/t
Van der Berg et al.[40]	1.4301	1.99	Coetzee et al. [64]	1.4301	1.28
		2.22			2.24
		3.4			2.23
		3.43			1.15
		4.43		1.4401	1.42
		4.47			2.05
		5.75			2.13
		5.85			1.37
		6.63		1.4003	1.35
		7.03			2.2
	1.4512	1.8			2.25
		1.87			1.38
		3	Lecce et al. [65]	1.4301	2.04
		3.26			2.04
		4.2			2.04
		4.31			2.04
		5.36			1.53
		5.97			1.53
		6.24		1.4003	2.02
		7.09			2.02
	1.4016	1.94			1.52
		2.39			1.52
		3.12		1.4016	2.15
		3.53			2.21
		4.32			2.21
		4.61			2.21
		5.3			2.21
		6.09			2.21
		6.54			2.21
		7.27			2.21
	1.4003	1.61			2.21
		2.25			
		3.08			
		3.16			
		4.09			
		4.33		MAX	7.27
		5.1		MIN	1.15
		5.64		MEAN	3.31
		6.25		SD	1.78
		6.7		MEAN + 2SD	**6.87**

Table G.0.1 Collected data for press-braked sections.

Cold-rolled sections					
Published by	Material grade	r_i/t	Published by	Material grade	r_i/t
Afshan et al. [47]	1.4301	0.51	Ganping Shu et al. [7]	1.4301	0.60
		0.38			0.75
	1.4301/1.4307	1.19			0.81
		1.48			0.76
	1.4301/1.4307	1.26			0.73
		1.14			0.61
	1.4571	1.08			0.65
		1.27			0.56
	1.4571	1.22			0.38
		1.27			0.37
	1.4404	1.24			0.90
		1.43			0.87
	1.4404	1.15			1.10
		1.34			1.28
	1.4509	1.32			0.85
		1.31			0.75
	1.4509	0.87	Gardner et al. [56]	1.4318	1.30
		0.86			0.81
	1.4509	0.79			1.30
		0.77			1.47
	1.4003	1.37			0.98
		1.47			0.98
	1.4003	1.27			1.31
		1.49			1.31
	1.4162	1.39	Gardner et al. [38]	1.4301	0.84
		1.39			1.18
	S355J2H	1.55			0.68
		1.42			1.57
	S355J2H	0.77			0.93
		0.77			1.46
	S355J2H	0.72	Huang et al. [29]	1.4162	0.70
		0.78			0.67
	S355J2H	1.14			0.40
		1.27			0.40
Rasmussen et al. [66]	1.4301	0.83			0.48
Gardner [42]	1.4301	1.20			0.81
		0.68			
		1.60		MAX	1.60
		0.92		MIN	0.37
		1.46		MEAN	1.02
Gardner et al. [67]	1.4318	1.31		SD	0.34
		0.99		MEAN + 2SD	**1.69**

Table G.0.2 Collected data for cold-rolled sections.